Volume 70A
Number 1
Jan.–Feb. 1966

Physics and Chemistry

U.S. DEPARTMENT OF COMMERCE

SECTION A

JOURNAL OF RESEARCH

NATIONAL BUREAU OF STANDARDS

Journal of Research

of the

National Bureau of Standards

A. Physics and Chemistry

Jan.–Feb. • 1966

VOLUME • 70A

NUMBER • 1

Editor: C. W. Beckett

Associate Editors: D. D. Wagman
J. M. Richardson

Publication dates:
Feb. 1, Apr. 1, June 1, Aug. 1, Oct. 1, Dec. 1, 1966

JOURNAL OF RESEARCH

The National Bureau of Standards Journal of Research reports research and development in the fields of activity shown at right. Also included from time to time are survey articles on topics closely related to the Bureau's scientific and technical program.

The Journal is published in three separate sections as follows:

A. Physics and Chemistry

Contains papers of interest primarily to scientists working in these fields. Issued six times a year. Annual subscription: domestic, $5.00; foreign, $6.00. Single copy, $1.00.

B. Mathematics and Mathematical Physics

Presents studies and compilations designed mainly for the mathematician and the theoretical physicist. Issued quarterly. Annual subscription: domestic, $2.25; foreign, $2.75. Single copy, 75c.

C. Engineering and Instrumentation

Reports research and development results of interest chiefly to the engineer and the applied scientist. Issued quarterly. Annual subscription: domestic, $2.75; foreign, $3.50. Single copy, 75c.

The National Bureau of Standards is a principal focal point in the Federal Government for assuring maximum application of the physical and engineering sciences to the advancement of technology in industry and commerce. Its responsibilities include development and maintenance of the national standards of measurement, and the provision of means for making measurements consistent with those standards; determination of physical constants and properties of materials; development of methods for testing materials, mechanisms, and structures, and making such tests as may be necessary, particularly for government agencies; cooperation in the establishment of standard practices for incorporation in codes and specifications; advisory service to government agencies on scientific and technical problems; invention and development of devices to serve special needs of the Government; assistance to industry, business and consumers in the development and acceptance of commercial standards and simplified trade practice recommendations; administration of programs in cooperation with United States business groups and standards organizations for the development of international standards of practice; and maintenance of a clearinghouse for the collection and dissemination of scientific, technical and engineering information. The scope of the Bureau's activities is suggested in the following listing of its three Institutes and their organizational units.

Institute for Basic Standards. Applied Mathematics. Electricity. Metrology. Mechanics. Heat. Atomic Physics. Physical Chemistry. Laboratory Astrophysics.* Radiation Physics. Radio Standards Laboratory.* Radio Standards Physics & Radio Standards Engineering. Office of Standard Reference Data.

Institute for Materials Research. Analytical Chemistry. Polymers. Metallurgy. Inorganic Materials. Reactor Radiations. Cryogenics.* Materials Evaluation Laboratory. Office of Standard Reference Materials.

Institute for Applied Technology. Building Research. Information Technology. Performance Test Development. Electronic Instrumentation. Textile and Apparel Technology Center. Technical Analysis. Office of Weights and Measures. Office of Engineering Standards. Office of Invention and Innovation. Office of Technical Resources. Clearinghouse for Federal Scientific and Technical Information.**

*Located at Boulder, Colo., 80301.
**Located at 5285 Port Royal Road, Springfield, Va., 22171.

U.S. DEPARTMENT OF COMMERCE
John T. Connor, Secretary

NATIONAL BUREAU OF STANDARDS
A. V. Astin, Director

Order all publications from the Superintendent of Documents
U.S. Government Printing Office, Washington, D.C., 20402

Use of funds for printing this publication approved by the Director of the Bureau of the Budget (June 19, 1961).

JOURNAL OF RESEARCH of the National Bureau of Standards—A. Physics and Chemistry
Vol. 70A, No. 1, January–February 1966

Optical and Magnetic Spectra of Bis-*N*-Propylsalicylaldiminato Copper (II)

Curt W. Reimann, Gerald F. Kokoszka, and Harry C. Allen, Jr.

(October 8, 1965)

The electronic and electron spin resonance spectra of bis-*N*-propylsalicylaldiminato copper (II) have been measured. The measurements show that the *g*-tensor has some rhombic character with $g_z = 2.225$, $g_x = 2.064$, and $g_y = 2.038$. Four *d-d* transitions were observed in the electronic spectrum at 14,800, 16,800, 19,800, and 22,000 cm^{-1}. A consistent set of assignments has been made based on the polarization data of the bands. These results are compared to the results from other similar molecules.

Key Words: Bis-*N*-propylsalicylaldiminato copper (II), optical spectra-four *d-d* transitions, paramagnetic resonance—three *g* values, square planar complex.

1. Introduction

Considerable data are now available on the electronic spectra and magnetic properties of bis-copper (II) complexes with bidentate ligands attached to ring systems [1–9].[1] Almost without exception, for a square planar configuration, the ligand field axes in the molecular plane have been found to point toward the ligand ring system even though the molecular geometry about the copper would seem to favor axes along the copper ligand bonds. These complexes generally contain a center of symmetry so that in the simplest approximation the *d-d* transitions are forbidden. To account for the observation of these transitions a vibronic mechanism is usually invoked.

The spectra of bis-salicylaldiminato copper (II) [$CuSal_2$] and bis-*N*-methylsalicylaliminato copper (II) [Cu(*m*-Sal)$_2$], for which the crystal structures are known, have been studied [2]. These spectra have been interpreted by assuming that the ligand field symmetry at the cupric ion is described by the point group D_{2h}. Unfortunately all four possible *d-d* transitions could not be observed for either molecule making it necessary to speculate on the reasons why only certain transitions are active. Although the interpretation seems reasonable, there are still some unanswered questions about it [3].

Preliminary data on bis-*N*-propylsalicylaldiminato copper (II) [Cu(*p*-Sal)$_2$] indicated that this complex would be particularly suited for a detailed study that might resolve some of the unanswered questions even though the complete crystal structure of the molecule is not known. Four *d-d* transitions are observed in the optical spectrum and the *g*-tensor has a rhombic distortion. Preliminary x-ray data revealed that there is only one molecule per unit cell thus ruling out any spectral ambiguities arising from crystallographically nonequivalent sites.

[1] Figures in brackets indicate the literature references at the end of this paper.

2. Experimental Prodecure

Samples of Cu(*p*-Sal)$_2$ were kindly supplied by Mrs. Paula Wood. Suitable single crystals were grown by evaporation from an acetone solution.

Analysis: Calculated, C—61.92%, H—6.24%, N—7.22%, Cu—16.38%.
Found, C—61.9%, H—6.2%, N—7.2%, Cu—16.4%.

X-ray examination showed that the crystals of Cu(*p*-Sal)$_2$ are triclinic with a measured cell volume of 462 Å^3. The calculated density based on one molecule per unit cell is 1.39 gm/cm^3 which is to be compared to the measured value of 1.40 gm/cm^3.

The magnetic studies were carried out at 25 °C and −196 °C using a X-band spectrometer with 100 kHz modulation and a K-band spectrometer with 6 kHz modulation. The principal axes of the *g*-tensor were determined by trial and error because of the absence of crystal symmetry. The principal *g*-values are given in table 1. The uncertainties quoted represent primarily a measure of the uncertainty in the alinement of the crystals in the applied magnetic field. The spectrum of a powdered polycrystalline sample was also observed. It was interpreted by the method of Kneubuhl [10] yielding results in agreement with the single crystal measurements. The peak-to-peak line widths at 77 °K are about 18 G in the *xy*-plane and about 60 G along the *z*-axis. Such line widths indicate a considerable amount of exchange interaction.

Optical spectra were taken on a spectrophotometer. Light incident on the crystal was polarized by means of Glan-Thomsen polarizers. Spectra were taken in two crystal faces whose orientation with respect to the experimentally determined magnetic axes is shown in figure 1. The *ab* face is nearly perpendicular to the molecular plane which is assumed to be the magnetic *xy*-plane. The other face corresponds very nearly to this *xy*-plane.

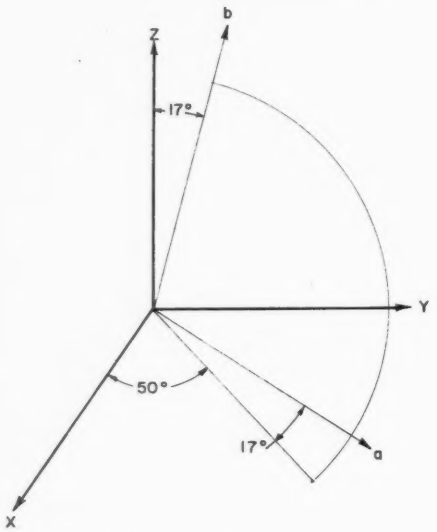

FIGURE 1. *Orientation of the* ab *face with respect to the principal magnetic axes.*

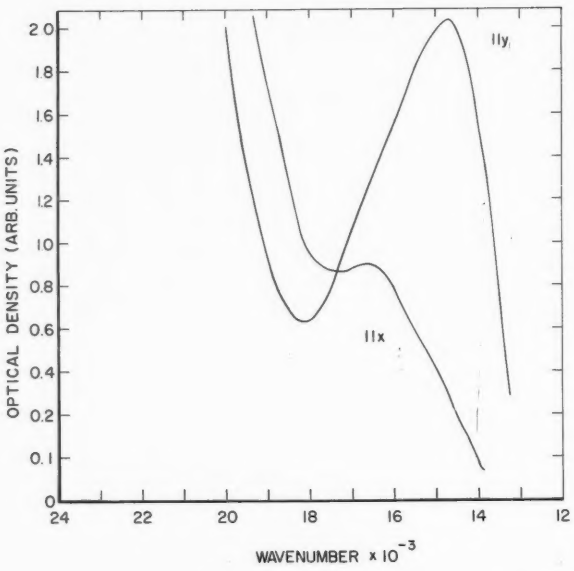

FIGURE 3. *Polarized absorption spectra of* Cu(p-Sal)$_2$ *at 77 °K with light incident in the* xy*-plane.*

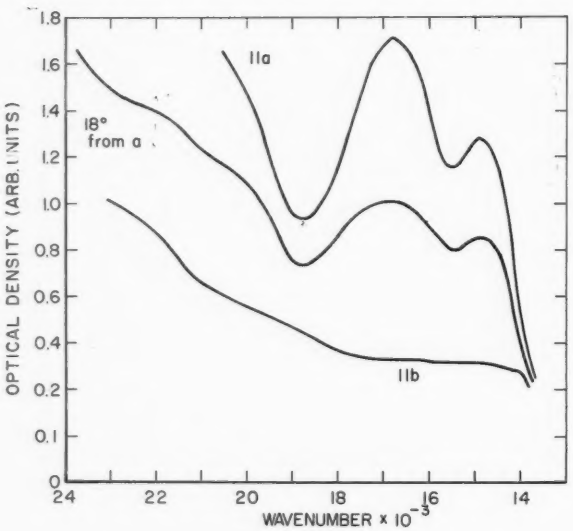

FIGURE 2. *Polarized absorption spectra of* Cu(p-Sal)$_2$ *at 77 °K with light incident on the* ab *face.*

Figure 2 shows the polarized spectra along *a* and *b*. The parallel to *a* spectrum shows two strong bands (14,800 and 16,800 cm^{-1}) while the parallel to *b* spectrum shows two relatively weak bands (19,800 and 22,000 cm^{-1}). The presence of four bands is clearly revealed in the spectrum taken approximately 18° from *a* in the *ab* face.

The spectra taken with light polarized parallel to *x* and to *y* in the *xy*-plane is shown in figure 3. Charge transfer and/or ligand absorption above 20,000 cm^{-1} preclude the observation of the two high frequency bands in this orientation. The two low-frequency bands are strongly polarized in the plane of the molecule while the two high-frequency bands have a *z*-component. Whether these latter bands also have an *x* or *y* component could not be established because of the strong overlapping absorption mentioned previously. These data are summarized in table 1.

TABLE 1. *Optical transitions* (cm^{-1})

Cu(*p*-Sal)$_2$	Cu(*m*-Sal)$_2$	Cu(Sal)$_2$
14,800 (*x*, *y*) 16,800 (*x*, *y*) 19,800 (*z*) 22,000 (*z*)	15,000 (*x*, *y*) 17,000 (*x*, *y*) 20,500 (*z*)	16,500 (*x*, *y*) 18,500 (*x*, *y*)
e.p.r. data		
	Cu(*p*-Sal)$_2$	Cu(Sal)$_2$[a]
g_x	2.064 ± 0.004	2.050$_0$
g_y	2.038 ± .004	2.040$_3$
g_z	2.225 ± .006	2.200$_0$

3. Interpretation of Results

The geometry for this type molecule is shown in figure 4 [11, 12]. The highest symmetry consistent with this model is the point group C_{2h}. This symmetry leaves the position of the *x*- and *y*-axes in the molecular plane undefined. In $CuSal_2$ and Cu(*m*-Sal)$_2$ the *y*-

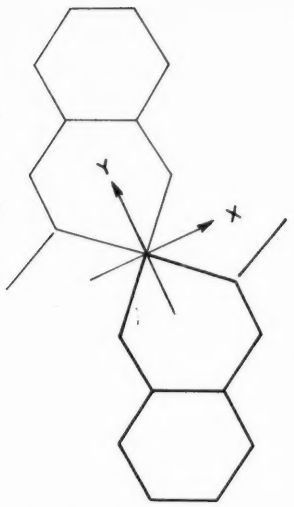

FIGURE 4. *Schematic representation of the geometry of the* $Cu(Sal)_2$*-type complex showing the location of the x- and y-magnetic axes.*

axis was found to pass through the interior N-Cu-O angle as shown. The ligand field axes of $Cu(p\text{-}Sal)_2$ were found to be identical from both optical and magnetic measurements and are assumed to be oriented in the same manner as in the closely related molecules.

The observed g-values can be accounted for on the basis of a ground state that is essentially $d_{x^2-y^2}$ or essentially d_{xy}. The polarized electronic spectrum does not lead to a differentiation either, since in C_{2h} both states belong to the symmetry species A_g. In table 2, the polarization of the various expected transitions is summarized assuming that the appropriate point group is C_{2h} and that the transitions become allowed through a vibronic mechanism. This same table would hold if the roles of d_{xy} and $d_{x^2-y^2}$ were interchanged.

TABLE 2. *Polarization of allowed vibronic transitions in* C_{2h}

Transition	Species of vibration	
	A_u	B_u
$\|xy> \rightarrow \|z^2>$	z	x,y 14,800
$\|xy> \rightarrow \|x^2-y^2>$	z	x,y 16,800
$\|xy> \rightarrow \|xz>$	x,y	z 19,800
$\|xy> \rightarrow \|yz>$	x,y	z 22,000

The assignment given in table 2 seems to be the most logical and agrees with the assignments made previously in $CuSal_2$ and $Cu(m\text{-}Sal)_2$ [1–3]. This means that the transitions become allowed through a vibronic mechanism involving a B_u vibration. Again this is in accord with the previous work [1–2].

The disturbing part of this interpretation is that it does not provide an unambiguous determination of the electronic ground state. However, intuitive arguments based on the fact that the d_{xy} orbital points directly at the ligands lead to the conclusion that d_{xy} must be the orbital containing the unpaired electron.

4. Bonding Parameters

The magnetic and optical data can be used to gain some insight into the nature of the bonding in $Cu(p\text{-}Sal)_2$. The wavefunctions which describe this complex are taken to be a linear combination of copper d-orbitals and ligand orbitals of the same symmetry species. The d_{z^2}, d_{xy}, and $d_{x^2-y^2}$ orbitals belong to the irreducible representation A_g in the point group C_{2h} and can therefore mix. As a first approximation, however, we have assumed they may be treated separately. The wavefunctions [6] are:

$$|xy> = \alpha d_{xy} - \tfrac{1}{2}\alpha' [-\sigma_{xy}^{(1)} + \sigma_{xy}^{(2)} + \sigma_{xy}^{(3)} - \sigma_{xy}^{(4)}]$$

$$|x^2-y^2> = \beta d_{x^2-y^2} - \tfrac{1}{2}(1-\beta^2)^{1/2}[-p_{xy}^{(1)} - p_{xy}^{(2)} + p_{xy}^{(3)} + p_{xy}^{(4)}]$$

$$|z^2> = \gamma d_{z^2} = \tfrac{1}{2}(1-\gamma^2)^{1/2}[\sigma_{xy}^{(1)} + \sigma_{xy}^{(2)} - \sigma_{xy}^{(3)} - \sigma_{xy}^{(4)}]$$

$$|yz> = \delta' d_{xy} - \tfrac{1}{2}(1-\delta'^2)^{1/2}[p_z^{(1)} + p_z^{(2)} - p_z^{(3)} - p_z^{(4)}]$$

$$|xz> = d_{xz}.$$

The g-values which are the experimental parameters in the usual spin Hamiltonian can then be related to the free ion spin-orbit coupling constant, the electronic energy levels and the bonding parameters by the equations

$$g_z = 2.002 - \frac{8\lambda}{\Delta_{x^2-y^2}}[\alpha^2\beta^2 - \alpha\alpha'\beta^2 S - \alpha\alpha'\beta(1-\beta^2)^{1/2}\frac{T(n)}{2}]$$

$$g_x = 2.002 - \frac{2\lambda}{\Delta_{xz}}[\alpha^2 - \alpha\alpha' S]$$

$$g_y = 2.002 - \frac{2\lambda}{\Delta_{yz}}[\alpha^2\delta'^2 - \alpha\alpha'\delta'^2 S].$$

The values for the S and $T(n)$ integrals are assumed to be the average of calculated values for oxygen and nitrogen. Using the assignments $\Delta_{x^2-y^2} = 16{,}800$ cm^{-1}, $\Delta_{xz} = 19{,}800$ cm^{-1}, and $\Delta_{yz} = 22{,}000$ cm^{-1}, the bonding parameters are found to be $\alpha = 0.89$, $\beta = 0.85$, and $\delta' = 0.76$. The values indicate that the pi bonding to the ring system can play an important role in stabilizing some chelating complexes. Gersmann and Swalen [6] also calculated values for bonding parameters in chelating complexes. In their studies the two in-plane g-values were approximately equal and differences in the optical transitions were used to

reach conclusions about the strength of the pi bond. In Cu(p-Sal)$_2$ the $|xz>$ and $|yz>$ energy levels are found to be rather close together and the nature of the bonding manifests itself in rather different in-plane g-values.

It is interesting to use the magnetic data of Maki and McGarvey and estimates of the bonding parameters for Cu(Sal)$_2$ to calculate the expected positions of the $|xz>$ and $|yz>$ levels in that complex. The work of Kivelson and Neiman [7] suggests that α^2 would be about 0.76 and we assume that δ' is about the same as in Cu(p-Sal)$_2$. The $|xz>$ level is then expected to be at 18,200 cm^{-1} and the $|yz>$ level is calculated to be at about 24,700 cm^{-1}. The latter band would be masked by the charge transfer spectra, while the former falls in the same region of the spectrum as the two more intense $A_g \rightarrow A_g$ transitions. Ferguson [2] has suggested that a small z component in the spectrum might indeed be present in this spectral region. This assignment of energy levels is also in qualitative agreement with the work of Gersmann and Swalen.

(Paper 70A1–380)

5. Conclusions

The electronic and magnetic spectra of Cu(p-Sal)$_2$ support the contention that the effective symmetry at the cupric ion is lower than axial. Moreover, these data appear to be best accounted for in terms of a model which supposes the ground-state molecular orbital is essentially d_{xy}.

6. References

[1] J. Ferguson, R. L. Belford, and T. S. Piper, J. Chem. Phys. **37,** 1569 (1962).
[2] J. Ferguson, J. Chem. Phys. **35,** 1612 (1961).
[3] T. S. Piper and R. L. Belford, Mol. Phys. **5,** 169 (1962).
[4] D. P. Graddon, J. Inorg. & Nucl. Chem. **14,** 111 (1960).
[5] J. M. Waters and T. N. Waters, J. Chem. Soc. 2489 (1964).
[6] H. R. Gersmann and J. D. Swalen, J. Chem. Phys. **36,** 3221 (1962).
[7] R. Neiman and D. Kivelson, J. Chem. Phys. **35,** 149, 156, 162 (1961).
[8] A. H. Maki and B. R. McGarvey, J. Chem. Phys. **29,** 31, 35 (1958).
[9] G. F. Kokoszka, H. C. Allen, Jr., and G. Gordon, J. Chem. Phys. **42,** 3730 (1965).
[10] F. K. Kneubuhl, J. Chem. Phys. **33,** 1074 (1960).
[11] J. M. Stewart and E. C. Lingafelter, Acta. Cryst. **12,** 842 (1959).
[12] E. C. Lingafelter, G. L. Simmons, B. Morosin, C. Scheringer, and C. Freiburg, Acta. Cryst. **14,** 1222 (1961).

JOURNAL OF RESEARCH of the National Bureau of Standards—A. Physics and Chemistry
Vol. 70A, No. 1, January–February 1966

Phase Equilibria in the System Niobium Pentoxide–Germanium Dioxide

Ernest M. Levin

(October 11, 1965)

The phase equilibrium diagram for the system Nb_2O_5—GeO_2 has been determined experimentally, using the quenching technique and examining the samples by optical microscopy and x-ray powder diffractometry. The system contains one compound, $9Nb_2O_5 \cdot GeO_2$, which melts incongruently at 1420 °C. A eutectic between this compound and GeO_2 is located at about 97 mol percent GeO_2 and 1090 °C. The system does not show liquid immiscibility, and it is concluded that the ionic field strength limit for two-liquid separation in the series of glass formers occurs with the Nb^{+5} cation.

Key Words: Germanium dioxide, immiscibility, niobium pentoxide, phase equilibria.

1. Introduction

Liquid immiscibility in binary oxide systems appears to be confined to the glass forming systems. In a systematic search for the principles underlying two-liquid formation it is necessary to examine the effect of different glass-forming cations, e.g., B^{+3}, Ge^{+4}, Si^{+4}, and also of different modifier cations, i.e., with varying charges and ionic radii. Many binary phase diagrams of glass formers with modifier oxides from Groups I and II of the Periodic Table have been reported [1].[1] Only a few systems with modifier oxides from Groups III and IV have been reported. Two pertinent systems from Group V have been published: $Nb_2O_5-SiO_2$ [2] and $Nb_2O_5-V_2O_5$ [3]. Finally, in Group VI, phase relationships in the system $WO_3-B_2O_3$ [4] have been established.

Determination of the phase diagrams of Nb_2O_5 with B_2O_3, GeO_2, and P_2O_5 has been undertaken in order to complete the study of the effect of a cation of high charge (Nb^{+5}) on immiscibility in a series of glass formers. This paper, therefore, reports the phase equilibrium relations in the $Nb_2O_5-GeO_2$ system and its bearing on immiscibility.

2. Sample Preparation and Test Methods

Starting materials for the preparation of mixtures consisted of high purity niobium pentoxide and electronic grade germanium dioxide, designated by the manufacturers as over 99.7 percent and 99.9+ percent pure, respectively. The Nb_2O_5 contained the following impurities when examined by the general qualitative spectrochemical method: Si—less than 0.1 percent; Fe, Sn, Ti—0.001 to 0.01 percent; Ca, Mg—0.0001 to 0.001 percent, Cu—? Spectrographic analysis of the GeO_2 showed: Si—0.001 to 0.01 percent; Ca, Mg—0.0001 to 0.001 percent; Cu—less than 0.0001 percent, Ag, Al, Fe—?

Calculated amounts of Nb_2O_5 and GeO_2 sufficient to yield 4-g batches, on an ignited basis, were weighed into plastic containers and blended with a high-speed mechanical mixer. The mixtures were formed into discs 16 mm in diameter by pressing in a mold at approximately 20,000 lb/in^2. The disks were placed in covered platinum crucibles and calcined in air at 800 °C for 15 hr, using an electrically heated furnace. The fired disks were ground in an agate mortar, remixed, pressed, and given a second heat treatment at about 900 °C for 12 hr. The complete process of grinding and pressing was repeated a third time, and the specimens were heated in the range of 900 to 1000 °C for 12 hr. Formulated compositions were used in constructing the phase diagram. Analyses of two small samples for Nb_2O_5 only, by the Analytical Chemistry Division, were about 0.75 percent low.

The quenching technique was used to obtain subsolidus and liquidus data on samples sealed in Pt tubes. Constant temperature control of the quenching furnace to within ±2 °C was achieved with a self-adjusting a-c bridge-type controller. Quenched samples were examined with the binocular and polarizing microscopes and by x-ray powder diffractometry (Ni-filtered CuK_α radiation) using a high-angle Geiger-counter diffractometer. The technique of sample preparation as well as the apparatus and method have been described in previous publications [5].

The solidus value was deduced from observation of the first temperature at which the sample showed slumping, coupled with x-ray evidence that one of the phases was disappearing. The liquidus temperature was indicated by the formation of a concave meniscus, coupled with microscopic evidence of a quenched glass (for several compositions rich in GeO_2) or x-ray evidence of large amounts of low-temperature niobia-type phases. The polarizing microscope was of limited value in the latter case.

Temperatures were measured with a Pt versus 90 Pt:10 Rh thermocouple which was taken from lengths of thermocouple wire which originally had been calibrated by the temperature physics section.

[1] Figures in brackets indicate the literature references at the end of this paper.

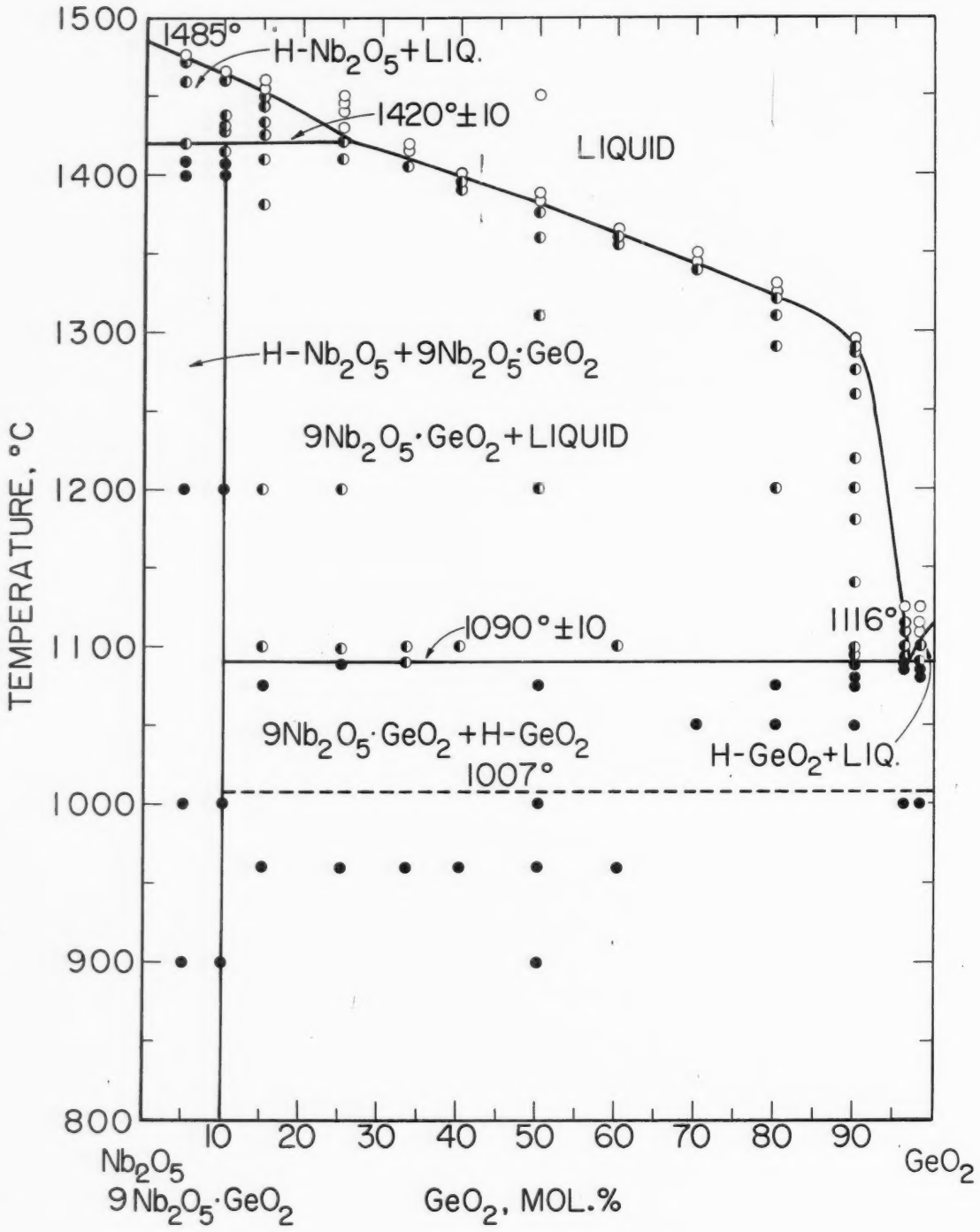

FIGURE 1. *Phase equilibrium diagram for the system* $Nb_2O_5-GeO_2$.
●–No melting; ◐–partial melting; ○–complete melting.
H–Nb_2O_5–High-temperature form of Nb_2O_5.
H–GeO_2–Quartz form of GeO_2.

Temperatures are given on the International Practical Temperature Scale of 1961. During the course of the experiments the thermocouple was checked against the melting points of gold (1063 °C) and of barium disilicate (1420 °C). The overall maximum uncertainty of the temperature values reported herein is estimated to be within ± 10 °C.

3. Results and Discussions

3.1. Nb_2O_5 and GeO_2 Components

No quenching experiments were made with the components, as they were the same materials that had been used previously in phase equilibirum studies originating in this laboratory [3, 6, 7].

The Nb_2O_5 used as starting material gave an x-ray pattern of poorly crystalline low-Nb_2O_5 [8]. The so-called high temperature, monoclinic form [9] was the only stable modification encountered in the present work. This finding agrees with that reported in studies of other binary phase diagrams [9, 10].

The GeO_2 used as starting material was the high-temperature (quartz form) polymorph, and it was the only form detected throughout the experiments. In pure GeO_2 the transition from the low to the high form is given at 1007 °C [11], and the phase diagram is constructed on the assumption of no solid solubility of niobia in germania.

3.2. Phase Diagram

Figure 1 shows the phase diagram for the system. Table 1 lists the compositions studied, the important heat treatments, and the phases identified, as well as the indices for several quenched phases. The system is characterized by one eutectic point at about 97.0 mole percent, GeO_2 (3.0% Nb_2O_5) and 1090 °C and by one peritectic point at about 25 percent GeO_2 (75% Nb_2O_5) and 1420 °C. The latter temperature corresponds to the incongruent melting point of $9Nb_2O_5 \cdot GeO_2$, the only binary compound found in the system.

TABLE 1. *Experimental data* [1] *for compositions in the binary system* $Nb_2O_5-GeO_2$

Composition		Heat treatment [2]		Results		Notes
Nb_2O_5	GeO_2	Temp.	Time	Physical observation	X-ray diffraction analyses [3]	
Mole %	*Mole %*	*°C*	*Hours*			
2.0	98.0	1000	12	No melting.	$GeO_2 + 9Nb_2O_5 \cdot GeO_2$	
		1080	1	No melting.	$GeO_2 + 9Nb_2O_5 \cdot GeO_2$	
		1084	1.25	No melting.	$GeO_2 + 9Nb_2O_5 \cdot GeO_2$	
		1090	1.25	Start of melting.	$GeO_2 + 9Nb_2O_5 \cdot GeO_2$	Solidus.
		1100	1	Considerable melting.	$GeO_2 + [9Nb_2O_5 \cdot GeO_2]$	
		1109	16	Complete melting.	Glass + $[9Nb_2O_5 \cdot GeO_2]$	
		1114	2	Complete melting.	Glass + $[9Nb_2O_5 \cdot GeO_2]$	$N_{Li} = 1.613$ (25°).
4.0	96.0	1000	12	No melting.	$GeO_2 + 9Nb_2O_5 \cdot GeO_2$	
		1086	1.25	No melting.	$GeO_2 + 9Nb_2O_5 \cdot GeO_2$	
		1089	1.5	No melting.	$GeO_2 + Nb_2O_5 \cdot GeO_2$	
		1093	1	Partial melting.	$[GeO_2] + 9Nb_2O_5 \cdot GeO_2$	
		1099	1.5	Considerable melting.	$9Nb_2O_5 \cdot GeO_2 + [GeO_2]$	
		1109	1.5	Complete melting.	Glass + $[9Nb_2O_5 \cdot GeO_2]$	$N_{Li} = 1.616$ (25°)
10.0	90.0	1050	15	No melting.	$GeO_2 + 9Nb_2O_5 \cdot GeO_2$	
		1075	67.5	No melting.	$GeO_2 + 9Nb_2O_5 \cdot GeO_2$	1098°/18 hr starting material.
		1088	18	No melting.	$GeO_2 + 9Nb_2O_5 \cdot GeO_2$	
		1095	2	Start of melting.	$9Nb_2O_5 \cdot GeO_2 + GeO_2$	
		1098	18	Partial melting.	$9Nb_2O_5 \cdot GeO_2$ + glass	
		1200	2	Partial melting.	$9Nb_2O_5 \cdot GeO_2$ + glass	
		1275	1.5	Considerable melting.	$9Nb_2O_5 \cdot GeO_2$ + glass	
		1287	2	Almost melted.	$9Nb_2O_5 \cdot GeO_2$ + glass	$N_{Li} = 1.711$ (25°).
		1291	2	Almost melted.		
		1295	1.75	Complete melting.	$[L - Nb_2O_5^s]$ + glass	$N_{Li} = 1.723$ (25°).
20.0	80.0	1050	15	No melting.	$GeO_2 + 9Nb_2O_5 \cdot GeO_2$	
		1075	67.5	No melting.	$GeO_2 + 9Nb_2O_5 \cdot GeO_2$	
		1200	5	Partial melting.	GeO_2 + glass	
		1310	1.5	Considerable melting.	$9Nb_2O_5 \cdot GeO_2 + [L - Nb_2O_5^s]$	$N_{Li} \approx 1.771$ (25°).
		1320	1	Almost melted.	$9Nb_2O_5 \cdot GeO_2 + [L - Nb_2O_5^s]$	
		1325	1	Complete melting.		$N_{Li} \approx 1.84$.
		1330	2	Complete melting.	$[L - Nb_2O_5^s]$	
30.0	70.0	1050	15	No melting.	$GeO_2 + 9Nb_2O_5 \cdot GeO_2$	
		1339	1.5	Considerable melting.	$9Nb_2O_5 \cdot GeO_2 + [L - Nb_2O_5^s]$	
		1344	2	Complete melting.	$[L - Nb_2O_5^s]$	
40.0	60.0	960	2.5	No melting.	$9Nb_2O_5 \cdot GeO_2 + GeO_2$	
		1100	15	Partial melting.	$9Nb_2O_5 \cdot GeO_2$ + glass	
		1355	1.5	Considerable melting.	$9Nb_2O_5 \cdot GeO_2 + [L - Nb_2O_5^s]$	
		1360	2	Almost melted.	$[L - Nb_2O_5^s] + 9Nb_2O_5 \cdot GeO_2$	
		1365	1.25	Complete melting.	$[L - Nb_2O_5^s]$	

TABLE 1. *Experimental data [1] for compositions in the binary system* $Nb_2O_5-GeO_2$ – Continued

Composition		Heat treatment [2]		Results		Notes
Nb_2O_5	GeO_2	Temp.	Time	Physical observation	X-ray diffraction analyses [3]	
Mole %	*Mole %*	*°C*	*Hours*			
50.0	50.0	900	1.75	No melting.	$GeO_2 + 9Nb_2O_5 \cdot GeO_2 + [Nb_2O_5]$	
		960	456	No melting.	$9Nb_2O_5 \cdot GeO_2 + GeO_2$	L – GeO_2 not formed.
		1000	1.75	No melting.	$9Nb_2O_5 \cdot GeO_2 + GeO_2$	
		1075	144	No melting.	$9Nb_2O_5 \cdot GeO_2 + GeO_2$	
		1200	5	Partial melting.	$9Nb_2O_5 \cdot GeO_2$	
		1375	1.5	Considerable melting.	$9Nb_2O_5 \cdot GeO_2 + [L-Nb_2O_5^2]$	
		1379	1.5	Almost melted.	$[L-Nb_2O_5^2] + 9Nb_2O_5 \cdot GeO_2$	
		1383	1.5	Complete melting.	$[L-Nb_2O_5^2]$	
		1450	2	Complete melting.	$[L-Nb_2O_5^2]$	
60.0	40.0	960	2.5	No melting.	$9Nb_2O_5 \cdot GeO_2 + GeO_2$	
		1100	15	Just melting.	$9Nb_2O_5 \cdot GeO_2$	
		1390	1.5	Considerable melting.	$9Nb_2O_5 \cdot GeO_2 + [L-Nb_2O_5^2]$	
		1395	2	Almost melted.	$[L-Nb_2O_5^2] + 9Nb_2O_5 \cdot GeO_2$	
		1400	1.5	Complete melting.	$[L-Nb_2O_5^2]$	
66.7	33.3	960	2.5	No melting.	$9Nb_2O_5 \cdot GeO_2 + GeO_2$	
		1090	18	Start of melting.	$9Nb_2O_5 \cdot GeO_2$	At solidus.
		1100	15	Slight melting.	$9Nb_2O_5 \cdot GeO_2$ + glass	
		1405	1	Considerable melting.	$9Nb_2O_5 \cdot GeO_2 + [L-Nb_2O_5^2]$	
		1414	1	Complete melting.	$[L-Nb_2O_5^2] + 9Nb_2O_5 \cdot GeO_2$	
75.0	25.0	960	2.5	No melting.	$9Nb_2O_5 \cdot GeO_2 + GeO_2$	
		1090	15	No melting.	$9Nb_2O_5 \cdot GeO_2 + GeO_2$	
		1098	18	Slight melting.	$9Nb_2O_5 \cdot GeO_2$	
		1200	5	Some melting.	$9Nb_2O_5 \cdot GeO_2$	
		1410	1.1	Partial melting.	$9Nb_2O_5 \cdot GeO_2$	
		1421	2	Considerable melting.	$9Nb_2O_5 \cdot GeO_2 + [L-Nb_2O_5^2]$	
		1430	1.25	Complete melting.	$[L-Nb_2O_5^2] + [9Nb_2O_5 \cdot GeO_2]$	
		1438	3.5	Complete melting.	$[L-Nb_2O_5^2]$	
85.0	15.0	960	2.5	No melting.	$9Nb_2O_5 \cdot GeO_2 + GeO_2$	
		1075	144	No melting.	$9Nb_2O_5 \cdot GeO_2 + GeO_2$	
		1100	16	Slight melting.	$9Nb_2O_5 \cdot GeO_2$ + glass	
		1200	5	Slight melting.	$9Nb_2O_5 \cdot GeO_2$	
		1409	65	Partial melting.	$9Nb_2O_5 \cdot GeO_2$	
		1427	1.5	Partial melting.	$9Nb_2O_5 \cdot GeO_2$	
		1433	9	Partial melting.	$[9Nb_2O_5 \cdot GeO_2] + H-Nb_2O_5$	Decomp. $9Nb_2O_5 \cdot GeO_2$.
		1442	3	Considerable melting.	$[9Nb_2O_5 \cdot GeO_2] + H-Nb_2O_5 + [L-Nb_2O_5^2]$	
		1450	1.5	Considerable melting.	$[9Nb_2O_5 \cdot GeO_2] + H-Nb_2O_5 + [L-Nb_2O_5^2]$	
		1455	2	Complete melting.	$[L-Nb_2O_5^2]$	
90.0	10.0	900	12	No melting.	$Nb_2O_5 + 9Nb_2O_5 \cdot GeO_2$	Nonequilibrium.
		1000	12	No melting.	$9Nb_2O_5 \cdot GeO_2 + H-Nb_2O_5$	Nonequilibrium.
		1200	5	No melting.	$9Nb_2O_5 \cdot GeO_2$	Single phase.
		1401	2	No melting.	$9Nb_2O_5 \cdot GeO_2$	
		1409	1.75	No melting.	$9Nb_2O_5 \cdot GeO_2$	
		1415	2	Slight slumping.	$9Nb_2O_5 \cdot GeO_2 + H-Nb_2O_5$	At decomp. $9Nb_2O_5 \cdot GeO_2$.
		1427	2	Partial melting.	$H-Nb_2O_5 + [9Nb_2O_5 \cdot GeO_2]$	
		1460	1.5	Considerable melting.	$[9Nb_2O_5 \cdot GeO_2] + H-Nb_2O_5 + [L-Nb_2O_5^2]$	
		1465	1.5	Complete melting.	$[L-Nb_2O_5^2]$	
95.0	5.0	900	12	No melting.	$Nb_2O_5 + 9Nb_2O_5 \cdot GeO_2 + [GeO_2]$	Nonequilibrium.
		1000	12	No melting.	$Nb_2O_5 + 9Nb_2O_5 \cdot GeO_2 + [GeO_2]$	Nonequilibrium.
		1200	5	No melting.	$H-Nb_2O_5 + 9Nb_2O_5 \cdot GeO_2$	
		1400	1.5	No melting.	$H-Nb_2O_5 + 9Nb_2O_5 \cdot GeO_2$	
		1409	2.75	No melting.	$H-Nb_2O_5 + 9Nb_2O_5 \cdot GeO_2$	
		1421	2	Slight melting.	$H-Nb_2O_5 + 9Nb_2O_5 \cdot GeO_2$	At decomp. $9Nb_2O_5 \cdot GeO_2$.
		1459	1.5	Slight melting.	$H-Nb_2O_5 + [9Nb_2O_5 \cdot GeO_2]$	
		1472	1.5	Considerable melting.	$H-Nb_2O_5 + [9Nb_2O_5 \cdot GeO_2] + [L-Nb_2O_5^2]$	
		1476	1.5	Complete melting.	$[L-Nb_2O_5^2] + [H-Nb_2O_5]$	

[1] Only definitive data are given: figure 1 shows all of the heat treatments.
[2] Specimens quenched in sealed Pt tubes.
[3] Phases indentified are listed in order of amount present at room temperature. Brackets enclose phases not necessarily present at the elevated temperature or not believed to be in final equilibrium Only the high-temperature, hexagonal (quartz form) of GeO_2(H-GeO_2) was observed in these experiments. H–Nb_2O_5 and L–Nb_2O_5 refer to high and low temperature forms, respectively. Glass identified as a broad diffuse band in 18° to 28° – 2θ range.
[4] This phase quenched from the liquid indexes on a hexagonal unit cell basis (table 2).
[5] This phase quenched from the liquid indexes on a pseudo-orthorhombic basis (table 2).

3.3. Compound $9Nb_2O_5 \cdot GeO_2$

This compound was reported by Waring and Roth [12] to be a tetragonal phase conforming to the general type $10M_2O_5 \cdot 90M'_2O_5$ apparently isostructural with $Ta_2O_5 \cdot 2Nb_2O_5$. The existence of this phase and the unit cell dimensions [2] were verified in the present study. The phase formed readily throughout the system at temperatures above 1000 °C. Decomposition of the phase above the incongruent melting point (1420 °C) was sluggish. For example, a sample of composition 85 percent Nb_2O_5 heated at 1433 °C for 9 hr (table 1) still showed a considerable proportion of the compound.

In the eight reported isostructural compounds [12] of the general type $10M_2O_5 \cdot 90M'_2O_5$, Ge^{+4} is the only

[2] $a = 15.70$ Å, $c = 3.817$ Å.

cation not pentavalent. It would be instructive for crystal chemical reasons to know if the compound composition were indeed exactly $9Nb_2O_5 \cdot GeO_2$. Results of the present study are consistent with the 9:1 ratio and indicate no solid solution region. However, limitations in the sensitivity of microscopic and x-ray detection of homogeneity preclude an unequivocal statement of the compound composition. For example, the ratio $10Nb_2O_5 \cdot GeO_2$ contains 90.9 mole percent Nb_2O_5, and would not be distinguishable from the 9:1 composition.

3.4. Metastable Phases Quenched From Liquid

Two metastable low niobia-like phases were obtained from quenched liquids (see table 1, footnotes d and e, and table 2). Samples of composition 50 Nb_2O_5: 50 GeO_2 and richer in niobia when quenched from the liquid gave a phase that could be partially indexed on the basis of low-Ta_2O_5 [13]. The several unindexed peaks (table 2), however, indicate that this cell is at best a subcell of low-Nb_2O_5. The pseudo-orthorhombic cell has unit cell dimensions: $a=6.17$ Å, $b=3.64$ Å, and $c=3.92$ Å.

Samples in the composition range $30Nb_2O_5:70GeO_2$ to $10Nb_2O_5:90GeO_2$ quenched from the liquid to give a phase that could be indexed on a hexagonal unit cell basis: $a=3.60$ Å, $c=3.90$ Å, $c/a=1.088$. In table 2 the coincidence of orthorhombic indices as related to the hexagonal indices is indicated. Thus, the orthorhombic (110) and (200) become the hexagonal (100), etc.

Quenches from the liquid of samples of composition $40Nb_2O_5:60GeO_2$, intermediate between the composition ranges for the two metastable phases, showed both phases (table 1). It should be noted, however, that no detectable change in unit cell dimensions with changing composition was noted for either metastable phase. Furthermore, as some GeO_2-rich glass was present in the quenched specimens, the exact composition limits of the metastable phases cannot be specified.

3.5. Application to Liquid Immiscibility Theory

From the standpoint of liquid immiscibility considerations, this system is noteworthy because of the absence of expected immiscibility. It is instructive to consider the following binary systems of Nb_2O_5 with the glass formers: B_2O_3, SiO_2, and GeO_2.

The $Nb_2O_5-B_2O_3$ [14] and $Nb_2O_5-SiO_2$ [2] systems have large regions of immiscibility, whereas the $Nb_2O_5-GeO_2$ system shows complete miscibility. In the hexavalent group of modifier cations, only the $WO_3-B_2O_3$ system has been reported [4]; and this system does not exhibit liquid immiscibility. The ionic field strength [3] (i.f.s.) of Nb^{+5} is greater than that of Ge^{+4}, slightly greater than that of B^{+3}, and less than that of Si^{+4}; the i.f.s. of W^{+6} is considerably greater than that of B^{+3}, Ge^{+4}, and Si^{+4}.

From the above information on immiscibility in oxide systems and i.f.s. of the modifier cations it may be concluded that the existence of immiscibility, per se, is not directly related to the extent of immiscibility. Whereas structural considerations determine the

[3] e.g., calculated as $\frac{Z}{(R_+ + 1.40)^2}$, where Z is the cationic charge and R_+ and 1.40 are the ionic radii of the cation and oxygen, respectively.

TABLE 2. *X-ray diffraction powder data for metastable low niobia-type phases quenched from liquid* (CuK_α *radiation*)

$50Nb_2O_5:50GeO_2$ (quenched from 1450 °C/2hr)					$20Nb_2O_5:80GeO_2$ (quenched from 1330 °C/2hr)				
hkl [1]	d	I/I_0	$1/d^2_{obs}$	$1/d^2_{calc}$	hkl [2]	d	I/I_0	$1/d^2_{obs}$	$1/d^2_{calc}$
	5.18	8	0.0373						
001	3.922	100	.0650	0.0650	001	3.912	93	0.0653	0.0653
110	3.136	94	.1017	.1017	100	3.114	100	.1031	.1031
200	3.084	63	.1052	.1051					
	2.731	4	.1341						
111	2.449	45	.1667	.1667	101	2.437	43	.1684	.1684
201	2.425	25	.1701						
	2.116	7	.2234						
	2.010	8	.2475						
002	1.9604	25	.2602	.2602	002	1.9568	18	.2612	.2612
020	1.8212	11	.3015	.3016	110	1.7987	18	.3091	.3093
310	1.7908	20	.3118	.3118					
112	1.6625	15	.3618	.3618	102	1.6562	18	.3645	.3644
021	1.6570	14	.3642	.3666					
202	1.6537	14	.3657	.3653					
311	1.6297	10	.3765	.3769	111	1.6339	15	.3746	.3746
220	1.5690	7	.4062	.4067	200	1.5570	7	.4125	.4123
400	1.5436	4	.4197	.4203					
221	1.4576	7	.4708	.4717					
022	[3] 1.3358	4	.5605	.5618					
312	[3] 1.3214	5	.5727	.5720					

[1] Indices determined by analogy to low Ta_2O_5 [13], but refer only to a pseudocell as several peaks cannot be indexed. Unit cell dimensions of the pseudocell are: $a=6.17$ Å, $b=3.64$ Å, $c=3.92$ Å.
[2] Hexagonal unit cell dimensions: $a=3.59_6$ Å, $c=3.91_3$ Å, $c/a=1.088$.
[3] Broad peak.

extent of the immiscible region [15], i.f.s. relationships between the glass-forming cation and the modifier cation largely govern the presence or absence of immiscibility. Just as the differences in i.f.s. between the modifier cation with oxygen and the glass-forming cation with oxygen can be too large to produce immiscibility, they may also be too small. The maximum i.f.s. difference occurs in the series of glass formers with Ba^{+2}, and the minimum occurs with Nb^{+5}. It may also be concluded that none of the hexavalent ions, e.g., Mo^{+6}, Te^{+6}, Cr^{+6}, will show immiscibility phenomenon. These principles will be elaborated in future publications [16].

4. Summary

The phase equilibrium diagram for the system $Nb_2O_5-GeO_2$ has been constructed from "quenching" data on 13 selected compositions. Solidus and liquidus values were determined by examination of the samples with the binocular and polarizing microscopes and x-ray powder diffractometry.

The system was found to contain: one compound, $9Nb_2O_5 \cdot GeO_2$, melting incongruently at 1420 °C; one eutectic point between GeO_2 and the compound, located at about 97 mole percent GeO_2 and 1090 °C; and one peritectic point at about 25 mole percent GeO_2 and 1420 °C.

Although the 9:1 ratio of oxides in the $9Nb_2O_5 \cdot GeO_2$ compound is consistent with the results, various limitations in the experimental method preclude an unequivocal statement as to the exactness of this ratio.

Two metastable low niobia-type phases were obtained from quenched liquids. A quenched liquid of composition $50Nb_2O_5:50GeO_2$ gave an x-ray powder pattern that could be partially indexed on a subcell of low Nb_2O_5. It had pseudo-orthorhombic unit cell dimensions of $a=6.17$ Å, $b=3.64$ Å, $c=3.92$ Å. The pattern of quenched liquid of composition $20Nb_2O_5:80GeO_2$ was indexed on a hexagonal unit cell basis: $a=3.59_6$ Å, $c=3.91_3$ Å.

Application of the results to liquid immiscibility theory leads one to the conclusion that a cation may have too strong an ionic field strength, as well as one that is too weak, to produce two-liquid separation. Furthermore, the limiting maximum occurs in the series of Nb_2O_5 with the glass formers, as B_2O_3 and SiO_2 both show large regions of immiscibility.

The author expresses his sincere appreciation to Robert S. Roth who aided in the interpretation of the x-ray data.

5. References

[1] E. M. Levin, C. R. Robbins, and H. F. McMurdie, Phase Diagrams for Ceramists, The American Ceramic Society, Inc., 601 pp., 2064 figs., Columbus, Ohio.
[2] M. Ibrahim and N. F. H. Bright, J. Am. Ceram. Soc. **45,** [5], 221–222 (1962).
[3] J. L. Waring and R. S. Roth, J. Res. NBS **69A** (Phys. and Chem.) No. 2, 119–129 (1965).
[4] E. M. Levin, J. Am. Ceram. Soc., **48,** [9] 491–492 (1965).
[5] (a) E. M. Levin, C. R. Robbins, and J. L. Waring, J. Am. Ceram. Soc. **44** [2], 87–91 (1961).
(b) E. M. Levin and C. L. McDaniel, J. Am. Ceram. Soc. **45** [8], 355–360 (1962).
[6] R. S. Roth and J. L. Waring, J. Res. NBS **65A** (Phys. and Chem.) No. 4, 337–344 (1961).
[7] C. R. Robbins and E. M. Levin, Am. J. Sci. **257,** 63–70 (1959).
[8] G. Brauer, Z. anorg. Allgem. Chem. **248,** 1 (1948).
[9] R. S. Roth, J. Res. NBS **62** [1], 27–38 (1959) RP2925.
[10] F. Holzberg, A. Reisman, M. Berry, and M. Berkenblit, J. Am. Chem. Soc. **79,** 2039 (1957).
[11] F. Dachille and R. Roy, Geol. Soc. America Bull. **67** [12], pt. 2, 168–83 (abstract) (1956).
[12] J. L. Waring and R. S. Roth, Acta Cryst. **17,** pt. 4, 455–456 (1964).
[13] K. Lehovec, J. Less-Common Metals **7,** 397–410 (1964).
[14] E. M. Levin, J. Res. NBS **70A** (Phys. and Chem.) No. 1, 11–16 (1966).
[15] E. M. Levin and S. Block, J. Am. Ceram. Soc. **40** [3], 95–106; [4] 113–118 (1957).
[16] E. M. Levin, Structural interpretation of immiscibility in oxide systems: parts IV, V, and VI, in preparation.

(Paper 70A1–381)

JOURNAL OF RESEARCH of the National Bureau of Standards—A. Physics and Chemistry
Vol. 70A, No. 1, January–February 1966

Phase Equilibria in the System Niobium Pentoxide–Boric Acid

Ernest M. Levin

(October 11, 1965)

The phase-equilibrium diagram for the system $Nb_2O_5-B_2O_3$ was determined experimentally using the quenching technique and examining the samples by optical microscopy and x-ray powder diffractometry. The system contains one binary compound of approximate composition "$3Nb_2O_5 \cdot B_2O_3$," which melts incongruently at about 1150 °C to $H-Nb_2O_5$ and B_2O_3-rich liquid. A large region of liquid immiscibility extends, at 1352 °C, from 10 mole percent Nb_2O_5 to 65.7 mole percent Nb_2O_5. The theoretically calculated extent of immiscibility is in reasonable agreement with the experimentally determined value.

Key Words: Boric oxide, immiscibility, niobium pentoxide, oxides, phase equilibria.

1. Introduction

Consistent with the objective expressed in the Introduction to the preceding paper on the system $Nb_2O_5-GeO_2$ [1],[1] the systematic study of immiscibility was extended to include the phase relations in the system $Nb_2O_5-B_2O_3$. The Nb^{5+} cation has a high charge and moderate ionic radius, 0.69 Å; and, consequently, a high ionic field strength. Notwithstanding the high field strength, the $Nb_2O_5-GeO_2$ system does not show liquid immiscibility. However, the $Nb_2O_5-SiO_2$ system was found to contain a large region of immiscibility [2]. Based on the observation that no case has been reported in which liquid immiscibility exists for the silicate system but not for the corresponding borate system, immiscibility in the $Nb_2O_5-B_2O_3$ system was to be expected. Furthermore, the system offered a possible opportunity to apply and to extend the principles of immiscibility developed mainly from systems of borates with the oxides of divalent cations.

2. Sample Preparation and Test Methods

Starting materials for the preparation of mixtures consisted of high-purity niobium pentoxide and reagent grade boric acid powder. The Nb_2O_5 contained the following impurities when examined by the general qualitative spectrochemical method: Si—less than 0.1 percent; Fe, Sn, Ti—0.001 to 0.01 percent; Ca, Mg—0.0001 to 0.001 percent; Cu—? The boric acid was of especially high purity, containing only faint traces (0.0001 to 0.001%) of Mg and Si.

Three-gram batches, on an ignited basis, of the starting materials were formulated by mixing or grinding, pressing, and heating for 4 hr, at three successively higher temperatures: 700, 800, and about 900 °C. Phase equilibrium relations were studied by the well-established quenching technique. Samples were heated in sealed Pt tubes for periods of 1 to 336 hr. Temperatures were measured with a calibrated Pt-90Pt:10 Rh thermocouple. Quenched samples were examined with the binocular and polarizing microscopes and by x-ray powder diffractometry (Ni-filtered CuK_α radiation) using a high-angle Geiger-counter diffractometer. The technique and details of sample preparation, apparatus, and method have been described in previous publications [3] and were the same as for the study of the $Nb_2O_5-GeO_2$ system [1]. The overall maximum uncertainty of the liquidus temperatures reported are estimated to be within ±10 °C.

It should be noted that the polarizing microscope was of limited value because clear homogeneous glass was not observed, even for the compositions richest in B_2O_3. Quenched liquid devitrified, to lesser or greater extent, and the grains appeared brownish, finely mottled, and very weakly birefringent, when viewed under the microscope.

3. Chemical Analysis

Formulated compositions were analyzed by the Analytical Chemistry Division. For most of the compositions only the Nb_2O_5 content was determined, by titration of an unbuffed solution at *p*H 4.5 with standard EDTA solution. Percent B_2O_3 was estimated by difference from 100 percent. Analyses of three compositions (formulated at 25, 50, and 66.7 mole percent Nb_2O_5) as well as analysis of the mechanically separated heavy and light devitrified liquids in the immiscibility region were made for both Nb_2O_5 and B_2O_3. B_2O_3 was determined by titration of a neutral solution (*p*H 7.00) with standard NaOH solution, after the additions of manitol. Nb_2O_5 was determined from the weight of the ignited residue. Analyzed values were used in constructing the phase diagram. Those compositions for which one of the components was determined by difference have an estimated uncertainty of about 2 mole percent. Those for which both components were analyzed have an estimated accuracy of better than 1 mole percent.

[1] Figures in brackets indicate the literature references at the end of this paper.

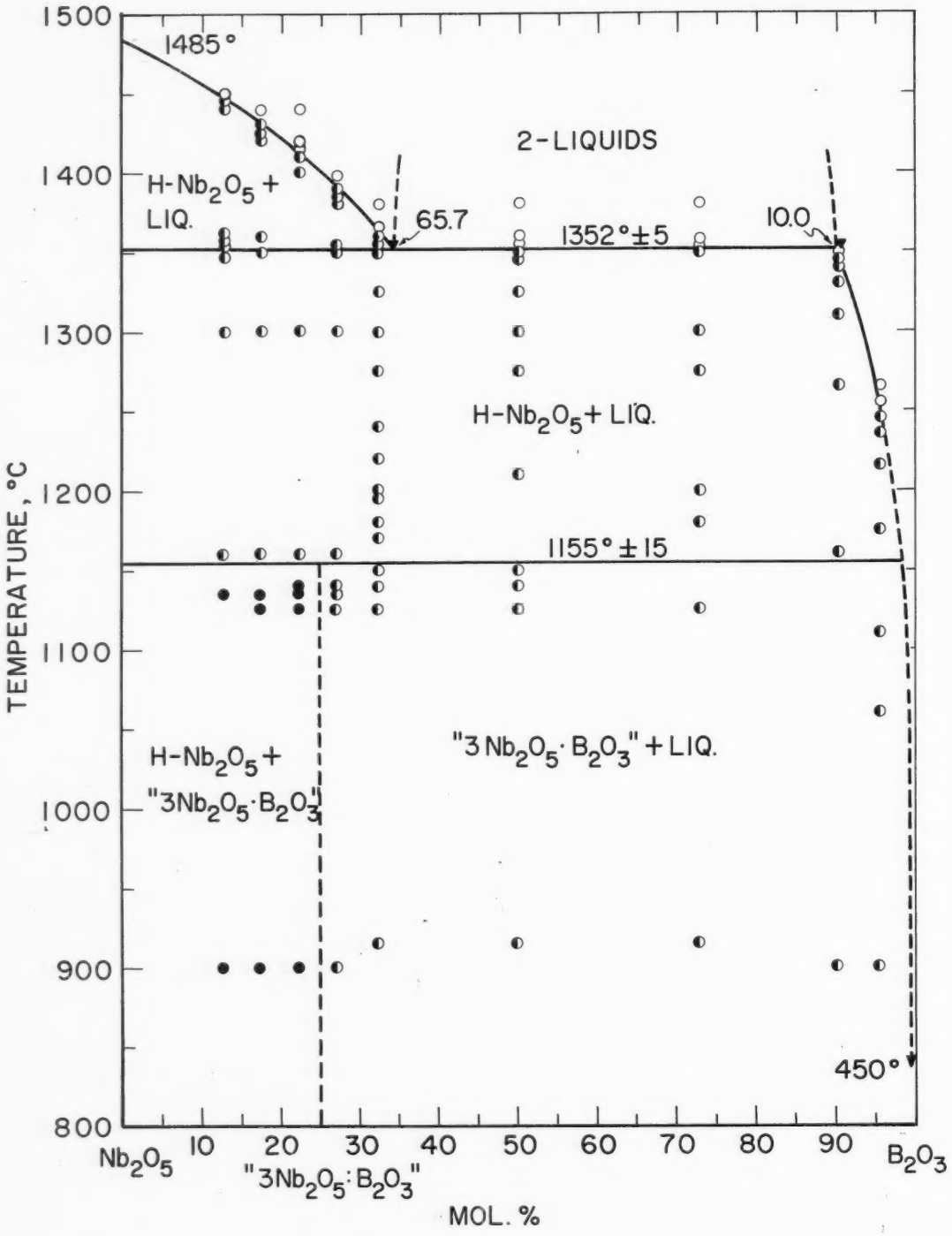

FIGURE 1. *Phase diagram for the system* $Nb_2O_5-B_2O_3$.
●–No melting; ◐–partial melting; ○–complete melting;
▼–chemically analyzed value of mechanically separated phases in two liquid regions.

4. Results and Discussion

4.1. Nb_2O_5 and B_2O_3 Components

No quenching experiments were made with the components, as they were the same materials that had been used previously in phase equilibrium studies originating in this laboratory [3, 4]. As regards the Nb_2O_5 component, the same remarks pertain as for the $Nb_2O_5-GeO_2$ system [1]. For purposes of consistency with previous publications the indicated melting temperature of B_2O_3 is given as 450 °C, although this value may be 5° to 10° low [5].

4.2. Phase Diagram

The phase diagram for the system is shown in figure 1, and table 1 lists the compositions studied, heat treatments, and phases identified. The system is characterised by a large region of liquid immiscibility, extending from about 10 mole percent to 65.7 mole percent Nb_2O_5, and by a binary compound, "$3Nb_2O_5 \cdot B_2O_3$" melting incongruently at 1150 °C, some 200° below the monotectic.

The two triangles in figure 1 designate the chemically analyzed values for the B_2O_3-rich and the Nb_2O_5-

TABLE 1. *Experimental data for compositions in the binary system* $Nb_2O_5-B_2O_3$

Composition [1]		Heat treatment [2]		Results		Notes
Nb_2O_5	B_2O_3	Temp.	Time	Physical observation	X-ray diffraction analyses [3]	
Mole %	*Mole %*	*°C*	*Hour*			
4.4	95.6	900	3	Considerable melting.	3:1 + glass hump + $[H_3BO_3]$	
		1061	1	Considerable melting.		
		1109	1.5	Considerable melting.	3:1 + glass hump + $[L-Nb_2O_5]$	No $H-Nb_2O_5$ detected.
		1175	1	Considerable melting.	3:1 + glass hump + $[L-Nb_2O_5]$	
		1216	1	Considerable melting.	$[H_3BO_3]$ + 3:1 + $[L-Nb_2O_5]$ + $H-Nb_2O_5$	Tube leaked.
		1235	2	Considerable melting.	$[L-Nb_2O_5]$ + 3:1 + $[H_3BO_3]$ + $H-Nb_2O_5$	
		1246	2	Near complete melting.	3:1 + $[H_3BO_3]$ + $[L-Nb_2O_5]$ + $H-Nb_2O_5$	
		1256	2	Complete melting.	$[L-Nb_2O_5]$ + [3:1]	
		1265	2	Complete melting.	$[L-Nb_2O_5]$ + [3:1]	
9.7	90.3	900	3	Some melting.	3:1 + glass hump	
		1161	68	Considerable melting.	3:1 + $H-Nb_2O_5$	Above decomp. 3:1.
		1265	2	Considerable melting.	$[L-Nb_2O_5]$ + 3:1	Very weak x-ray pattern.
		1310	1.5	Considerable melting.	3:1 + $[L-Nb_2O_5]$ + $H-Nb_2O_5$	
		1331	1.5	Considerable melting.	3:1 + $[L-Nb_2O_5]$ + $H-Nb_2O_5$	
		1339	1.5	Considerable melting.	3:1 + $[L-Nb_2O_5]$ + $[H_3BO_3]$	Tube leaked.
		1345	1.5	Near complete melting.	$[L-Nb_2O_5]$ + 3:1 + $H-Nb_2O_5$	
		1350	1.5	Complete melting.	$[L-Nb_2O_5]$	One liquid.
27.2	72.8	915	4	Slight melting.	3:1	B_2O_3-rich glass present.
		1180	53.5	Some melting.	3:1 + $H-Nb_2O_5$	Above decomp. 3:1.
		1200	66.5	Some melting.	3:1 + $H-Nb_2O_5$	
		1275	15	Some melting.	3:1 + $H-Nb_2O_5$	
		1300	18	Some melting.	$H-Nb_2O_5$ + 3:1 + $[L-Nb_2O_5]$	
		1300	18		3:1 + $H-Nb_2O_5$	Shows reversibility:
		1125	117			3:1 ↔ $H-Nb_2O_5$ + liquid.
		1349	2	Some melting.	$H-Nb_2O_5$ + $[L-Nb_2O_5]$ + 3:1	
		1354	1.5	Complete melting.	$[L-Nb_2O_5]$ + $[H-Nb_2O_5]$	Above monotectic.
		1357	1	Complete melting.		Chem. Analysis of each phase.
		1380	2	Complete melting.		
50.2	49.8	915	4	Slight melting.	3:1	
		1140	69	Slight melting.	3:1 + $[H_3BO_3]$	
		1150	45	Some melting.	3:1	
		1210	40	Some melting.	3:1 + $H-Nb_2O_5$	Above decomp. 3:1.
		1275	15	Some melting.	$H-Nb_2O_5$ + 3:1	
		1300	18	Considerable melting.	$H-Nb_2O_5$ + 3:1	
		1300	18		3:1 + $H-Nb_2O_5$	Shows reversibility:
		1125	117			3:1 ↔ $H-Nb_2O_5$ + liquid.
		1325	1	Considerable melting.	3:1 + $H-Nb_2O_5$	
		1345	1.25	Considerable melting.	3:1 + $H-Nb_2O_5$	
		1350	1	Considerable melting.	$H-Nb_2O_5$ + $[L-Nb_2O_5]$ + 3:1	Decomp. 3:1 sluggish.
		1356	1.5	Complete melting.	$[H-Nb_2O_5]$ + $[L-Nb_2O_5]$	Above monotectic.
		1360	1.25	Complete melting.		For chem. analysis.
		1380	2	Complete melting.		Above monotectic.
67.8	32.2	915	4	Slight melting.	3:1	B_2O_3-rich glass present.
		1140	69	Slight melting.	3:1	
		1150	45	Slight melting.	3:1	
		1170	20	Melting.	3:1 + $H-Nb_2O_5$(?)	
		1180	53.5	Melting.	3:1 + $H-Nb_2O_5$	
		1194	1.75	Melting.	3:1	Decomp. 3:1 sluggish.
		1200	66.5	Melting.	3:1 + $H-Nb_2O_5$	
		1220	8.5	Melting.	3:1 + $H-Nb_2O_5$	
		1240	1.5	Melting.	3:1 + $H-Nb_2O_5$	
		1275	1.5	Melting.	$H-Nb_2O_5$ + 3:1	
		1300	18	Melting.	$H-Nb_2O_5$ + 3:1 (?)	
		1300	18		3:1 + $H-Nb_2O_5$	Shows reversibility:
		1125	117			3:1 ↔ $H-Nb_2O_5$ + liquid.
		1325	1		3:1 + $H-Nb_2O_5$	
		1350	1		$H-Nb_2O_5$ + $[L-Nb_2O_5]$	Above monotectic.
		1356	1	Considerable melting.	$H-Nb_2O_5$	
		1361	1.5	Near complete melting.	$H-Nb_2O_5$ + [3:1]	
		1367	1	Complete melting.	$[L-Nb_2O_5]$ + [3:1]	One liquid.
		1380	2	Complete melting.	$[L-Nb_2O_5]$ + [3:1]	

TABLE 1. *Experimental data for compositions in the binary system* $Nb_2O_5-B_2O_3$ – Continued

Composition [1]		Heat treatment [2]			Results	
Nb_2O_5	B_2O_5	Temp.	Time	Physical observation	X-ray diffraction analyses [3]	Notes
Mole %	*Mole %*	*°C*	*Hour*			
73.0	27.0	900	3	Opalescent.	3:1	
		1135	336	Opalescent.	3:1	
		1140	69	Opalescent.	3:1	
		1161	68	Opalescent.	3:1 + H – Nb_2O_5	Above decomp. 3:1.
		1300	18	Opalescent.	H – Nb_2O_5 + 3:1 (?)	
		1300	18		H – Nb_2O_5 + 3:1	Shows reversibility:
		1125	117			3:1 ↔ H – Nb_2O_5 + liquid.
		1351	1.5	Slight melting.	H – Nb_2O_5	
		1355	1.5	Melting.	H – Nb_2O_5 + 3:1	Above monotectic.
		1380	1.5	Considerable melting.	H – Nb_2O_5 + 3:1	
		1385	1.5	Near complete melting.	H – Nb_2O_5 + [L – Nb_2O_5] + 3:1	
		1390	1.5	Near complete melting.	[L – Nb_2O_5] + H – Nb_2O_5 + 3:1	
		1398	1.5	Complete melting.	[H – Nb_2O_5] + [L – Nb_2O_5] + [3:1]	All devitrify from liquid.
77.8	22.2	900	3	No melting.	3:1	
		1135	336	No melting.	3:1	
		1140	69	No melting.	3:1	
		1161	68	Slight melting.	3:1 + H – Nb_2O_5	Above decomp. 3:1.
		1300	18	Opalescent.	H – Nb_2O_5 + 3:1 (?)	
		1300	18		H – Nb_2O_5 + 3:1	Shows reversibility:
		1125	117			3:1 ↔ H – Nb_2O_5 + liquid.
		1401	1	Considerable melting.	H – Nb_2O_5 + [L – Nb_2O_5] + 3:1	
		1409	2.5	Near complete melting.	H – Nb_2O_5 + [L – Nb_2O_5] + 3:1	
		1415	1.5	Complete melting.	[H – Nb_2O_5] + [L – Nb_2O_5] + [3:1]	
		1420	1	Complete melting.	[H – Nb_2O_5] + [L – Nb_2O_5]	
		1440	1	Complete melting.	[L – Nb_2O_5] + [H – Nb_2O_5]	
82.9	17.1	900	3	No melting.	3:1	
		1135	336	No melting.	3:1 + H – Nb_2O_5	
		1161	68	Slight melting.	3:1 + H – Nb_2O_5	Above decomp. 3:1.
		1300	18	Melting.	H – Nb_2O_5 + 3:1 (?)	
		1300	18		H – Nb_2O_5 + 3:1	Reversibility sluggish.
		1125	117			
		1349	3	Melting.	H – Nb_2O_5 + [L – Nb_2O_5]	Below monotectic.
		1359	3	Considerable melting.	H – Nb_2O_5 + [L – Nb_2O_5]	Above monotectic.
		1420	1	Considerable melting.	H – Nb_2O_5 + [L – Nb_2O_5] + 3:1	
		1425	1.5	Near complete melting.	H – Nb_2O_5 + 3:1 (?)	
		1430	1	At liquidus.	[H – Nb_2O_5] + [L – Nb_2O_5] + [3:1 (?)]	
		1440	1	Complete melting.	[H – Nb_2O_5] + [L – Nb_2O_5]	
87.2	12.8	900	3	No melting.	3:1 + H – Nb_2O_5 (?)	
		1135	336	No melting.	3:1 + H – Nb_2O_5	
		1161	68	Melting.	3:1 + H – Nb_2O_5	Above decomp. 3:1.
		1300	18	Melting.	H – Nb_2O_5 + 3:1 (?)	
		1348	2	Melting.	H – Nb_2O_5	$N_{gl} < 1.47$, below monotectic.
		1356	2	Moderate melting.	H – Nb_2O_5	Above monotectic.
		1358	1.5	Moderate melting.	H – Nb_2O_5	
		1362	1.5	Moderate melting.	H – Nb_2O_5	
		1440	1	Considerable melting.	H – Nb_2O_5 + 3:1 (?)	
		1445	1	Near complete melting.	H – Nb_2O_5 + [L – Nb_2O_5] + [3:1]	
		1450	1	Complete melting.	[L – Nb_2O_5] + [H – Nb_2O_5]	

[1] Analyzed value for Nb_2O_5; B_2O_3, by difference.
[2] Specimens quenched in sealed Pt tubes.
[3] Phases identified are listed in order of amount present at room temperature. Phases not necessarily present at the elevated temperatures are enclosed in brackets. 3:1 refers to $3Nb_2O_5 \cdot B_2O_3$, the most likely composition of the binary compound.

rich devitrified liquids which were mechanically separated from samples quenched from above the monotectic. When the Pt was removed from the quenched specimens, two distinct layers were clearly visible. The top layer appeared opalescent white and was found to be hard and glassy when ground. An index of refraction of approximately 1.51 ± 0.01 was determined for clear portions of some of the grains. The lower layer appeared crystalline, metallic grey in color. Under the microscope the grains were dark and very weakly birefringent. The x-ray powder patterns showed that the top layer (B_2O_3-rich) contained low-Nb_2O_5 with a trace of high-Nb_2O_5, whereas the lower layer (Nb_2O_5-rich) contained appreciable high-Nb_2O_5, low-Nb_2O_5, and a small amount of "$3Nb_2O_5 \cdot B_2O_3$."

Homogeneous glasses were never obtained for any composition as the liquids devitrified on quenching. X-ray examination showed either low-Nb_2O_5, high-Nb_2O_5, "$3Nb_2O_5 \cdot B_2O_3$", or combinations. The low-Nb_2O_5 phase corresponded to the pseudo-orthorhombic subcell of low-Nb_2O_5 found for some of the quenched liquids in the $Nb_2O_5-GeO_2$ system. It had the same unit cell dimensions [1]. The metastable low-temperature niobia-type phase of hexagonal symmetry occurring in the GeO_2 system was not found.

4.3. Compound "$3Nb_2O_5 \cdot B_2O_3$"

The exact composition of this compound could not be determined because of insufficient sensitivity, in this instance, of the microscopic and x-ray methods together with some uncertainty in the chemical analyses. Therefore, the 3:1 ratio of oxides is given as the most probable.

The compound formed readily for all compositions in the system. It melted incongruently at about 1150 °C to liquid and $H-Nb_2O_5$. However, disappearance of the compound above the melting point was extremely sluggish. The compound could be detected in diminishing amounts up to the monotectic and liquidus temperatures (see table 1). Even compositions heated at 1161 °C for 68 hr showed appreciable amounts of the compound, but the appearance of $H-Nb_2O_5$ indicated that the temperature was above the incongruent melting point. X-ray powder diffraction data suitable for identification is given in table 2. The pattern is of low symmetry with regions of closely spaced low-intensity peaks and could not be indexed.

TABLE 2. *X-ray powder diffraction data* (CuK_α *radiation) for the compound* "$3Nb_2O_5 \cdot B_2O_3$"

(Pattern of low symmetry and could not be indexed)

d	I/I_0	d	I/I_0
Å	%	Å	%
*14.4(b)	4	2.434	3
7.16	7	2.389	6
6.93	6	2.369	4
4.774	34	2.337	3
4.741	27	2.302	17
3.770	71	*2.094(b)	3
3.584	90	2.049	26
3.553	100	2.033	27
3.170	12	1.9125	33
2.864	6	*1.7918(b)	5
2.833	10	1.7746	10
2.773	57	1.7697	10
*2.730(b)	7	1.6995	22
2.675	9	1.6874	21
2.576	6	1.6842	23
2.520	7	*1.5838(b)	6
2.506	9	1.5769	16
2.473	4		

*b = broad peak.

4.4. Application to Liquid Immiscibility Theory

The niobium borate and niobium silicate systems both contain large regions of immiscibility, whereas the niobium germanate system shows complete liquid miscibility. Thus, as previously discussed [1], the niobium cation possesses a critical ionic field strength for the formation of two liquids with the glass-forming cations.

With data on immiscibility in the niobium borate and silicate systems, it is possible to test and to extend the principles of immiscibility developed mostly from data on the divalent cations to the cations of high charge. A fundamental consideration in the structural approach is the average number of oxygens associated with a modifier cation, in the modifier-rich liquid. Once this value is known, statement of the nominal composition is a routine calculation. The oxygen-volume method, discussed in previous publications [3, 6] is an attempt to make a reasonable estimate of this number.

TABLE 3. *Calculated composition of modifier-rich liquids, in* #0/Nb *and in mole percent* Nb_2O_5, *based on the oxygen-volume method [6] and two values both for the niobium separation and the volume of space occupied by* 0^{-2} (V_0).

System	Experimental		Calculated from Nb–Nb separation:					
			of 4.18 Å [2(1.40+0.69)], and				of 4.08 Å, and	
			V_0=17 Å^3		V_0=19 Å^3		V_0=19 Å^3	
	Nb_2O_5	#0/Nb	#0/Nb	Nb_2O_5	#0/Nb	Nb_2O_5	#0/Nb	Nb_2O_5
	Mole %			*Mole %*		*Mole %*		*Mole %*
$Nb_2O_5-B_2O_3$	65.7	3.28	4.18	47.2	3.72	55.1	3.45	61.1
$Nb_2O_5-SiO_2$ [2]	47.5	3.61	4.18	37.4	3.72	45.0	3.45	51.2

Table 3, column 3 gives the number of oxygens per modifier cation calculated directly from the experimentally determined composition of the modifier-rich liquid. For example, in the $Nb_2O_5-B_2O_3$ system:

$$\#0/Nb = \frac{5 \times 0.657 + 3(1.00 - 0.657)}{2 \times 0.657} = 3.28.$$

Similarly, in the $Nb_2O_5-SiO_2$ system:

$$\#0/Nb = \frac{5 \times 0.475 + 2(1.00 - 0.475)}{2 \times 0.475} = 3.61.$$

As a first approximation the number of oxygens per cation may be considered independent of the glass-forming cation. Using the data in column 3 for one of the systems, it is possible to calculate the composition of the modifier-rich liquid in the other system. The calculation yields 57.5 mole percent Nb_2O_5 in the borate system,[2] using the 3.61 value, and 56.2 mole percent Nb_2O_5 in the silicate system, using the 3.28 value. The calculated value in the borate system is about 8 mole percent low, that in the silicate system about 9 mole percent high. As will be shown later, this seemingly large discrepancy is due to the sensitivity of the calculations in the niobium oxide systems.

Table 3 (columns 4–7) lists the calculated #0/Nb and the corresponding mole percent Nb_2O_5, based on the oxygen-volume method using a Nb–O–Nb bond angle of 180° and Ahrens' ionic radii for Nb^{+5} and O^{-2}. In the original papers on immiscibility the value of 17 Å^3 was taken as the average volume of space occupied by an oxygen atom in the modifier-rich liquid.

[2] Nominal oxide formula $= \frac{Nb_2O_5 \cdot (2 \times 3.61 - 5)}{3} B_2O_3 = Nb_2O_5 \cdot 0.74B_2O_3$ (57.5 mole % Nb_2O_5).

An analysis of the experimental data in about 40 borate and silicate systems showing immiscibility [7] gives an empirical value of about 19 Å^3. Therefore, in table 3 calculations are given for both oxygen values. It may be seen that for the 19 Å^3 value in the silica case agreement is good between the calculated mole percent Nb_2O_5 (45.0) and the experimental one (47.5). In the borate case the calculated value is 11 mole percent low.

For the case of small highly charged modifier cations, such as niobium, the calculations are very sensitive to cationic radius because a small difference in separation has a large effect on the calculated number of oxygen per cation. For example, using a separation of only 0.1 Å less than 4.18, will increase the calculated value by about 6 mole percent (column 9); and the calculated number of oxygens per niobium (column 8) is intermediate between 3.28 and 3.61, the experimentally determined values for the borate and silicate systems, respectively. Gatehouse and Wadsley [8], from a crystal structure determination of high-Nb_2O_5, have concluded that in Nb_2O_5 the average ionic radius of O^{2-} is 1.40 Å and that of Nb^{5+}, 0.59 Å. The latter value is 0.1 Å less than Ahrens' ionic radius.

5. Summary

The phase equilibrium diagram for the system $Nb_2O_5-B_2O_3$ was constructed from "quenching" data on nine selected compositions. Solidus and liquidus values were determined by examination of the samples with the binocular and polarizing microscopes and x-ray powder diffractometry.

The system was found to contain one binary compound, "$3Nb_2O_5 \cdot B_2O_3$", which melts incongruently at about 1150 °C, some 200 below a monotectic. The liquidus is characterized by a large two-liquid region, at 1352 °C, extending from about 10 mole percent Nb_2O_5 to 65.7 mole percent Nb_2O_5.

Experimental limitations precluded an unequivocal statement of the composition of the "$3Nb_2O_5 \cdot B_2O_3$" compound. Above the incongruent melting point its decomposition to $H-Nb_2O_5$ and B_2O_3-rich liquid is sluggish. X-ray powder data suitable for identification is listed.

In the modifier-rich liquid in the immiscibility region, an average of 3.28 oxygen are associated with each Nb atom, as compared to 3.61 for the corresponding silicate system. Calculation of the composition of the modifier-rich liquid, by the oxygen-volume method, gives acceptable agreement with the experimentally determined value, considering that for cations of large valence the calculation is sensitive to small changes in the parameters.

6. References

[1] E. M. Levin, J. Res. NBS **70A** (Phys. and Chem.), No. 1, 5–10 (1966).

[2] M. Ibrahim and N. F. H. Bright, J. Am. Ceram. Soc. **45** [5], 221–22 (1962).

[3] (a) E. M. Levin, C. R. Robbins, and J. L. Waring, J. Am. Ceram. Soc. **44** [2], 87–91 (1961).
(b) E. M. Levin and C. L. McDaniel, J. Am. Ceram. Soc. **45** [8], 355–60 (1962).

[4] (a) J. L. Waring and R. S. Roth, J. Res. NBS **69A** (Phys. and Chem.), No. 2, 119–29 (1965).
(b) R. S. Roth and J. L. Waring, J. Res. NBS **65A** (Phys. and Chem.), No. 4, 337–44 (1961).

[5] T. J. Rockett and W. R. Foster, J. Am. Ceram. Soc. **48** [2], 75–80 (1965).

[6] E. M. Levin and S. Block, J. Am. Ceram. Soc. **40** [3], 95–106; [4], 113–18 (1957).

[7] E. M. Levin, Structural interpretation of immiscibility: parts IV, V, and VI, in preparation.

[8] B. M. Gatehouse and A. D. Wadsley, Acta Cryst. **17** [12], 1545–54 (1964).

(Paper 70A1–382)

JOURNAL OF RESEARCH of the National Bureau of Standards—A. Physics and Chemistry
Vol. 70A, No. 1, January–February 1966

The Solution to a Nonlinear Lamm Equation in the Faxén Approximation

Irwin H. Billick and George H. Weiss*

(October 5, 1965)

An exact solution in the Faxén approximation is given for the Lamm equation in which the sedimentation coefficient is related to concentration as $s=s_0(1-kc)$. It is shown that the solution in this case can be expressed in terms of the solution to the linear case ($k=0$) with a modified argument. The boundary sharpening phenomenon expresses itself very clearly in the solution presented here.

Key Words: Sedimentation, Lamm equation, concentration dependence, nonlinear.

Solutions of the Lamm equation for constant diffusion and sedimentation coefficients have found wide application in the analysis of data from the ultracentrifuge [1].[1] It is known that both the sedimentation and the diffusion coefficients depend on concentration, and in particular, the sedimentation coefficient can be approximated by

$$s=s_0/(1+kc) \tag{1}$$

where s_0 is the sedimentation coefficient at infinite dilution and k is a constant which is a measure of nonlinearity. Fujita has shown that if the relation of eq (1) is replaced by

$$s=s_0(1-kc) \tag{2}$$

while the diffusion coefficient remains independent of concentration, the resulting Lamm equation can be linearized rigorously [2]. Fujita solved this Lamm equation in the Faxén regime by an approximation technique. It is the purpose of this paper to show that an exact solution of the Lamm equation is possible in the Faxén regime, and that the solution for the nonlinear case can be written entirely in terms of the solution to the linear problem. The technique exploited in this paper was originally suggested in a preliminary note [3] although the result given there contains an error. Our solution then enables one to derive an expansion in powers of the time variable to as high a degree as desired, whereas Fujita's original solution was limited in this respect. The Lamm equation can also be solved with the *ansatz* of eq (2) in the rectangular approximation [4], and an Archibald solution which takes account of boundary conditions can be written [5]. A detailed comparison between solutions of the Lamm equation with the two forms of sedimentation coefficient given by eqs (1) and (2) will be presented elsewhere [6].

*National Cancer Institute, National Institutes of Health, Bethesda, Md.

[1] Figures in brackets indicate the literature references at the end of this paper.

792-867 O–66–2

The Lamm equation will be written

$$\frac{\partial c}{\partial t}=\frac{1}{r}\frac{\partial}{\partial r}\left(rD\frac{\partial c}{\partial r}-s_0\omega^2r^2(1-kc)c\right) \tag{3}$$

in terms of the solute concentration c, the diffusion coefficient D, sedimentation coefficient s_0, and angular frequency ω. Let r_0 be the radial position of the meniscus, and c_0 be the initial concentration. Then the transformations

$$\theta=c/c_0, \qquad \epsilon=2D/(s_0\omega^2r_0^2) \qquad x=(r/r_0)^2, \qquad \tau=2\omega^2s_0t \qquad \alpha=kc_0 \tag{4}$$

convert eq (3) into

$$\frac{\partial\theta}{\partial\tau}=\frac{\partial}{\partial x}\left\{\epsilon x\frac{\partial\theta}{\partial x}-x\theta(1-\alpha\theta)\right\}. \tag{5}$$

This equation can be linearized by introducing a new dependent variable $u(x, \tau)$ by

$$\theta(x, \tau)=\frac{\epsilon}{\alpha}\frac{\partial}{\partial x}\ln u(x, \tau). \tag{6}$$

It proves convenient to also define new independent variables by

$$z=2(xe^{-\tau})^{1/2}, \qquad \zeta=1-e^{-\tau} \tag{7}$$

which, together with eqs (5) and (6) implies that u satisfies

$$\frac{1}{\epsilon}\frac{\partial u}{\partial\zeta}=\frac{\partial^2u}{\partial z^2}-\frac{1}{z}\frac{\partial u}{\partial z} \tag{8}$$

which is to be solved with the initial condition

$$u(\sigma, 0)=1, \qquad 0\leq\sigma\leq 2=\exp\frac{\alpha}{4\epsilon}(\sigma^2-4), \qquad \sigma>2. \tag{9}$$

We can solve eq (8) by a separation of variables. A general solution for which $\partial u/\partial z$ remains finite at $x=0$ is

$$u(z, \zeta)=A+Bz^2+z\int_0^\infty g(\lambda)J_1(\lambda z)e^{-\lambda^2\epsilon\zeta}d\lambda \tag{10}$$

where A and B are constants, and $g(\lambda)$ is to be determined from initial conditions. Notice that the first two terms are solutions to the homogeneous equation obtained by setting $\partial u/\partial\zeta=0$. Initially we have

$$u(z, 0)-A-Bz^2=z\int_0^\infty g(\lambda)J_1(\lambda z)d\lambda \tag{11}$$

where $g(\lambda)$ can be calculated by regarding the right-hand side as a Hankel transform [6]. In this way we find

$$g(\lambda)=\lambda\int_0^\infty J_1(\lambda\sigma)[u(\sigma, 0)-A-B\sigma^2]d\sigma. \tag{12}$$

Hence $u(z, \zeta)$ is given by [7]

$$u(z_1\zeta) = A + Bz^2 + z\int_0^\infty [u(\sigma, 0) - A - B\sigma^2]d\sigma \int_0^\infty \lambda J_1(\lambda\sigma)J_1(\lambda z)e^{-\lambda^2\epsilon\zeta}d\lambda$$

$$= A + Bz^2 + \frac{z}{2\epsilon\zeta}e^{-\frac{z^2}{4\epsilon\zeta}} \int_0^\infty e^{-\frac{\sigma^2}{4\epsilon\zeta}} I_1\left(\frac{z\sigma}{2\epsilon\zeta}\right)[u(\sigma, 0) - A - B\sigma^2]d\sigma \qquad (13)$$

where $I_1(\mu)$ is a Bessel function of the first kind, with imaginary argument.

Since

$$\int_0^\infty \sigma^2 e^{-\frac{\sigma^2}{4\epsilon\zeta}} I_1\left(\frac{z\sigma}{2\epsilon\zeta}\right)d\sigma = 2z\epsilon\zeta e^{\frac{z^2}{4\epsilon\zeta}} \qquad (14)$$

we see that the terms containing B cancel. The constant A can be determined by requiring that the limiting solution for $\alpha \to 0$ agree with the known Faxén solution for constant s and D. It can easily be verified that this is equivalent to setting $A = 1$. Hence an expression for $u(z, \zeta)$ is

$$u(z, \zeta) = 1 + \frac{z}{2\epsilon\zeta}\int_2^\infty e^{-\frac{(z^2+\sigma^2)}{4\epsilon\zeta}} I_1\left(\frac{z\sigma}{2\epsilon\zeta}\right)[e^{\frac{\alpha}{4\epsilon}(\sigma^2-4)} - 1]d\sigma. \qquad (15)$$

It will prove convenient for later purposes to perform an integration by parts, noting that $I_1(y) = dI_0(y)/dy$. This leads to the expression

$$u(z, \zeta) = 1 + \frac{1}{2\epsilon\zeta}\int_2^\infty \sigma e^{-\frac{(z^2+\sigma^2)}{4\epsilon\zeta}} I_0\left(\frac{z\sigma}{2\epsilon\zeta}\right)[(1-\alpha\zeta)e^{\frac{\alpha}{4\epsilon}(\sigma^2-4)} - 1]d\sigma. \qquad (16)$$

Differentiation according to eq (6) together with an integration by parts leads to an expression for $\theta(z, \zeta)$,

$$\theta(z, \zeta) = \frac{1-\zeta}{2\epsilon\zeta u(z, \zeta)}\int_2^\infty \sigma e^{-\frac{(z^2+\sigma^2)}{4\epsilon\zeta}} I_0\left(\frac{z\sigma}{2\epsilon\zeta}\right)e^{\frac{\alpha}{4\epsilon}(\sigma^2-4)}d\sigma. \qquad (17)$$

When $\alpha = 0$ this relation reduces to the known Faxén solution, which will be denoted by $\theta_0(z, \zeta)$:

$$\theta_0(z, \zeta) = \frac{1-\zeta}{2\epsilon\zeta}\int_2^\infty \sigma e^{-\frac{(\sigma^2+z^2)}{4\epsilon\zeta}} I_0\left(\frac{z\sigma}{2\epsilon\zeta}\right)d\sigma. \qquad (18)$$

We now notice that all of the integrals appearing in the expression for $\theta(z, \zeta)$ have the same general form of an exponential of a quadratic in σ, multiplied by the common factor

$$\sigma \exp\left[-\frac{(\sigma^2+z^2)}{4\epsilon\zeta}\right] I_0\left(\frac{z\sigma}{2\epsilon\zeta}\right).$$

Hence all of the integrals are expressible in terms of θ_0 provided that the arguments are properly chosen. After some algebra it is found that

$$\theta(z, \zeta) = \frac{1-\zeta}{1-(\alpha+1)\zeta} \frac{e^{-\frac{\alpha}{\epsilon}\left[1-\frac{z^2}{4(1-\alpha\zeta)}\right]}\theta_0(z^*, \zeta^*)}{1 + \frac{1-\alpha\zeta}{1-(\alpha+1)\zeta}e^{-\frac{\alpha}{\epsilon}\left[1-\frac{z^2}{4(1-\alpha\zeta)}\right]}\theta_0(z^*, \zeta^*) - \frac{1}{1-\zeta}\theta_0(z, \zeta)} \qquad (19)$$

where

$$z^*=\frac{z}{1-\alpha\zeta},\ \zeta^*=\frac{\zeta}{1-\alpha\zeta}. \tag{20}$$

Simple properties of the solution follow immediately from the representation of eq (19). The parameter α/ϵ which appears in the expression of eq (19) is commonly greater than 10 for values of D, s, and ω^2 (which validate the approximation of eq (2)) and the Faxén approximation. Hence the exponential terms in eq (19) predominate when

$$\frac{z^2}{4(1-\alpha\zeta)}-1 \tag{21}$$

is positive by an order of magnitude greater than ϵ/α. When this is the case we have

$$\theta(z,\zeta)\sim\frac{1-\zeta}{1-\alpha\zeta}=[\alpha+(1-\alpha)e^{\tau}]^{-1} \tag{22}$$

which defines the behavior of the plateau region. This can also be verified directly from eq (5). When the quantity of eq (21) is negative by an order of magnitude greater than ϵ/α, $\theta(z,\zeta)$ is effectively equal to zero. The transition region occurs from values of r for which

$$\frac{z^2}{4(1-\alpha\zeta)}-1=0\left(\frac{\epsilon}{\alpha}\right). \tag{23}$$

Thus, in the limit $\epsilon=0$ the transition region (from essentially zero to a plateau value) is very sharp, and for fixed ϵ and increasing α the transition region also becomes sharper, as indeed is well known. If the gradients are denoted by $G(z,\zeta)$ and $G_0(z,\zeta)$, i.e.,

$$G(z,\zeta)=\frac{\partial\theta}{\partial(r/r_0)},\qquad G_0(z,\zeta)=\frac{\partial\theta_0}{\partial(r/r_0)} \tag{24}$$

then we can write for $G(z,\zeta)$:

$$G(z,\zeta)=\frac{1}{1-\alpha\zeta}\frac{G_0(z,\zeta)}{F(z,z^*,\zeta,\zeta^*)}+\frac{1-\zeta}{1-\alpha\zeta}\frac{\left(1-\frac{1}{1-\zeta}\theta_0(z,\zeta)\right)}{F^2(z,z^*,\zeta,\zeta^*)}$$

$$\times\left\{\frac{\alpha}{4\epsilon}\frac{(1-\zeta)^{1/2}}{1-(\alpha+1)\zeta}e^{-\frac{\alpha}{\epsilon}\left[1-\frac{z^2}{4(1-\alpha\zeta)}\right]}\theta_0(z^*,\zeta^*)+\frac{e^{-\frac{\alpha}{\epsilon}\left[1-\frac{z^2}{4(1-\alpha\zeta)}\right]}}{1-(\alpha+1)\zeta}G_0(z^*,\zeta^*)-\frac{1}{1-\zeta}G_0(z,\zeta)\right\} \tag{25}$$

where

$$F(z,z^*,\zeta,\zeta^*)=1+\frac{1-\alpha\zeta}{1-(\alpha+1)\zeta}e^{-\frac{\alpha}{\epsilon}\left[1-\frac{z^2}{4(1-\alpha\zeta)}\right]}\theta_0(z^*,\zeta^*)-\frac{1}{1-\zeta}\theta_0(z,\zeta). \tag{26}$$

It is possible now to derive successive approximations to $\theta(z,\zeta)$ by expanding it in powers of $(\epsilon\zeta)^{1/2}$. That this is the natural parameter for the expansion will be seen later. Since $\theta(z,\zeta)$ depends only on $\theta_0(z,\zeta)$ we must first consider the expansion of the latter function for small ζ. For small ζ the Bessel function $I_0\left(\frac{z\sigma}{2\epsilon\zeta}\right)$ has the asymptotic expansion [7]

$$I_0\left(\frac{z\sigma}{2\epsilon\zeta}\right) \sim \sqrt{\frac{\epsilon\zeta}{\pi z\sigma}}\, e^{\frac{z\sigma}{2\epsilon\zeta}} \sum_{j=0}^{\infty} B_j \left(\frac{2\epsilon\zeta}{z\sigma}\right)^j \tag{27}$$

where

$$B_j = \frac{(-1)^j}{2j!}\,\frac{\Gamma(j+\frac{1}{2})}{\Gamma(-j+\frac{1}{2})}. \tag{28}$$

Therefore $\theta_0(z, \zeta)$ has the expansion

$$\theta_0(z, \zeta) \sim \frac{e^{-\tau}}{2\sqrt{\pi z\epsilon\zeta}} \sum_{j=0}^{\infty} B_j \left(\frac{2\epsilon\zeta}{z}\right)^j \int_2^{\infty} e^{-\frac{(\sigma-z)}{4\epsilon\zeta}}\, \frac{d\sigma}{\sigma^{j-1/2}}$$

$$= \frac{e^{-\tau}}{\sqrt{2\pi z}} \sum_{j=0}^{\infty} B_j \left(\frac{2\epsilon\zeta}{z}\right)^j \int_{\frac{2-z}{\sqrt{2\epsilon\zeta}}}^{\infty} e^{-u^2/2}\, \frac{du}{(z+u\sqrt{2\epsilon\zeta})^{j-1/2}}. \tag{29}$$

We now consider the integrals which appear in this series and expand them in powers of $(\epsilon\zeta)^{1/2}$. To carry out this expansion we write, for fixed u and small ζ

$$(z+u\sqrt{2\epsilon\zeta})^{-j+1/2} = \sum_{r=0}^{\infty} \binom{-j+1/2}{r} u^r (2\epsilon\zeta)^{r/2}\, z^{-j-r+1/2}. \tag{30}$$

This can be further transformed by noting the identity

$$\binom{-j+1/2}{r} = (-1)^r \binom{r+j-3/2}{r}. \tag{31}$$

Finally, combining eqs (29), (30), and (31) we find that the complete asymptotic expansion of the Faxén solution can be written as

$$\theta_0(z, \zeta) \sim \frac{1-\zeta}{\sqrt{2\pi}} \sum_{j=0}^{\infty} \sum_{m=2j}^{\infty} (-1)^m\, B_j \binom{m-j-3/2}{j-3/2} \frac{(2\epsilon\zeta)^{m/2}}{z^m}\, U_{m-2j}\left(\frac{2-z}{\sqrt{2\epsilon\zeta}}\right) \tag{32}$$

where the $U_r(y)$ are defined by

$$U_r(y) = \int_y^{\infty} u^r e^{-u^2/2}\, du. \tag{33}$$

In particular, the first two terms of eq (32) yield the usual Faxén approximation

$$\theta_0 \sim \frac{e^{-\tau}}{\sqrt{2\pi}} \left\{ U_0\left(\frac{2-z}{\sqrt{2\epsilon\zeta}}\right) + \frac{1}{z}\left(\frac{\epsilon\zeta}{2}\right)^{1/2} e^{-\frac{(2-z)^2}{4\epsilon\zeta}} \right\} \tag{34}$$

in which $U_0(y)$ can be expressed in terms of an error function. A complete asymptotic expansion for $\theta(z, \zeta)$ can now be obtained by combining eqs (19) and (32). Similarly, $\partial\theta/\partial(r/r_0)$ is expressible in terms of $\theta_0(z, \zeta)$ and its derivative, $G_0(z, \zeta)$, which has the expansion

$$G_0(z, \zeta) \sim \frac{e^{-\tau}}{\sqrt{2\pi}} \sum_{j=0}^{\infty} \sum_{m=2j}^{\infty} (-1)^m B_j \binom{m-j-3/2}{j-3/2} \frac{(2\epsilon\zeta)^{m/2}}{z^m}$$

$$\times \left\{ -\frac{m}{z}\, U_{m-2j}\left(\frac{2-z}{\sqrt{2\epsilon\zeta}}\right) + \frac{(2-z)^{m-2j}}{(2\epsilon\zeta)^{\frac{m-2j+1}{2}}}\, e^{-\frac{(2-z)^2}{4\epsilon\zeta}} \right\}. \tag{35}$$

The lowest order Faxén approximation to $\theta(z, \zeta)$ is

$$\theta(z, \zeta) = \theta_p(\zeta) \left[1 - \frac{1-\phi\left(\frac{2-z}{\sqrt{2\epsilon\zeta}}\right)}{1-\phi\left(\frac{2-z}{\sqrt{2\epsilon\zeta}}\right) + e^{-\frac{\alpha}{\epsilon}\left[1-\frac{z^2}{4(1-\alpha\zeta)}\right]} \phi\left(\frac{2-z^*}{\sqrt{2\epsilon\zeta^*}}\right)} \right] \tag{36}$$

where $\theta_p(\zeta)$ is the normalized plateau concentration (eq (22)) and $\phi(\mu)=(2\pi)^{-1/2}\int_{\mu}^{\infty}\exp(-x^2/2)\,dx$ is the complementary error function. To this approximation, the gradient is

$$\frac{\partial\theta}{\partial(r/r_0)}=2e^{-\tau/2}\frac{\partial\theta}{\partial z}=\frac{e^{-\tau/2-\frac{\alpha}{\epsilon}\left[1-\frac{z^2}{4(1-\alpha\zeta)}\right]}}{D}$$

$$\times\left\{\frac{1}{\sqrt{\pi\epsilon\zeta}}\phi\left(\frac{2-z^*}{\sqrt{2\epsilon\zeta^*}}\right)e^{-\frac{(z-z^*)^2}{4\epsilon\zeta^*}}+\frac{1}{\sqrt{\pi\epsilon\zeta^*}}\left(1-\phi\left(\frac{2-z}{\sqrt{2\epsilon\zeta}}\right)\right)e^{-\frac{(2-z)^2}{4\epsilon\zeta}}\right.$$

$$\left.+\frac{\alpha z}{\epsilon(1-\alpha\zeta)}\phi\left(\frac{2-z^*}{\sqrt{2\epsilon\zeta^*}}\right)\left(1-\phi\left(\frac{2-z}{\sqrt{2\epsilon\zeta}}\right)\right)\right\} \tag{37}$$

where

$$D=1-\phi\left(\frac{2-z}{\sqrt{2\epsilon\zeta}}\right)+e^{-\frac{\alpha}{\epsilon}\left[1-\frac{z^2}{4(1-\alpha\zeta)}\right]}\phi\left(\frac{2-z^*}{\sqrt{2\epsilon\zeta^*}}\right). \tag{38}$$

When α is set equal to 0 eq (37) reduces to the known Faxén solution.

Fujita [2] showed that in his approximation the position of the maximum is given by

$$r_{\max}=r_0e^{\tau}[1-\alpha(1-e^{-\tau})]. \tag{39}$$

The result of eq (19) implies that this is modified to

$$r_{\max}=r_0e^{\tau}[1-\alpha(1-e^{-\tau})][1+f]. \tag{40}$$

The factor f is generally of the order of 0.1 or less and therefore Fujita's result for the position of the maximum gradient is sufficient for all practical purposes. It also follows that Fujita's calculations for the height-area ratio are sufficiently good for practical purposes.

References

[1] H. Fujita, Mathematical Theory of Sedimentation Analysis (Academic Press, New York, 1962).

[2] H. Fujita, Effects of a concentration dependence of the sedimentation coefficient in velocity ultracentrifugation, J. Chem. Phys. **24,** 1084 (1956).

[3] I. H. Billick, G. H. Weiss, Exact Faxén solution for centrifugation when sedimentation depends linearly on concentration, Nature, **201,** 912 (1964).

[4] G. H. Weiss, D. A. Yphantis, Rectangular approximation for concentration dependence in the ultracentrifuge, J. Chem. Phys. **42,** 2117 (1965).

[5] G. H. Weiss, An Archibald type solution to a non-linear Lamm equation, Nature **202,** 792 (1964).

[6] M. Dishon, G. H. Weiss, and D. A. Yphantis, Numerical solutions to the Lamm equation, to appear in Biopolymers.

[7] I. M. Ryshik, I. S. Gradstein, Tables of Series, Products, and Integrals, 2d edition (Plenum Press, New York, 1963).

(Paper 70A1–383)

JOURNAL OF RESEARCH of the National Bureau of Standards—A. Physics and Chemistry
Vol. 70A, No. 1, January–February 1966

A Line Formula Notation System for Coordination Compounds: III. Deviations From Idealized Configurations

E. Silverton* and R. F. Pasternack**

(October 22, 1965)

A linear notation describing the true configuration of a coordination complex has been developed to supplement the McDonnell-Pasternack representation of the idealized configuration. Criteria for determining major deviations from the ideal configuration are proposed. The symmetry of the true configuration is described with the aid of point-group notation; ligand sites are designated according to the system developed by McDonnell and Pasternack.

Key Words: Configuration, coordination, inorganic, linear notation, point-group, symmetry.

A previous study [1, 2][1] has led to a method of ciphering coordination complexes using a set of idealized structures. However, many important properties (spectra, magnetic susceptibility, etc.) of this class of compounds depend on the true symmetry of the species. Indeed, for certain group M atoms [1], the idealized structure is never closely approached in Nature. Cupric hexacoordinate complexes, for example, never appear octahedral, but always show large distortions. It is therefore appropriate to include the true configuration in the store of information about the given substance.

The idealized structure is represented in File I by the McDonnell-Pasternack cipher and the true configuration (if it differs from the ideal) is described in File II in terms of its point group notation [3]. As the transition from the ideal to the nonideal configuration is a gradual one, a criterion is set to distinguish the so-called "minor" deviations from the "major" deviations. A deviation is termed major when it cannot be attributed to inaccuracies in atomic parameters. If the apparent deviation of a bond length or angle is 2.3 times as large as the corresponding estimated standard deviation (e.s.d.)[2] the deviation is taken to be real [5]. The e.s.d. thus serves as a criterion for classifying apparent deviations. When all deviations are minor, the structure is treated ideally, and the symbol "#" is stored in File II. File II is omitted when the structural information[3] given is insufficient to derive deviations.

The accuracy of structure determinations reported in the literature covers a wide range, although the trend is to more accurate determinations. This presents a problem in the consideration of deviations: a deviation classified as a minor in a relatively inaccurate determination can be major in an accurately determined structure. Therefore, if no major deviations are disclosed in a structure, does this indicate a close approach to ideality or merely reflect a low degree of accuracy in the structure determination? To resolve this question it seems appropriate to grade the quality of a structure determination according to its minimum significant deviation from ideality. As the classification of deviations is based upon e.s.d., this becomes a natural criterion in assigning the above-described grades. The proposed grades are in table 1.

TABLE 1. *Proposed grades*

Grade	e.s.d. of Ligand-metal bond	e.s.d. of Ligand-metal-ligand
	(Å)	*Angle (deg)*
A	≤ 0.01	≤ 0.3
B	0.01 – 0.03	0.3 – 0.6
C	0.03 – 0.05	0.6 – 0.7
D	> 0.05	> 0.7
	and all two-dimensional structure determinations.	

The point group of the true configuration contains only those symmetry elements of the idealized configuration from which there are no major deviations. Therefore, the first step in determining the true configuration is to test the symmetry elements of the idealized configuration for deviations. Ligands are treated as identical spheres (bidentates are represented by two spheres, tridentates by three, etc.) in determining symmetry elements. Three types of symmetry elements are used in point-group notation: inversion center, rotation axis, and reflection plane (mirror plane). Combinations of these symmetry elements produce additional symmetry elements: rotoreflection axis (alternating axis) and rotoinversion axis (inversion axis). An n-fold axis of rotation rotates each atom $360°/n$ about the axis, generating N atoms in a plane perpendicular to the axis. Therefore the conditions for an n-fold are (1) the n atoms display the axial symmetry, (2) the n atoms are coplanar, (3) the plane of the n atoms is perpendicular to the rotation axis. Deviations from these conditions may be expressed in different ways. The following are possible criteria

*Present address: National Institutes of Health, Bethesda, Md.
**Present address: Department of Chemistry, Ithaca College, Ithaca, New York.

[1] Figures in brackets indicate the literature references at the end of this paper.
[2] The e.s.d. measures the precision of bond distances and angles. See reference [4].
[3] For the purposes of this paper, the structural data are taken from crystallographic studies.

for testing axial symmetry: (1) the distances of the *n* atoms from the axis of rotation, (2) the interatomic distances between adjacent planar atoms, and (3) the angle subtended by adjacent planar atoms and the rotation axis. The e.s.d. of the corresponding bond distance or angle is used in classifying possible deviations from the average value. Two ways of expressing degree of coplanarity are (1) distances of the atoms from the mean plane, and (2) the sum of the interior angles in the polygon formed by the *n* atoms. In the first case, the apparent deviation is compared with the e.s.d. of the atomic coordinates and the e.s.d. of the angles are used in the second case.

Any molecule with an atom lying on a symmetry element of the space group [4] will contain that symmetry element. (These space-group positions are called special positions.) Thus, if an atom in a coordination complex occupies a special position, the true configuration of the coordination complex will contain the symmetry element corresponding to the special position.

After the point group of the true configuration is determined, a rotational axis is selected according to the following criteria:

1. The highest-order axis.
2. The axis coinciding with the highest-order axis of the idealized structure.
3. The axis containing the earliest locant-designator.
4. The axis perpendicular to the plane containing the earliest locant-designator.

The senior end of the axis is the one passing through the most senior (earliest) locant position (or the plane containing the most senior locant position) at first difference.

The cipher describing the true configuration makes use of the enumeration pattern and locant designation given in File I [1]. In the idealized configuration the assignment of ligands to locant sites may be arbitrary for identical ligands occupying positions in a plane equidistant from the axis or occupying equivalent positions on the axis. However, if distortions from the idealized configuration exist, these ligand sites may no longer be equivalent. In this case ligands are assigned locants in order of increasing distance from the axis of rotation (if they lie in a plane) or from the group M atom (if they lie on the axis). The File II cipher begins with the Schoenflies notation [7, 3] for the point group of the true configuration, followed by a comma. The order (2, 3, 4, etc.) of the selected rotational axis is cited next, followed by an opening brace. Atoms are cited as they appear along the axis (starting from the senior end), separating atoms at different levels by slashes. Atoms not on the axis and equidistant from the axis, lying in a plane perpendicular to the axis, are separated by commas and enclosed within parentheses. A period precedes the opening parenthesis. If another set of atoms lies in the same plane at a greater distance from the axis, the sets are cited in order of increasing distance and are separated by periods. Atoms within parentheses are cited (1) in numerical order,[5] and (2) in alphabetic order of the locants. If an axial atom lies on the above described plane, it is cited before the initial period. If a single nonaxial atom occurs, it is preceded by a period. The cipher is completed by a closing brace, followed by the grade.

The following examples illustrate various degrees of deviation from the ideal configuration as well as the use of the criteria for testing symmetry elements.

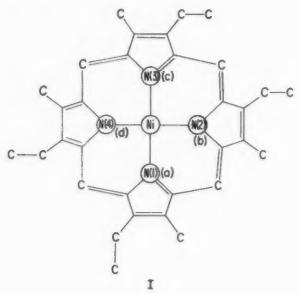

I

EXAMPLE I. Nickel Etioprophyrin II [8]
$NiC_{32}H_{36}N_4$ (I)
Type: square planar (point group D_{4h}).
Special positions: Ni at $\bar{4}$M2, N on a mirror plane and C on a 2-fold axis.
Grade: D.
File I cipher [6]: ni{1,4B} ≪ 5L(L=@5LN[1a]L(
=L@5L=N[1b]L(=L@5LN[1c]

L(L=@[1])=L(CM)LM=)LM
=L(CM))L(CM)=LM)
=N[1d]L[1]L(CM)=LM.

The square planar configuration contains the following combination of symmetry elements: a 4-fold axis with four 2-fold axes and a mirror plane perpendicular to it. The conditions for a 4-fold axis through the nickel atom are that the four nitrogen atoms (1) be equidistant from the nickel, (2) subtend 90° angles with the nickel, and (3) be coplanar with the nickel atom. Note that the third condition also satisfies the requirement for a mirror plane perpendicular to the 4-fold axis. Since the nitrogen atoms lie on two perpendicular mirror planes intersecting at the nickel atom, the first two conditions are satisfied. The third condition will be discussed later.

[4] The 230 space groups describe all combinations of symmetry elements possible in crystals. See reference [6].

[5] A number referring to the coordination center is used if more than one coordination center exists.

[6] The square planar configuration is referred to as 4B in the File I cipher. See reference [1].

The four potential 2-fold axes are as follows:
(1) An axis bisecting angles N(1)NiN(2) and N(3)NiN(4),
(2) an axis bisecting angles N(2)NiN(3) and N(1)NiN(4),
(3) an axis through N(1), N(3), and Ni,
(4) an axis through N(2), N(4), and Ni.

The first two axes are the ones on which the carbon atoms lie. If the third axis exists, N(2) and N(4) must be related by 2-fold symmetry. This is true if N(2) and N(4) are coplanar with N(1), N(2), and Ni. Similarly this condition also satisfies the requirements for the fourth axis. A look at the atomic coordinates of nitrogen and nickel shows that the condition would be met if the *z*-coordinate of nitrogen were 0.125. The *z*-coordinate is 0.122, a deviation of 0.003 from the ideal. As the standard deviation of the *z*-coordinate is approximately 0.002, the deviation is minor.[7] Since there are no deviations from the ideal configuration, File II contains "#, D" where D is the grade.

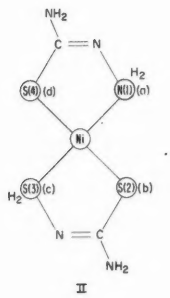

II

EXAMPLE II. Bis(thiosemicarbazidato)nickel(II)[9] $Ni[SC(NH_2)=NNH_2]_2$(II)
Type: square planar (point group D_{4h}).
Special positions: Ni on center of inversion.
Grade: B
File I cipher: ni{1,4B} ≪ C(S[1b,1d])Z(=NZ[1a, 1c]) ≫ 2.

The point group D_{4h} contains a 4-fold axis with four 2-fold axes and a mirror plane perpendicular to it.

The conditions for a 4-fold axis through the nickel atom are that the ligand atom to nickel distances be equal (see table 2,a) and the angles subtended by adjacent ligands and the nickel atom be 90° (see table 2,b).

The deviations from 4-fold symmetry are major.

[7] The apparent deviation is less than 2.3 times the e.s.d.

TABLE 2 *Bond parameters*

	Deviations	e.s.d.
a NiS, NiN 2.155, 1.911Å	0.122Å	0.014Å
b N(1)NiS(4), N(1)NiS(2) 81.7, 98.3°	8.3°	.4°

There are five possible 2-fold axes:
(1) An axis through the nickel atom perpendicular to the plane of the ligands.
(2) An axis through the two nitrogens and the nickel atom.
(3) An axis through the two sulfurs and the nickel atom.
(4) & (5) Two axes bisecting the N-Ni-S angles.

Axis (1) is the only one having no major deviation. Axes (2) and (3) show major deviations from the required N-Ni-S angles. Axes (4) and (5) show major deviations in the ligand to metal distances.

The special position of the nickel atom requires that it be coplanar with the four ligands. Thus the symmetry elements of the true configuration are a 2-fold axis with a mirror plane perpendicular to it; that is, C_{2h}. File II is written:

$$C_{2h}, 2\{1 \cdot (a,c) \cdot (b,d)\}B.$$

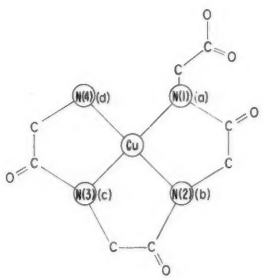

III

EXAMPLE III. Disodium *N*-[*N*-(*N*-glycylglycyl) glycyl]glycinocuprate(II) decahydrate[10] $Na_2[CuNH_2(CH_2CON)_3CH_2COO] \cdot 10H_2O$ (III)
Type: square planar (point group D_{4h}).
Special positions: None.
Grade: A.
File I cipher: [cu{1,4B} ≪ C(O)V{CN[1a,1b,1c]CV} 3CZ[1d] ≫]Θ2.

Again the configuration is square planar, but in this case no atoms occupy special positions and so all symmetry elements must be tested.

The potential 4-fold axis passes through the copper atom perpendicular to the plane of the nitrogen atoms. Therefore the four ligands should be equidistant from the copper atom (see table 3a, a, b, c, d) and subtend equal angles with the axis (see table 3b, e, f, g, h).

The deviations from 4-fold symmetry are major. The five potential 2-fold axes which have been described in Example II all show major deviations in this case. Axes (1) and (3) require that CuN(4)=CuN(2). Axis (2) requires that the angles subtended by adjacent ligands and the copper atom be 90°. The conditions for axes (4) and (5) include CuN(4)=CuN(3) and CuN(1)=CuN(4), respectively.

TABLE 3a. *Distances* (Å)

			Deviations from average	e.s.d.
			Å	Å
a	CuN(4)	2.028	0.08	0.005
b	CuN(3)	1.923	.03	.004
c	CuN(2)	1.912	.04	.004
d	CuN(1)	1.944	.01	.004

TABLE 3b. *Angles (degrees)*

			Deviations from average	e.s.d.
			Degrees	*Degrees*
e	N(3)CuN(4)	83.5	6.5	0.2
f	N(1)CuN(4)	109.8	19.8	.2
g	N(1)CuN(2)	84.0	6.0	.2
h	N(3)CuN(2)	82.8	7.2	.2

The remaining possible symmetry element is a mirror plane through the copper and the four ligands. Two criteria for planarity are (1) the sum of the angles subtended by adjacent ligands and the copper atom and (2) the deviations from the mean plane. The sum of the angles is 360.1°, indicating a minor deviation. The deviations from the mean plane are listed in table 4.

The deviations from the mean plane are major. This contradiction between the two criteria is not unexpected as the second is more sensitive to small deviations.

File II is written:

$$C_1,1\ \{1\cdot b\cdot c\cdot a\cdot d\}A.$$

TABLE 4 *Deviations from mean plane*

	Atom	Deviation	e.s.d.
		Å	Å
a	Cu	0.029	0.009
b	N(4)	.046	.017
c	N(3)	.048	.017
d	N(2)	.040	.017
e	N(1)	.039	.017

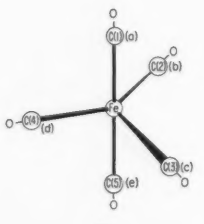

IV

EXAMPLE IV: Iron [II] pentacarbonyl $Fe(CO)_5$ (IV)
Type: trigonal bipyramid (point group D_{3h}).
Special positions: Fe and C_2 on 2-fold axis.
Grade: D.
File I cipher: fe{1,5A}≪C[1a,1b,1c,1d,1e]0:V⩾5.

TABLE 5a. *Bonds* (Å)

			e.s.d.
			Å
a	C(2)-Fe	1.76	0.03
b	C(3)-Fe	1.80	.02
c	C(4)-Fe	1.80	.02

TABLE 5b. *Angles (degrees)*

			e.s.d.
			Degrees
d	C(2)-Fe-C(3)	122	1
e	C(3)-Fe-C(4)	116	1
f	C(2)-Fe-C(4)	122	1
g	C(1)-Fe-C(2)	88	1
h	C(5)-Fe-C(2)	88	1
i	C(1)-Fe-C(3)	90	1
j	C(5)-Fe-C(3)	92	1

The point group D_{3h} consists of a 3-fold axis with three 2-fold axes and a mirror plane perpendicular to it. The potential 3-fold axis passes through C(1), C(5), and Fe perpendicular to the plane of ligands C(2), C(3), and C(4). The conditions for 3-fold symmetry are (1) that ligands C(2), C(3), and C(4) be equidistant from the iron atom, and (2) that each angle subtended by any two of these ligands and the iron atom be 120. An examination of the parameters listed in table 5a shows a major deviation (parameter e) from the above conditions. The three possible 2-fold axes are (1) an axis through C(2) bisecting the angle subtended by ligands C(3) and C(4) and the iron atom, (2) an axis through C(3) bisecting the angle subtended by ligands C(2) and C(4) and the iron atom, and (3) an axis through C(4) bisecting the angle subtended by ligands C(2) and C(3) and the iron atom. The first 2-fold axis need not be tested for deviations since the iron atom and ligand C(2) lie on a 2-fold axis of the space group (i.e., a special position). The following conditions are required by the second and third 2-fold axes respectively:

$$C(2)FeC(3) = C(3)FeC(4)$$

$$C(2)FeC(4) = C(3)FeC(4)$$

Inspection of table 5b reveals major deviations from these conditions. The final symmetry element of D_{3h} to be tested is a mirror plane containing ligands C(2), C(3), and C(4) and the iron atom. The conditions for the mirror plane are (1) that ligands C(1) and C(5)

be equidistant from the mirror plane,[8] (2) that the line connecting ligands C(1) and C(5) be perpendicular to the mirror plane, (see table 5b, g–j) and (3) that the sum of the angles subtended by ligands C(2), C(3), and C(4) and the iron atom be 360° (see table 5b, d, e, f). Therefore, the mirror plane is a valid symmetry element. The point group of the true configuration is C_{2v}. File II is written:

$$C_{2v},\ 2\{b/1\cdot(a,\ e)/\cdot(c,\ d)\}D.$$

References

[1] P. M. McDonnell and R. F. Pasternack, J. Chem. Doc. **5,** 56 (1965).

[2] R. F. Pasternack and P. M. McDonnell, Inorg. Chem. **4,** 600 (1965).

[3] F. A. Cotton, Chemical Applications of Group Theory, pp. 38–39 (Interscience Publishers, New York, N.Y., 1963).

[4] D. W. J. Cruickshank, Acta Cryst. **2,** 65 (1949).

[5] H. Lipson and W. Cochran, The Determination of Crystal Structures. The Crystalline State, Vol. **III,** p. 309 (G. Bell and Sons, London, 1957).

[6] International Tables for X-ray Crystallography, Vol. **I** (The Kynoch Press, Birmingham, England, 1952).

[7] A. Schoenflies, Krystallsysteme und Krystallstructur, Leipzig, 1891.

[8] M. B. Crute, Acta. Cryst. **12,** 24 (1959).

[9] L. Cavalca, M. Nardelli, and G. Fava, Acta Cryst. **15,** 1139 (1962).

[10] H. C. Freeman and M. R. Taylor, Acta Cryst. **18,** 939 (1965).

[11] J. Donohue and A. Caron, Acta Cryst. **17,** 663 (1964).

[8] C(1) and C(5) are related by the 2-fold axis, which lies in the mirror plane, and are therefore equidistant from the plane.

(Paper 70A1–384)

JOURNAL OF RESEARCH of the National Bureau of Standards—A. Physics and Chemistry
Vol. 70A, No. 1, January–February 1966

The Spherulitic Crystallization of Isotactic Polypropylene From Solution: On the Evolution of Monoclinic Spherulites From Dendritic Chain-Folded Crystal Precursors[1]

F. Khoury

(October 19, 1965)

Polypropylene can be crystallized in the form of monoclinic (Natta) spherulites from moderately concentrated solutions of the polymer in different solvents. A study is presented involving both optical and electron microscopy which has led to the characterization of the unusual structure and morphology of the dendritic precursor crystals from which such spherulites evolve, as well as the manner in which these precursors degenerate progressively into spherulites.

The *overall* shape of the above mentioned polypropylene dendrites approximates that of a rectangular parallelepiped (reference axes x, y, z, where $x/y \approx 1.1$ and $y > 2z$). These dendrites consist of a dense but not compact network of monolayer chain-folded lamellar branches which traverse the dendrite *diagonally* with respect to its rectangular x, y cross section, the fold surfaces of the individual lamellar branches (i.e., those faces *between* which the constituent molecules in each branch fold back and forth) being normal to the x, y cross section. Electron diffraction data indicate that the orientation of the **b**-crystallographic axis is unique throughout the cross-hatched array of lamellar branches and is parallel to z, the latter axis corresponding to the direction of slowest growth of the dendrite as a whole as well as its constituent branches. It has also been deduced on the basis of the above features coupled with electron diffraction data and consideration of two different but plausible model twinned dendrites that the fold surfaces of the lamellar branches are (001) and that the angle between the **c**-crystallographic axis in intercrossing branches is circa 80°. The possible origin of this unusual mode of twinning, which involves an 80° change in the orientation of the chain axes in offspring branches from that in parent branches, is briefly presented.

The process of evolution of monoclinic polypropylene spherulites from the unusually twinned dendritic crystal precursors is contrasted with the evolution of spherulites in other polymers; furthermore, the relevance of the observations presented in this study to an understanding of the origin of the previously reported atypical fine structures exhibited by monoclinic spherulites of polypropylene crystallized from the melt, is discussed.

Key Words: Chain-folded, crystal, dendritic, electron microscopy, isotactic, monoclinic, morphology, optical microscopy, polymer, polypropylene, precursor, spherulite.

1. Introduction

The purpose of this communication is to report on the outcome of an investigation of the nature of some crystallization habits exhibited by isotactic polypropylene when the polymer is crystallized from moderately concentrated solutions (in the range 3/4 to 10 percent) in some solvents. Specifically, the relevance of various observations derived from this study to the further elucidation of the mechanism of growth and hitherto little understood origin of the atypical fine structures of spherulites of the monoclinic crystalline modification of polypropylene will be discussed in detail.

The spherulitic crystallization of polypropylene in thin films of the polymer crystallized from the melt under isothermal conditions at temperatures in the range 110 to 148 °C has been characterized by Padden and Keith [1][2] who found that spherulites exhibiting different optical properties are formed in this temperature range. A complementary study by Keith et al., [2] of the structure of these different types of spherulites using microbeam x-ray diffraction techniques revealed that all the spherulites that are formed at temperatures above 132 °C and the majority of the spherulites formed below 132 °C possess the monoclinic crystalline structure proposed by Natta et al., [3] for isotactic polypropylene.[3]

[1] Portions of the work described in this paper were presented before the Division of High Polymer Physics of the American Physical Society in March 1963, March 1964, and March 1965. The observations described in section 3, involving the crystallization of polypropylene from xylene and mineral oil, were made during the author's association with the Avisun Corp., Marcus Hook, Pa. All other work was carried out at NBS under partial financial support from the Advanced Research Projects Agency.

[2] Figures in brackets indicate the literature references at the end of this paper.

[3] The monoclinic unit cell parameters are: $a = 6.65$ Å, $b = 20.96$ Å, $c = 6.50$ Å, $\beta = 99°20'$. Four chains in a 3_1 helical configuration pass through the unit cell which contains 12 monomer units. The axes of the helical chains are oriented parallel to the c-axis of the cell [3].

The optical characteristics (birefringence) of these monoclinic spherulites were found to depend on the temperature at which they are formed. Briefly, Padden and Keith [1] point out that the majority of the monoclinic spherulites grown below 132 °C and above 138 °C are respectively positively birefringent and negatively birefringent. While these are the predominant types of monoclinic spherulites formed in these temperature ranges, an appreciable number of "mixed" [4] spherulites of the same crystalline modification are also formed in these temperature ranges. Further, most of the monoclinic spherulites formed in the range 134 to 138 °C are of the mixed type.

The exact origin of the differences in the optical properties of the various types of monoclinic spherulites is not known. The preferred radial crystallographic orientations in both the positive and negative spherulites, as deduced from microbeam x-ray diffraction data, are indistinguishable. According to Keith et al., [2] in both these types of spherulites the **c**-crystallographic axis, and hence the axes of the helical chains, are oriented at an angle of 65 to 70° to the radius. The **b**-axis orientation is tangential.

In addition to the predominantly positive and fewer mixed monoclinic spherulites which grow at temperatures below 132 °C, Padden and Keith [1] observed that a few negatively birefringent spherulites are formed also in the same temperature range (110 to 132 °C). These rarer spherulites possess an apparently pseudohexagonal metastable crystalline structure [2, 4, 5]. The axes of the chain molecules are normal to the radial direction in such spherulites [1, 2].

Spherulites of the more common monoclinic crystalline modification and the rarer hexagonal crystalline modification of polypropylene exhibit highly contrasting fine structures. The morphology of the rarer hexagonal spherulites is similar to that commonly exhibited by spherulites in numerous other polymers [6]. Surface replicas of hexagonal spherulites formed in thin films of polymer reveal, as described by Geil [6], a radiating fine structure consisting of thin lamellar structural units which extend radially outwards from the central regions of the spherulites. The crystallographic orientation in these spherulites as derived from both their optical properties as well as the microbeam x-ray diffraction experiments referred to above (which indicate that the chain molecules are oriented normal to the radius), coupled with the uniformity in thickness of the radiating lamellae normal to the radius, corroborate that these lamellae are most probably chain-folded single crystal structural units. The fold surfaces (i.e., the surfaces between which the molecules are folded regularly back and forth) of the lamellae are parallel to the radial direction as has been established in spherulites of other polymers, e.g., polyethylene, polyoxymethylene, and poly(4-methylpentene-1) [7].

[4] These spherulites do not exhibit symmetrical extinction characteristics between crossed polarizers; individual spherulites exhibit, randomly, positive birefringence, negative birefringence, or irregular transitions from one sign of birefringence to another along different radial paths.

In contrast with the radiating chain-folded lamellar morphology which, as indicated above, is characteristic of spherulites of numerous polymers, as well as those of the pseudohexagonal crystalline modification of polypropylene, spherulites of the monoclinic crystalline modification of polypropylene exhibit highly complex morphologies the nature and origin of which have hitherto been little understood. Brief descriptions of the morphology of such spherulites have been presented by Bailey [8] (see also Keller [9]) and Geil [10]. Bailey [8] has described spherulites which exhibit a cross-hatched morphology consisting apparently of interwoven or intercrossing radially and tangentially oriented "fibrils." Geil [10] describes positive and negative monoclinic spherulites as consisting of radially oriented ribbonlike or ropelike structural units which exhibit a transverse ribbed or corrugated morphology; apparently no specific morphological differences between the positively and negatively birefringent types of monoclinic spherulites have been observed.

Additional evidence of the unusual morphologies associated with the crystallization of polypropylene in its monoclinic crystalline modification has been further reported by Geil [11]. This evidence has been derived from a study of the morphology of extremely thin films of polypropylene crystallized by slow cooling from the melt on a substrate. Examination under the electron microscope revealed that those portions of the film which crystallized in the pseudohexagonal crystal modification consisted of thin (~ 150 Å thick) lamellar chain-folded crystal layers lying parallel to the substrate. Frequent instances of spiral development of superposed layers initiated by screw dislocations in basal lamellae were observed. In contrast, those regions of the polymer film which crystallized in the monoclinic modification were found to consist of "incipient spherulites" various portions of which exhibited differing morphologies. In some regions of these structures a distinctly cross-hatched fine structure akin to that reported by Bailey [8] was observed. Geil points out that the narrow structural units which may be seen to intercross at right angles within limited areas appear to be thicker normal to the substrate on which they grew than they are wide. The possibility is indicated by Geil [11] that they may be chain-folded single crystals the fold surfaces of which are oriented normal to the plane of the film. In other regions of these "incipient spherulites" individual broad ribbonlike structures were discerned which exhibited in their thicker parts a transverse striated fine structure, reminiscent of that exhibited by the constituent radiating units in positive and negative monoclinic spherulites [10].

The unorthodox morphologies of isotactic polypropylene in which the polymer crystallizes in its more common monoclinic crystalline modification clearly suggested that some fundamental differences must exist between the mechanism of evolution of monoclinic spherulites of that polymer and the mechanism leading to the formation of polymer spherulites that exhibit the more conventional radiating lamellar

fine structures. The original objectives of the present study were to (a) investigate the nature of the habits and fine structures of crystalline aggregates that hot moderately concentrated solutions of polypropylene yield in suspension in solvent when they are cooled to lower temperatures, and (b) determine whether any information relevant to the elucidation of the origin of the complex morphologies exhibited by the relatively intractable melt-grown monoclinic spherulites could be derived from the structural characterization of crystalline aggregates grown from solution (under different conditions) that are more accessible to detailed morphological investigations.

It will first be shown in what ensues that polypropylene can be readily crystallized from solution in the form of monoclinic spherulites in suspension. Experiments will subsequently be described, the outcome of which has been to provide a detailed insight into the unorthodox nature of the crystal precursors from which monoclinic spherulites evolve when formed from solution. The direct relevance of the observations derived from the latter experiments to an understanding of the origin of the atypical fine structures of melt-grown monoclinic spherulites will be pointed out. Finally, the nature of an underlying fundamental phenomenological difference between the mechanism of formation of spherulites of the monoclinic crystalline modification of polypropylene and that of polymer spherulites which exhibit the more typical radiating lamellar or fibrillar morphologies will be discussed.

2. Experimental Procedures

2.1. Materials

Isotactic polypropylene in powder form having a number average (osmotic) molecular weight of 98000 [12] was used in all the experiments. The solvents used were: mineral oil (medicinal grade, specific gravity according to manufacturer 0.880–0.900 at 15.6 °C), xylene (A.C.S. reagent grade, boiling range 139 to 139.3 °C) and amyl acetate (purified). The xylene and amyl acetate were distilled before use.

2.2. Solutions

Unless otherwise stated, solution concentrations are expressed throughout as weight (grams) of polymer per volume (100 cm^3) of solvent at room temperature. In general polymer solutions were prepared by adding the polypropylene powder to solvent at room temperature in a Pyrex flask and then immersing the flask and its contents for half an hour in a bath held isothermally at an appropriate elevated temperature, i.e., at 180 °C for the mineral oil preparations, and at 140 °C for both the xylene and amyl acetate preparations. The resulting solutions were then either cooled continuously to room temperature (sec. 3.1) or transferred to constant temperature baths held at lower temperatures (sec. 3.2a; 4). Details pertaining specifically to some individual experiments are given in appropriate parts of the paper.

2.3. Optical Microscopy

With the exception of some experiments described in section 3.2b, the various structural entities precipitated from solution under different conditions were examined under the optical microscope at room temperature while still in suspension in liquid using either polarizing or phase contrast optics. In the latter case contrast was often enhanced by either exchanging or highly diluting the original solvent in which the various structures were in suspension at room temperature with a liquid of appropriate refractive index. Cargille Refractive Index Liquids were used in such instances. Unless otherwise stated, all optical micrographs shown in the paper represent the types of structures that will be discussed as they variously appear when seen in different perspectives (we refer specifically here to structures that are not spherulites) while in suspension in a liquid medium.

2.4. Electron Microscopy

A JEM 6A [5] electron microscope was used in the study described in section 4. The precautions required in examining the crystals described therein, in transmission, and the technique used in replicating their surfaces are presented in the selfsame section.

3. Results and Discussion

3.1. Preliminary Evidence of the Spherulitic Crystallization of Polypropylene From Solution in Its Monoclinic Crystalline Modification

Exploratory experiments revealed that when hot 3/4-percent and 10 percent solutions of polypropylene in mineral oil or xylene are cooled continuously to room temperature at ~ 0.5 °C/min, the polymer crystallizes in the form of spherulites in suspension in solvent.

The mineral oil solutions yielded only positively birefringent monoclinic spherulites, examples of which as seen under the polarizing microscope while still in suspension in solvent are shown in figures 1 and 2.

In contrast, the xylene solutions yielded spherulites exhibiting various birefringent properties depending on the initial polymer concentration. Thus, whereas all the spherulites grown from the 3/4 percent xylene solution were negatively birefringent (fig. 3), the 10 percent xylene solution yielded on cooling a preponderance of spherulites of different sizes exhibiting "mixed" birefringent characteristics as well as a few smaller distinctly negatively birefringent spherulites. The mixed spherulites were essentially of two general types, namely, some which exhibit an overall irregular change from positive birefringence in the central regions to negative birefringence nearer the periphery,

[5] Instrument identified by trade name in order to adequately specify equipment used. Such identification in no way implies endorsement or recommendation by the National Bureau of Standards.

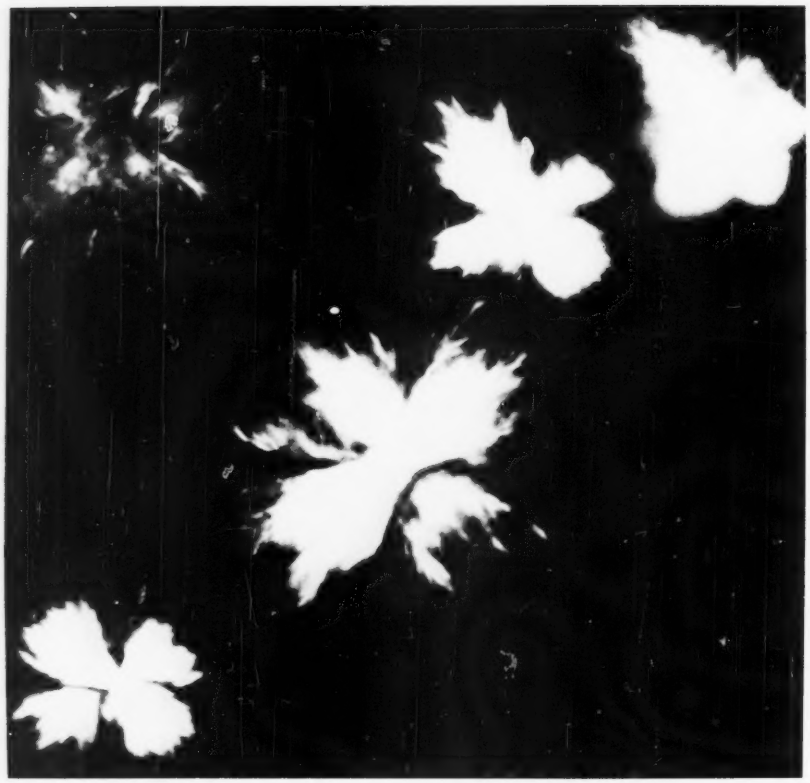

FIGURE 1. *Positively birefringent spherulites grown on cooling a 0.75 percent solution of polypropylene in mineral oil.*
Crossed polarizers, ×600.

and others which exhibit asymmetric birefringent characteristics along different radial paths (see footnote 3). Examples of spherulites grown from a 10 percent xylene solution are shown in figure 4.

Wide-angle x-ray diffraction patterns (powder) obtained from samples consisting of spherulites formed from the 3/4 percent and 10 percent xylene solutions were characteristic of the monoclinic crystalline modification of polypropylene proposed by Natta et al., [3]. An x-ray powder pattern obtained from a sample of the negatively birefringent spherulites formed from the more dilute xylene solution is shown in figure 5 in which the four prominent 110, 040, 130, and composite 111, 13$\bar{1}$, 041 rings characteristic of monoclinic polypropylene may be readily detected.

The various solution-grown spherulites described briefly above are by no means rigid structures. They undergo varying degrees of deformation after elimination of the solvent by direct drying (xylene preparations) or by suitable extraction (mineral oil preparations). The extent of deformation to irregular shapes was pronounced in the less compact spherulites grown from the dilute polymer solutions. The spherulites grown from the 10 percent xylene solution, however, underwent only some radial shrinkage on drying while still retaining their spherical shape. Examples of spherulites removed from the latter preparation as they appear under oblique incident illumination after drying are shown in figure 6.

Further study aimed specifically at determining the origin of the different birefringent characteristics of the various types of spherulites referred to above was not attempted. It is clear, however, that the birefringent characteristics of individual spherulites grown from the 10 percent xylene solution depend on the temperature range within which they develop during the cooling cycle. The available observations indicate that lower crystallization temperatures lead to the formation of negatively birefringent spherulites, as evidenced by the fact that the smallest spherulites formed in this preparation were negatively birefringent. This is further substantiated by the, albeit irregular, change in sign of birefringence (from positive in the interior to negative nearer the periphery) exhibited by many of the larger "mixed" spherulites. That lower

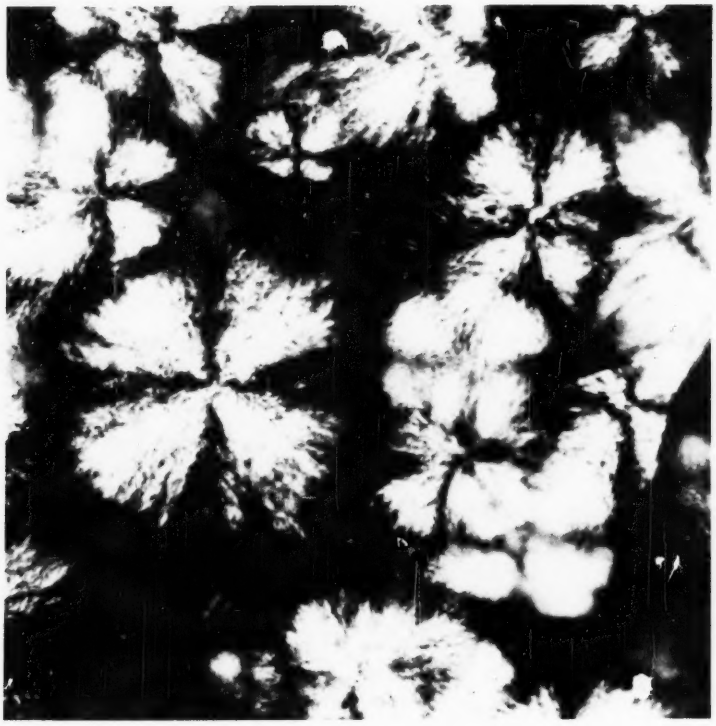

FIGURE 2. *Positively birefringent spherulites grown on cooling a 10 percent solution of polypropylene in mineral oil.*
Crossed polarizers, × 220.

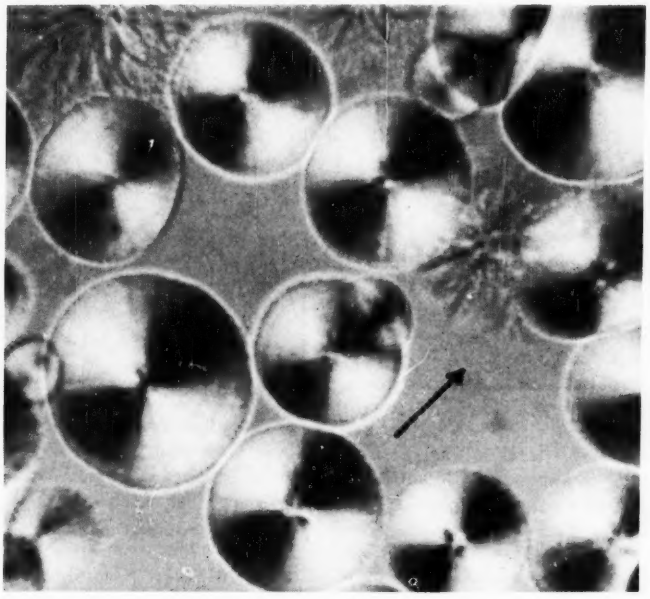

FIGURE 3. *Negatively birefringent spherulites grown on cooling a 0.75 percent solution of polypropylene in xylene.*
Crossed polarizers and 1/4 λ compensator (slow direction of vibration of compensator indicated by arrow), × 370.

792-867 O-66-3

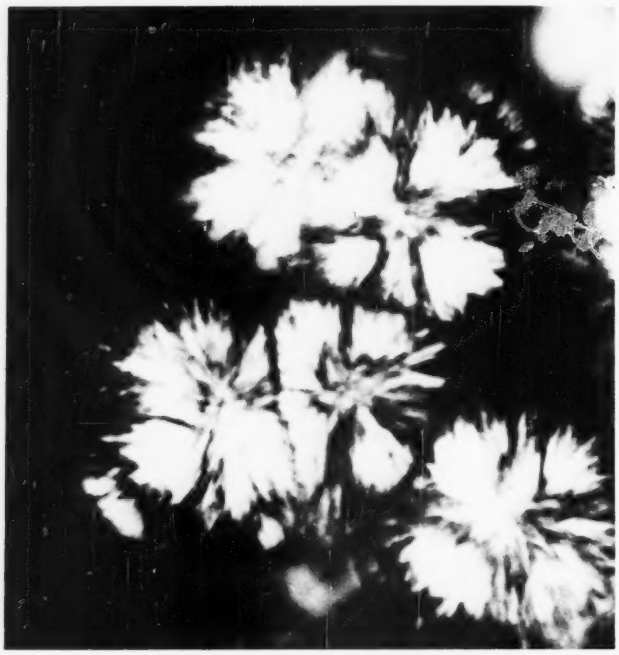

FIGURE 4. *Spherulites exhibiting "mixed" birefringent characteristics grown on cooling a 10 percent solution of polypropylene in xylene.*
Crossed polarizers. × 470.

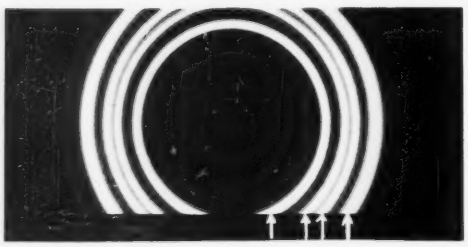

FIGURE 5. *Wide angle x-ray powder pattern obtained from a sample of negatively birefringent spherulites formed on cooling a 0.75 percent solution of polypropylene in xylene.*
Vertical bars identify inner 110, 040, 130 and composite 111, $13\bar{1}$, 041 rings characteristic of the monoclinic (Natta) crystalline modification of polypropylene.

temperatures of crystallization lead to the formation of negatively birefringent monoclinic spherulites from a 10 percent xylene solution, was further substantiated by the fact that when such a solution is rapidly quenched in liquid nitrogen (rate of cooling to room temperature ~ 44 °C/min) only negatively birefringent spherulites are formed.

3.2. On the Nature of the Early Stages of Formation of Monoclinic Spherulites From Solution

a. The Habits of Polypropylene Crystallized From 3/4 percent Solutions of the Polymer in Mineral Oil Under Isothermal Conditions (80 to 112 °C)

At 80 and 90 °C the polymer crystallizes very rapidly. The solutions yield positively birefringent monoclinic spherulites similar to those shown in figure 1. At higher temperatures, however, in the range 105 to 112 °C individual solutions yield in addition to relatively more compact positively birefringent monoclinic

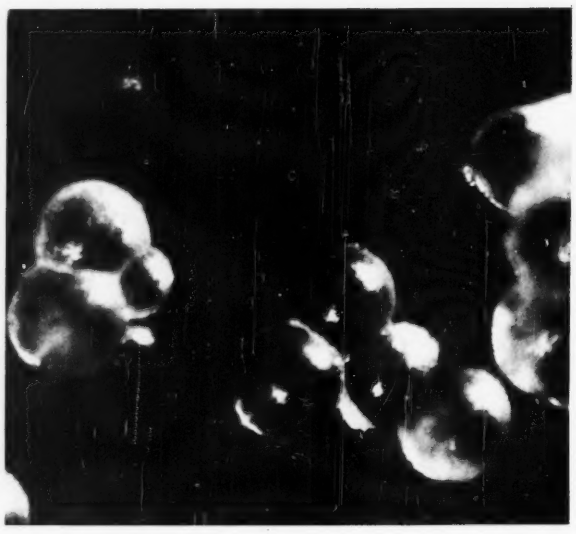

FIGURE 6. *Spherulites grown on cooling a 10 percent solution of polypropylene in xylene.*
They are depicted as seen under oblique (unpolarized) incident illumination after having dried in air at room temperature. × 270.

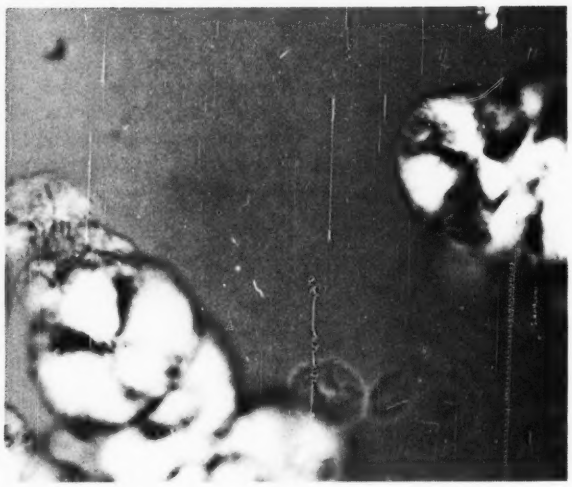

FIGURE 7. *Positively birefringent spherulites and smaller aspherical aggregates grown from a 0.75 percent solution of polypropylene in mineral oil at 112 °C.*
Polarizers crossed at 80°. ×370.

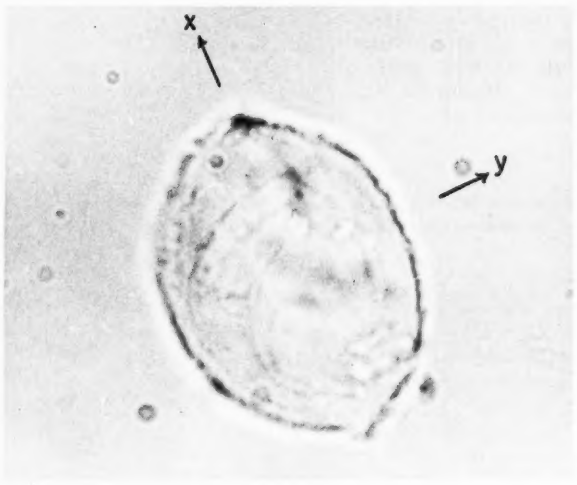

FIGURE 8. *Crystalline aggregate grown from a 0.75 percent solution of polypropylene in mineral oil at 112 °C.*
Note elliptical profile of aggregate when seen as depicted here along an axis (z) at right angles to its plane (x,y) of preferential development. Unpolarized light. × 1,930.

spherulites of different sizes (fig. 7), numerous smaller rigid nonspherulitic monoclinic crystalline aggregates[6] which exhibit differing but related habits. The respective shapes of these various aggregates were readily deduced by observing them (after crystallization was completed and the solutions cooled to room temperature) as they tumbled, or were induced to tumble slowly, in suspension in liquid under the optical microscope in transmission either in unpolarized light or more appropriately using phase contrast optics.

An example is shown in figure 8 of an aggregate typical of many that are formed in the temperature range 105 to 112 °C. These aggregates exhibit characteristically contrasting profiles when viewed along different directions. Observing such structures as they tumbled in a liquid medium revealed that they possess a plane of preferential development. When they are oriented so as to occupy a maximum surface area in the field of view of the microscope they exhibit, as may be seen in figure 8, an essentially elliptically shaped profile. For the sake of convenience in what follows, the major and minor axes of the aggregate cross section depicted in figure 8 will be referred to below as the (x) and (y) axes, respectively, and the axis normal to the (x,y) plane (the plane of preferential development) as the (z) axis. When such an aggregate is viewed along any axis lying in the (x, y) plane (i.e., if the aggregate shown in figure 8 is rotated through 90° from the position depicted therein about any axis normal to the microscope axis), it exhibits an essentially incipient sheaflike appearance as shown in figure 9. Overall growth along the (z) direction is substantially slower than in the (x,y) plane, the relative disparity in growth being roughly characterized by the following overall (x, y, z) dimensions: $\sim 30\ \mu \times 20\ \mu \times 5\ \mu$ (i.e., x:y:$z \sim$ 6:4:1). In actual fact these aggregates are somewhat thicker along the (z)-direction in the peripheral regions than at the center. This is more clearly revealed by examining these structures under the phase contrast microscope, as may be

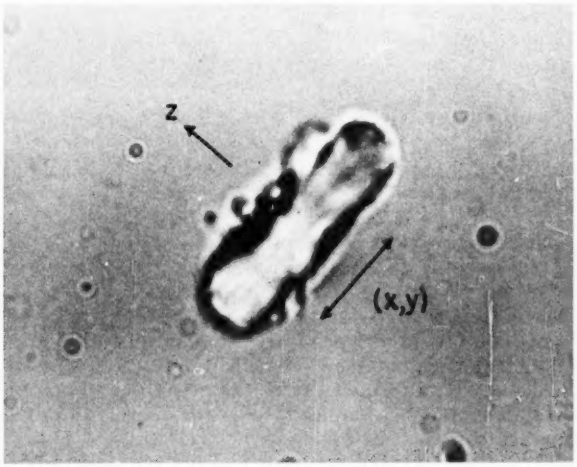

FIGURE 9. *Aggregate similar to that shown in figure 8 but viewed edge-on along an axis parallel to its plane* (x,y) *of preferential development.*
Unpolarized light, × 1,930.

[6] The term aggregate is used throughout this paper in a generic sense to denote any structural entity which has grown from solution and which could not be outrightly characterized as being an individual coherent crystal or a spherulite. Different types of aggregates will be differentiated by suitable adjuncts (e.g., elliptical, apparent or pseudopolyhedral, etc.) referring variously to distinguishing shape characteristics.

FIGURE 10. *Cluster of variously oriented structures grown from a 0.75 percent polypropylene solution in mineral oil at 112 °C.*
Note optically denser peripheral regions of elliptical aggregate (arrow). Phase Contrast. × 1450.

seen in figure 10, in which the distinctly darker peripheral regions in the appropriately oriented "elliptical" aggregate present in the field of view can be clearly discerned.

In addition to the type of aggregate described above, still smaller aggregates exhibiting different but related habits are also formed under the same conditions of crystallization. Examples typical of these different aggregates, as seen under the phase contrast microscope, are shown in figure 11. They are essentially planar structures which exhibit respectively the characteristic profiles seen in figure 11 (a to d) when viewed along an axis normal to their plane of preferential development.

The smallest aggregates (fig. 11a), which are relatively rare, exhibit parallel lateral edges and a distinctly concave profile at the extremities of their longer axis. This latter aspect is also evident in the slightly larger structures (fig. 11b) in which, however, the longer lateral edges are slightly convex. The lateral sides of the still larger structures (fig. 11c, d) are pronouncedly convex and these aggregates also exhibit a distinctly re-entrant or notched appearance at opposite extremities along the bisectrix parallel to their direction of preferred overall growth. As mentioned earlier, the aggregate types shown in figure 11

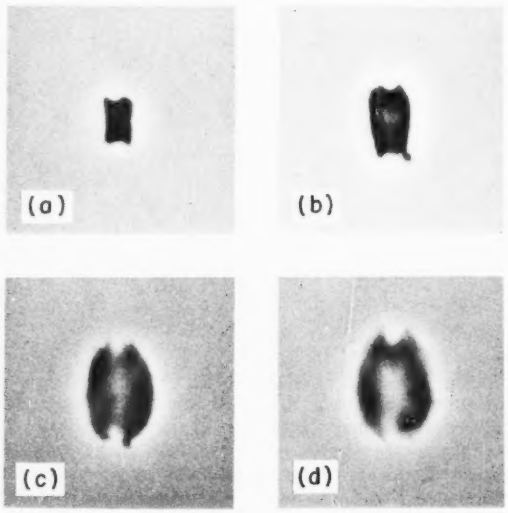

FIGURE 11. *Examples of other aggregates also formed from a 0.75 polypropylene solution in mineral oil at 112 °C.*
Each is depicted as seen along an axis at right angles to its plane of preferential development. Note pronounced concavity of shorter edges of aggregates in (a), (b), as well as the pronounced convexity of the lateral edges and notched appearance at opposite extremities of aggregates in (c), (d). Phase Contrast. × 1,050.

are thinner ($< 5\ \mu$) than they are long or broad. They, too, however, as in the case of the elliptical structures described above, are slightly thicker in the peripheral regions than at the center. They all exhibit incipient sheaflike appearances when viewed on edge (i.e., along any axis in the plane of the respective cross sections depicted in figure 11). A view is shown in figure 12 including a few "notched" aggregates of the type shown in figure 11c, d lying flat on a substrate and several other nonspherulitic aggregates similar to those described above, oriented with their plane of preferential growth parallel to the axis of the phase contrast microscope.

A comparison of the relative sizes and corresponding habit features of the types of aggregates shown in figure 11 which had all formed under the same conditions as the elliptical structures shown in figures 8 and 10, indicates an evident size-habit trend (increased convexity of the lateral sides and progressive filling in of the re-entrant extremities) which strongly suggested that these structures might well represent early successive stages in the formation of the larger "elliptical" structures (figs. 8 to 10), but further development of which had been arrested due to depletion of the polymer from the solution. By the same token, since the spherulites (fig. 7) that are formed under the same conditions as the types of aggregates described above were larger than the elliptical structures formed at the same temperatures in individual solutions, the possibility was envisaged that the elliptical and other aggregates are representative of the early successive transient structures that develop progressively during the initial stages of growth of individual monoclinic spherulites. This was confirmed by some experiments described below.

b. Direct Microscopic Observations of the Growth of Monoclinic Spherulites From Concentrated Solutions of Polypropylene in Mineral Oil

The procedure adopted in these experiments was facilitated by the low volatility of the mineral oil at the temperatures at which the experiments were carried out. Appropriate weights of powdered polypropylene and mineral oil were deposited on a microscope slide at room temperature. The polymer-solvent mixture was then covered with a thin coverglass and placed in the heating chamber of a Leitz heating stage (Model 350) mounted on the rotating stage of a phase contrast microscope. The temperature of the heating stage was then raised to 200 °C and maintained at that temperature for approximately 10 min. The temperature was then lowered by suitable adjustment of the current supply to the hot stage and maintained within ± 1 °C of a predetermined temperature at which the rate of spherulite formation was slow enough to be recorded with a conventional photographic

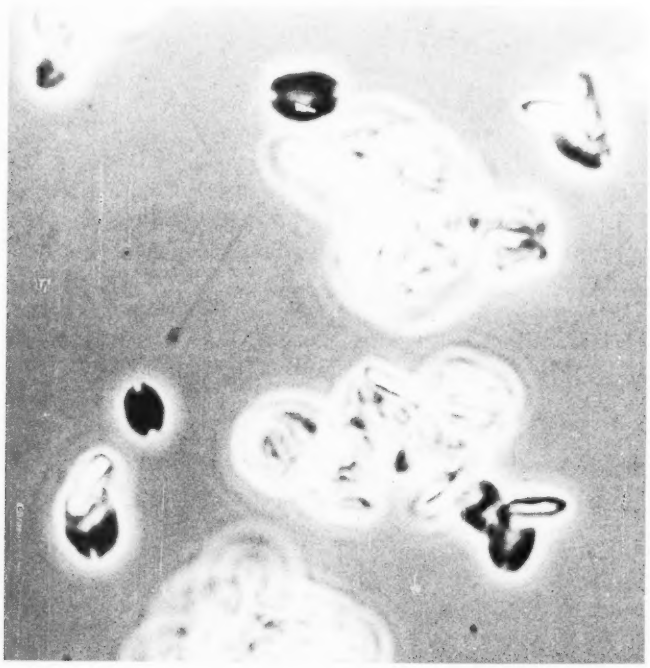

FIGURE 12. *General view including numerous randomly oriented aggregates from the same preparation as those shown in figures 7 to 11.*
Phase Contrast, × 660.

camera. The vertical size of the heating stage and the mechanically restricted vertical travel of the phase contrast condenser system used were such that suitable illumination could be obtained only for low and medium power phase contrast objectives. All direct observations and photographic recordings were made using a × 20 phase contrast objective. The sequences described below were recorded within a period of 30 to 45 min.

A sequence of micrographs depicting successive stages of growth of an individual positively birefringent monoclinic spherulite from a 5 percent (w/w) solution of the polymer at 113 °C is shown in figure 13 (a to h). The thickness of the solution between the glass slides was of the order of 50 μ. The similarity between the profile of the initial successive transitional structures depicted in figure 13a,b, and that of the aggregates shown in figure 11c,d, and figure 12 is clearly evident.

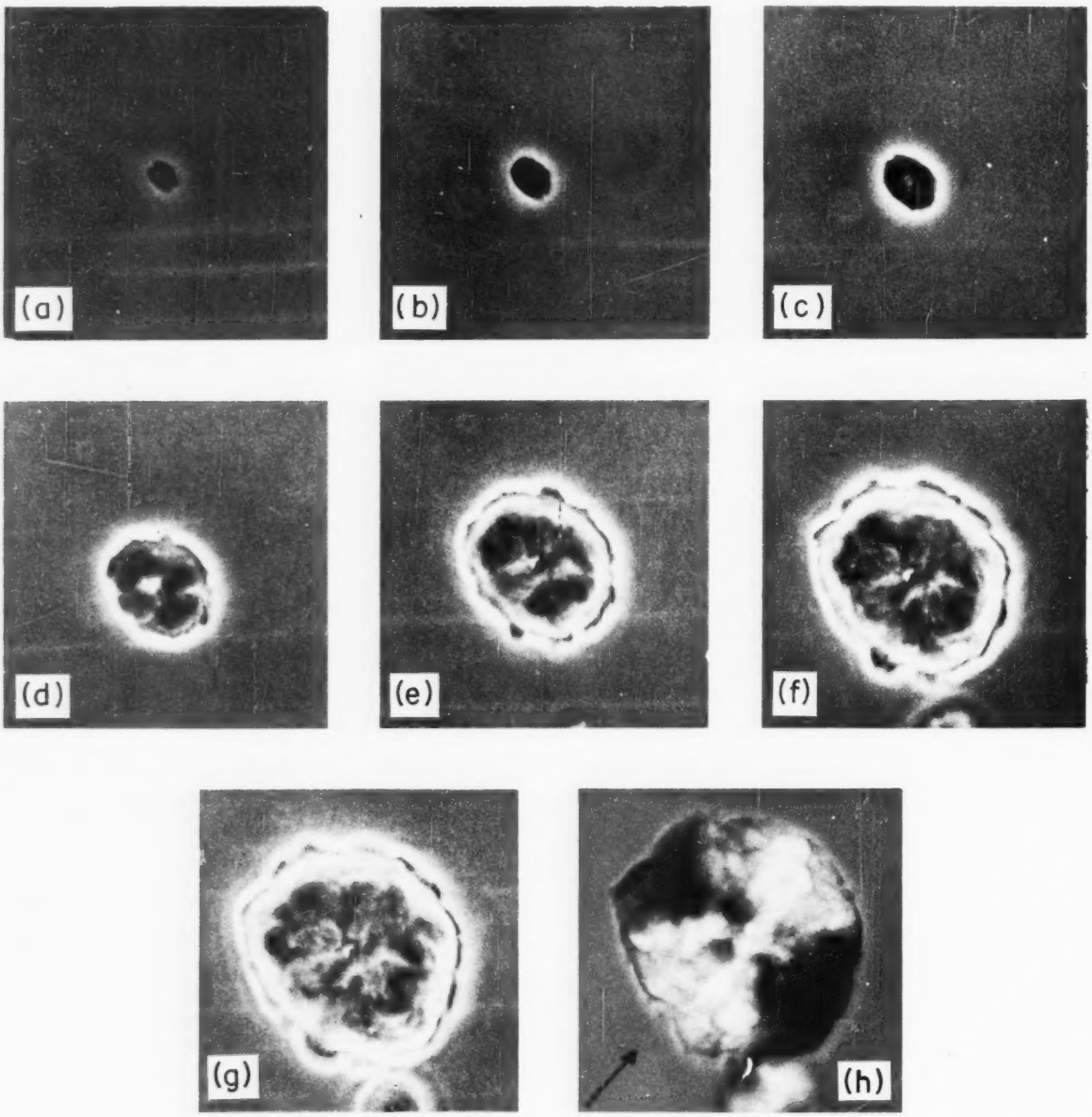

FIGURE 13. *Time lapse sequence depicting the growth of a positively birefringent spherulite from a 5 percent solution of polypropylene in mineral oil at 113 °C.*

(a–g) Phase contrast. (h) Crossed polarizers and 1/4 λ compensator (arrow indicates slow direction of vibration of compensator). × 670.

Note the convex lateral edges of the successive structures shown in figure 13a,b, and the re-entrant or notched appearance these transitional aggregates exhibit at opposite extremities. This latter feature, which is less pronounced at the more advanced stage of development represented in figure 13b, becomes progressively less evident on subsequent growth and disappears eventually, at which stage the developing structure exhibits an essentially elliptical profile (as seen in figure 13c,d) which corresponds to that of the aggregates shown in figures 8 and 10. Subsequent stages of growth culminating in the development of a monoclinic spherulite are shown in figure 13 (e to h). Figure 13h represents the spherulite thus formed as seen between crossed polarizers and a quarter wave compensator revealing its positively birefringent character.

In some instances it was possible to observe and record the growth of individual spherulites at even earlier stages of development than has been depicted

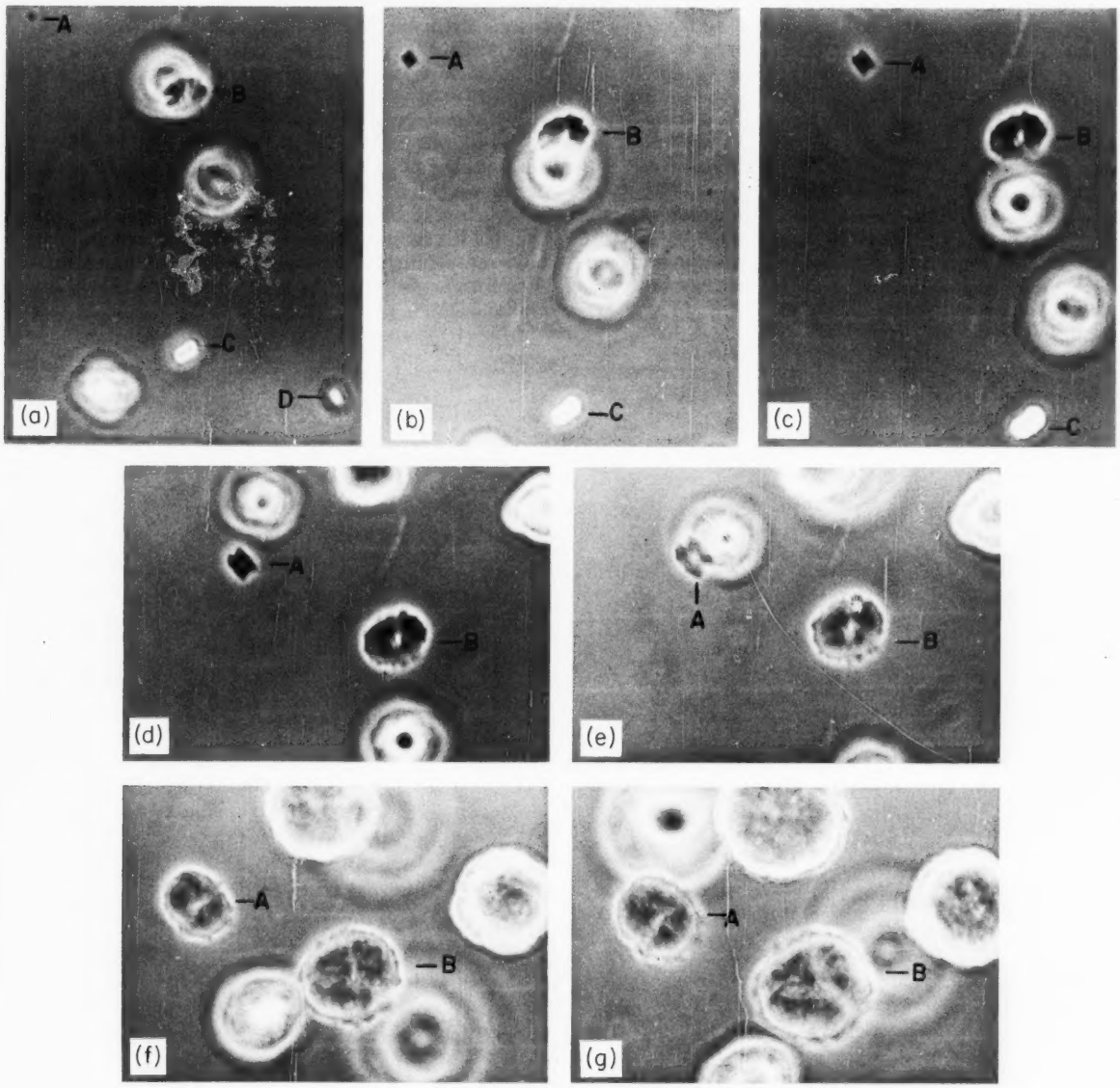

FIGURE 14. *Time lapse sequence depicting successive early stages (A) in the growth of a positively birefringent spherulite from a 12 percent solution of polypropylene in mineral oil at 116 °C.*

Identity of (A) which was moving slowly in solution is facilitated by reference to companion aggregate (B) which was moving along with it. Note rectangular profile of (A) in frame (b), a very slight concavity of its shorter edges may be detected. See text for comments on (C), (D) in frames (a–c). Phase Contrast. ×410.

in the sequence shown above. Correspondingly, the very initial resolvable precursor structure was found to exhibit (when appropriately oriented) a rectangular (almost square) profile. Early stages of development of an individual monoclinic spherulite from a 12 percent (w/w) solution of polypropylene in mineral oil at 116 °C are depicted in the sequence of micrographs shown in figure 14. The particular structure (A) the growth of which was followed in this sequence was moving very slowly in the solution; its identity is confirmed in figure 14 (a to g) by a reference aggregate (B), at a more advanced stage of growth, which was moving along with it (note the elliptical profile of B).

The apparently rectangular (almost square) profile of the first clearly resolvable precursor seen in figure 14b is evident. At the growth stages depicted in figure 14c,d the profile of the growing structure can be seen to correspond with that of the smallest and rarer aggregates (of the type shown in fig. 11a,b) described in the previous subsection. Note the longer lateral edges and the distinctly cusped appearance (concave with respect to the interior) of the shorter edges of the growing aggregate (A) in figure 14c,d. The aggregate subsequently assumes on further growth a profile similar to that of the structures shown in figure 11c,d. At the more advanced stages of growth depicted in figure 14 (f to g) the aggregate may be seen to exhibit an essentially elliptical profile—it eventually developed into a positively birefringent spherulite.

On the basis of the evident similarity between the transient precursors seen in the sequences shown in figures 13, 14, and the aggregates described in the previous subsection (3.2a), it is to be expected that their appearance would vary significantly depending on their orientation with respect to the direction of viewing, hence the contrasting appearance of precursors C (fig. 14 a to c) and D (fig. 14a). It may be readily deduced that they are respectively oriented with their plane of preferential development essentially normal to the plane of the field of view photographed in figure 14.

In summary, the observations described in this section provide a gross insight into the nature of the early stages of development of monoclinic spherulites of polypropylene. Further opportunity to characterize in finer detail the early stages of development of such spherulites is clearly provided by the ready accessibility of the representative precursors of the spherulites formed from the ¾ percent mineral oil solutions.

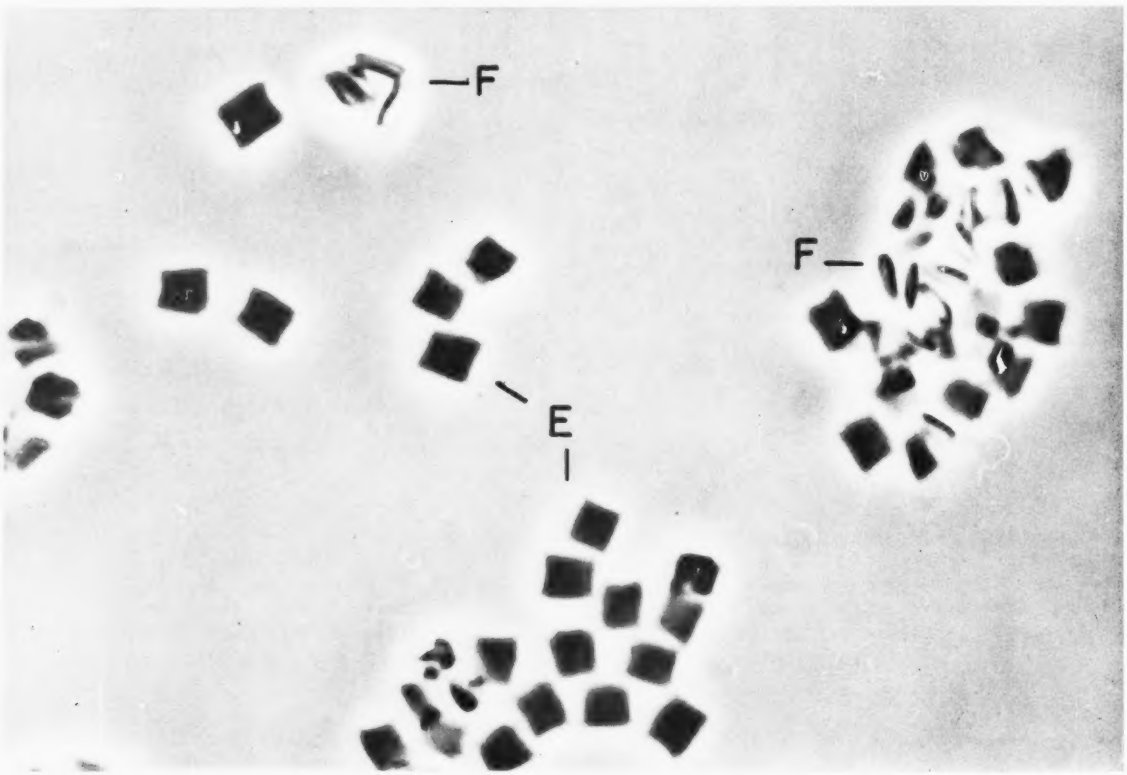

FIGURE 15. *Pseudopolyhedral aggregates grown from a 0.75 percent solution of polypropylene in amyl acetate at 114 °C.*
(E) denotes aggregates lying with their plane of preferential development parallel to the substrate. (F) denotes the same type of aggregate viewed edge-on. Note rectangular profile of aggregates (E) as well as the slightly concave nature of their shorter edges. Phase Contrast. × 1,400.

Clearly these structures can be readily isolated from the latter preparations and subjected to an electron microscopic study using replicating techniques in order to characterize the nature of their fine structure.

The apparently polyhedral earliest precursors which develop during the initial stages of formation of the spherulites are of particular initial interest, however. Similar essentially planar objects exhibiting a square or slightly rectangular profile have been respectively observed by Leugering [13] and Geil [14] to form during the initial stages of growth of monoclinic spherulites from the melt. In short, the formation of such initial structures is not a peculiar characteristic of the mode of growth of monoclinic spherulites under the specific conditions of crystallization described in this section—it is evidently a phenomenon of more general occurrence. The discovery that 3/4 percent solutions of polypropylene in amyl acetate yield, at temperatures between 110 to 115 °C, monoclinic crystalline aggregates the shape of which (see fig. 15) coincides with that of the above-mentioned initial apparently polyhedral precursors of monoclinic polypropylene spherulites, was therefore particularly gratifying [15]. The outcome of an optical and electron microscopic study, which has led to the characterization of the highly unorthodox structure of these model counterparts of the earliest microscopically resolvable spherulite precursors, is discussed in the ensuing section. It will be shown that they are not polyhedral objects, but possess instead a complex fine structure which is distinctly dendritic in character.

4. On the Morphology of Model Counterparts of the Pseudopolyhedral Precursors of Monoclinic Spherulites of Polypropylene

The observations presented in this section were derived from an optical and electron microscopic study of crystalline aggregates grown from 3/4 percent solutions of polypropylene in amyl acetate at 114 °C. Within 6 hr at that temperature the solutions exhibit a very faint cloudiness indicating the onset of crystallization. The particular solution from which the aggregates shown in figure 15 were formed was held at 114 °C for 10 days. At the end of this period, the solvent and suspended aggregates were poured into a special filtration vessel maintained at 114 °C. The type of vessel used was essentially similar in design to a filtering apparatus previously described by Bassett et al., [16]. The preparation was filtered isothermally and washed several times with fresh amyl acetate preheated to 114 °C. Care was taken not to allow the filtrate to dry between successive washings. After a final addition of hot fresh solvent, filtration was stopped, and the vessel allowed to cool to room temperature.

The characteristic monoclinic [3] wide angle x-ray diffraction pattern (powder pattern) obtained from a sample consisting of randomly oriented aggregates formed at 114 °C is shown in figure 16.

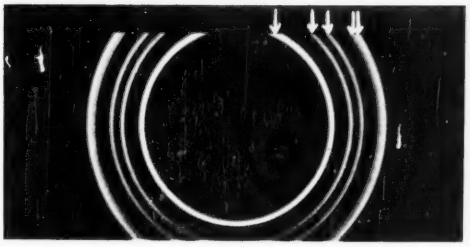

FIGURE 16. *Wide angle x-ray powder pattern from a sample consisting of pseudopolyhedral structures of the type shown in figure 15.*
The inner 110, 040, 130 and composite 111, 13$\bar{1}$, 041, monoclinic polypropylene rings are indicated by vertical bars.

4.1. Observations Derived From Optical (Phase Contrast) Microscopy

Examination of the aggregates formed in the preparation described above at high magnifications under the phase contrast microscope as they tumbled in suspension in liquid revealed that they possess a planar habit, and that when viewed along an axis normal to their plane of preferential development (e.g., the aggregates marked (E) in fig. 15) they exhibit an essentially rectangular (almost square) profile. Characteristically however, the shorter of the two pairs of lateral edges appear either slightly cusped near the apices or are slightly curved, concave with respect to the interior of the aggregate. The length of the longer pair of lateral edges was generally in the range 5 to 7 μ. The thickness of these structures along the axis normal to their plane of preferential development, i.e., along the direction normal to the cross section whose peripheral characteristics have been just described, is of the order of 1 to 2 μ. When viewed edge-on as is the case of aggregates marked (F) in figure 15, they exhibit a rodlike or blunt spindlelike appearance.

In so far as one could ascertain under the optical microscope the aggregates appeared to possess substantial overall rigidity. No detectable changes in profile were observed under the phase contrast microscope when they were allowed to dry in air at room temperature. This feature is further confirmed by the electron microscopic observations presented below and will be discussed in a later part of the paper.

4.2. Observations Derived From Electron Microscopy

a. Direct Examination in Transmission

The aggregates were deposited on electron microscope grids covered with a carbon film and examined directly in the electron microscope. It became immediately evident that they were highly susceptible to the electron beam. At levels of illumination that were high enough to permit clear visual examination of the image formed on the fluorescent screen of the microscope, the aggregates were invariably observed to shrivel up extremely rapidly. This drawback was

overcome by scanning the grids and photographing the aggregates at very low intensities and by limiting the area of the specimen grid exposed to the electron beam at any given time to approximately one grid square. This was accomplished by the conventional method of using the double condenser system of the microscope and appropriately defocusing the second condenser lens.

Under such conditions of low illumination it was possible to discern only faintly the outline of individual aggregates on the microscope screen. Consecutive micrographs recorded within 30 sec of exposure of individual aggregates to the electron beam under such conditions of low "illumination" revealed no detectable morphological changes in that period of time. Within two minutes, however, substantial changes in overall shape were discerned, even visually.

Electron micrographs depicting three individual aggregates photographed immediately after being exposed to the electron beam are shown in figures 17, 18, and 19a. These aggregates originate from the same preparation as the structures shown in figure 15. Two characteristic features detected under the optical microscope are clearly revealed in these electron micrographs, namely, the overall essentially rectangular profile of each aggregate and the slightly cusped or concave nature of the shorter "sides." The length to breadth ratio of the aggregates (as determined from the length of the central axes bisecting opposite sides) was generally found to be of the order of 1.1:1.

As would be expected from the 1 to 2 μ thickness of these structures they are essentially opaque to the electron beam, particularly so in the somewhat thicker central regions. Nevertheless, transmission electron micrographs generally revealed two characteristic morphological features. First, what appeared to be narrow diagonally oriented spikelike outgrowths were frequently seen protruding from the edges of the aggregates, as may be seen in particular in figures 17 and 19a. Second, a weakly discernible diagonally oriented cross-hatched appearance which could be traced from the peripheral regions for a limited distance into the interior, as may be seen for example in figure 18, was frequently detected in the electron micrographs.

In addition to the above-mentioned features apparently spurious lamellar single crystallike outgrowths, as may be seen for example near the apex (G) of the aggregate partially in view in figure 18, were occasionally observed in the peripheral regions of some aggregates.

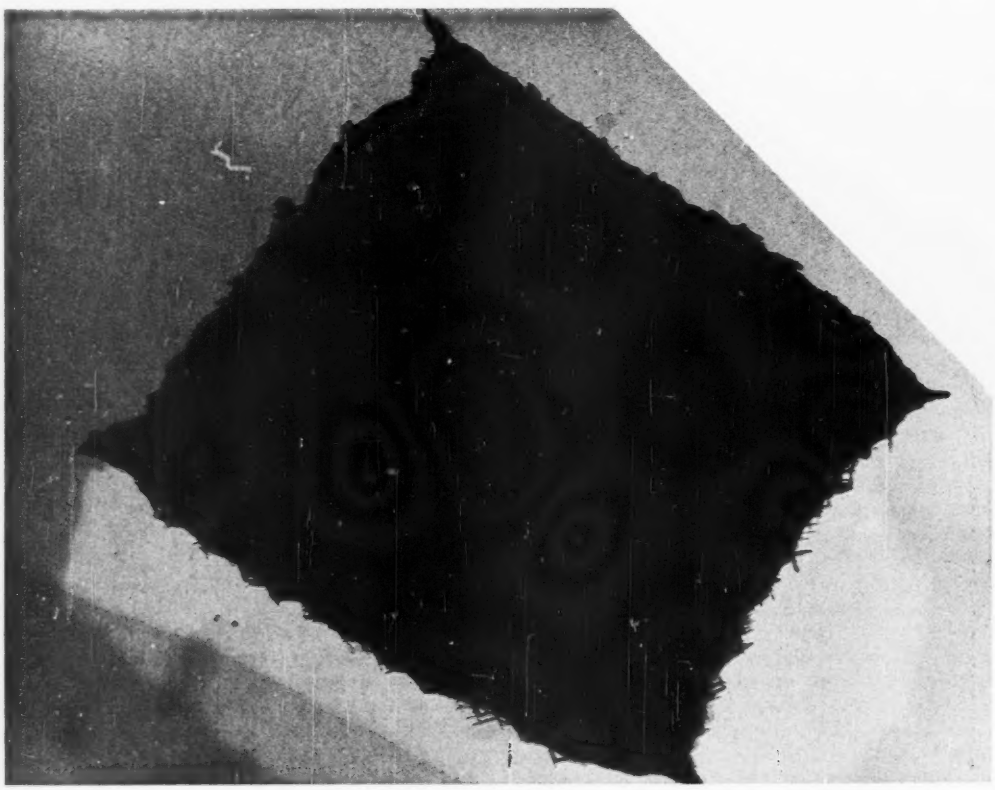

FIGURE 17. *Electron micrograph of a pseudopolyhedral polypropylene aggregate of the type shown in figure 15.* Note overall essentially rectangular profile of the aggregate as well as the diagonally oriented spikelike outgrowths protruding from its periphery. Also note slightly concave profile of one of its shorter "sides." Shadowed (Pt.-Pd). × 16,800.

The consequence of prolonged exposure to the electron beam is shown in figure 19b. The aggregates were always observed to undergo preferential overall shrinkage along a direction normal to their longer axis as may be readily ascertained by comparing figure 19a and figure 19b. No further change in aspect was observed beyond the stage of shriveling depicted in the latter electron micrograph even when the intensity of illumination is substantially increased. The specificity of the mode in which the aggregates deform remains unexplained. The change they undergo when exposed to the electron beam is primarily attributable to melting or partial melting resulting from the heating effects of the electron beam and the poor dissipation of heat generated by the impinging electrons due to the low thermal conductivity of the aggregates and their supporting carbon film. It is to be expected that the polypropylene chains undergo cross-linking on exposure to the electron beam [17]. On the basis of established experience, for example contrasting the behavior of these aggregates with that of polyethylene single crystals, it may be readily assumed that the occurrence of cross-linking (which leads to a loss of crystallinity in polyethylene crystals without their undergoing a change in shape) is not the prime factor leading to the drastic deformation which the aggregates undergo when irradiated.

b. Electron Microscopic Examination of Surface Replicas

In order further to elucidate the nature of the fine structure of the aggregates, replicas of their large surfaces were prepared using the method of shadow transfer. For this purpose, the aggregates were initially deposited on a glass slide and allowed to dry in air at room temperature; they were then shadowed with metal (80 percent Pt-20 percent Pd alloy). A backing film of carbon was subsequently evaporated onto the shadowed aggregates on the slide. The resulting composite metal-carbon "film" thus formed was floated over distilled water. The aggregates were found to adhere to the film, portions of which

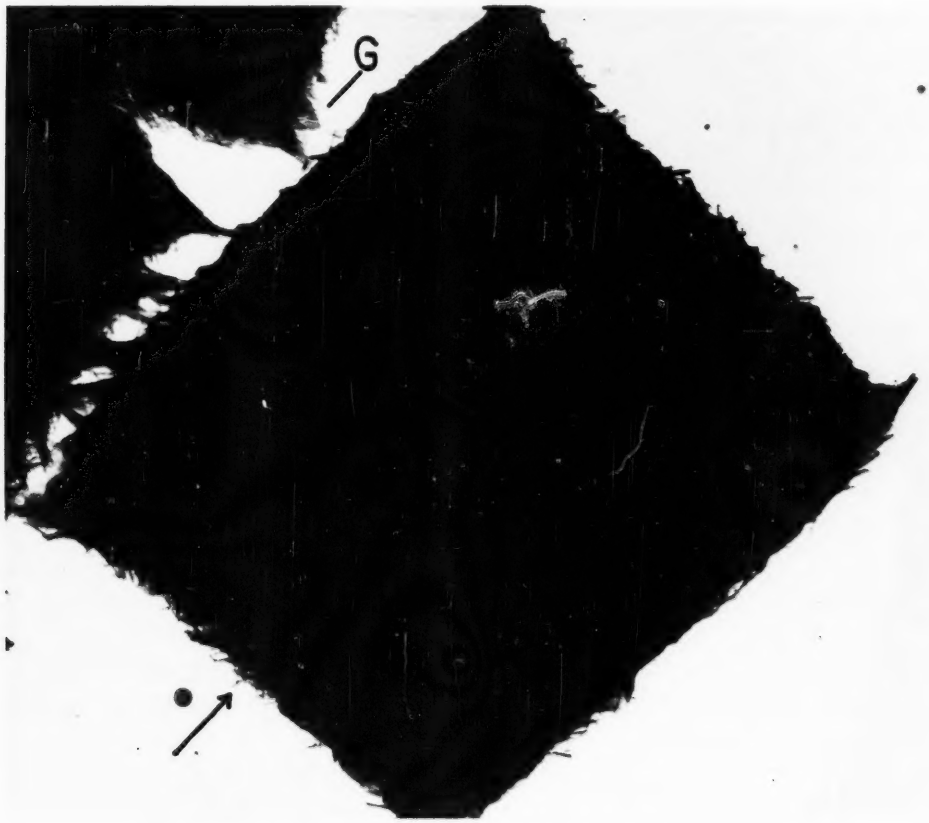

FIGURE 18. *Electron micrograph of a pseudopolyhedral polypropylene aggregate.*
Note the faintly discernible diagonally oriented cross-hatched appearance extending inwards from one of the shorter edges of the aggregate indicated by the arrow near the left-hand corner of the figure. Also note apparent lamellar character of outgrowths (G) near the apex of another neighboring aggregate. Shadowed Pt-Pd × 16,400.

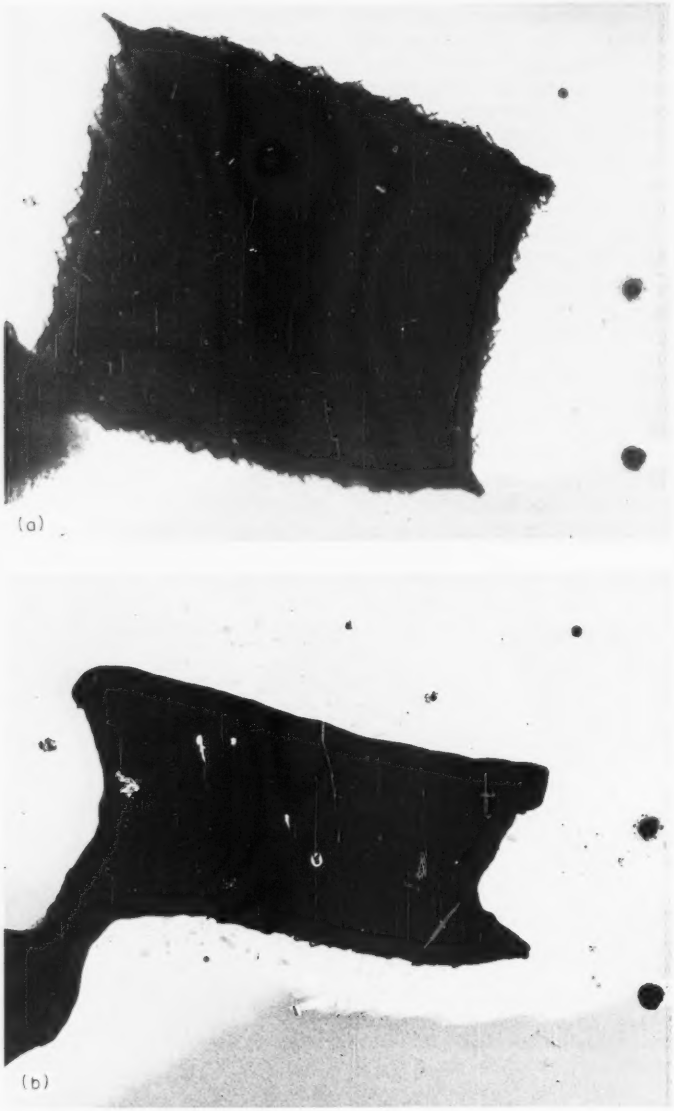

FIGURE 19. *Electron micrographs depicting effect of prolonged exposure to the electron beam.*

(a) Micrograph recorded at low intensity immediately after exposure to the electron beam. (b) Micrograph of same aggregate after 2 min exposure to the electron beam. Note characteristic preferential shrinkage at right angles to the longer edges of the aggregate. Shadowed (Pt-Pd) × 13,300.

were then picked up on electron microscope grids and allowed to dry in air at room temperature. Some difficulty was encountered in dissolving the aggregates from the metal-carbon replicating medium but they were effectively dissolved by immersing the replicas supported on the grids in excess distilled decalin, heating the solvent to 160 °C, and maintaining it at that temperature under a blanket of nitrogen for 18 hr.

Replicas of the large aggregate surfaces prepared in the manner described above revealed, as may be seen in figure 20, a distinct cross-hatched surface texture consisting of a network of narrow (150 to 200 Å) apparently intercrossing structural units which traverse the surface for varying distances diagonally

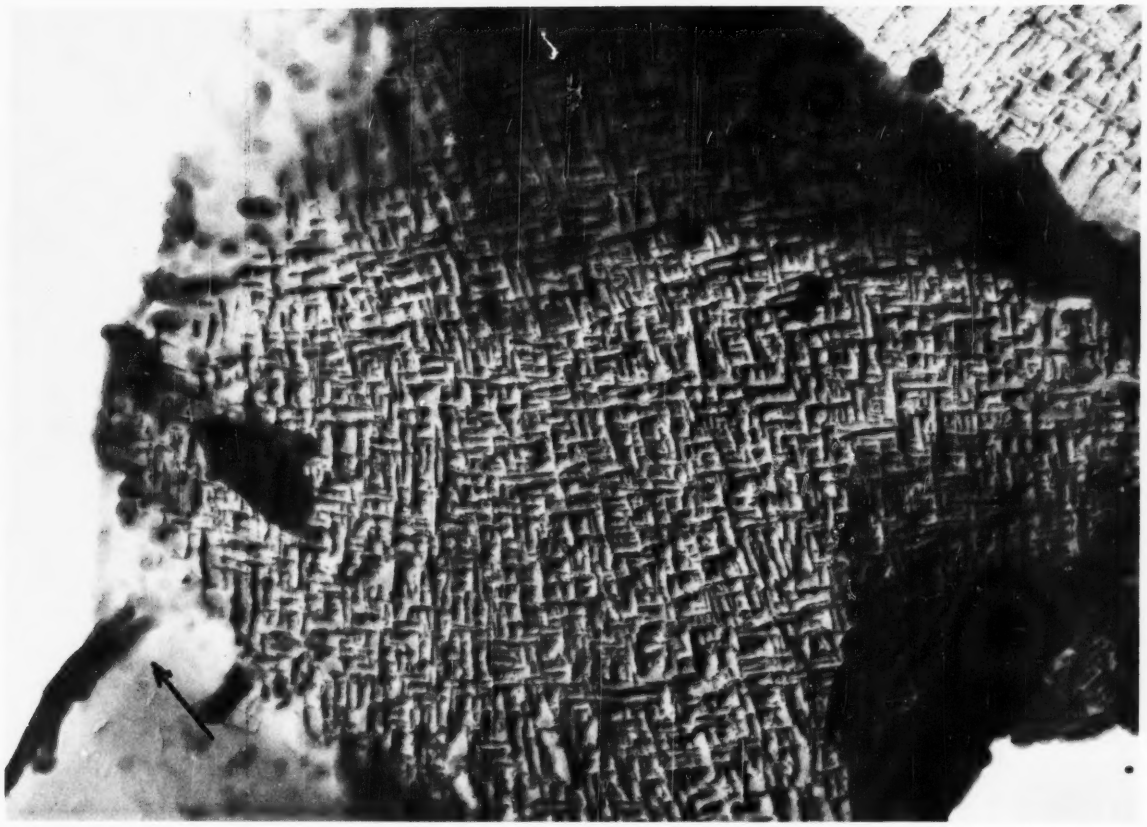

FIGURE 20. *Electron micrograph of a shadow transfer replica of the surface of a pseudopolyhedral polypropylene aggregate.* Arrow in left hand corner of micrograph indicates orientation of longer lateral edges of the aggregate. Note distinct cross-hatched surface texture consisting of a network of narrow (150 to 200 Å) apparently intercrossing structural units which traverse the surface diagonally with respect to the rectangular periphery. ×24,100.

with respect to the aggregate periphery. A magnified view of the central portion of the replica depicted in figure 20 is shown in figure 21 in which the dense but not compact network of narrow diagonally oriented structural units is clearly seen.

In summary, the preliminary morphological observations derived from the examination of the aggregates in transmission and by replication clearly established that they possess a composite fine structure having the earmarks of a crystallographically specific pattern of growth which is dendritic in character—the narrow diagonally oriented structural units being readily identifiable as elementary (primary, secondary, etc.) dendrite branches.

On the basis of the foregoing morphological observations several questions immediately arose, inter alia: How is growth propagated normal to the plane of preferential development of the aggregates? What is the nature of the molecular organization in the constituent branches? A possible clue relating to the nature of both these aspects was provided by the occasionally observed lamellar, and hence one could reasonably presume chain-folded, single crystallike peripheral outgrowths revealed, as mentioned earlier, in transmission electron micrographs of some aggregates. The apparently spurious nature of these lamellar outgrowths seemed inconsistent with the highly organized fine structure revealed by the surface replicas (in particular) which evidently reflected a highly specific mechanism of growth. This consideration led to the conjecture that these lamellae might simply be individual branches of the type revealed by the replicas (the narrow diagonally oriented structural units pointed out in figs. 20 and 21) which, however, were being seen in a different perspective as a consequence of localized distortions undergone inadvertently by the aggregates in their peripheral regions on being transferred to, or during subsequent drying on, the electron microscope sample grids.

In short, the possibility was considered that the narrow diagonally oriented branches revealed by the replicas are lamellar chain-folded single crystallike structures whose fold surfaces are normal or preferentially normal to the aggregate plane of preferential development. Clearly, this would readily account for the apparent uniform width of the branches when viewed along that same direction. Substantiation of the foregoing conjectures is presented below.

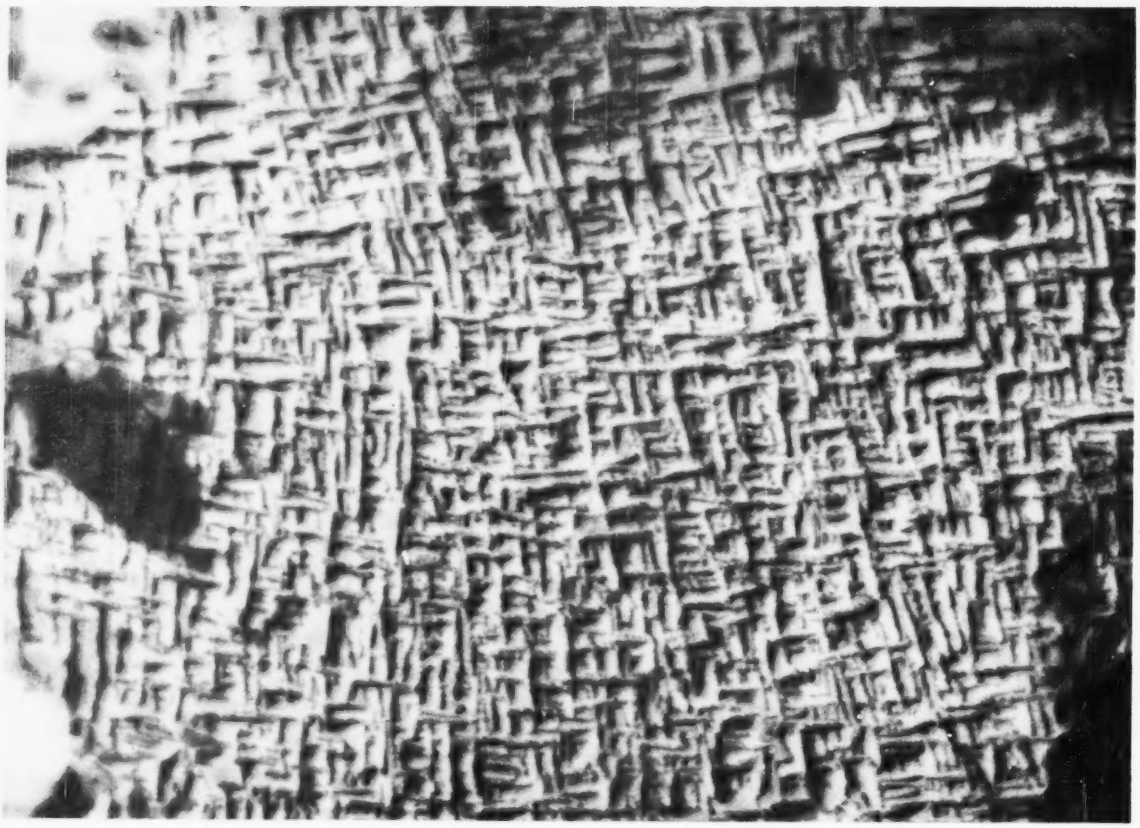

FIGURE 21. *Magnified view of central portion of replica shown in figure 20.*
Note dense but not compact network of intercrossing structural units. ×39000.

c. Morphological Observations on the Pseudopolyhedral Spherulite Precursors Isolated From the Mother Liquor at an Early Stage of Growth

Further elucidation of the nature of the internal structure and mechanism of growth of the aggregates discussed in the previous two subsections was provided by isolating such aggregates from the mother liquor at a relatively early stage in their growth and examining the fine structure of these smaller (and hence more electron transparent) precursors electronmicroscopically in transmission.

Examination under the phase contrast microscope of aliquot samples removed periodically from a ¾-percent solution of polypropylene in amyl acetate from which the polymer was crystallizing at 114 °C, revealed that after a period of approximately 9 hr at that temperature, the average size of the aggregates formed was approximately half that of those discussed in the preceding subsections. At this point the solution was filtered isothermally in the manner described earlier. Fresh solvent preheated to 114 °C was added intermittently to the preparation during filtration to wash away polymer still in solution. Care was taken not to allow the residue to dry between successive additions of fresh solvent in order to prevent the formation of a compact mat of aggregates on the filter which might be difficult to redisperse. Inevitably however, the aggregates were repeatedly drawn together during the process of filtration thus giving rise to a high incidence of random interaggregate impingement and subsequent adherence as a consequence of superficial intergrowing at regions of contact particularly during the early stages of filtration.

The intergrowing and consequent adherence of groups of randomly oriented aggregates as rigid clusters which remained as such after transfer and drying on the carbon coated electron microscope grids proved to be highly beneficial. It provided, as demonstrated below, a means of examining aggregates in widely different perspectives ranging from "normal" to edge-on viewing; [7] clearly such widely divergent viewings, equivalent to tilting an individual aggregate through 90° could not have been easily accomplished otherwise in the electron microscope.

[7] i.e., along directions normal to their plane of preferential development and along directions parallel to their plane of preferential development respectively.

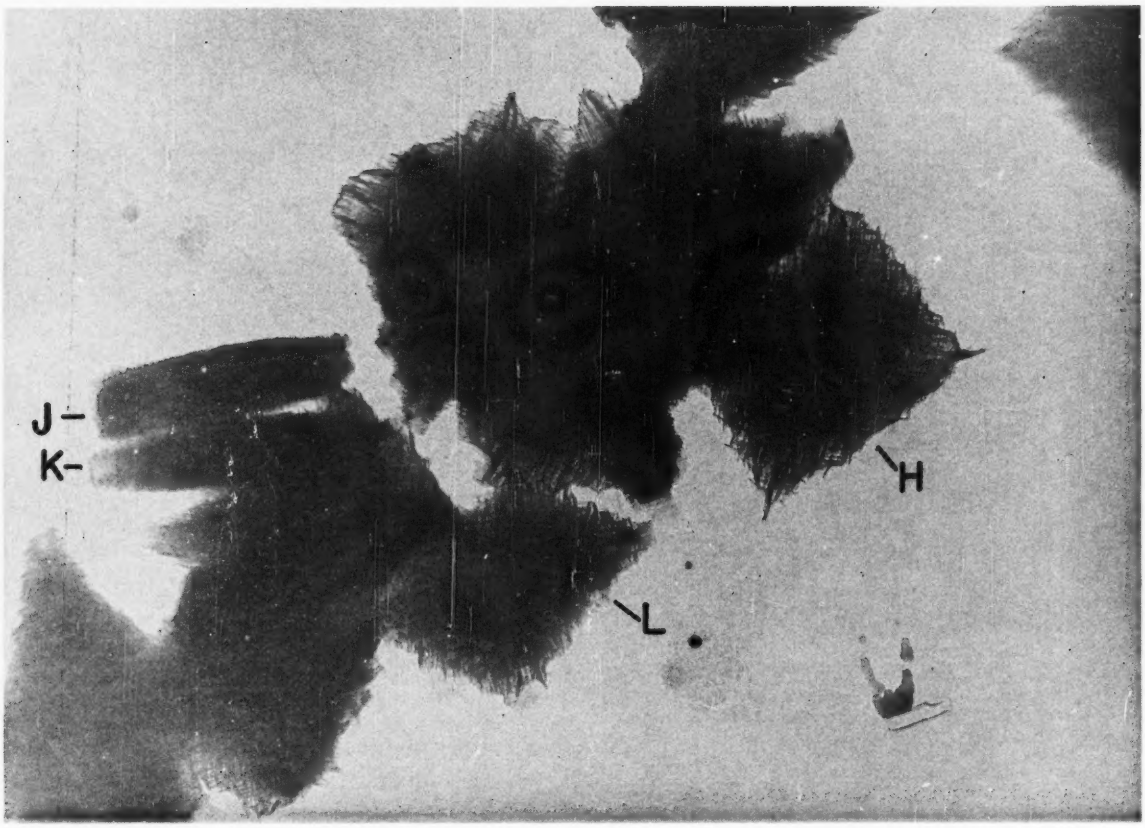

FIGURE 22. *Electron micrograph of a cluster of variously oriented "half-grown" pseudopolyhedral polypropylene aggregates.*
(H) is oriented with its plane of preferential development at right angles to the microscope axis, (J) and (K) are viewed edge-on, and (L) is an aggregate at an inclination intermediate between the extreme orientations represented by (H), (J) and (K). ×12,800.

An electron micrograph depicting a cluster of "half-grown" aggregates isolated from the mother liqour at 114 °C in the manner described above, is shown in figure 22. Characteristically the aggregates are variously oriented; in particular, aggregate (H) (note its rectangular profile) is oriented "normally" with respect to the microscope axis, whereas aggregates (J) and (K) are oriented on edge. The plane of aggregate (L) is inclined to the substrate. It should be pointed out that these "half-grown" aggregates were found also to be susceptible to the heating effects of the electron beam, hence the precautions described earlier (i.e., scanning and photographing at low beam intensities and suitably limiting the area of a specimen grid exposed to the electron beam at any time) had to be resorted to. The characteristic morphological features exhibited by the aggregates when viewed "normally" and edge-on are considered in detail below.

An examination of electron micrographs of aggregates oriented with their plane at right angles to the electron beam revealed the following structural characteristics which may be readily discerned in the representative aggregate shown in figure 23. First, they exhibit an overall rectangular (almost square) profile, their length to breadth ratio being of the order of 1.1:1. On average they were found to be about 2.5 μ long. Second, they exhibit a highly regular fine structure consisting of a dense but not compact "network" of narrow diagonally oriented branches. This evidently dendritic cross-hatched fine structure could in all instances be traced throughout each aggregate thus oriented from the thicker central regions to the periphery. The width of the constituent branches (based on the measurement of those branches that are individually resolvable in the peripheral regions) is of the order of 150 to 200 Å.

On the basis of geometric considerations (length/breadth ratio), the acute angle subtended at the center of the crystals by the diagonally oriented branches (i.e., the angle subtended at the center by the shorter aggregate edges) is estimated to be ~85°. Accurate direct interbranch angular measurements are frustrated by the overall opacity of the crystals which are 0.5 μ–0.75 μ thick.

These observations further confirmed that the cross-hatched surface structure revealed by the replicas of the larger precursors described earlier is character-

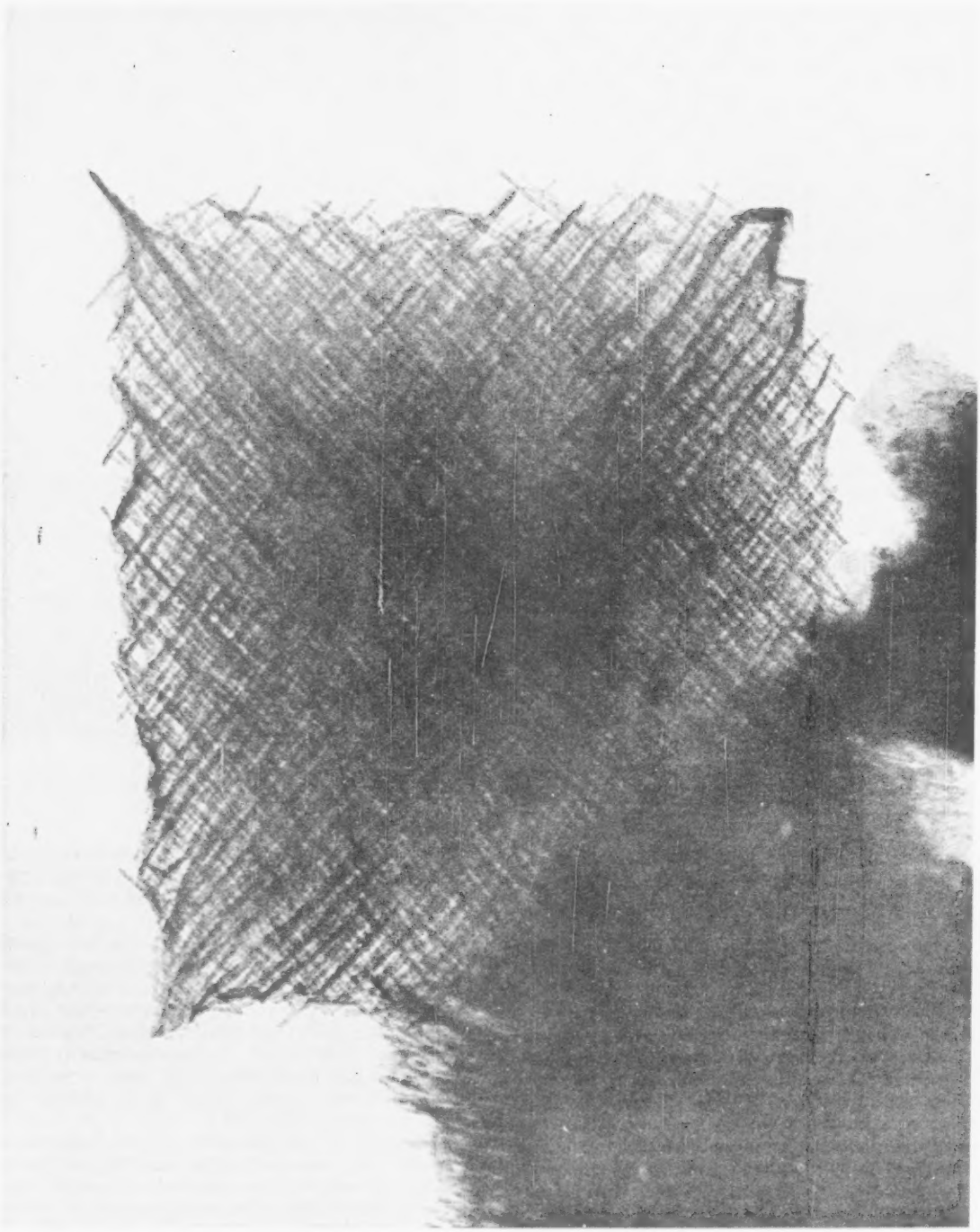

FIGURE 23. *Electron micrograph revealing the distinctly dendritic crystal character of the polypropylene aggregates grown from 0.75 percent solutions of polypropylene in amyl acetate at 114 °C.*
Note rectangular overall profile of the crystal as well as network of narrow diagonally oriented branches. ×49,900.

FIGURE 24. *Electron micrograph of potypropylene dendrite similar to that shown in figure 23 but viewed edge-on.*
Note cigar shaped profile of the dendrite as well as lamellar outgrowths (arrows) protruding at both extremities. ×53,000.

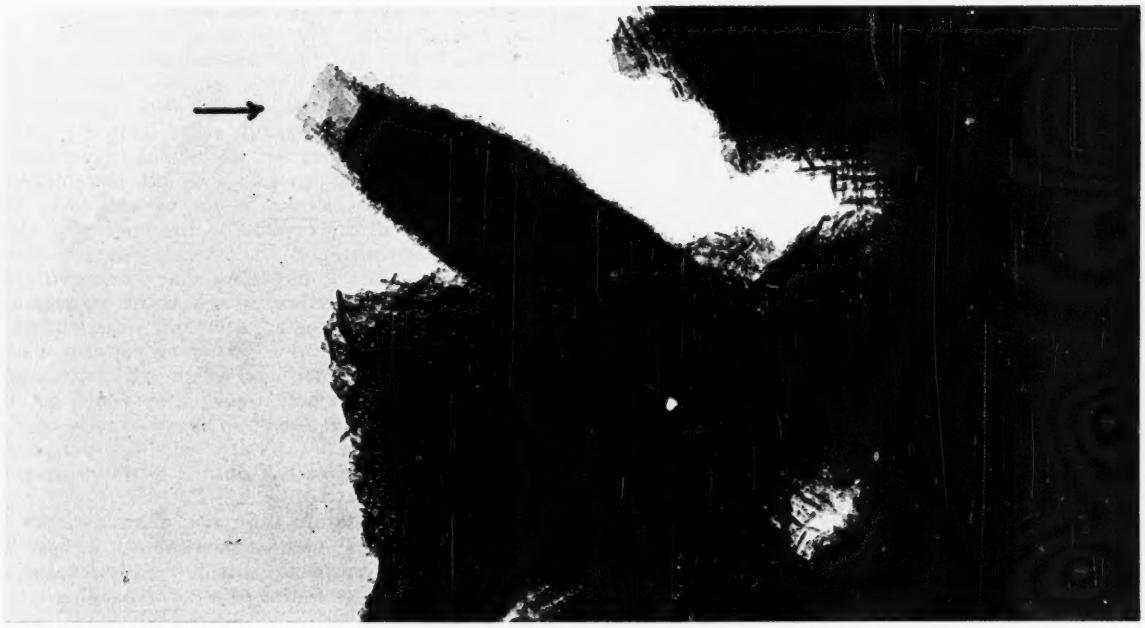

FIGURE 25. *Cluster of dendrites from same preparation as those shown in figures 22 to 24.*
Note lamellar outgrowths (arrow) at extremity of dendrite viewed edge-on. ×26,100.

792-867 O-66-4

istic of their internal structure. The continuity of the same dendritic pattern of branch propagation parallel to the plane of preferential development of the smaller precursors just described and the larger aggregates discussed in the previous subsections is evident. Some loss of specificity in the mode of propagation of the branches as these dendrites become larger is however suggested by regional deviations in parallelism of the branches revealed by the replicas of the bigger dendrites and by the apparent concavity of their shorter "sides."

We turn now to a consideration of how these evidently dendritic crystals propagate along the direction normal to their plane of preferential development. In this respect the structural features exhibited by the smaller "half-grown" dendrites when viewed edge-on (as exemplified in fig. 22 (structures J, K) and figs. 24, 25) were examined. When viewed thus, i.e., along directions parallel to their plane of preferential development, they exhibit a cigar-shaped profile; they were on average found to be 0.75 μ wide at the center and somewhat narrower at the extremities, which is consistent with the observed decrease in overall opacity to the electron beam from the central to the peripheral regions when they are viewed as shown in figure 22 (H) and figure 23. In all instances in which the dendrites were examined edge-on, distinctly lamellar single crystallike outgrowths were observed protruding from their extremities as may be seen in figures 24 and 25; further the profile of these lamellae always formed a natural extension of the overall cigar-shaped contour of the dendrites (see both extremities of the dendrite shown in fig. 24 and the one visible extremity of the dendrite shown in fig. 25). This latter feature, coupled with the general observation that no such lamellae were seen protruding elsewhere in dendrites examined in edge-on perspective indicated that the lamellae are not spurious outgrowths but are the extremities of constituent diagonally oriented branches which extend from the interior to the rectangular periphery of the crystals.

The evidence presented in the preceding paragraph substantiates the proposition advanced earlier that the uniformly narrow diagonally oriented dendrite branches are chain-folded crystal entities whose fold surfaces are oriented at right angles to the dendrite plane of preferential development. These branches once formed can be readily visualized to develop in a continuous fashion at right angles to that plane as well as diagonally during the growth process. A simplified and essentially self-explanatory schematic representation of the mode of growth of these polypropylene dendrites as presently envisaged is shown in figure 26. For the sake of simplicity only four primary and two secondary branches are depicted; their respective fold surfaces (f) (i.e., the faces between which the molecules fold back and forth) are also identified. Clearly, profuse crystallographically specific branching involving a dihedral angle of $\sim 85°$ between the fold surfaces in parent and offspring branches is envisaged.

The apparent overall rigidity of the dendrites may be attributed to interlocking at points where branches impinge and grow "around" one another as depicted in figure 26.

It should be emphasized at this stage that the pattern of development exhibited by these dendritic crystals is highly unusual. It is common experience that solution-grown chain-folded polymer crystals (lamellae) generally thicken along a direction normal to their fold surfaces through the agency of screw dislocations (with Burger's vectors parallel to the chain segments). These dislocations give rise to the formation of additional chain-folded terraces which are coplanar with the basal lamella.[8] As far as this author is aware, no previous instances have been reported, in the context of chain-folded crystals of other polymers, of the occurrence of the repeated formation of lamellar outgrowths the fold surfaces of which are oriented at a substantial and specific angle ($\sim 85°$ in the present instance) to the fold surfaces of the parent lamellae from which they have grown, as exemplified by the polypropylene crystals described herein.

Further elucidation of the structure and mechanism of growth of these unusual dendritic crystals clearly required their characterization on a crystallographic basis. Some observations pertaining to the nature of the molecular orientation in the dendrites are presented below.

d. On the Crystallography of the Dendrites

The birefringent properties of the dendrites were determined by examining the crystals orthoscopically under a polarizing microscope while they were in suspension in amyl acetate and other liquid media at room temperature. The resulting observations are described below and their significance in so far as providing a rough indication of the nature of the molecular orientation in the dendrite branches is discussed in conjunction with some limited electron diffraction data. Electron diffraction experiments have been somewhat frustrated by the instability of the crystals in the electron beam, as well as by the overall opacity of the crystals to the impinging electrons. In a few instances the crystals were preserved long enough at low illuminations that a selected area electron diffraction pattern as well as the corresponding selected area including a crystal were recorded photographically. The few diffraction patterns which have so far been recorded, and which will be discussed presently, were extremely weak; they could not be discerned visually on the fluorescent screen of the electron microscope. Evidently only the peripheral regions of the dendrites contributed to the diffraction patterns.

The room temperature extinction characteristics of the larger dendrites (such as those shown in figs. 15, 17 to 21), when variously oriented with respect to crossed polarizers as well as the corresponding inter-

[8] The situation is somewhat more complex in the case of hollow pyramidal crystals. In such instances the additional layers are also hollow pyramidal and coaxial with the "basal" layer [18].

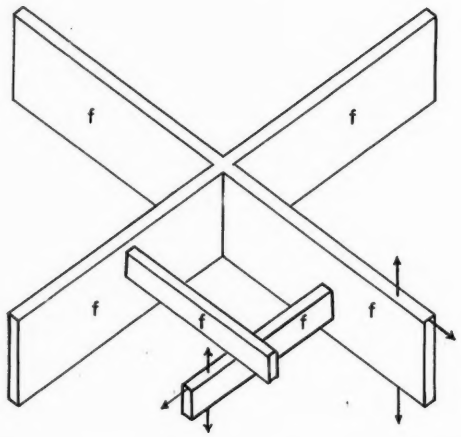

FIGURE 26. *Simplified schematic representation of the structure and mode of branch propagation of the polypropylene dendrites described in figures 15 to 25.*
The faces between which the chain molecules in individual branches fold back and forth are denoted (f).

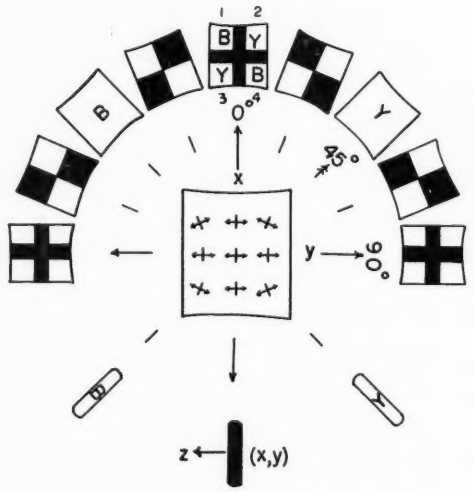

FIGURE 27. *Schematic representation of birefringent properties of the larger dendrites shown in figures 15 to 21.*
Shaded areas denote regions of extinction between crossed polarizers whose privileged directions of vibrations are horizontal and vertical in the diagram. B = 2nd order blue and Y = 1st order yellow interference colors observed when a 1st order red compensator is inserted between dendrite and analyser. Slow privileged direction of compensator is parallel to arrow pointing to 45° position. The orientation of the slow direction of vibration of light traveling at right angles to the *x,y* cross section of the dendrite is indicated by the arrowed arms of the crosses in the central diagram.

ference colors observed after insertion of a first order red retardation plate between the crystals and the analyzer, are summarized in figure 27.[9] For the sake of brevity in the ensuing discussion, the long and short axes which bisect the plane of the dendrites will be referred to as the *x* and *y* axes respectively, as shown in figure 27. The axis normal to the dendrite plane (i.e., the *x,y* plane) is denoted *z*.

When viewed along axes parallel to the *x,y* plane, the dendrites exhibit positive birefringence with respect to that plane (note interference colors when *x,y* plane is parallel to $\pm 45°$ positions in lower half of fig. 27) and become extinguished when the latter plane is oriented parallel to the privileged directions of the crossed polarizers (0° and 90° positions, lower part of fig. 27). When viewed along the *z*-axis, the dendrites exhibit throughout negative birefringence with respect to the *x*-direction (cf. interference colors with compensator inserted when *x* is at $\pm 45°$ to the privileged directions of the crossed polarizers, upper half of fig. 27). Consideration of the extinction characteristics and interference colors observed as a dendrite is rotated through 180° about the *z*-axis indicates however that whereas the slow privileged direction of vibration of light which has traversed the crystal is oriented normal to the *x*-axis in the regions situated along and adjoining the *x* and *y* axes, it deviates symmetrically by up to $\pm 22\frac{1}{2}°$ from that orientation in the regions close to the apices. The sense of this deviation in orientation of the slow privileged direction of vibration near each of the four apices is as indicated in the central diagram in figure 27.

The extinction characteristics of the smaller dendrites (from the same preparation as those shown in figs. 22 to 26) were also examined under the polarizing microscope. So far as could be ascertained, considering their small size, their optical properties were essentially similar to those of the larger dendrites. The deviation in extinction angle between the axial regions and the apices appeared to be somewhat less pronounced (i.e., $< 22\frac{1}{2}°$) than was the case in the larger dendrites.

Assuming that the refractive index ellipsoid of monoclinic polypropylene is uniaxial and positive and that the major axis of the ellipsoid is parallel (as indicated by calculations based on bond polarizabilities [18]) to the **c**-axis of the unit cell (i.e., parallel to the axes of the helical molecules), the positive birefringence exhibited by the dendrites with respect to the *x,y* plane (lower part of fig. 27) indicates that the chain molecules are preferentially oriented parallel to that plane. This was substantiated by an electron diffraction pattern (fig. 28a) obtained from a dendrite oriented edge-on (fig. 28b) with respect to the electron beam. In view of the opacity of the interior of the dendrite to the

[9] The same general characteristics depicted in figure 27 were exhibited by (i) as-grown crystals in suspension in amyl acetate, (ii) crystals which had been dried and reimmersed in either amyl acetate or Cargille immersion liquids having refractive indices in the range 1.440–1.560, (iii) as-grown crystals in suspension in amyl acetate diluted with an excess of Cargille immersion liquids having refraction indices in the range indicated in (ii).

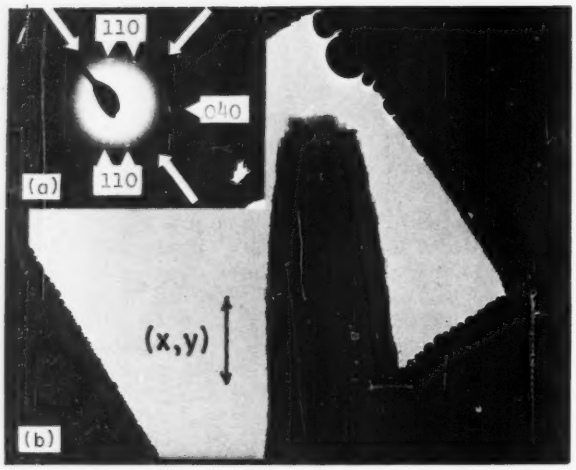

FIGURE 28. *(a) Insert: Electron diffraction pattern from a dendrite oriented edge-on with respect to the electron beam. (b) Corresponding electron micrograph, ×7,267, of portion of dendrite giving rise to diffraction pattern in (a).*

This dendrite was formed under the same conditions as those shown in figures 15 to 25, the preparation was however filtered isothermally after being held for 18 hr at 114 °C. Angle of rotation of image with respect to diffraction pattern is 8° counterclockwise. Unmarked arrows indicate position of weak 130 spots. Disposition of diffraction spots indicates that the **b**-crystallographic axis is oriented horizontally and the **c**-axis at right angles to the field of view.

impinging electrons, the pattern may be readily attributed to the transparent branches (note their lamellar character) protruding at its extremity. The diffraction spots recorded in figure 28a are reflections from {110}, (040), and {130} planes. The disposition of the spots corresponds to that to be expected from a monoclinic crystal of polypropylene oriented with its **c**-axis parallel to the electron beam, i.e., parallel to the *x,y* plane of the dendrite in figure 28b, and with its **b**-crystallographic axis (note the disposition of the 040 spot) essentially at right angles to both the beam direction and the *x,y* plane.

On the basis of the latter observations, i.e., that the **b**-axis in the dendrite branches is oriented at right angles to the *x,y* plane of the dendrite, and that the **c**-axis in the branches is oriented parallel to that plane, it follows that the **a**-axis in individual branches must also lie parallel to that plane. In this respect, two crystallographically distinguishable but morphologically similar hypothetical "twinned" dendritic crystals may be envisaged whose respective morphologies would coincide closely with the experimental observations described above. The **b**-axis projections of these two hypothetical models I and II, based on the unit cell parameters given by Natta et al., [3], are depicted schematically in figures 29a and 30a. The corresponding relationships between the orientation of the **a**- and **c**-axes in their constituent branches are

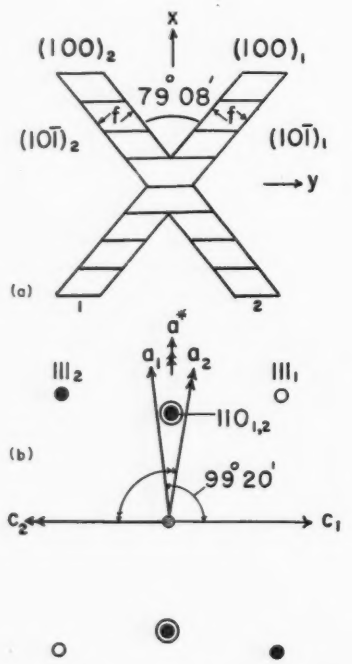

FIGURE 29. (a) **b**-*axis projection of Model I twinned dendrite. Striations in branches indicate orientation of chain segments in each branch.* (b). *Diagram showing relative lattice orientations in twinned branches in (a), as well as projected disposition of 110 and 111 reciprocal lattice points* (d_{110} = 6.25 Å, d_{111} = 4.2 Å) *with respect to the dendrite.*

○ Reciprocal lattice points corresponding to a_1c_1. ● Reciprocal lattice points corresponding to a_2c_2.

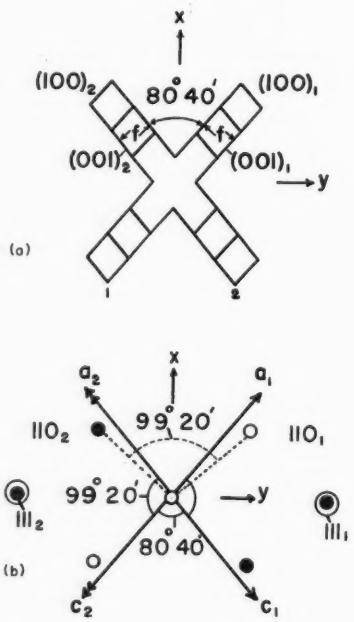

FIGURE 30. (a). **b**-*axis projection of Model II twinned dendrite. (b) Diagram showing relative lattice orientations in twinned branches in (a) as well as projected disposition of 110 and 111 reciprocal lattice points with respect to the dendrite.*

○ Reciprocal lattice points corresponding to a_1c_1. ● Reciprocal lattice points corresponding to a_2c_2.

shown in figures 29b and 30b. The fold surfaces (f) of individual branches are viewed edge-on in both models as depicted in figures 29a and 30a. In both models the acute dihedral angle between the fold surfaces of the intercrossing branches is circa 80° (cf. experimentally estimated angle ~ 85°). In order to compare the essential features of these models with respect to experimental observations we identify the axes bisecting the acute and obtuse angles between the dendrite branches as the x and y reference axes respectively (cf. the x- and y-axes which have been referred to previously in the discussion of the experimentally observed optical properties of the dendrites (fig. 27)).

The essential and contrasting features of models I and II are summarized below:

Model I. The dominant feature of this model is that the axes of the constituent helical molecules, and hence the **c**-axis, in all the branches are oriented throughout the whole structure parallel to y. The **a*** and [001] axes in the "intercrossing" (twinned) branches in this model are parallel to x and y respectively. The respective lattice orientations in the twinned branches are such as to be brought into coincidence by rotation through 180° either about x (i.e., **a***) as shown in figure 32 or about y (i.e., [001]). It may be noted that **a*** which is normal to the **b**-axis in the monoclinic unit cell of polypropylene, is very closely parallel to the [601] axis in the cell, and that the (10$\bar{6}$) planes are very closely normal to the (100) planes. Individual branches in this model are bound by (10$\bar{1}$), (100) and (010) faces (the latter which are parallel to the x,y cross section are not shown in fig. 29a). The (10$\bar{1}$) faces, which are the fold surfaces, are denoted (f) in figure 29a.

Model II. In this model (fig. 30) it is assumed that the fold surfaces are parallel to the (001) planes in each branch whose other faces are parallel to the (100) and (010) planes. It is also assumed that the (100) planes in individual branches are parallel to the (001) planes in branches that "cross" them. The chain molecules in intercrossing branches are symmetrically inclinded at 49° 40′ to y in the x,y plane, and the twinned lattice orientations are such as to be brought into coincidence by rotation through 180° about x. It may be noted that the [10$\bar{1}$] and [101] axes in the branches are very nearly parallel to x and y respectively.

Both Models I and II conform with the experimental observation that the **b**-axis in the dendrites is oriented at right angles to their x,y plane. That the overall development of the dendrites is slowest at right angles to the latter plane may be accounted for in both models if it is envisaged that the growth of individual branches occurs more rapidly along the direction normal to their (100) faces (i.e., along **a***) than along [010].

In summary, therefore, on the basis of the two models discussed above, the possibility was envisaged, as an initial guide, that the mechanism of propagation of the dendritic monoclinic polypropylene crystals may involve either repeated twinning through 180° lattice rotations about **a*** or [001] as in figure 29a, or about an axis at right angles to the **b**-crystallographic axis and almost coincident to [10$\bar{1}$] as in figure 30a.

Using the two model twinned crystals I and II as a basis of reference, we turn now to a consideration of the experimentally observed optical properties of the dendrites about their x,y cross section (upper half of fig. 27), in conjunction with some electron diffraction data obtained from their peripheral regions with the crystals oriented with their x,y cross section at right angles to the electron beam.

The optical feature of the dendrites which initially strikes attention is the overall negative birefrigence they exhibit with respect to their x-axis since, a priori, this feature is consistent with the orientation of the chain molecules in Model I. The birefringence with respect to the x-axis was measured however, and found to be of the order of -0.007 birefringence units.[10] This value is rather lower than would be expected when considered in the light of birefringence-draw ratio data obtained by Keedy et al., [19] from drawn filaments of isotactic polypropylene. A value closer to -0.03 birefringence units with respect to x would be expected of a structure corresponding to Model I.

While the low birefringence of the crystals with respect to x argues against Model I this feature alone could not be used to discriminate unambiguously against this model in view of the uncertainty involved in the determination of the overall thickness of the dendrites at right angles to the x,y cross section, coupled with the fact that these structures are not solid objects and that consequently their effective thickness is most probably lower than the overall thickness which was used to calculate their birefringence.

A further factor adding to the uncertainty in interpreting the low value of the observed birefringence unambiguously in terms of a precursor model is the fact that the extinction behavior of the dendrites, which is not uniform throughout their x,y cross section (fig. 27), indicates deviations (albeit symmetrical) in average molecular orientation about that cross section. We turn, therefore, to the outcome of electron diffraction experiments which, although subject to complications associated with the latter factor, nevertheless provide a more direct means of crystallographic characterization.

Two typically weak electron diffraction patterns obtained from smaller dendrites (same preparation as the crystals shown in figs. 22 to 25) are shown in figures 31 and 32. Interpretation of these patterns is provided by consideration of figure 33 in which the **b**-axis projection of the monoclinic unit cell of polypropylene is depicted together with the corresponding projection of the reciprocal lattice. The projected dispositions of the 110 and 111 reciprocal

[10] These measurements were made on the larger dendrites from the same preparation as those shown in figure 15. The dendrites in suspension in amyl acetate were deposited on a glass slide. Partial evaporation of excess solvent was allowed to occur in air after which an excess of a Cargille immersion liquid whose refractive index (1.510) corresponded to the isotropic refractive index of highly crystalline unoriented polypropylene [2] was added to the deposit. Possible contributions of form birefrigence were thus minimized. The birefrigence measurements were carried out with a Berek compensator.

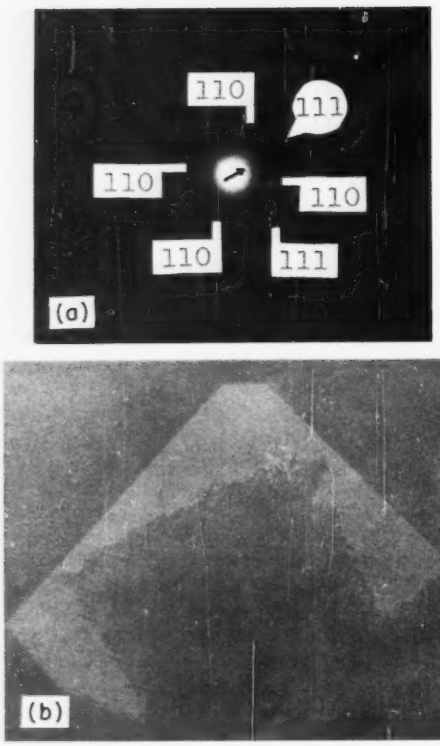

FIGURE 31. *(a) Electron diffraction pattern obtained from the dendrite shown in (b). Correction made for relative rotation of the image with respect to the diffraction pattern.*
Central arrow in (a) indicates orientation of *x*-axis of dendrite with respect to the diffraction pattern. Magnification in (b) × 14800.

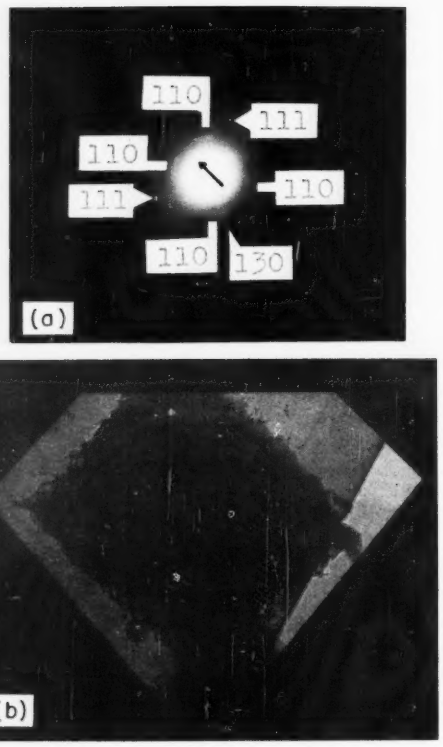

FIGURE 32. *(a) Electron diffraction pattern obtained from dendrite shown in (b). Correction made for relative rotation of the image with respect to the diffraction pattern.*
Central arrow in (a) indicates orientation of *x*-axis of dendrite with respect to the diffraction pattern. Magnification in (b) × 14800.

lattice points with respect to the unit cell (real space) are also shown in the same figure. The angles of inclination of the (110) and (111) real space planes with respect to the **ac** plane of the unit cell are 73° and 80°, respectively. In anticipation of what follows the projected dispositions of the 110 and 111 reciprocal lattice points with respect to the **b**-axis projections of the model twinned crystals I and II shown in figures 29 and 30 may be considered.

The diffraction patterns shown in figures 31 and 32 have one particular feature in common, namely, in both cases four inner diametrically paired 110 reflections ($d = 6.28$ Å) are discernible. The acute angle between the two pairs is 85° in figure 30 and ~ 62° in figure 31, some uncertainty being involved in the estimation of the latter angle in view of the arced and unevenly spotty nature of the reflections; hence the choice of the midpoints of the arcs is subject to some arbitrariness. The feature of interest which will be returned to presently is the apparently twinned disposition of these 110 reflections, the bisector of the acute angle between the two pairs being closely coincident in orientation with the *x*-axis of the dendrites.

In addition to the 110 reflections, individual (i.e., unpaired) spots or arcs corresponding to an interplanar spacing of 4.15–4.20 Å which could thus be indexed 111 are pointed out in figures 30 and 31. An individual arced reflection corresponding to a spacing of 4.75 Å, hence indexed 130, may also be seen in figure 31.

Some complicating factors arising from the very nature of the dendrites must be contended with in attempting to interpret the diffraction patterns in figures 31, 32, and the variations between them. First, the weakness of the patterns, which, as indicated earlier, could not be discerned visually on the fluorescent screen of the electron microscope, indicates that they are essentially contributed to only by the extremities of those branches that extend to the thinner peripheral regions of the dendrites. Second, it can be anticipated that distortions or relative displacements undergone by the branches in the peripheral regions as a consequence of surface tension forces incurred during drying could give rise to a situation approximating that of precessing the undistorted structure with respect to the electron beam. In principle, if the **a**- and **c**-axes in the branches are oriented parallel to the *x*,*y* cross section, the (110), (111) and (130) planes would not satisfy the Bragg condition for diffraction (Bragg angle $< 1°$ for an 80 kv electron

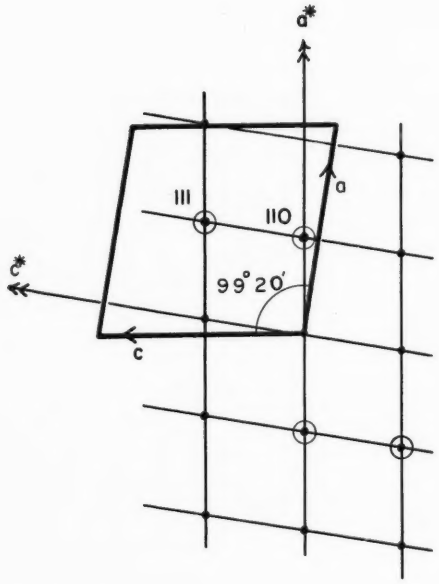

FIGURE 33. **b**-*axis projection of monoclinic unit cell of polypropylene, and corresponding projection of the reciprocal lattice indicating projected disposition of the 110 and 111 reciprocal lattice points.*
b* which is parallel to **b** is normal to the plane of the diagram. (d_{110} = 6.25 Å, d_{111} = 4.2Å).

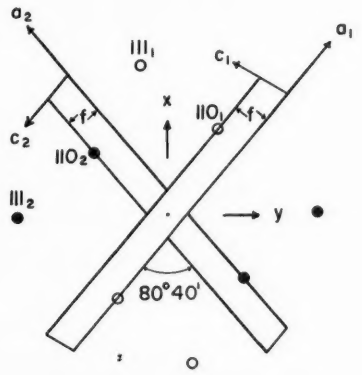

FIGURE 34. *Schematic representation of the* **b**-*axis projection of "twinned" branches in which the angle between their respective fold surfaces (f) is 80° 40', their lattice orientations being related by an 80° 40' rotation about* **b**.
The projected disposition of the 110 and 111 reciprocal lattice points is also shown. ○ Points corresponding to a_1c_1. ● Points corresponding to a_2c_2.

beam). The presence of these reflections can, however, be attributed to distortions in the network of branches; their resulting dispositions, however, would not be expected to coincide precisely with precession patterns (about the **b**-axis) corresponding to either models I or II. Some deductions may nevertheless be based on the disposition of the 110 arcs in figures 31 and 32, with respect to the *x*-axis of the dendrites.

If the structure of the dendrites corresponded with Model I the 110 reflections from the twinned branches would coincide and be expected to fall along, or be spread about, an axis parallel to *x* as may be deduced from figure 29b. The diffraction patterns shown in figures 31 and 32 in which the angle between the paired 110 reflections are 85° and ~ 62° respectively therefore argue against Model I. The corresponding angle for Model II however is ~ 100°. The discrepancy observed in the angle between the 110 reflections with respect to Model II may be attributed to distortions incurred by the crystal on drying, evidence for which may be detected in the electron micrographs shown in figures 31, 32, and, in a secondary way, to possible as-grown misorientations between the dendrite branches (see sec. 5 for discussion concerning possible origin of such misorientations). The same factors could also account for the fact that the reflections marked 111 on rectangular backgrounds in figures 31 and 32 do not fall along the axis parallel to *y* as would be expected of Model II. In some instances however as indicated for example in figure 31, arced 111 reflections (circular background) included in the acute angle between the paired 110 reflections were observed. Unless it is assumed that they are artifacts associated with deformations in the dendrites, they raise the possibility that the lattice orientations in intercrossing branches may be related by an 80° 40′ rotation about the **b**-axis as shown in figure 34. It should be noted in the latter instance, however, that whereas the chain axes in the twinned branches are respectively oriented at 80° 40′ to one another as is the case in Model II, they are not symmetrically inclined with respect to *x*. Furthermore, whereas the chain molecules in branch (1), figure 34, are parallel to the fold surfaces of branch (2), the reverse does not hold, thus implying the unlikely possibility that there exist two different modes of formation of offspring branches from parent branches. Assuming, for reasons which will be discussed later (see sec. 5), that the formation of offspring branches from parent branches occurs through the epitaxial deposition of chain molecules on and parallel to the fold surfaces of parent branches, the development of branches (2) from branch (1) can be envisaged. The formation of branch (1) from branch (2) does not comply with the above assumption which is however satisfied by model II.

In summary, while realizing that the interpretation of the twinned nature of the dendrites presented in previous paragraphs is subject to ambiguities associated with the problem that they are not perfectly rigid entities, it appears nevertheless that the structure of these crystals corresponds closely to that depicted in Model II shown in figure 30. It is of interest to note in this respect that Geil [11] has reported that electron diffraction patterns obtained from those areas in very thin melt crystallized polypropylene

films which exhibit a woven morphology indicate that the chain molecules lie parallel to the plane of the films and that the **a**-axis in the interweaving structural units is either parallel or perpendicular to the long axis of these units, the orientation being indeterminate in view of the interwoven disposition of the units. On the basis of the findings reported in the present paper it can thus be concluded that the **a**-axis in the individual interweaving units is parallel to their long axis and that the **c**-axis is transverse to their length. Reciprocally, Geil's observation lends further credence to Model II. In addition, following our observation that the polypropylene dendrites described herein could be grown from solutions of polypropylene in amyl acetate, Sauer, Richardson, and Morrow [20] have observed that similar dendrites exhibiting however a much more open structure (i.e., less profuse branching) could be grown from very dilute solutions of the polymer in α-chloronaphthalene. These structures collapse and distort pronouncedly on drying with the result that individual lathlike lamellar branches protruding from the collapsed dendrite and lying with their fold surfaces parallel to the substrate were observed. Electron diffraction patterns from such lamellae as reported by Sauer et al., show that the chain molecules are oriented at right angles (or closely so) to the plane of the lamellae and that the **a**-axis is parallel to the long axis of the laths. These features are consistent with Model II.

5. Discussion and Conclusions

The coincidence between the overall shape of the dendritic polypropylene crystals described in section 4 with that of the earliest microscopically detectable apparently polyhedral objects which are observed to develop during the initial stages of growth of monoclinic spherulites (sec. 3.2b) leads to the conclusion that their fine structures must be similar. In short, it is deduced on the basis of the present study that monoclinic polypropylene spherulites evolve from initially formed dendritic crystal precursors whose fine structure and mode of propagation is similar to that of the highly unusual crystals shown in figures 15 to 26.

The diagram shown in figure 35 represents schematically the respective profiles of the smaller and larger dendrites described in section 4. Also shown in the same figure is the corresponding cross-sectional profile exhibited by the transient and still essentially planar structures whose development corresponds, as shown in section 3 to a stage in the evolution of a monoclinic spherulite that is intermediate between the initially formed pseudopolyhedral precursor (dendritic crystal) and the ultimate spherulite.

Consideration of figure 35 clearly reveals the specific manner in which the dendritic precursor changes progressively in shape as it evolves into a spherulite. This feature suggests that the characteristically observed increase in concavity of the shorter "edges" and convexity of the longer edges of the dendritic

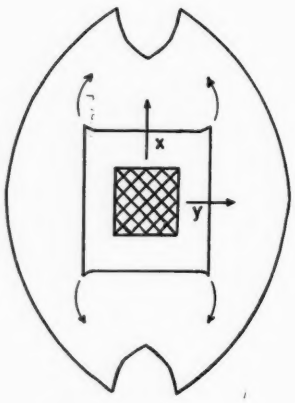

FIGURE 35. *Comparison of x,y cross sections of smaller and larger dendrites with that of the corresponding cross section of a notched aggregate representative of a more advanced stage in the evolution of a monoclinic spherulite.*

precursor, followed by the characteristic symmetrical pincer pattern of filling in at the concave extremities leading to an intermediate elliptically profiled aggregate, must be the result of a progressive degeneration of the apparently regular pattern of propagation through branching associated with the precursor initially.

Before proceeding into a further discussion of the unusual habit of the dendritic precursors of the monoclinic spherulites, and the apparently specific manner in which they degenerate into spherulites, it is instructive first to consider the observations reported in previous sections in a more general perspective. With this purpose in mind, current views relating to the mechanism of formation of polymer spherulites are summarized below. This will serve further to emphasize the nature of the atypical features associated with the formation of monoclinic polypropylene spherulites.

The more common morphological forms adopted by crystalline polymers may be classified into essentially three categories. These are in ascending degree of morphological complexity: lamellar chain-folded single crystals (planar or hollow pyramidal), axialites, and spherulites.

The term axialite was first coined by Bassett, Keller, and Mitsuhashi [18] to a species of solution-grown crystalline aggregates of polyethylene which consist of chain folded lamellae splaying about a common axis parallel to the **b**-crystallographic axis of the lamellae. When viewed along this common axis the axialites exhibit a sheaflike appearance, whereas they exhibit polygonal or oval shaped profiles when viewed at right angles to that axis. The contrasting appearance of these axialites when viewed in different perspectives led to the suggestion [18] that the sheaflike objects from which polymer spherulites grown in thin films from the melt have been frequently observed to evolve,

as well as the hedrites [21] also observed in thin melt crystallized films of several polymers [21, 22, 23], are axialite type structures seen respectively in different perspectives. This generalization has been substantiated and elaborated on further by Keith [24] in a paper in which the relations among the different types of morphological forms commonly exhibited by polymers are discussed, in the context of spherulite formation, in terms of the role played by fractionation and impurity segregation in the crystallization of polymers [25, 26].

According to Keith [24] axialites and spherulites represent respectively successive stages in the evolution of an initially formed lamellar chain-folded crystal growing (e.g., from the melt) under the influence of impurity species which give rise to cellulation at the growth fronts of the crystal along which the chain molecules accrue in a regularly folded manner. Morphological evidence supporting this view has been presented in the case of isotactic polystyrene in particular. It appears, as suggested by Keith [24], that the single crystal → axialite → spherulite pattern of evolution associated with the formation of spherulites in the latter polymer is, with minor variations, generally characteristic of polymer spherulites which exhibit, when fully grown, conventional radiating lamellar fine structures such as found in polyethylene, polyoxymethylene, polyoxyethylene and poly(4-methylpentene-1) [7]. The same growth scheme applies most probably to spherulites of the *hexagonal* crystalline modification of polypropylene.

It is evident that the pattern of evolution of monoclinic polypropylene spherulites differs in a fundamental manner from the lamellar single crystal (planar or hollow pyramidal) → axialite → spherulite pattern of spherulite formation summarized above. The origin of this difference as well as the atypical fine structures exhibited by monoclinic polypropylene spherulites [8, 11] is clearly traceable to the unorthodox nature of the dendritic crystal precursors described herein, from which such spherulites evolve. The factors governing the unusual habit of these dendritic crystals of polypropylene are still obscure. Some considerations relating to their mode of initial propagation and progressive degeneration into spherulites may nevertheless be speculated on.

The puzzling feature about these polypropylene crystals is, as indicated by the diffraction data, that the orientations of the chain axes in the two families of "intercrossing" branches in these crystals are not coincident. This feature represents a departure from the generally encountered compliance of the habits and mechanisms of growth of polymer single as well as twinned crystals [27] with the inherently characteristic parallel mode of chain packing which long chain compounds adopt in the crystalline state.

Clearly the 80° change in chain orientation between parent and offspring branches implicit in twinned Model II (fig. 30) raises the evident question, namely, how does an offspring branch in which the chain segments (and fold surfaces) are oriented at 80° to those in a parent branch develop from the latter in such a specific manner? One would expect that such a change in lattice orientation between parent and offspring branches would involve an interim boundary region of considerable disorder between them if one assumes that there exist a substantial number of tie molecules between individual branches and their offshoots. It is difficult to envisage that crystallographic information of a specific nature could be transmitted through such a region, particularly so in view of the 80° change in chain orientation involved. In short, the mechanism of branching of the dendrites still remains obscure. It may be speculated, however, that the formation of new branches could be initiated by the epitaxial accretion of individual molecules in a regularly folded conformation onto the fold surfaces (i.e., the (001) faces) of parent branches such that the chain segments lie parallel to the latter faces. The resulting monomolecular "steps" formed by such individual molecules might then be envisaged to develop further through the parallel accretion of fresh molecules onto them. Such an epitaxial mode of development of new branches evidently presupposes that some topographical features of the (001) fold surfaces in the parent branches must favor the initial deposition of individual molecules parallel to these faces in a specific manner such that their chain segments are also oriented at right angles to the **b**-crystallographic axis in the parent branch. This latter feature must be assumed in order to account for the parallel orientation of the **b**-axis in both parent and offspring branches.

We turn now to a consideration of the nature of possible factors which lead to the progressive evolution of the dendritic crystal precursors discussed above into monoclinic spherulitic aggregates.

It has been pointed out earlier that the progressive transition in shape (see growth sequences in figs. 13, 14, and diagrammatic representation, fig. 35) which the dendrites undergo as they evolve into spherulites must be a consequence of progressive deviations from the apparent crystallographically specific pattern of branch propagation which characterizes their earliest stages of development.

Evidence has been obtained which indicates that the propagation of new lamellar branches from the fold surfaces of chain-folded parent lamellae in the manner depicted schematically in figure 26 remains however basically an intrinsic and continuing feature of the mechanism of evolution of the dendrites into spherulites. Briefly, it is pointed out in this latter respect that exploratory experiments have revealed that polypropylene crystallizes uniformly in the form of "notched" type aggregates, examples of which are shown in figure 36, from 0.01 percent amyl acetate solutions at 100 °C. Surface replicas [11] of these aggregates of which the shape is similar to that of the transient structures which develop during the still

[11] The preparation was filtered isothermally in the manner described earlier. The replicas were prepared by the same technique as that used for the dendrites described in section 4.

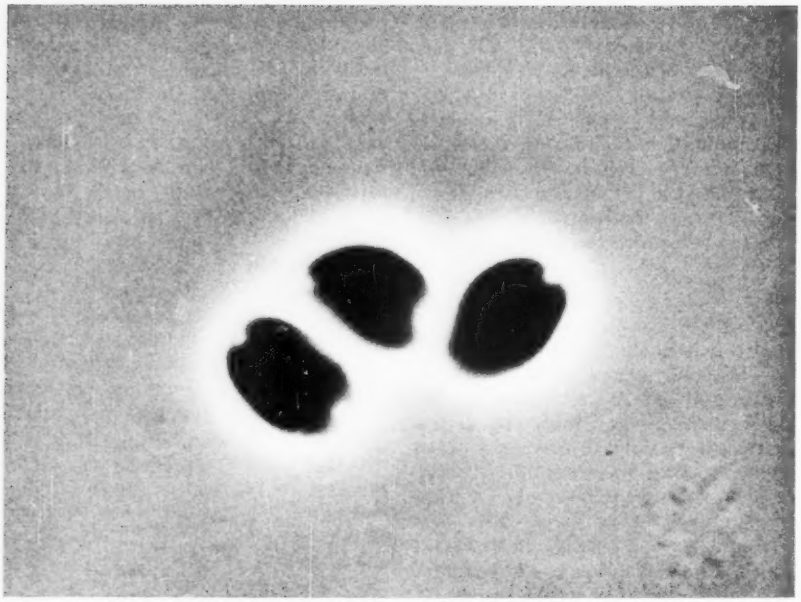

FIGURE 36. *Notched aggregates grown from a 0.01 percent solution of polypropylene in amyl acetate at 100 °C.*
Phase Contrast × 2100.

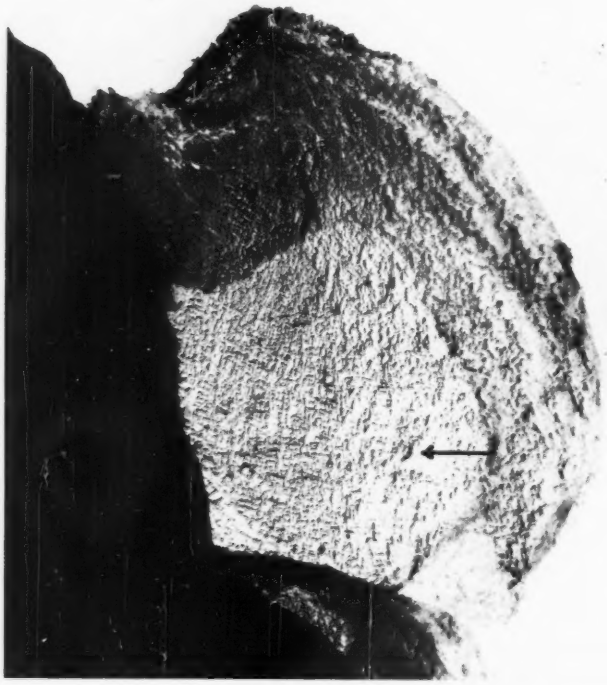

FIGURE 37. *Replica of an aggregate similar to those shown in figure 36.*
A cross-hatched fine structure is faintly discernible at this relatively low magnification. Arrow points to mark identifying region shown at higher magnification in figure 38. × 10800.

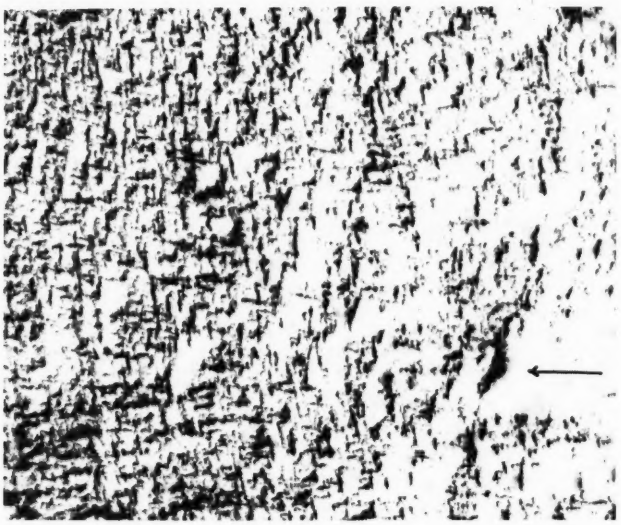

FIGURE 38. *A view at higher magnification of a portion (note arrow) of the replica shown in figure 37, revealing the cross-hatched surface texture of the replicated aggregate.*
×33200.

relatively early stages of evolution of the initial dendritic crystal precursors into spherulites revealed, as shown in figures 37 and 38, a distinctly cross-hatched fine structure clearly related to that of the dendrites described in section 4.

Two factors, one possibly intrinsically associated with the folded conformation of the chain molecules in the lamellar branches, and the other environmental, may be considered, that contribute to the progressive degeneration of the dendritic crystal precursors into spherulites.

With respect to the first of the two factors indicated above, recent quantitative measurements of lattice distortions arising from the chain folds in polymer crystals reported by Bassett [28] may be pointed out. These measurements have been derived from an analysis of Moiré patterns exhibited under the electron microscope by bilayer crystals of polyoxymethylene and poly(4-methylpentene-1) in particular. It has been shown that the spacing of a family of planes parallel to the chain molecules in crystals of these two polymers differs depending on whether or not the planes contain the chain folds. Such lattice distortions are attributed to the bulkiness of the folds which give rise to a slight increase in spacing between planes along which the molecules accrue in a regularly folded conformation. Bassett et al., [29] present evidence suggesting that the resulting distortion of the tetragonal subcell in simple (four-sectored) lamellar crystals of poly(4-methylpentene-1) causes the lamellae to adopt a very slightly curved ("conicalness"), as distinct from planar overall shape. It would appear that the highly curved bowl-shaped tetragonal crystals of poly(4-methylpentene-1) consisting of multisectored chain folded layers observed recently by Khoury and Barnes [30], as well as the orthorhombic crystals of polybutene-1 which, as reported by Holland and Miller [31], are curled up in the form of tubelike structures, owe their distinctly curved habits to lattice distortions associated with the chain folds in their constituent lamellae. It also seems very likely that the well established twisting of the constituent radiating lamellae in certain species of polymer spherulites [32, 33, 34] is also a consequence of lattice distortions associated with chain folds [35]. In short, there exists a widespread body of evidence of the formation of chain-folded lamellae that are curved in some manner, as well as some direct and circumstantial evidence indicating that this phenomenon may be associated with lattice distortions due to the bulkiness of the folds in their constituent molecules.

On the basis of the phenomena indicated in the foregoing paragraph the possibility may be envisaged that the lamellar branches in the polypropylene dendrites may develop as very slightly curved rather than planar laths. Such an effect would clearly lead cumulatively to progressively more pronounced misorientations between newly formed branches throughout the dendrite and hence to a slow change in overall shape of the developing structure.

Direct detection of a possible very slight curvature of individual branches in the dendrites described in section 4 is clearly hindered by the impossibility of tracing individual branches unequivocally for appreciable distances. Deviations in the relative orientations of the dendrite branches may however be seen in the

replicas of the larger dendrites shown in figures 20 and 21. In addition, the slight change in profile of the dendrites between the stages of growth corresponding to the smaller and larger crystals described in section 4, as evidenced by the more pronounced concavity of the shorter edges of the latter, coupled with the symmetrical deviations in extinction (about the *x,y* cross section) between crossed polarizers, distinctly exhibited by the larger dendrites, suggests the contribution of a factor inherent in the very nature of the structure and mode of propagation of the dendrites to their progressive change in shape. It is merely pointed out in this respect, that a tendency of the four primary branches (i.e., those lying along the diagonals of the rectangular *x,y* cross section of the dendrites) which play a major role in the propagation of the crystals, to curve inwards towards the interior of the crystal in the manner indicated in exaggerated fashion by the arrows in figure 35 would account for the characteristic manner in which the overall shape of the dendrites changes progressively during their early stages of evolution into spherulites.

We turn now to a brief discussion of the role played by environmental factors on the mode of propagation of the dendritic crystal precursors and their progressive evolution into spherulites under isothermal conditions. The influence of temperature, and hence rate of growth, as well as rejected impurity species (e.g., atactic molecules and low molecular weight chains) on the mode of propagation of the dendritic crystal precursors needs to be considered in this respect. Some indication of the effect of these factors may be obtained from a consideration of their influence on the development of individual dendrite branches. We may borrow in this respect from the views advanced by Keith [24] relating to the influence of impurity segregation at the growth fronts of a chain-folded polymer crystal.

It may be anticipated that whether growth occurs from solution or from the melt, an inpurity-rich layer surrounds the dendrite, thus leading to cellulation in the form of pronounced reentrances developing at those faces of each branch at which growth occurs through the parallel accretion of chain molecules (i.e., the (100) and (010) faces). Lattice misorientations between neighboring "cells" may then be expected to lead to the progressive acquisition of a polycrystalline character by each branch, as has been observed for example in the case of individual polystyrene chain-folded lamellae growing from the melt. Intrabranch lattice misorientations would evidently lead to misorientations between offspring branches growing from different regions of the fold surfaces of a parent branch and hence would contribute cumulatively to the progressive degeneration of the initial dendritic crystal into a spherulite.

Recapitulating, therefore, it is considered that the characteristic development of monoclinic spherulites from the particular species of dendritic crystals described in this paper is brought about cumulatively as a consequence of (a) the curving of individual dendrite branches due to lattice distortions associated with chain folds, and (b) the progressive acquisition of a polycrystalline character by individual branches growing under the influence of rejected impurity species. At low undercoolings and hence slow growth rates which favor the diffusion of impurities away from the growth fronts of the constituent dendrite branches the disruptive effects of cellulation are minimized in particular. Under such conditions the progressive transition from dendritic crystal to spherulite will be gradual and the initial precursor dendrite may attain, as has been observed, microscopic (optical) proportions before exhibiting pronounced signs of degeneration. At high undercoolings, however, the dendrite to spherulite transition would occur much earlier in the growth sequence at the submicroscopic level of resolution with the result that no initial pseudo-polyhedral precursor will be observed.

The considerations presented in the preceeding three paragraphs have been only concerned with the influence of rejected impurity species on the *degeneration* of the dendritic precursors. An important consideration arises however regarding the influence of impurity rejected species on the frequency with which offspring branches develop from a parent branch in these dendritic precursors. In this respect the possibility cannot be discounted that the development of discrete offspring branches from the fold surfaces [(001) faces] of a parent lamella may actually result from the favored epitaxial accretion of molecules (assuming the epitaxial mode of development of branches suggested earlier holds) only on specific asperities on the fold surfaces of parent lamellae, and not necessarily due to a cellular pattern of monomolecular deposition of chains parallel to fold surfaces having an initial uniform topography. Carrying this latter conjecture further, it would follow that the frequency of branching will be governed by the number of branch-initiating asperities per unit area of the (001) faces, such as for example localized steps formed on those faces due to irregularities or fluctuations in the fold period of the constituent chain molecules in the parent lamella, which in turn may well be governed by the environmental conditions.

In conclusion, while the present study provides some detailed insight into the nature of the early stages of evolution of monoclinic polypropylene spherulites from solution as well as from the melt, a final analysis will have to account for the preferred molecular orientation with respect to the radial direction in the fully grown spherulites, information on which is, as indicated in the introduction, at present limited to monoclinic spherulites grown from the melt in the range of 110 to 148 °C [2]. While such a detailed analysis is beyond the scope of the present study, it may be pointed out at this stage that the preferred tangential orientation of the **b**-crystallographic axis in melt grown spherulites [2] correlates with the observation that growth is slowest parallel to the **b**-crystallographic axis in the branches of the dendritic precursor crystals. The average 65° to 70° inclination of the chain molecules with respect to the radial direction in these spherulites [2] still remains unexplained at this stage.

The author thanks E. Passaglia for the benefit of many helpful and critical discussions. Thanks are due to P. H. Geil for the loan of unpublished electron diffraction patterns.

6. References

[1] F. J. Padden, Jr., and H. D. Keith, J. Appl. Phys. **30,** 1479 (1959).
[2] H. D. Keith, F. J. Padden, Jr., N. M. Walter, and H. W. Wyckoff, J. Appl. Phys. **30,** 1485 (1959).
[3] G. Natta, P. Corradini, M. Cesari, Atti, accad. nazl. Lincei. Rend. Classe sci. fis. mat. e nat. **21,** 365 (1956).
[4] E. J. Addink and J. Beintema, Polymer (London) **2,** 185 (1961).
[5] A. Turner-Jones, Jean M. Aizlewood, and D. R. Beckett, Makromolekulare Chem. **75,** 134 (1964).
[6] P. H. Geil, Polymer Single Crystals, ch. IV, p. 269 (Interscience, New York, 1963).
[7] P. H. Geil, Polymer Single Crystals, ch. IV, p. 223 (Interscience, New York, 1963).
[8] G. W. Bailey, J. Polymer Sci. **62,** 241 (1962).
[9] A. Keller, Kolloid-Z. **165,** 15 (1959).
[10] P. H. Geil, Polymer Single Crystals, ch. IV, p. 270 (Interscience, New York, 1963).
[11] P. H. Geil. Polymer Single Crystals, ch. III, p. 214–220 (Interscience, New York, 1963).
[12] A. Hiltz. Private communication.
[13] H. J. Leugering, Makromolekulare Chem. **68,** 223 (1963).
[14] P. H. Geil, Polymer Single Crystals (Interscience New York, 1963, ch. III, p. 211).
[15] F. Khoury, Bull. Am. Phys. Soc. Series II, **9,** 275 (1964), Paper JA 4.
[16] D. C. Bassett and A. Keller, Phil. Mag. **7,** 1553 (1962).
[17] R. Salovey and F. R. Dammont, J. Polymer Sci. **A1,** 2155 (1963).
[18] D. C. Bassett, A. Keller and S. Mitsuhashi, J. Polymer Sci. **A1,** 763 (1963).
[19] D. A. Keedy, J. Powers and R. S. Stein, J. Appl. Phys. **31,** 1911 (1960).
[20] J. A. Sauer, G. C. Richardson and D. R. Morrow, Bull. Am. Phys. Soc. Series II, **10,** 354 (1965) Paper EG8.
[21] P. H. Geil in Growth and Perfection of Crystals, p. 579 (John Wiley & Sons, Inc., New York, N.Y., 1958).
[22] H. J. Leugering, Kolloid-Z **172,** 184 (1960).
[23] F. Danusso and F. Sabbioni, Rend. Inst. Lombardo Sci. Lettere **A92** 435 (1958).
[24] H. D. Keith, J. Polymer Sci. **2A,** 4339 (1964).
[25] H. D. Keith and F. J. Padden, Jr., J. Appl. Phys. **34,** 2409 (1963).
[26] H. D. Keith and F. J. Padden, Jr., J. Appl. Phys. **35,** 1270, 1286 (1964).
[27] P. H. Geil, Polymer Single Crystals, ch. II (Interscience New York, 1963).
[28] D. C. Bassett, Phil. Mag. **10,** 595 (1964).
[29] D. C. Bassett, F. R. Dammont and R. Salovey, Polymer (London) **5,** 579 (1964).
[30] F. Khoury and J. D. Barnes, Bull. Am. Phys. Soc. Series II **10,** 366 (1965) Papers HG3, HG4.
[31] V. F. Holland and R. L. Miller, J. Appl. Phys. **35,** 3241 (1964).
[32] H. D. Keith and F. J. Padden, Jr., J. Polymer Sci. **39,** 101, 123 (1959).
[33] F. P. Price, J. Polymer Sci. **39,** 139 (1959).
[34] A. Keller, J. Polymer Sci. **39,** 151 (1959).
[35] J. D. Hoffman and J. L. Lauritzen, Jr., J. Res. NBS **65A** (Phys. and Chem.) No. 4, 297 (1961).

(Paper 70A1–385)

JOURNAL OF RESEARCH of the National Bureau of Standards—A. Physics and Chemistry
Vol. 70A, No. 1, January–February 1966

Wavelengths, Intensities, and Zeeman Patterns in Ytterbium Spectra (Yb I, II, III, IV)

William F. Meggers and Charles H. Corliss

(October 19, 1965)

In 1937, Meggers and Scribner published a paper on arc and spark spectra of ytterbium providing wavelengths, relative intensities, and spectrum numbers of 1668 spectral lines, including about 400 for Yb I, 1250 for Yb II, and 12 for Yb III. That work was handicapped by impure materials and conventional light sources. When pure ytterbium metal and new light sources became available in 1950, Meggers and Corliss decided to make a new description of ytterbium spectra. This new description includes data for 7300 spectral lines with wavelengths between 2000 Å and 12000 Å distributed as follows: 1800 belong to Yb I, 5100 to Yb II, 430 to Yb III, and 5 to Yb IV. The Zeeman effect on 1300 lines has been observed in magnetic field intensities ranging from 3.7 to 9.358 tesla (37000 to 93580 gauss). These data were obtained for chemical identifications and for structural analyses of the first two spectra of ytterbium.

Key Words: Spectra of ytterbium: ytterbium. spectra of: Zeeman effect in ytterbium: wavelengths of ytterbium.

1. Introduction

Although ytterbium was discovered in 1907, Meggers and Scribner [1][1] provided, in 1937, the first useful description of conventional arc and spark spectra of this element. That publication reviewed all earlier work and presented measured wavelengths of 1668 spectral lines ranging from 2073.70 Å to 10321.64 Å and estimated relative intensities from 1 to 2000. On the basis of relative intensities in arc and spark light sources, that description included the first deliberate assignment of lines to three successive spectra (about 400 to Yb I, 1250 to Yb II, and a dozen to Yb III), and for the first two provided the identification of electron configurations, spectral terms and series.

During the first half of this century, the major obstacle in making useful descriptions of the spectra that characterize the so-called rare earths was the difficulty in obtaining pure samples. For example [1] "our first measurements of Yb spectra were made in 1929 when samples of Lu and Yb oxides, prepared by Auer and obtained from Eder in 1919, were available. Although the chemical separation was far from complete, it was possible to make a fairly satisfactory assignment of lines to Lu and Yb by simultaneous comparison of arc and spark. However, both salts contained some Tm as impurity which could not be completely identified without comparable data for Tm spectra. The first sample of Tm salt available for this purpose was generously supplied in 1933 by B. S. Hopkins, University of Illinois, who also supplied three samples of Yb oxide; one of which contained more Lu than Tm, another more Tm than Lu, and the third was entirely free from both Lu and Tm but contained considerable lanthanum."

Through the courtesy of G. R. Harrison, Meggers in 1939 photographed the first Zeeman patterns of ytterbium lines by using the Bitter magnet and the concave gratings at the Massachusetts Institute of Technology. These results were an accidental by-product of the first attempt to observe the magnetic splitting of thulium lines, as the purest sample of thulium then available contained about 15 percent of ytterbium. These Zeeman data, and further observations of spark spectra, enabled Meggers [2] to confirm and greatly extend the earlier quantum interpretation of the Yb II spectrum [1], but it also became obvious that the structural analyses of Yb spectra could not be satisfactorily extended without additional experimental data.

Since 1945, several contributions to the data of ytterbium spectra have been presented by others. Gatterer and Junkes [3] presented wavelengths and relative intensities of 1476 ytterbium lines observed in arc and spark spectra between 2262.25 Å and 7448.33 Å, but most wavelengths were taken from earlier tables, estimated intensities were given on a scale of 1 to 10, and in many cases it was impossible to sort the lines into Yb I and Yb II spectra.

A valuable extension to information concerning ytterbium spectra was made in 1959 by Humphreys and Paul [4] who used electrodeless lamps. They reported the wavelengths and relative intensities of 49 infrared lines dispersed by a grating spectrometer and detected with a lead-sulfide cell. The wavelengths ranged from 10267.05 Å to 24,552.51 Å and the intensities from 3 to 30000; no separation of Yb I and Yb II was attempted.

In 1961, Bryant [5] reported on "the spectra of doubly and triply ionized ytterbium." By using three different electrical discharges (hot spark, mild spark, high-voltage arc), Bryant succeeded in photographing 5900 lines (from 677 Å to 11262 Å); he attempted to assign each line to its proper spectrum, either Yb I, Yb II, Yb III, or Yb IV. His list contains 4550 lines with wavelengths greater than 2000 Å. We have

[1] Figures in brackets indicate the literature references on page 106. .

changed some of his assignments, failed to find some of his lines, but increased the total number longer than 2000 Å by 60 percent.

In 1962, Allen [6] reported on "the Zeeman effect of the arc and spark spectra of ytterbium and thulium." Those spectra were excited in a d-c arc between impregnated electrodes mounted in bored poles of an electromagnet with a maximum field intensity of 2.55 tesla (25500 gauss). Although Zeeman patterns are tabulated for 350 ytterbium lines, only 20 are resolved; most of the remainder are listed as pseudo triplets or quartets.

Prior to 1947, individual (lanthanon) rare earths were usually extracted from natural mixtures by fractional crystallization. In order to obtain a comparatively pure sample, it was often necessary to repeat this operation thousands of times. A more efficient technique, ion-exchange chromatography involving the use of absorption columns of organic resins, was developed in 1947. By this method since 1950, large quantities of (99.99%) pure lanthanons have been accumulated as by-products of the purification and concentration of thorium and uranium as nuclear fuels. Thus, the former major handicap to spectroscopic investigation of lanthanon spectra has vanished and high-purity metals are now obtainable from various commercial sources at moderate cost [7]. Furthermore, since 1950, new types of light sources such as electrodeless lamps excited by microwaves, and sliding sparks, have been developed. These emit stronger and cleaner spectra than the d-c arcs and a-c sparks previously used at atmospheric pressure. These recent important improvements in materials and methods of observing persuaded us, in 1958, to undertake another description of ytterbium spectra. The present description contains 7300 lines (2000 to 12000 Å) and 1300 Zeeman patterns; it should be adequate for chemical identifications and for further progress in the structural analyses of ytterbium spectra. In fact, new analyses and quantum interpretations of Yb I and Yb II are now approaching completion and will be reported in separate papers.

2. Experiments

To obtain spectra of rare-earth elements, it was formerly customary to burn chemical compounds (oxides) of them on carbon, copper, or silver electrodes of electrical arcs or sparks at atmospheric pressure. Those sources favored the excitation of ionic spectra, masked many lines near those of the electrode materials, or of atmospheric gases, and caused undue widening of the lines because of high temperature and pressure. During the past decade, all these defects have been removed by the introduction of electrodeless evacuated lamps containing minute samples of metallic halides excited at moderate temperatures and reduced pressures by microwaves, as described by Corliss, Bozman, and Westfall [8] and demonstrated by Corliss and Meggers [9] for hafnium.

Our first ytterbium lamps were made with bromine compounds but the Yb spectra were found to contain, in addition to Br lines, many troublesome diatomic molecular bands due to YbBr. Since Yb has relatively low melting (824 °C) and boiling (1193 °C) points, new lamps were made containing only pure metal and a small pressure of noble gas as described by Meggers and Westfall [10] and by Zelikoff, Wyckoff, Aschenbrand, and Loomis [11]. Excited with microwaves, these lamps produced extremely intense Yb I spectra and most of Yb II but only a trace of Yb III. A slightly different form of lamp, also containing pure Yb metal and noble gas, was operated as a ring-discharge with high frequency in a surrounding solenoid; it greatly enhanced the intensity of Yb II relative to Yb I, and in addition excited Yb III and Yb IV peripherally.

In 1937, Meggers and Scribner [1] observed only 400 lines belonging to neutral ytterbium atoms and remarked that "The Yb I spectrum is surprisingly simple but may not be fully developed in the arc." In 1958, when Corliss and Meggers [9] undertook to make an improved description of hafnium spectra, they found that the number of recorded lines belonging to Hf I was greatly increased by using (instead of d-c arcs) electrodeless lamps containing hafnium halides excited by microwaves. This experience prompted us to apply this type of excitation to ytterbium halides to obtain a more complete development of the first spectrum. Our first ytterbium lamps, accordingly, were charged with $YbBr_3$ prepared by dissolving pure Yb_2O_3 in a mixture of HBr and Br_2 in water solution at about 300 °C. The spectra emitted by these lamps were satisfactory in the ultraviolet, but the visible region was partly obscured by strong bands of YbBr. We then decided to avoid the use of metal halides since ytterbium has relatively low melting and boiling points. A 100-mg portion of pure Yb metal was placed in a 7-mm o.d. quartz tube with a hemispherical window blown at one end. This tube was evacuated, outgassed, and filled with 7 torr of argon gas. With the argon excited in a microwave field of 2450 MHz, a Bunsen flame was applied to the portion of the tube containing the ytterbium metal. A green glow, characteristic of the arc spectrum of ytterbium, appeared and became dazzlingly brilliant as the temperature rose to make the quartz tube a dull red. At that temperature (ca. 600 °C), ytterbium has a vapor pressure of about 0.01 torr. The lifetime of this type of lamp is limited by the diffusion and ultimate condensation of ytterbium vapor onto the window, which then becomes opaque. In our lamps, this generally took place after about 20 hr of operation. Spectral regions where argon lines interfere with ytterbium were reobserved with lamps containing pure Yb metal and helium gas. In that case, a reservoir with a capacity of about 50 to 100 cm^3 was necessary to maintain the gas pressure because helium gradually escapes through hot quartz.

These ytterbium lamps emit an intense and very clean spectrum consisting primarily of Yb I with numerous lines of Yb II present but none of Yb III. Because Yb I and Yb II contain some prominently outstanding lines, our first spectrograms on nonbacked photographic plates were marred by opaque patches

of halation extending 1 cm on either side of the strong images; all subsequent exposures were made on black-backed plates.

To distinguish and identify successive spectra of ytterbium, a light source of higher excitation was required for comparison. This we found in the ring-discharge discovered, named, and described by J. J. Thompson [12] in 1891. Although Thompson suggested that his light source might serve spectroscopy, it never became popular. However, in 1923, the Bloch brothers [13] demonstrated that the proper use of a Thompson tube permitted them to record simultaneously four successive spectra of mercury and distinguish them by observing different intensity gradients along the diameter or radius of the tube. Nearly 40 years later, in like manner, we succeeded in recording simultaneously four successive spectra of ytterbium, distinguished by radial intensity gradients in spectral-line images obtained from a single source, the ring-discharge or Thompson tube.

In our experiments, a 100 mg lump of pure ytterbium metal was placed in a Vycor tube (18 mm o.d. and 150 mm long) closed at one end with a plane quartz window. This tube was evacuated, outgassed, and sealed after being filled with helium to a pressure of 6 torr. The tube was then surrounded by a solenoid (25 mm diam by 140 mm long) of 20 turns of platinum wire which was connected into the discharge circuit of a high-voltage spark apparatus with capacitance of 0.001 μF charged to 20,000 V and discharged through a 6-mm gap. Peak current in the solenoid was about 500 A.

The platinum solenoid and the enclosed ytterbium lamp were mounted with their axes on the optical axis of the spectrograph, and the tube was focused on the slit. When excited, the cold tube emitted a dull reddish glow due to the helium present. A Bunsen burner set beneath the solenoid brought the platinum coils to a bright red heat and the discharge in the tube changed to a bright blue-green as ytterbium was vaporized and excited.

Unlike the ordinary spark in air, the Thompson tube produces clean ytterbium spectra of sharp lines. When it is photographed beside the microwave discharge, the spectra of neutral and ionized atoms are easily distinguished. The first spectrum is strongest in the microwave discharge and considerably weaker in the ring discharge where it appears with maximum intensity on the axis of the tube. The second spectrum is generally much stronger and more fully developed in the ring discharge than in the microwave discharge because the latter lacks energy for the excitation of higher states in ions. The third and fourth spectra appear only in the ring discharge where they are observed only near or at the walls of the tube, fading toward the axis.

It appears that the energy for excitation of spectra in the Thompson tube has its minimum value on the axis and maximum at the walls. Consequently, when the tube is viewed end-on, by focusing the diameter of the tube on the slit of a stigmatic spectrograph, the lines characteristic of neutral atoms are stronger at the center and lines belonging to singly ionized atoms are nearly uniform in intensity along the diameter, whereas lines due to doubly or trebly ionized atoms are absent at the center but are observed near the wall with noticeably different intensity gradients.

The spectra of microwave and ring discharges of ytterbium were photographed side-by-side together with short images of superposed standards from iron arcs or from thorium-iodide tubes. To disperse and focus the spectra, four concave gratings of 6.5 m radius, in Wadsworth-type mountings, were used. The short ultraviolet region from 2000 Å to 2500 Å was photographed in the first order of two (30,000 lines per inch) gratings with a plate factor of 2.4 Å/mm. In the range 2500 Å to 4500 Å, the spectra were recorded in the second order of either grating with a plate factor of 0.87 Å/mm, and the same setting served to record the range 5000 Å to 9000 Å in the first order with a plate factor of 1.74 Å/mm. In the latter case, a colored glass filter was placed before the slit to absorb the second and third orders, and special dye-sensitized plates recorded the first order. The spectral range 7000 Å to 10000 Å was photographed with a third grating having 15,000 lines per inch and plate factor of 5 Å/mm, and the infrared observations were extended to 12000 Å with a fourth grating, ruled 7,500 lines per inch, whose plate factor was 10 Å/mm.

The above-mentioned spectrograms yielded wavelengths and estimated relative intensities of about 7000 ytterbium lines and, with few exceptions, they all appeared as sharp emission lines. In particular, there was no detectable absorption or self-reversal in any lines emitted by our sources. After our line list was compiled, Sugar [14] developed a new light source specifically for producing self-reversed lines in both the first and second spectra of rare-earth elements. The first observations with this light source were made in 1962 by Sugar with ytterbium electrodes. Those spectrograms (covering 2400 Å to 7000 Å) were evaluated by Meggers who found that 22 lines of Yb I and 50 of Yb II were absorbed or self-reversed; these are indicated by A and by R or *r* respectively, following the intensity number in our table of ytterbium spectra.

The final contribution to our table of ytterbium lines was made in 1963 by Nissan Spector who was photographing the spectra of erbium emitted by a sliding spark; he kindly substituted ytterbium electrodes for erbium and photographed the spectral range 6600 Å to 11600 A with this source. A description of this source was given by Sugar [15]. These spectrograms were presented to Meggers who found that below 8000 Å they were practically identical with those from the Thompson tube, but beyond 9000 Å they added several hundred lines to our list, many of which have been explained as transitions between previously established Yb II energy levels. Some ytterbium lines appear slightly hazy (h) in the sliding spark.

A major contribution to this description of ytterbium spectra is found in the data on Zeeman effect. As noted in the introduction, the first Zeeman patterns

792-867 O-66-5

of ytterbium lines were obtained accidentally in 1939 when they appeared as impurities in a thulium sample under investigation at MIT. Those Zeeman spectrograms were made with a d-c arc in the Bitter magnet [16] with field intensities at 7.30, 8.50, and 9.358 tesla; both factors favored ionization so that Zeeman patterns were recorded only for strong lines of Yb II or Yb III and none for Yb I. The total number of ytterbium lines with Zeeman patterns on MIT spectrograms was about 400, and in favorable cases the resolution reached 0.05 Lorentz unit, but most of the lines lay between 2200 Å and 4300 Å.

To extend and supplement the Zeeman data for ytterbium obtained at MIT in 1939, we resumed investigations in 1959 at the National Bureau of Standards where a Weiss magnet (with ferro-cobalt pole pieces) was used. When that magnet was animated with 15 kW, it produced a field intensity of 3.70 T in a pole gap of 5 mm. Special electrodeless lamps containing pure ytterbium metal (and argon gas) were made of quartz tubing 4 mm o.d. to be inserted and excited between the pole pieces of the magnet. Care was taken to vaporize the metal only in that portion of the lamp located in the region of uniform magnetic field between the pole pieces. The lamp was viewed end-on and focused on the slit of the spectrograph containing a concave grating with 30,000 groves per inch, the same one used in the first and second orders to describe ytterbium spectra between 2000 Å and 9000 Å. A Wollaston prism was inserted on the optical axis; it produced a vertical separation of polarized components of Zeeman patterns (parallel or normal to the lines of force) and, since the spectrograph was stigmatic, it recorded all components simultaneously without mixing any. Indeed, the Wollaston was placed where it separated the polarized components sufficiently to insert a narrow strip of "no field" exposure to the ytterbium spectra, useful for recognizing asymmetrical or overlapping Zeeman patterns, and for assigning unresolved patterns to their proper spectrum by noting the reduced intensity of the first spectrum relative to the second in the magnetic field. The magnetic field intensity was calibrated with standard splittings of ubiquitous impurity lines, principally of calcium, magnesium, sodium, and silicon. In this series of Zeeman-effect observations, the highest resolution achieved was about 0.10 Lorentz unit. The first results of Zeeman patterns in Yb I were announced by Meggers and Corliss [17] in 1960.

3. Results

These investigations, extending intermittently over a quarter century, resulted in the condensed data displayed in table 1, in which successive columns contain measured wavelengths (in air), estimated relative intensities and other attributes in two or more sources, successive spectra assignments, and types of Zeeman patterns.

In general, the wavelengths are the average of two to four or five measurements, and are regarded reliable to 0.01 Å in most cases. In the range 2500 Å to 4500 Å, photographed with our highest dispersion, most strong lines were accompanied by two or more Rowland ghosts. In such cases, the ghosts contributed to the wavelength determination of the parent line, but were scratched from the final list. When the average deviation from the mean of several values was less than 0.005 Å, the third decimal was retained.

Because of the electronic structures of ytterbium atoms and ions (deduced from their spectra), their spectra are characterized by an extraordinary range of line intensities. In table 1, these are roughly estimated from photographic images of illuminated slits and assigned numerical values from 1 to 100,000. In spite of their crudeness, these estimates of relative intensities in the same and in different light sources provide general criteria for assigning lines to their proper spectrum (Yb I or Yb II) and in the same spectrum they often distinguish lines of different excitation. Yb III and Yb IV lines were not excited in microwave discharges but could be seen in spectra of the Thompson tube where they were distinguished by radial intensity gradients. Literal symbols following intensity numbers have the following meanings:

A = nearly all absorbed in the pulsed arc.
R = wide reversal in the pulsed arc.
r = narrow reversal in the pulsed arc.
d = double but not resolved.
e = enhanced near wall of Thompson tube.
h = hazy as distinguished from sharp.
H = very hazy.
l = shaded or displaced to longer waves.
s = shaded or displaced to shorter waves.

The above-mentioned estimates of spectral-line intensities and supplementary information on line attributes constitute the main criteria for sorting the observed lines in four successive spectra: Yb I from neutral Yb atom, Yb II from Yb^{+} ions, Yb III from Yb^{2+} ions, and Yb IV from Yb^{3+} ions. The assignment of observed lines to their proper spectrum is indicated by Roman numerals in column 4 of table 1; there are about 1800 lines for Yb I, 5100 for Yb II, 430 for Yb III, and 5 for Yb IV.

In the last column of table 1, we list the Zeeman-type numbers for about 1300 lines observed in strong magnetic fields. These numbers correspond to the classification of Back and Landé [18] who showed that only 7 types of Zeeman patterns exist, types 1, 2, 3, for energy levels of odd multiplicity, types 4, 5, 6 for even, and type 7 appearing in either multiplicity as a single undisplaced parallel (*p*) component and two symmetrically displaced normal (*n*) components. The Zeeman types in table 1 prove that Yb I and Yb III result from energy levels of odd multiplicity, and Yb II from even. Further details of the Zeeman patterns, including quantum numbers (J and L) and magnetic splitting factors (*g*) derived from them, will be presented in subsequent papers dealing with atomic energy levels and quantum interpretations of Yb I and Yb II spectra.

TABLE 1.—*Emission spectra of ytterbium*

Wavelength in air Å	Intensity: Meggers lamp	Intensity: Thompson lamp	Spectrum	Zeeman type
11603.94	20		I	
11559.05		5	II	
11442.70		1	II	
11299.78		5 h	II	
11277.83		1	II	
11262.27	250	10	I	
11060.25		2 h	II	
11051.05		2	II	
11035.15		1 h	II	
11023.37		1 h	II	
11002.95		4	II	
10980.47		3 h	II	
10959.94		1 h	II	
10943.17		1	II	
10882.92		1 h	II	
10856.25		1	II	
10845.53		3 h	II	
10830.36		100	II	
10829.11		40	II	
10810.82		5 h	II	
10802.47		4	II	
10776.11		1	II	
10774.38		1	II	
10770.10	2000	400	I	
10754.99		1	II	
10745.87		3	II	
10731.94		3	II	
10727.72	200	20	I	
10721.68		3 h	II	
10717.07		2	II	
10717.02	2		I	
10711.60		80 h	II	
10691.02		1 h	II	
10689.20		2 h	II	
10678.64		1	II	
10676.73		30	II	
10666.30		2 h	II	
10651.36		5	II	
10638.35		1	II	
10633.24	5		I	
10632.89		400 h	I	
10628.11		4	II	
10602.75		2 h	II	
10584.87		1	II	
10580.74		1	II	
10574.50		2 h	II	
10570.51		1	II	
10567.5	1		I	
10567.42		3	II	
10565.46		4	II	
10556.48		2 h	II	
10547.78		4	II	
10546.24		1	II	
10516.65		40	II	
10516.61	60		I	
10502.56		1	II	
10501.08		4	II	
10490.03		1	II	
10485.56		2	II	
10477.15		1 h	II	
10456.88		1	II	
10455.88		2	II	
10446.15		1	II	
10445.27		4 h	II	
10425,42		2	II	
10416.16		5	II	
10414.15		1	II	
10411.40		10	II	
10397.98		3	II	
10397.88	4		I	
10391.64		1 h	II	
10388.85		2 h	II	
10363.89		3	II	
10345.62		1 h	II	
10343.99		4 h	II	
10343.85	3		I	
10341.77	7		I	
10339.49		2 h	II	
10337.35		1 h	II	
10328.74		2 h	II	
10327.33		1	II	
10321.68	500	80	I	
10293.40		2 h	II	
10285.15		2	II	
10283.38		2	II	
10275.82		1	II	
10267.37	300	100	I	
10259.93		3 h	II	
10257.97		1 h	II	
10251.85		10	II	
10242.30		1 h	II	
10222.98		2 h	II	
10212.34		1 h	II	
10212.27	1		I	
10198.92		1 h	II	
10189.53		10 h	II	
10186.03		5	II	
10172.39		2	II	
10168.71		1 h	II	
10167.42		1 h	II	
10157.63		1	II	
10148.91		3	II	
10145.30		4 h	II	
10136.34		3 h	II	
10110.87	10		I	
10110.60		200	III	
10107.09		1	II	
10103.24		3	II	
10100.39		1 h	II	
10086.67		1	II	
10068.79		2 h	II	
10067.47		1	II	
10066.30		5	II	
10063.22		2 h	II	
10046.95		2	II	
10039.90		1	II	
10032.55		50	II	
10020.70		1	II	
10016.78		15	II	
10007.96		3	II	
10003.38		4	II	
9994.64		1	II	
9992.75		1	II	
9990.47		6	II	
9984.66		1	II	
9976.50	2	30	II	
9970.44	5		I	
9970.1		200H	II	
9959.25		2	II	
9953.32		4	II	
9945.98		4	II	
9940.23		3	II	
9932.98		1	II	
9915.99		6	II	
9914.02		2	II	
9904.5		3	II	
9896.50		20	II	
9894.20	8		I	
9893.9		100H	II	
9892.20		4 h	II	
9888.40	2		I	
9885.02		1	II	
9884.09		3	II	
9882.33	1		I	
9881.04		1	II	
9870.17	200	15	I	
9849.25		2 h	II	
9837.89		2 h	II	
9831.13	7		I	
9830.09		2	II	
9826.25		2	II	
9826.14	1		I	
9823.76	9		I	
9818.33		6 h	II	
9817.16	1		I	
9816.25		2 h	II	
9800.41		1	II	
9799.96	400	10	I	
9797.67		6	II	
9775.49	1		I	
9770.61		2 h	II	
9760.38	200	1000	II	
9745.39		7	II	
9735.10		1	II	
9734.62	2		I	
9718.81	3		I	
9717.58		2	II	
9716.88		8	II	
9711.44		5	II	
9706.65		10	II	
9705.60		3 h	II	
9700.26		2 h	II	
9695.71	2		I	
9694.33		2	II	
9693.72		50	II	
9688.77	25		I	
9678.00	1	5	II	
9677.56		1	II	
9671.78		1	II	
9670.80	5		I	
9669.62		1	II	
9669.03		2	II	
9664.23		20	II	
9663.60		1	II	
9663.09		2	II	
9661.01		6 h	II	
9659.43	2		I	
9657.25		3	II	
9656.05	20		I	

TABLE 1.—*Emission spectra of ytterbium*—Continued

Wavelength in air Å	Intensity: Meggers lamp	Intensity: Thompson lamp	Spectrum	Zeeman type
9648.86		3	II	
9644.92		2 h	II	
9640.78	2		I	
9637.59		3 h	II	
9630.97		5	II	
9629.04		2	II	
9623.60		9 h	II	
9619.82		3 h	II	
9613.49		1	II	
9611.30		2	II	
9610.77		2	II	
9608.81		2	II	
9606.08	3		I	
9602.64		20	II	
9600.55		2 h	II	
9595.60		2 h	II	
9594.26		2 h	II	
9592.23	1		I	
9589.34	1		I	
9589.14		7 h	II	
9580.31	30		I	
9578.21		1	II	
9577.45		3	II	
9572.65	5		I	
9564.64		3	II	
9559.83		5	II	
9555.55		5	II	
9536.43		3	II	
9532.71		8 h	II	
9532.64	1		I	
9531.83		20	II	
9527.91		3 h	II	
9524.36	300	6	I	
9522.68		4 h	II	
9520.19		3	II	
9512.32	2		I	
9511.61		3	II	
9505.71	2		I	
9504.03		1	II	
9498.90		3	II	
9496.63		10	II	
9490.85		2	II	
9482.44		20	II	
9475.35		1	II	
9474.20		2 h	II	
9468.54	2	3	I,II	
9468.20		10 h	II	
9464.03		4 h	II	
9457.07		6 h	II	
9445.45		6 h	II	
9442.75		7	II	
9428.10		30	II	
9423.79		3 d	II	
9417.09		5	II	
9408.11		4	II	
9405.75		3	II	
9404.73		10	II	
9397.79		2 h	II	
9390.61		8 h	II	
9388.32		2	II	
9382.31	2		I	
9380.18		15	II	
9378.29		3	II	
9377.90	7		I	
9372.12		3	II	
9367.86		1	II	
9367.21		2	II	
9352.58	8	80	II	
9349.25	80	300	II	
9341.89		4 h	II	
9334.67		3	II	
9328.56		3 h	II	
9325.68		20 h	II	
9324.60		2 h	II	
9321.14		2 h	II	
9320.30		1	II	
9316.58		1	II	
9314.88	2	40	II	
9304.35	1000	80	I	
9302.74		2	II	
9301.33		3	II	
9299.67		1	II	
9298.90	3		I	
9298.74		6	II	
9291.74	2		I	
9289.87	4	100	II	
9287.36		1	II	
9272.68	3	30	II	
9271.84		2	II	
9263.73		4 h	II	
9261.11		4 h	II	
9258.76	1		I	
9257.70		8	II	
9253.57	7	70	II	
9252.27		3	II	
9251.95	1	5	II	
9245.69		2 h	II	
9241.86		2	II	
9230.17	7		I	
9226.17		6 h	II	
9224.21	6		I	
9220.77		7 h	II	
9218.26		1	II	
9217.40		6	II	
9215.28		5	II	
9211.07		2	II	
9207.65		7 h	II	
9196.5		20H	II	
9192.40		3 h	II	
9191.41		3	II	
9190.18		5 h	II	
9188.34	10		I	
9187.53		4	II	
9187.01		1	II	
9182.32		5 h	II	
9178.52		5	II	
9177.47	1		I	
9176.14	1		I	
9175.76		2 h	II	
9172.59		2 h	II	
9170.70		3 h	II	
9168.70		2 h	II	
9167.06	3	40	II	
9163.69		15	II	
9162.85		2	II	
9158.62		15	II	
9155.30	40		I	
9152.45		8H	II	
9150.60		1 h	II	
9149.57		2 h	II	
9142.22		7	II	
9141.37		15	II	
9140.64	10		I	
9133.17	3	60	II	
9128.47	20		I	
9127.08		1	II	
9126.00		7 h	II	
9123.62		2	II	
9122.30		15	II	
9121.10	3		I	
9120.52		5 h	II	
9117.68	100	4	I	
9113.24		7 h	II	
9105.95		15 h	II	
9104.10	200	7	I	
9097.69	2		I	
9096.88		20	II	
9094.57		4	II	
9089.55	2 d		I	
9083.98		3 h	II	
9082.61		7	II	
9080.35	1	60	II	
9077.91		4	II	
9076.21		2	II	
9073.18	1		I	
9069.22	20		I	
9066.47		1	II	
9062.06		15	II	
9057.08		3 h	II	
9055.35		2	II	
9045.47	1		I	
9043.95	5		I	
9040.38		3 h	II	
9039.08	1		I	
9035.02	2	20	II	
9029.62		2	II	
9021.00		100 h l	II	
9020.90	10		I	
9017.02		5 h	II	
9016.21	2		I	
9014.27		2	II	
9004.83		3	II	
9004.21	10	150	II	
8997.66	400	10	I	
8985.71	8	60	II	
8982.45		2	II	
8980.79	3		I	
8980.74		20	II	
8978.58		6	II	
8971.65		3 h	II	
8967.71		5	II	
8959.06	2	70	II	
8956.72		9	II	
8952.23		6	II	
8948.02	2		I	
8947.78		6	II	
8946.66		5	II	
8946.38	1		I	
8942.87		3	II	

TABLE 1.—*Emission spectra of ytterbium*—Continued

Wavelength in air Å	Intensity: Meggers lamp	Intensity: Thompson lamp	Spectrum	Zeeman type
8930.12		1	II	
8927.38		4	II	
8922.56		100 h	II	
8922.50	1000	40	I	
8912.14	4	60	II	
8907.81		2 h	II	
8902.99	2		I	
8902.92		7 h	II	
8898.89	1		I	
8897.61		1	II	
8896.50		4	II	
8890.45	5	50	II	
8888.66	3		I	
8883.16	10		I	
8874.68	2		I	
8874.53		9	II	
8873.33		4	II	
8867.40		1	II	
8865.65		1	II	
8864.18		1	II	
8864.06	2		I	
8863.98		4	II	
8862.12		3	II	
8861.70		1	II	
8855.12	50	300	II	
8851.05		1	II	
8849.52		1	II	
8848.83	4	60	II	
8842.64		2	II	
8839.24		10	II	
8831.38	2		I	
8829.26	30		I	
8827.46	1		I	
8825.52		2	II	
8822.45		7	II	
8815.52		9	II	
8806.80	6		I	
8806.05		2	II	
8800.32		2 h	II	
8797.99	5	100	II	
8794.91	5		I	
8788.45	5		I	
8783.76		2	II	
8783.75	4		I	
8781.96	1	10	II	6
8780.63	10		I	
8762.42		5	II	5
8761.26		2	II	
8750.88		1 h	II	
8749.10		40	II	4
8744.27		1	II	
8742.84		7	II	
8742.45		10	II	7
8740.48		5	II	
8737.78		10	II	7
8736.45	20		I	
8736.03	4		I	
8735.23		1	II	
8731.29	30		I	
8725.19		10	II	
8724.18	4		I	
8723.33		1	II	
8717.80	1		I	
8710.15		4	II	4
8699.84		1	II	
8697.67		1	II	
8691.24		1	II	
8686.28	2		I	
8681.93	3		I	
8679.50	2		I	
8672.34		5	II	7
8671.53		1	II	
8670.82	2		I	
8667.69	50		I	
8663.92	10		I	
8663.39		4 h	III	
8661.59	5		I	
8659.04		15	II	4
8655.52	15 h		I	
8654.91	100		I	
8654.42	20		I	
8650.23	2		I	
8641.86		15	II	
8634.68	9		I	
8633.25		1	II	
8621.62		2	II	6
8620.75		1	II	
8612.57	50		I	
8607.49	200	400	II	6
8603.56	80		I	
8601.25	1		I	
8597.22		2 h	III	
8594.75	2		I	
8594.57		8	II	
8592.85		10	II	5
8592.00	200		I	
8591.26	20		I	
8590.94	20		I	
8590.08	1		I	
8587.89		1	II	
8585.99	20		I	
8585.00		1	II	
8584.20	2		I	
8579.08		7	II	6
8575.25	10		I	
8574.91	2		I	
8566.83		2	II	
8561.74		20	II	6
8558.47	2 h		I	
8556.90		4	II	
8554.92		2	II	6
8548.15		1	II	
8546.26	40		I	
8543.66		5	II	
8535.68	20		I	
8532.59		1	II	
8528.08	10		I	
8527.65		1	II	
8525.66	3		I	
8525.54		1	II	
8524.07	3		I	
8523.93	5 h		I	
8522.92	2		I	
8520.34	50		I	
8520.12	7		I	
8519.66	20		I	
8518.01	20		I	
8517.54		2 h	II	
8516.60	2		I	
8515.78	3		I	
8515.24	2		I	
8508.02	10		I	
8505.96	2		I	
8503.56		1 h	II	
8502.18		3	II	4
8500.55		2	II	
8494.37	50		I	
8493.74	4		I	
8489.90		30 e	III	
8487.84	1		I	
8485.10	30		I	
8483.31		2	II	
8481.03		2	II	
8480.27		2 h	II	
8477.79		2 h	II	
8474.21	3		I	
8473.35		2	II	
8465.75		15	II	6
8463.32	1		I	
8462.25	4		I	
8460.54		2	II	
8458.72		1	II	
8455.87	4	30	II	4
8446.74	5		I	
8446.35	20		I	
8446.32		6	II	
8443.99	5		I	
8438.92		1	II	
8438.42		2	II	
8437.07		3	II	
8435.61		3	II	
8430.76	2		I	
8429.59	3		I	
8428.83		15	II	4
8428.24	10		I	
8427.26		3	II	
8424.89		1	II	
8423.84	1		I	
8418.43	10		I	
8416.53	20		I	
8411.84	1	100	II	4
8408.89		3	II	
8403.58		2	II	
8400.65	20		I	
8400.61		1	II	
8400.35	5		I	
8400.01		20	III	
8396.79		8	II	4
8392.00		4 h	III	
8391.62	3		I	
8383.90	2		I	
8381.26		20	II	
8380.03		3	II	
8379.39		8	II	
8378.93	6		I	
8378.34		3	II	
8376.33	2		I	
8375.94	40		I	
8374.40		15	II	4

TABLE 1.—*Emission spectra of ytterbium*—Continued

Wavelength in air Å	Intensity: Meggers lamp	Intensity: Thompson lamp	Spectrum	Zeeman type
8371.77		2 h	II	
8360.09	2		I	
8356.75		5	II	
8352.37		4	II	
8352.03	2		I	
8350.15		9	II	
8349.52	2 h		I	
8347.14		2 h	II	
8346.11	3 h		I	
8343.49		2	II	
8342.51		8	II	
8341.30		2	II	
8336.34		5	II	
8335.12	1		I	
8334.43		10	II	
8333.30	10		I	
8331.71		2 h	II	
8327.88		30 e	III	
8327.71	3		I	
8326.86		10 e	III	
8325.18	800	5	I	3
8320.33	8		I	
8318.01		1	II	
8317.43	20		I	
8310.61	3		I	
8310.53		2	II	7
8310.38		2	II	
8309.10	2		I	
8308.40		1	II	
8307.67		2	II	
8306.38	2		I	
8301.74		15	II	6
8299.77	2		I	
8296.83	4		I	
8294.85	150		I	
8291.01		20	II	
8289.25		3	II	
8283.78		15	II	6
8282.14		2	II	
8280.60		2	II	
8276.29		2 h	II	
8267.90		2	II	
8267.87	10		I	
8266.52		7	II	
8266.06	2		I	
8265.64	2		I	
8263.64	4	150	II	4
8262.66		3	III	
8261.70		1	II	
8260.66		3	III	
8259.34	1		I	
8257.79		7 h	III	
8249.18	50		I	
8246.48		1 h	II	
8242.95	1		I	
8242.03	1		I	
8241.66		5	II	
8240.67	2		I	
8240.01		1	II	
8237.20		2	II	
8234.61	15		I	
8230.78		1	II	
8227.41		1	II	
8225.59	1 h		I	
8225.41		5	II	6
8224.13	10		I	
8221.74	10		I	
8221.35	10		I	
8220.44	2		I	
8213.96	9		I	
8213.64		30	II	6
8213.24		10	II	6
8213.02	30		I	
8212.03	5		I	
8210.33	4		I	
8207.98	40		I	
8206.55		3	II	
8200.20	1		I	
8199.08		1	II	
8197.43	6		I	
8194.83		2	II	
8192.40		30	II	4
8190.61		10	II	7
8190.31	5		I	
8189.53		2	II	
8183.28		1	II	
8180.75	10		I	
8180.64	30		I	
8180.34		2 h	II	
8179.01		4	II	
8178.46		4	II	
8178.14		3	II	
8177.37		2 e	III	
8173.60		3 h	II	
8171.82	1	30	II	5
8169.69		1 h	II	
8169.29		2 h	II	
8166.73		4 h	II	
8166.05		1	II	
8162.00		2 h	II	
8158.49	5	80	II	5
8157.40		150	II	6
8155.12		3	II	
8149.08		15	II	6
8148.83		3	II	
8146.64		1	II	
8145.56	20		I	
8145.36	5		I	
8143.81		2 h	II	
8142.47		20	II	4
8140.67		6 e	III	
8140.53	2		I	
8139.18		6 e	III	
8137.92		2	II	
8136.38	9		I	
8133.01		8	II	
8131.92		2	II	
8124.50		15	II	
8123.85		9	II	
8122.77	1		I	
8122.49		5	II	4
8121.35		3 h	II	
8121.12		2	II	
8118.80	5	150	II	4
8117.44		10 e	III	
8116.08	10		I	
8115.46		6	II	
8114.26	9		I	
8111.71	90		I	
8111.61		9	II	
8111.19	2	10	II	6
8109.79	100		I	
8104.44		5	II	4
8103.22		1	II	
8101.64		1	II	
8100.20		3 h	II	
8098.66	2		I	
8097.06		1	II	
8095.74	1		I	
8093.03		8	II	6
8092.95	3		I	
8091.73	1000	10	I	1
8089.66	7		I	
8086.68	10		I	
8085.56	4		I	
8084.74		9	II	4
8084.50	1		I	
8079.47		5	II	6
8078.10		2	II	
8076.95		1	II	
8075.92	2	40	II	6
8074.53		7	II	5
8071.28	10		I	
8070.00	50		I	
8067.21	7		I	
8066.72	2	50	II	6
8066.43	7		I	
8066.17		9 e	III	
8063.02	2	60	II	4
8058.91	80		I	
8056.20	10		I	
8056.02		20 e	III	
8055.12	20		I	
8053.43	50	500	II	6
8052.35	20		I	
8051.48	20		I	
8049.03	5	30	II	6
8042.91	4		I	
8042.63		5	II	
8039.83	200	2	I	1
8038.16		10	II	
8035.53		4	II	5
8034.43		1	II	
8034.08		2	III	
8023.46	1	20	II	
8023.11	3		I	
8022.93		10	II	
8021.62	3	150	II	6
8018.74	3		I	
8013.17		15	II	6
8009.53	4	50	II	4
8007.83	15	300	II	4
8002.73	1	20	II	4
8001.30		2 h	II	
7994.90		30	II	4
7990.35	30		I	
7984.31		4	II	
7971.46		100 e	III	
7968.09	1	6	II	

TABLE 1.—*Emission spectra of ytterbium*—Continued

Wavelength in air	Intensity		Spectrum	Zeeman type	Wavelength in air	Intensity		Spectrum	Zeeman type	Wavelength in air	Intensity		Spectrum	Zeeman type
	Meggers lamp	Thompson lamp				Meggers lamp	Thompson lamp				Meggers lamp	Thompson lamp		
Å					Å					Å				
7964.12	2	80	II	4	7772.78		2	II		7623.44		4 e	III	
7958.80		3	II		7771.01	4		I		7616.50		2	II	
7958.48	2	40	II	6	7767.43		2	II		7616.34	3		I	
7950.35	2	60	II	6	7766.02		2	II		7611.69		15	II	5
7950.01		2	II		7761.45	2		I		7611.28	3		I	
7947.60	1	40	II	4	7760.49	5		I		7607.09		2	II	
7946.26	50		I		7758.04	500	20	I	7	7603.42	2		I	
7933.25	2		I		7753.91	2	5	II		7599.13		20	II	6
7930.04		8	II	4	7753.29		6	II		7598.01	2		I	
7928.71		7	II		7749.38		1	II		7596.22	200	1	I	
7924.65	4		I		7746.98	6 h		I		7595.20		2	III	
7922.40	4000	100	I	1	7745.93		5	II	5	7588.43	8		I	
7918.41		3	III		7744.97	5		I		7582.93		40	II	4
7913.30		6	II		7741.94		3	II		7582.90	30		I	
7912.46		10	II		7741.66		2	II	7	7581.32		2 e	III	
7910.08	10		I		7741.15		2	II		7579.97	1	60	II	5
7906.25		2 h	II		7737.59	1	8	II	4	7576.94		4 e	III	
7904.82	10	200	II	4	7734.53	200	2	I	3	7576.41	2		I	
7899.54		5	II	6	7732.46		4 h	II		7572.81		5	II	
7897.90		2	II		7732.35		6	II	6	7566.65		15	II	4
7896.38	100		I		7719.82		15	II		7561.76		8 e	III	
7895.51		3 h	III		7719.23		40	II	6	7561.42	4		I	
7895.08	1000	50	I	2	7717.58	6		I		7560.18		1	II	
7893.10		20 e	III		7713.74		4 e	III		7556.13	1	40	II	6
7892.39		80 e	III		7707.28		2 h	III		7555.14	1	60	II	4
7891.93		1	II		7706.29	2 h		I		7547.08	5		I	
7889.78		3	III		7702.72		2 h	III		7541.56		2	III	
7885.17		2	III		7699.48	20000	2000	I	1	7541.10	5	80	II	4
7883.96	2		I		7697.62		5	II		7539.25		8 e	III	
7877.06	60		I		7693.21		6 e	III		7537.40		1	II	
7875.15	10		I		7692.75	5 h		I		7533.09		3	II	
7874.10	1	20	II	5	7684.25		4 h	III		7530.78		3	II	
7865.13		7	II	5	7683.77		9	II	5	7529.61		3	III	
7856.20		4	II	4	7679.91	200	1	I	1	7528.07		8	II	
7851.06		3 h	III		7678.20		1	II		7527.46	10000	200	I	1
7849.85		6	II		7676.62		8	II	6	7522.92		7 e	III	
7848.49		15	II	4	7666.57		1	II		7522.73	200	2	I	
7844.11	20	2	I	6	7664.41		70 e	III		7520.94		4	II	
7840.45	1	40	II	4	7664.11		2 h	III		7520.46		15	II	6
7839.17		1 h	II		7662.08	2		I		7517.94		2	II	
7834.65	15		I		7659.90	20		I		7516.24		2	II	
7833.02		9	II	4	7659.40		3 h	III		7513.50		4 e	III	
7825.52	1	50	II	6	7659.14	50		I		7512.86		15	II	
7824.64		3	II		7657.60	100		I		7508.07		8	II	5
7822.78		8 e	III		7655.71		5	II	4	7507.59	5		I	
7821.37	2		I		7650.02	4		I		7503.32		1 h	II	
7820.89	50		I		7648.88		4	II	6	7501.33		1 h	II	
7815.52		5	II	5	7645.84		8	II	6	7500.09		3 h	II	
7811.96	1	8	II	4	7641.45	3		I		7499.87	30		I	
7809.48		8 e	III		7640.63		1 h	II		7496.33	100	2	I	
7808.64		4	II	6	7639.47		4	II	4	7496.24		20	II	
7806.11		3	II		7637.27	15		I		7495.15		2	II	
7804.57		6	II		7636.65		3	II		7494.37		3	II	
7803.65	20	300	II	6	7635.53		4 h	III		7492.34	1	6	II	4
7802.01		9	II		7634.62		6	II		7483.19		2	II	
7801.17		8	II		7633.95	6	100	II	4	7482.80		1	II	
7799.44		3	II		7631.81		4	II		7481.04		6	II	7
7799.33	1		I		7630.87		1	II		7478.77	4		I	
7793.72		2 h	III		7630.48		9	II		7477.86	1	5	II	
7789.80	2		I		7630.00		8	II		7477.61	7	200	II	7
7785.02		3	II	4	7627.45	1	50	II	5	7475.24		2	II	
7777.96	1	7	II	6	7627.24	1	70	II	7	7474.72		4 e	III	
7777.49		6	II	5	7623.90	20		I		7473.32		5	II	

TABLE 1.—*Emission spectra of ytterbium*—Continued

Wavelength in air Å	Intensity: Meggers lamp	Intensity: Thompson lamp	Spectrum	Zeeman type
7472.44	2		I	
7469.44	60		I	
7468.09		8	II	
7467.58	40	30	I	
7464.10	5	60	II	4
7462.71		5 e	III	
7458.79	5 h		I	
7456.86		15 e	III	
7456.20		2	II	
7451.21		1	II	
7449.60		1	II	
7448.28	6000	100	I	7
7447.37	1	60	II	7
7444.20		2	II	
7439.84	1	80	II	5
7438.92	25	1	I	
7433.39	4	30	II	5
7429.51	2	40	II	4
7429.10		2	II	
7422.15	40	200	II	5
7421.04		2	II	
7419.60	1	40	II	4
7419.22	10		I	
7419.06		8	II	
7418.49		4	II	
7418.15		3	II	
7416.64	40		I	
7414.13	5		I	
7411.63		4	II	5
7411.17	200	2	I	
7410.94		8 e	III	
7410.01		80 e	III	
7406.00	10	150	II	6
7405.93	6		I	
7404.35	10		I	
7402.70		2	II	
7402.45		1	II	
7400.97		5	II	
7400.67	7		I	
7399.98		10 e	III	
7398.50		3 e	III	
7397.10	1	40	II	4
7396.04		1	II	
7393.34	4	30	II	4
7393.03		1	II	
7389.22	6	150	II	5
7387.69	2		I	
7384.50	7	150	II	7
7383.00		2	II	
7382.17	3		I	
7377.73	20	400	II	
7377.43	10	300	II	
7373.06	3	15	II	4
7367.93		8 e	III	
7367.78		20	II	4
7362.92	2	15	II	5
7362.83		60	II	
7361.90	200	1	I	
7356.90	3		I	
7354.17		4	II	6
7350.42		15	II	
7350.04	6000	100	I	3
7346.60	3		I	
7342.30	10	400	II	4
7341.64		4	II	
7339.99	10		I	
7339.80		60	II	7
7334.01	50		I	
7331.31	1	80	II	6
7329.29		2	II	
7328.57	8		I	
7327.87	500	2	I	1
7325.07		2	II	
7323.32	4		I	
7318.77		1	II	
7317.74		30	II	7
7313.18		15	II	
7313.05	3000	50	I	2
7311.02		10 e	III	
7310.70	400	1	I	
7309.19		40	II	5
7306.63	1	100	II	5
7305.92		8	II	
7305.22	2500	50	I	3
7304.54		5 e	III	
7302.15		15	II	4
7298.05	8 h		I	
7294.50		1	II	
7290.56		3	II	
7287.96		2	II	
7285.02		1	II	
7284.70		1	II	
7279.67		5	II	
7278.37		30	II	4
7275.02		1 e	III	
7268.03		4	II	
7266.55		1 e	III	
7266.37		1 e	III	
7265.76		10	II	7
7259.76		6	II	
7259.56		3	II	
7256.62	20		I	
7253.76	40		I	
7251.55	30	200	II	6
7244.41	2000	40	I	3
7238.95	1	80	II	
7238.73	4	80	II	
7235.42	1	40	II	6
7234.00		3 e	III	
7229.70		3 e	III	
7228.98		2	II	5
7227.21	5		I	
7222.72	20	150	II	6
7221.50		10	II	
7221.21	1	60	II	7
7220.38	2	50	II	5
7217.57		60	II	5
7209.65		1	II	
7209.38		2	II	
7209.10		8	II	
7208.29	4	200	II	7
7205.93	4		I	
7202.20	100	1	I	3
7201.09		20	II	7
7198.08	10 h		I	
7196.92	3		I	
7191.87		1	II	
7190.33	6		I	
7187.07	200	2	I	1
7182.60		2	II	
7175.48		300	II	6
7175.10	1000	10	I	3
7174.60		8	II	
7173.96	10		I	
7169.25	10		I	
7160.31	2		I	
7157.72		15 e	III	
7156.48	3		I	
7154.52		5	II	6
7153.51	3		I	
7152.40	10		I	
7148.16		2	II	
7147.94		8	II	
7145.13		4	II	7
7142.39	1	120	II	5
7141.28	6		I	
7137.67		2	II	
7136.82	5		I	
7135.61	10		I	
7134.85	5		I	
7134.83		2	II	
7128.94		2	II	
7126.81	2	100	II	5
7124.46		5	II	5
7117.99		10	II	6
7116.96		3	III	
7108.98	200	2	I	
7108.37		6	II	6
7105.34		1	III	
7101.66		10	II	4
7099.70		2	II	
7098.11		6	II	4
7089.40		1	II	
7086.08		20	II	4
7082.61		80	II	4
7081.81		4	II	
7080.77		1	II	
7080.53		40	II	6
7078.11		5	II	7
7077.07		1	II	
7074.60		2	II	
7072.12		4	II	4
7066.20		10	II	
7060.67		60	II	4
7060.41		2	II	
7056.72		4	II	5
7053.80	1	200	II	7
7052.58		10	II	5
7045.75		15	II	
7045.51		20	II	
7043.78	30	700	II	7
7037.04		10 e	III	
7032.91	2		I	
7031.52		30	II	6
7031.21	3		I	
7029.38		3	II	
7029.27		2	II	
7027.84	10	150	II	
7023.97		6	II	

TABLE 1.—*Emission spectra of ytterbium*—Continued

Wavelength in air Å	Intensity: Meggers lamp	Intensity: Thompson lamp	Spectrum	Zeeman type
7022.27		6	II	
7022.00	2	200	II	4
7020.18	500	4	I	
7019.48	2	20	II	5
7012.75		5	II	6
7003.90		1	II	
7002.14		1	II	
7001.79	3		I	
6999.88	50	800	II	6
6998.98		2	II	
6993.31	5	250	II	4
6990.51	100		I	
6985.15		20 e	III	
6981.99	20	300	II	4
6978.36		5	II	
6977.67	20	150	II	6
6977.30		1	II	
6976.89	3 h		I	
6973.58	10		I	
6970.54		7	II	
6968.73	1	30	II	6
6965.46	1		I	
6964.47		3	II	
6963.47		10	II	
6963.10	5	300	II	6
6959.11	1	10	II	5
6958.11	300	3	I	
6953.29	1		I	
6952.14		4	II	
6951.38	50		I	
6949.50		10	II	4
6944.95		30	II	6
6943.98	4		I	
6934.05	100	600	II	6
6929.57		9	III	
6926.08	1	30	II	5
6923.78		2	II	
6921.30		5	II	5
6916.78		1	II	
6916.10		3	II	
6915.84		4	II	7
6914.84	2		I	
6913.73	50	1	I	
6911.34		1	II	
6911.11	1	20	II	5
6908.92		2	II	
6902.28	2		I	
6901.06		2	II	
6897.78		1	II	
6897.31	1	40	II	5
6892.61	5		I	
6891.94	20		I	
6890.19		3	III	
6889.59	10	100	II	5
6888.76		2	II	
6886.95		8	II	4
6886.77		5	II	
6881.40	1	100	II	5
6877.93	2	250	II	7
6871.51		3	II	
6869.56	200	1	I	
6867.95		2	III	
6864.27	2	300	II	6
6862.08	2 h		I	
6857.64		2	II	
6854.67		7 e	III	
6850.64	4		I	
6844.05		1	II	
6843.02		2	II	
6842.87		3	III	
6840.56		3	III	
6833.56	4		I	
6831.17	7		I	
6830.99		2	II	
6829.80	1	70	II	
6828.90	2	200	II	4
6828.35		2	II	
6826.18		5	II	
6826.02		10	II	
6819.41		2	II	
6817.16	100		I	
6816.18		40	II	
6815.88	1	100	II	6
6813.65	5		I	
6812.42		2	II	
6809.30		5	II	4
6806.67	10		I	
6803.91		20	II	
6802.47	2	400	II	5
6799.60	60000R	6000	I	3
6798.29		2 h	II	
6796.80		2 h	II	
6792.58		30	II	
6790.82		20	II	6
6786.32		1	II	
6785.14	1	150	II	4
6784.80		4 e	III	
6782.17	1000	20	I	3
6779.74	2		I	
6777.22	600	10	I	
6776.87		2 e	III	
6775.79		2	II	
6773.47	2		I	
6772.42	1	50	II	6
6772.26	20		I	
6768.70	6000	1000	I	2
6765.67	40	1	I	
6765.24	200	1	I	7
6761.64	3 h		I	
6761.31		4	II	4
6759.10		15	II	4
6757.29	1		I	
6755.44	1	150	II	6
6754.69		3	II	
6753.01	2		I	
6751.45		10	II	
6751.17		2 e	III	
6749.40	1000	20	I	2
6746.64		6	II	
6745.23	30	600	II	7
6740.59		8	II	
6738.24		2	II	
6734.56		1	II	
6732.53		15	II	7
6732.17	2		I	
6731.02	5 h		I	
6728.37		1	II	
6727.61	400	2000	II	7
6727.12		20	II	
6724.92	1		I	
6724.36	1	30	II	6
6724.19		1	II	
6723.90		1	II	
6720.85	2		I	
6719.87	6 h		I	
6718.00	1	30	II	
6717.05	30		I	
6715.79	1000	20	I	7
6710.95		1	II	
6710.73		3	II	
6707.91	3		I	
6707.76	5		I	
6707.61		15	II	
6702.48	2		I	
6701.26	15		I	
6699.36	100	1000	II	4
6698.93		5	II	
6698.13		3	II	
6697.64	10 h		I	
6692.42	700	5	I	1
6689.84		15	II	
6689.28	10	150	II	5
6687.82	60		I	
6687.64		1	II	
6685.34		1	II	
6683.41		10	II	
6682.06		15	II	
6680.74		4	II	
6679.30	1	100	II	
6678.17	20000	1000	I	3
6673.08		10	II	4
6670.57		1	II	
6670.18		50	II	
6667.82	50000	2000	I	7
6666.78		20	II	
6666.55		40	II	4
6665.08		1	II	
6661.90	2	200	II	6
6658.43		60	II	6
6657.26		25	II	
6656.70	2		I	
6651.52		4	II	
6647.25		1	II	
6644.94		6	II	
6644.06	2	200	II	4
6643.55	10000	300	I	7
6642.12	10 h		I	
6640.88		15	II	
6640.79	7		I	
6639.62		3	II	
6639.34	150	1	I	
6639.19		5	II	
6636.54		2	II	
6636.42	6 h		I	
6634.28	5		I	
6632.40		2	II	
6630.85	2 h		I	
6626.73	800	2	I	2
6626.39		2 e	III	

TABLE 1.—*Emission spectra of ytterbium*—Continued

Wavelength in air Å	Intensity: Meggers lamp	Intensity: Thompson lamp	Spectrum	Zeeman type
6625.27	4 h		I	
6619.66		40	II	
6617.72		4	II	
6617.06	100	1000	II	6
6616.40	2	40	II	
6615.80	1	80	II	
6611.87		4	II	
6611.32		5	II	
6610.79		1 e	III	
6610.31		1	II	
6608.68		1	II	
6607.07	2000	40	I	1
6605.82	4	250	II	7
6604.45		50	II	
6600.68		7	II	
6600.03		2	II	
6594.65	3 h		I	
6593.25		50	II	
6592.69	2	150	II	7
6592.47	40		I	
6592.12		30	II	
6590.72	1	15	II	
6587.26		1	II	
6585.41	100	1000	II	6
6582.79	2	250	II	7
6578.10		20	II	
6574.10	2	200	II	6
6573.31		10	II	
6572.90	300	2	I	
6571.44	10	400	II	4
6570.94		9	II	
6568.35	60	1	I	
6567.60		9	II	
6565.72	1		I	
6563.38		2	II	
6562.35		5 h	II	
6561.65	3		I	
6560.94		1 h	II	
6559.65		2	II	
6557.46		4	II	
6555.15	1500	15	I	7
6553.35	900	9	I	3
6552.61		2	II	
6550.90	1		I	
6550.14	400	10	I	3
6549.16		6 e	III	
6548.53	2	200	II	6
6547.82	4 h		I	
6547.77		9	II	
6547.43	2		I	
6546.35		2	II	
6541.38	3	400	II	6
6540.36		1	II	
6539.33		3 e	III	
6538.31	20		I	
6531.71		5	II	
6531.26		4	II	
6531.00	25	1	I	
6527.01		25	II	
6526.36		3	II	
6523.19	2	250	II	
6521.51		25	II	
6513.78	5		I	
6512.23		1 e	III	
6509.09	60	1	I	
6508.81	1		I	
6507.98	2		I	
6507.15		1	II	
6505.29	1		I	
6503.96	3		I	
6503.01	50	500	II	4
6502.28		20	II	
6500.70	2	30	II	
6498.79	1	20	II	
6493.58		5	II	
6492.73	10	700	II	4
6491.18		5	II	
6490.32		20	II	
6489.06	80000R	10000	I	2
6488.47		200	II	
6487.08		10	II	
6486.74		50	II	
6485.55	10	200 h	II	
6477.98	5		I	
6477.63		6	II	
6476.36		1	II	
6475.98	8		I	
6474.74	30	1500	II	6
6470.17		1	II	
6468.88	70		I	
6468.18	1500	5	I	
6466.79		7	II	
6466.33		25 e	III	
6465.78		3 h	II	
6464.66	3		I	
6464.46	1		I	
6463.15	50	2000	II	7
6461.37	3 h		I	
6460.89	2		I	
6460.66	1		I	
6456.95	2	150	II	
6456.90	2		I	
6456.64	1		I	
6456.33	5		I	
6455.41	1000		I	
6455.23		4	II	
6453.30	1	150	II	
6453.11	10	150	II	
6452.73	1		I	
6452.46	1		I	
6452.10		15	II	
6450.88	40		I	
6450.10		4 e	III	
6449.59	1500	15	I	
6448.41	4 h		I	
6446.22	20		I	
6442.10		9	II	
6440.79	5	400	II	6
6437.98	1	150	II	
6435.61	3 h		I	
6433.44	15	1	I	
6432.73	1000	3000	II	5
6427.60	20	400	II	5
6423.67		5	II	
6421.53	1500	10	I	2
6421.04	400	20	I	
6417.91	20000	1000	I	2
6416.98		7	II	
6412.85		30	II	
6411.38		7 e	III	
6408.77	4		I	
6408.44	4		I	
6404.62	800	20	I	
6402.64		50	II	
6400.35	40000	2000	I	7
6397.15		2	II	
6396.68		1	II	
6396.09		7	II	
6393.91		3	II	
6393.74	700	5	I	2
6393.59		8	II	
6393.23	4	150	II	4
6389.69		10	II	
6387.68	100	2	I	
6386.84		25	II	
6382.92	20	200	II	7
6381.68	10		I	
6380.47		3	II	
6378.33		150 e	III	
6377.01	6	400	II	7
6376.74	1	20	II	
6374.81	4	80	II	5
6372.72	1500	20	I	1
6371.34		2 e	III	
6367.91		4	II	
6365.88		10 e	III	
6365.05	30		I	
6364.92		3	II	
6360.33		4	II	
6359.22	2 h		I	
6358.49	20		I	
6356.67	2	200	II	5
6355.38	20	1000	II	4
6354.39		20	II	
6348.85	2 h		I	
6348.05		10	II	
6347.32		20	II	
6347.08		4 e	III	
6345.74	40	400	II	
6344.97	3000	100	I	3
6343.54		7	II	
6343.01	8		I	
6342.65		1	II	
6341.41		6	II	
6340.93		15	II	7
6338.10		7	II	
6336.23	100	1	I	
6335.72	3000	70	I	1
6334.20		5	II	
6333.45	1	70	II	
6328.52		200 e	III	
6328.19	4		I	
6324.77	40	400	II	5
6324.43	1	90	II	4
6322.56	400	3	I	2
6318.91	20	1	I	
6317.78		2 e	III	
6313.61		1	II	
6312.99		20	II	6

TABLE 1.—*Emission spectra of ytterbium*—Continued

Wavelength in air	Intensity		Spectrum	Zeeman type	Wavelength in air	Intensity		Spectrum	Zeeman type	Wavelength in air	Intensity		Spectrum	Zeeman type
	Meggers lamp	Thompson lamp				Meggers lamp	Thompson lamp				Meggers lamp	Thompson lamp		
Å					Å					Å				
6311.10	2		I		6209.05	2		I		6121.91		9	II	
6309.82	20	1	I		6208.89	3	70	II		6120.30	5	250	II	
6308.15	400	2000	II	5	6208.10	10	500	II	6	6118.28	3000	100	I	7
6305.37	90	1	I		6206.49		3	II		6117.54	2	10	II	
6304.79	8		I		6204.88		4	II		6116.67	10	70	II	
6303.91		5	II		6204.20		4	II		6113.42	10		I	
6303.27	50	400	II	5	6198.67	20		I		6111.27	4000	60	I	2
6300.94		8	II		6196.90	3		I		6110.14	6	200	II	7
6299.71	2		I		6196.01		6	II		6108.32		2	II	
6297.95	90	1	I		6194.85	900	4	I	2	6106.18	5	200	II	6
6297.35	5	400	II		6192.32	60	1	I		6105.58	1	10	II	
6292.56		2	II		6191.14		7 h	II		6104.79		2 e	III	
6292.17	2	20	II		6190.78	15	1000	II	7	6101.83	40		I	
6291.06		5	II		6189.03	1	90	II		6099.35		3 e	III	
6286.25	2000	20	I	2	6187.08		20	II		6098.89		7	II	
6285.72		3	II		6185.43		2	II		6098.54	3	250	II	
6283.00		1 e	III		6184.05		1	II		6096.98	1	30	II	
6281.96		4	II		6183.01	2		I		6096.15	15	2	I	
6280.60		2	II		6182.14	1		I		6095.98		3	II	
6280.39		5 e	III		6181.78	100	2	I	7	6094.49	4		I	
6279.21		1 e	III		6178.81	1	20	II		6089.14	20	100	II	
6277.08	2	150	II	7	6178.63		3	II		6088.70	3	200	II	7
6274.78	2000	10000	II	6	6176.91	1		I		6087.44	20		I	
6271.15	6	250	II	4	6175.62	150	50	I		6086.48	2		I	
6270.31	3	100	II	5	6175.58		90	II	4	6083.86	1	30	II	
6269.95	1	40	II		6175.36		9	II		6083.29	5	200	II	5
6265.45	1	80	II	7	6174.70	1	60	II		6082.37	6	500	II	6
6262.89		15	II		6173.76		7	II		6082.21		10	II	
6262.43	1		I		6172.53	5		I		6076.55		2 e	III	
6261.50	2		I		6171.87	20		I		6075.21	3	200	II	7
6260.79	30	1500	II	7	6171.63	30	300	II	6	6074.10		1	II	
6257.03	20		I		6169.55	100	200	II		6073.17	7		I	
6255.43	200	2	I		6164.53		2	II		6070.19		20	II	
6251.31		2 e	III		6161.97	50		I		6068.64	1	60	II	
6250.39		1	II		6160.74	6		I		6066.51	15		I	
6249.54		1	II		6156.03	2		I		6065.72	300	3	I	2
6248.29		20	II		6152.57	800	4000	II	6	6063.01		4	II	
6247.99	1500	15	I	3	6150.63		70 h	II		6059.93		3	II	
6246.97	500	4000	II	4	6149.44		1	II		6059.22	6000	80	I	
6245.93		6	II		6148.50	15		I		6056.46	10	500	II	4
6244.69	3		I		6148.24	1		I		6055.85		40 e	III	
6244.39		1	II		6146.91	10	400	II	7	6054.57	4000	50	I	7
6242.25	1	30	II		6146.29		3	II		6053.61		3	II	
6239.67		3	II		6144.20	3 h		I		6052.88	100	900	II	5
6236.82		5 e	III		6142.83	1	60	II	7	6052.66		250	II	
6236.55	600	5	I		6141.70		1	II		6052.63	150		I	
6236.13	3	150	II	4	6141.05		3	II		6050.48	2		I	
6235.25	200	3	I		6140.72		5 e	III		6048.87		2	II	
6234.85	3	250	II	6	6140.56		2	II		6048.44	4000	50	I	1
6234.12	25		I		6135.42		2	II		6048.18	5	50	II	
6233.37	5	250	II	4	6134.28	7	200	II	4	6046.91	9		I	
6232.02		2	II		6133.56		3	II		6045.95	6 h		I	
6229.36		10	II		6132.95		25	II		6045.52		6	II	
6228.53	1		I		6131.53	1	80	II	5	6044.96	3 h		I	
6223.63	15	500	II	7	6130.67	1		I		6043.45		1	II	
6219.16	15		I		6128.51		5	II		6042.22	2	100	II	
6216.14		9	II		6128.18	10	300	II		6041.79	100	1	I	
6215.56	6	200	II	6	6127.92		10	II		6040.77	15	500	II	6
6214.22		100 e	III		6126.89		1	II		6038.82		9	II	
6213.74		3	II		6126.39	3	100	II		6035.72	400	4	I	7
6212.28		2	II		6124.63		3	II		6035.37	3		I	
6211.10		1	II		6123.68	1	30	II		6034.26	1		I	
6210.59	900	1	I		6122.99	40	250	II	6	6031.80	3000	40	I	3

TABLE 1.—*Emission spectra of ytterbium*—Continued

Wavelength in air Å	Intensity: Meggers lamp	Intensity: Thompson lamp	Spectrum	Zeeman type	Wavelength in air Å	Intensity: Meggers lamp	Intensity: Thompson lamp	Spectrum	Zeeman type	Wavelength in air Å	Intensity: Meggers lamp	Intensity: Thompson lamp	Spectrum	Zeeman type
6029.76		1	II		5965.48	1		I		5928.63	2		I	
6029.05	7 h		I		5964.12		1	II		5928.24		2	II	
6027.50	1 h		I		5963.60	2		I		5927.69	60		I	
6024.08	40	400	II	7	5962.51		2 e	III		5926.958	10		I	
6023.82	2 h l		I		5961.83	1	60	II	4	5926.688	5		I	
6021.92	10	400	II	6	5960.20	1		I		5925.46	600	5	I	2
6021.24		5 e	III		5960.04	10		I		5925.00	60		I	
6020.55	40	400	II		5959.33	1000	10	I	2	5924.498	15		I	
6018.16	5 h		I		5959.03		7	II		5924.165	2		I	
6017.70		2	II		5958.70	4000	100	I	1	5922.991	5		I	
6016.62	5	50	II		5956.86		7	II		5922.153	15		I	
6014.95	1500	10	I	1	5955.34	1500	8	I	2	5920.98		2	II	
6014.16	10		I		5954.19	2 h		I		5920.48	2		I	
6012.51		9	II		5950.93	5	250	II	6	5920.38	5	300	II	6
6012.16	1	15	II		5950.66	1500	10	I	3	5919.710	8		I	
6011.55		8	II		5949.83		20	II		5919.585	2		I	
6011.18	1		I		5949.02		10 d	III		5919.10		7	II	
6009.56	1	10	II		5948.98		5	II		5917.826	3		I	
6008.80	5	50	II		5947.71	2		I		5917.130	6		I	
6008.44	200	1	I		5947.54	1		I		5916.95		2	II	
6007.41	20	1000	II	4	5947.26	15	500	II	5	5916.00	5 h l		I	
6004.52	2000	20	I	3	5946.79	4 h l		I		5915.052	3		I	
6004.015		10	II		5946.23	1		I		5914.912	2	20	II	
6003.62	400	10	I	1	5946.00	40	2000	II	4	5914.415	5		I	
6003.33	2 h l		I		5945.44	8		I		5912.35	5 h l		I	
6002.52	3	90	II		5945.33	3		I		5912.15	2		I	
6001.05	1	30	II	6	5945.27	3		I		5911.55	5		I	
6000.91		8	II		5945.10	4		I		5911.35	20		I	
6000.28	20		I		5944.93	2		I		5910.10	4		I	
5999.95	1	30	II		5944.73	4		I		5909.33	2	10	II	
5998.71		25	II		5944.63	1	10	II		5909.10	2		I	
5996.84		1	II		5944.41	3		I		5908.36	400	1500	II	6
5993.95		1	II		5944.24	2		I		5906.45	2		I	
5993.704		15	II		5943.63	9		I		5906.33		2	II	
5991.51	2000	6000	II	6	5943.55	5	200	II		5905.85	2		I	
5990.01		10	II		5943.05	20	250	II		5905.22	3		I	
5989.33	5000	100	I	3	5942.89	3		I		5903.38	3	90	II	
5987.91	15	500	II		5942.73	3		I		5902.80		3	II	
5987.58	20		I		5942.02	4		I		5902.71	2		I	
5986.78	1	40	II		5941.72	2		I		5900.85		20	II	
5985.98		6 e	III		5941.29		2	II		5899.30	2		I	
5985.35	20	300	II	5	5941.04	1		I		5898.77	15	800	II	4
5984.98	3 h l		I		5940.68	20		I		5897.21	50	2500	II	7
5983.12	2		I		5940.63		1	II		5896.63		6 d	II	
5980.83	2		I		5939.35	2	8	II		5895.16	2		I	
5978.35	2		I		5938.15	1	10	II		5894.98	5		I	
5978.11		10	II		5936.68		20	II		5892.30		2	II	
5976.93		2	II		5936.49	900	10	I	1	5888.02		4	II	
5976.21	20		I		5935.88	2		I		5886.05	5		I	
5975.70	2		I		5935.56	2		I		5883.61		6	III	
5975.29	2		I		5935.05	20	1000	II	5	5882.80	100	600	II	
5974.63	2		I		5934.27	3		I		5877.68	10		I	
5973.49	2	20	II		5934.01		1	II		5874.67	2	200	II	7
5973.05		20 e	III		5933.775	2		I		5873.12		10	II	
5972.73	150	1	I		5932.98	2		I		5872.90		3	III	
5972.29		1	II		5932.562	4		I		5872.15		1	II	
5972.02		2	II		5931.853	3		I		5868.94		7	II	
5970.26		5	II		5931.73	3 h		I		5868.34	2	100	II	4
5969.95	3		I		5931.33		3 e	III		5866.69		6	II	
5969.84	2		I		5930.722	6		I		5866.48		1	II	
5968.23	2 h l		I		5929.82	4		I		5865.63	1	70	II	6
5966.86	2		I		5929.77		10	II		5863.86		3	II	
5966.43	20		I		5928.761	5		I		5863.37		1	II	

TABLE 1.—*Emission spectra of ytterbium*—Continued

Wavelength in air Å	Intensity: Meggers lamp	Intensity: Thompson lamp	Spectrum	Zeeman type
5862.90	1	15	II	
5861.53		3	III	
5861.11	10		I	
5854.89		3	II	
5854.510	4000	200	I	3
5854.30	5	70	II	
5853.84		3	II	
5852.92		5	II	
5847.18	1	40	II	6
5845.50	6 h		I	
5844.97		9 e	III	
5842.44	80	1	I	
5841.96	20		I	
5839.56		1	II	
5839.25	2 h		I	
5838.91	6 h		I	
5838.62	2	70	II	5
5838.27	70	1	I	
5837.14	600	4000	II	6
5836.18	1	50	II	
5835.53	1	30	II	
5834.58	200	3	I	
5833.99	5 h	200 h	II	
5833.62	20		I	
5832.12		2 e	III	
5831.82	300	3	I	3
5831.58		5	II	
5831.04		15	II	
5830.82	2		I	
5829.63	200	2	I	
5829.11	5 h		I	
5828.49		1	II	
5824.33	2	50	II	7
5823.36		2	II	
5820.17	2		I	
5819.99		3	II	
5819.41	50	1500	II	4
5814.76		2	II	
5813.58	3	40	II	5
5812.64	3 h		I	
5811.90	1	40	II	
5811.13	1	20	II	
5810.67	3000	7	I	1
5808.66	3	120	II	
5807.86		30	II	
5807.51	1	7	II	
5806.58	7		I	
5804.06	80	1	I	
5803.44	5000	80	I	2
5802.36	200	1	I	
5801.50		8	II	
5801.13	1	15	II	
5801.04	1	10	II	
5799.57	1	40	II	
5798.82	2 h		I	
5796.09	80		I	
5792.28	1	10	II	
5789.93	1500	15	I	
5789.63	100		I	
5789.17	2	50	II	
5788.74	1	15	II	
5787.86	500	5	I	
5786.59	20	150	II	5
5786.09	400	3	I	
5784.43	3 h		I	
5784.026	10		I	
5779.92		3 e	III	
5777.95	3	100	II	5
5777.29	1	10	II	
5775.61	1	50	II	
5774.34	500	5	I	
5773.82	1000	10	I	
5772.76		3	II	
5772.39	3 h l		I	
5771.66	500	2000	II	4
5769.44		6	II	
5767.95	3	30	II	
5767.20	20	800	II	6
5765.21	5 h		I	
5764.65	1	40	II	
5760.18	30	6	II	
5759.84	4 h		I	
5758.25	9		I	
5757.84	2	15	II	
5755.89	3000	40	I	3
5754.80	2	70	II	
5753.57	1	25	II	
5753.20	2		I	
5750.62		8	II	
5749.91	1000	400	II	3
5746.703		3	II	
5746.36	1	15	II	
5745.80	2000	30	I	1
5741.99	15		I	
5741.75		2	II	
5740.83		15 e	III	
5738.82		5	II	
5738.53	2		I	
5737.09		20	II	
5735.773	10	600	II	7
5735.50		5	II	
5734.26		3	II	
5733.00	2 h l		I	
5732.60	4 h l		I	
5731.94	6 h l		I	
5731.69		3	II	
5731.26	6 h l		I	
5730.41	7 h l		I	
5730.001	20	1500	II	5
5729.26	5 h l		I	
5728.853	150	5	I	
5728.58	5 h l		I	
5727.47	90		I	
5727.21		5	II	
5726.68	10 h		I	
5726.49		2	II	
5724.58	500	2	I	7
5724.21		3	II	
5723.70	600	7	I	
5722.743		8	II	
5719.99	20000	1000	I	3
5718.86		1	III	
5717.25	10	300	II	7
5716.70		2	II	
5713.73	20	500	II	4
5713.270	4	15	II	
5712.844		15	II	
5711.38	1		I	
5710.733		25	II	
5710.403	1	15	II	
5709.715		2	II	
5706.773	10	100	II	
5704.98	2	70	II	5
5704.14		3	II	
5701.922	250	3	I	3
5699.95	3000	50	I	1
5699.02		15	II	
5698.21	2		I	
5697.65		2	II	
5696.93	2		I	
5696.717		5	II	
5695.22		2	II	
5694.906		15	II	
5694.13		1	II	
5693.694	10	400	II	7
5689.917	1000	30	I	7
5689.67	3	70	II	
5688.48	200	3	I	
5687.14	1 d	20 d	II	
5686.53	80	800	II	6
5685.832	1	9	II	
5684.13	2		I	
5683.56	10	300	II	
5683.09	500	5	I	7
5679.270	1	15	II	
5679.180	2	8	II	
5675.180	2	50	II	
5674.31	10	150	II	7
5672.37		2	II	
5672.16		8	II	
5671.45		2 e	III	
5670.02	500	2	I	
5665.34		1	II	
5663.21	200	2	I	
5660.152		4	II	
5658.86		1 e	III	
5654.27	2	150	II	7
5653.24	3	200	II	7
5651.985	1000	4000	II	4
5642.446	40		I	
5637.812	80	600	II	6
5637.33	1	6	II	
5634.45		1	II	
5633.81		1 e	III	
5631.496	2	90	II	
5628.958	10		I	
5627.89	4	200	II	7
5625.92	20		I	
5624.494		10	II	
5620.88	1	70	II	
5620.19	50	700	II	4
5618.55		1	II	
5616.66	2 h		I	
5614.68	1		I	
5614.116	3		I	
5613.39	5 h		I	
5611.50	1		I	
5610.60	2		I	
5610.281	3		I	

TABLE 1.—*Emission spectra of ytterbium*—Continued

Wave-length in air	Intensity		Spectrum	Zeeman type	Wave-length in air	Intensity		Spectrum	Zeeman type	Wave-length in air	Intensity		Spectrum	Zeeman type
Å	Meggers lamp	Thompson lamp			Å	Meggers lamp	Thompson lamp			Å	Meggers lamp	Thompson lamp		
5609.89		1	II		5529.92	4	150	II	7	5458.088	2	60	II	
5609.44	1		I		5529.08	5	250	II	5	5457.427	4	150	II	
5608.914	1	50	II		5528.403	3		I		5455.046	5	250	II	4
5608.64		2	II		5527.81	50		I		5454.007	2500	25	I	1
5608.041	6		I		5526.37	5		I		5453.47	60	1	I	
5607.91		1	II		5524.544	3000	30	I	7	5449.84		1	II	
5607.345	10	150	II		5521.76	10		I		5449.270	500	2500	II	5
5607.124		4	II		5521.61		3	II		5448.565		4	II	
5606.64		1	II		5520.22	1	50	II	6	5445.492	1	40	II	
5605.847	3		I		5519.83		2	II		5441.615	2	5	II	
5604.145		9	II		5518.352	70	1	I		5441.259	200	1	I	
5602.35	2	20	II		5516.334		10	II		5440.548	10	200	II	
5602.264	3	40	II		5515.38		3	II		5438.01	2		I	
5600.45	10		I		5514.79	1		I		5435.27		6	II	
5598.14	2		I		5512.47	20		I		5432.89	400	6	I	
5597.189	800	10	I	7	5512.19	20		I		5432.71	60	1500	II	4
5595.84	5		I		5511.764	1	30	II	7	5431.167	2	80	II	
5591.19	10		I		5511.401	2	70	II	7	5429.838		8	II	
5590.10	10		I		5509.198		20	II		5428.162		2 e	III	
5588.452	500	4000	II	4	5509.046		3	II		5426.867	30	900	II	7
5587.249	200	2	I		5508.266		20	II	5	5425.445	100	1	I	
5586.362	2000	100	I	3	5507.70		1	II		5424.627	30	300	II	5
5585.426	400	5	I		5506.11	1500	5	I		5422.715		1	II	
5585.248		20	II		5505.49	20000	300	I	2	5421.361	7		I	
5583.57		1	II		5504.17	60		I		5420.608		7	II	
5582.236		2	II		5504.026	300	3	I		5417.421		9	II	
5581.778		8	II		5502.802	1	10	II		5414.258	6	200	II	7
5581.05	2	40	II		5501.37	2	20	II		5413.195	15		I	
5580.79	20	700	II	4	5499.65		2	II		5411.038	1	40	II	
5578.483		4	II		5498.75	5000	500	I	7	5410.635		15	II	
5578.232	2000	20	I	7	5498.390		3	II		5409.473	2	60	II	4
5576.250	5		I		5494.58		1	II		5408.348	100	2	I	
5575.705	10	100	II		5494.364	1	10	II		5408.092		4	II	
5573.64		1	II		5493.088	700	5	I	2	5405.541	60	1	I	
5572.528	30	300	II		5491.285	6		I		5404.899	300	5	I	
5568.11	10000	100	I	2	5490.847		3	II		5403.079	3000	100	I	1
5566.04		3	II		5489.633	80		I		5402.706		3	II	
5564.352		3	II		5488.883		8	II		5402.00	150	2	I	
5562.093	2000	200	I	3	5487.512	1	9	II		5399.71	50	500	II	7
5559.58		1	II		5486.535	7	150	II	6	5398.084		2 e	III	
5558.98	800	8	I		5483.212		3	II		5397.23		1	II	
5556.466	50000 A	10000	I	2	5481.925	20000	400	I	2	5395.73	20	300	II	7
5554.62	500	5	I		5479.806	1	50	II		5394.084		3	II	
5554.30		4	II		5479.122		2 d	II		5393.757	2500	90	I	1
5552.30		1 e	III		5478.50	100	1500	II	4	5393.37	5	150	II	6
5551.69		2	II		5477.206		9	II		5390.845	2500	40	I	3
5550.37		7	II		5476.90	2		I		5390.622	4000	150	I	1
5549.79		20	II		5475.706		10	II		5390.18		6	II	
5549.32		1	II		5475.132		4	II		5389.84	200	800	II	5
5548.918		50	II		5474.565	400	5	I		5387.99	90	8	I	
5548.79	100		I		5474.037	1500	15	I	1	5386.72	1	50	II	
5547.16	50	500	II	7	5471.17	30	400	II	5	5386.07		10	II	
5545.814	500	10	I		5469.353	400	5	I		5385.29	200	2	I	
5544.17		1 h	II		5468.387	150	2	I		5384.48	5	50	II	5
5543.96		8	II		5468.260		3	II		5383.95	3	60	II	
5540.03		10	II		5468.099	1		I		5382.55	2		I	
5539.053	20000	1000	I	1	5467.495	1	9	II		5380.94	1		I	
5538.016	50		I		5466.714	1	25	II		5380.54	500	7	I	2
5535.47	7		I		5464.894	6	200	II	7	5380.24	70	2	I	7
5533.21		7	II		5463.850		3	II		5379.15	6		I	
5533.14		10	II		5463.24	4		I		5376.97	5	250	II	7
5532.111		3	II		5463.12		10	II		5371.53		4	II	
5530.73	1	1	II		5460.74		4 e	III		5370.47		9	II	

TABLE 1.—*Emission spectra of ytterbium*—Continued

Wavelength in air Å	Intensity: Meggers lamp	Intensity: Thompson lamp	Spectrum	Zeeman type
5368.28	50	400	II	4
5367.78	10	100	II	
5367.35	4	60	II	7
5365.41	1	50	II	
5364.78		15	II	
5364.12		15	II	
5363.66	10000	200	I	2
5362.43	1	20	II	
5360.85		1	II	
5360.10	1	30	II	
5359.91	6	200	II	
5358.64	400	2000	II	6
5357.71		3	II	
5357.08	20	200	II	
5356.54	1	2	II	
5356.41		10	II	
5352.95	1000	6000	II	4
5351.29	5000	300	I	3
5350.474	2	40	II	
5349.626		5	II	
5349.10	1	6	II	
5348.208	300	3	I	
5347.22	1000	3000	II	4
5345.83	200	900	II	
5345.66	400	1500	II	
5342.99		7	II	
5341.10	2		I	
5339.69		1	II	
5339.312		15	II	
5338.75	10	100	II	7
5338.31	60		I	
5337.11		7	II	
5335.82	10		I	
5335.49	50		I	
5335.15	2000	7000	II	4
5334.02	100	200	II	
5331.536		20	II	
5330.92		1	II	
5330.79	1		I	
5330.348	6		I	
5328.526	3	50	II	
5327.593	4		I	
5324.778		7	II	
5324.486		9	II	
5323.10	300	3	I	1
5322.541		8	II	
5321.14	10	250	II	
5320.962	5		I	
5320.774		15	II	
5320.324	6		I	
5318.79		1	II	
5315.462		6	II	
5309.31	30	200	II	4
5307.74		6	II	
5306.506		40	II	
5300.935	100	2000	II	4
5299.852	2000	10	I	3
5297.153	150	4	I	
5297.02	50	1	I	
5295.755		5	II	
5293.726		3	II	
5291.99		10	II	
5291.077		5	II	
5290.578	150	3	I	
5290.08	2	20	II	
5289.45		2	II	
5289.178	1	5	II	
5288.51	2000	15	I	7
5287.45	3000	70	I	1
5287.285	5	100	II	
5286.12	2	100	II	
5283.825		3	II	
5283.00		1	II	
5281.210		20	II	
5280.522	1	50	II	
5279.53	1000	5000	II	4
5277.04	30000	3000	I	2
5275.592	1000	10	I	3
5271.473	400	20	I	
5266.964	15		I	
5265.63		8	II	
5265.558	40		I	
5264.238	10		I	
5263.570	6	200	II	6
5262.012	1	30	II	
5261.52		1	II	
5259.65		1	II	
5258.165	800	10	I	
5257.490	800	3000	II	6
5257.29	90		I	
5256.85		20	II	
5255.680	4	150	II	
5255.61	2		I	
5254.79		2 e	III	
5254.60		3	II	
5254.20	1	20	II	
5253.448	1		I	
5250.804	100	2	I	
5250.51	1	8	II	
5249.80	5	150	II	
5248.99		6	II	
5248.17		1	II	
5247.94	15		I	
5246.857	400	4	I	
5246.39	4	40	II	
5244.61	100	300	II	5
5244.11	10000	250	I	2
5243.56		1	II	
5243.41		4	II	
5243.15		2	II	
5240.51	300	1000	II	6
5239.25		2	II	
5236.66	3	150	II	
5234.28		2	II	
5232.537	6	40	II	
5230.292	60		I	
5229.963	1	60	II	
5228.172	1000	30	I	7
5227.271	4000	80	I	1
5227.01	1	70	II	
5226.18	20	150	II	
5224.53	1		I	
5222.68		3	II	
5221.606	50	1	I	
5220.82		5	II	
5220.41		10	II	
5218.792	1		I	
5217.936	3	70	II	7
5215.44	4	100	II	
5214.95	500	5	I	3
5212.232		25	II	
5211.604	6000	400	I	3
5209.54		1	II	
5205.574	4	30	II	
5204.57		1	II	
5202.87		1	II	
5201.32		1	II	
5201.21		2	II	
5200.74		4	II	
5200.54	50	500	II	4
5200.10	4		I	
5199.14		1	II	
5196.81	40		I	
5196.085	5000	200	I	3
5195.20	100	1	I	
5194.752	2000	80	I	
5193.850	2000	20	I	1
5189.89		7	II	
5189.50		8	II	
5189.14	200	2	I	
5188.89		9	II	
5187.33		3	II	
5185.15		1	II	
5184.66		1	II	
5184.15	150	1000	II	4
5182.755	2000	50	I	7
5180.641		5 e	III	
5180.355	15	150	II	6
5178.73	60		I	
5178.70	90	20	I	
5175.45	250	2	I	
5173.11	2	200	II	
5173.064	10	100	II	
5172.40		1	II	
5172.214	50	1	I	
5168.29	90		I	
5167.660		3	II	
5163.862	1		I	
5160.99		1	II	
5160.74		1 e	III	
5160.47	7		I	
5159.655		3	II	
5157.962	3	100	II	
5156.285	100	2	I	
5152.34	7	200	II	
5151.25		4	II	
5149.04		1	II	
5148.75	1		I	
5147.02	50	700	II	6
5146.37		3 e	III	
5142.28	3	100	II	
5141.64		3	II	
5140.38	120	2	I	
5140.11	20		I	
5139.53	900	10	I	1
5139.35	40		I	
5138.01		1	II	
5137.43	2	4	II	
5137.389	6		I	

TABLE 1.—*Emission spectra of ytterbium*—Continued

Wavelength in air	Intensity		Spectrum	Zeeman type
Å	Meggers lamp	Thompson lamp		
5137.23		1	II	
5136.76	2		I	
5136.49		1	II	
5135.98	200	1500	II	7
5133.42		1	II	
5132.71	90	1	I	
5132.40	1	60	II	
5131.01	1	10	II	
5130.711		2	II	
5130.56		1	II	
5130.523	100	2	I	
5130.30		8 e	III	
5130.095	7		I	
5129.688	200	2	I	
5129.56		60	II	
5128.55	3	100	II	
5127.64	2		I	
5126.80	2000	20	I	3
5121.58	30	300	II	6
5119.29	100	1	I	
5117.72	1	25	II	
5116.200		10	II	
5114.606	40	1	I	
5113.34	700	10	I	3
5111.89	2		I	
5111.47	1	60	II	
5107.58		1	II	
5106.95	1		I	
5106.12		1	II	
5105.75	600	30 h l	I	7
5105.028	10	150	II	
5104.85	2000	30	I	1
5104.42	20	400	II	
5103.724	5	1	I	
5103.644	5		I	
5101.810		3	II	
5101.57	3	80	II	
5100.08	100	1	I	
5099.11		3	II	
5097.75		2	II	
5095.99		3	II	
5093.92	2		I	
5090.77	80		I	
5090.628		15	II	
5088.92	1	30	II	
5088.275	15		I	
5087.89	4		I	
5087.61	10	150	II	4
5086.45	15		I	
5085.70	2	80	II	
5085.22		1	II	
5083.938	90	1	I	
5083.52		2	II	
5082.934		7	II	
5082.590	250	9	I	
5080.981	500	9	I	2
5076.957		6	II	
5076.744	5000	150	I	1
5075.813		8	II	
5074.609		80	II	
5074.34	20000	2000	I	1
5073.35		1	II	
5069.144	4000	150	I	7
5067.800	1500	40	I	2
5067.600		10	II	
5067.297	200	800	II	4
5065.74		1	II	
5065.488		4	II	
5063.605	8		I	
5062.938	30	300	II	6
5062.634		15	II	
5061.87		2 e	III	
5061.24		1	II	
5060.722	2		I	
5058.71		8	II	
5058.613	900	5	I	2
5057.275		2	II	
5055.933	15		I	
5055.485	2		I	
5054.94		15 e	III	
5052.90		2 e	III	
5051.096		2	II	
5050.77	15		I	
5049.832	5	250	II	5
5047.08		15 d	II	
5043.708	150	4	I	7
5043.28		1	II	
5042.982	3	20	II	7
5041.756		4	II	
5039.86		2	II	
5038.240		15	II	
5034.262	5	1	I	
5033.289	1	20	II	
5032.899	2		I	
5032.586	1	25	II	
5032.14	2		I	
5029.342		3	II	
5029.03	6		I	
5027.67	2000	80	I	2
5025.356	1	6	II	
5023.925	1	9	II	
5022.32		3 e	III	
5021.860	400	4	I	
5021.13	50	400	II	7
5019.691	1500	15	I	1
5017.80		3	II	
5014.98		2	II	
5014.472	20	250	II	6
5013.76		1	II	
5013.27		2	III	
5010.04		1	II	
5009.525	500	2000	II	7
5009.025		2	II	
5008.876	1	15	II	
5007.76		1	II	
5005.25		1	II	
5004.79	15		I	
5004.63		1	II	
5003.306	2		I	
5002.98	5	70	II	5
5000.452		2	II	
4998.87		3	II	
4998.266	3	15	II	
4996.604		4	II	
4994.74		1	II	
4993.32		1	II	
4992.786	2		I	
4992.654		6	II	
4992.520		7	II	
4992.102	2		I	
4989.924	6		I	
4989.794		4	II	
4989.57	100	1	I	
4988.383	1	15	II	
4988.022		1	II	
4987.292	1	15	II	
4986.88	6	3	II	
4985.36	2		I	
4982.82	2		I	
4981.34	1		I	
4978.62	1	9	II	
4976.65		2	II	
4975.86		4 e	III	
4974.16	2000	100	I	2
4973.90		15	II	
4972.42	10	2	I	
4972.26	1	20	II	
4971.20		8	II	
4970.41	40	7	I	
4970.203	3	4	II	
4967.35		2	II	
4966.902	10000R	700	I	3
4965.43	3	15	II	
4964.61		3 e	III	
4963.18		2	II	
4962.28	1		I	
4961.124		3	II	
4960.478		4 e	III	
4960.28	1		I	
4958.895		2	II	
4957.83	8		I	
4957.262		7	II	
4956.512	500	9	I	3
4955.98		1	II	
4954.68	3	50	II	7
4953.72	1		I	
4953.622		3	II	
4952.740		2	II	
4951.88	2		I	
4949.24		2	II	
4946.524		1	II	
4946.19		1	II	
4945.944		3	II	
4944.956	5	150	II	
4944.080	200	600	II	6
4942.742	20	200	II	
4942.254	250	3	I	
4940.53		2	II	
4938.828		4	II	
4937.222	100	2000	II	7
4935.50	20000R	2000	I	1
4932.81	5		I	
4931.953	1000	40	I	2
4931.16	5		I	
4930.78		1	II	
4929.31	1	20	II	7
4928.184		4	II	
4927.154		1	II	
4924.187		2	II	

TABLE 1.—*Emission spectra of ytterbium*—Continued

Wavelength in air	Intensity		Spectrum	Zeeman type	Wavelength in air	Intensity		Spectrum	Zeeman type	Wavelength in air	Intensity		Spectrum	Zeeman type
	Meggers lamp	Thompson lamp				Meggers lamp	Thompson lamp				Meggers lamp	Thompson lamp		
Å					Å					Å				
4923.747		1	II		4845.612	3		I		4778.982	200	7	I	3
4919.595	100	2	I		4841.918	50	2	I		4778.414		1	II	
4918.45		10	II		4841.47		2	II		4778.35		1	II	
4918.118	150	2	I	7	4841.153	50	150	II	6	4777.946		4	II	
4917.044	20	60	II	4	4839.462	2		I		4777.56		1	II	
4915.42		1	II		4839.279	1	15	II		4774.145	4	8	II	
4912.365	3000	100	I	3	4839.014	1	7	II		4773.839		8	II	
4909.81		3	II		4838.657	7		I		4773.13		3	II	
4906.335	50		I		4838.220	10	20	II		4772.43		2	II	
4906.27		9	II		4837.46	4000	100	I	2	4772.23		6	II	
4905.48		2	II		4837.045	500	1000	II		4772.000		2	II	
4904.93	1		I		4836.96	500	1000	II	6	4770.834	150	2	I	
4903.89	1	25	II		4834.926	1	10	II		4768.32		6	II	
4903.71	3	50	II	7	4834.72	10	100	II	4	4768.036		3	II	
4900.16		4	II		4834.23	2	3	II		4765.51	1		I	
4899.980		2	II		4833.55		1	II		4765.080	3		I	
4899.78	500	5	I	3	4833.24		1	II		4762.587	300	5	I	2
4898.42		15	II		4832.989	200	5	I		4761.55	2		I	
4897.90	2	40	II		4831.912	400	20	I		4761.139	2	40	II	
4897.08	5		I		4831.533	2	20	II		4758.320	80	4	I	7
4895.606	150	5	I		4831.30	600	10	I	3	4757.559	40	1	I	
4894.983	50	400	II	5	4830.704	500	10	I	2	4757.14		1	II	
4894.596	3000	400	I	1	4828.29	3		I		4756.36		1	II	
4894.296	50		I		4827.81		2	II		4755.15	4		I	
4893.465	500	5	I	7	4826.78		2	II		4754.370	5		I	
4891.992	200	4	I	7	4825.655	1		I		4752.91	100	400	II	6
4891.654		3	II		4824.28	1		I		4751.789	400	10	I	1
4891.056	1	8	II		4823.615		2	II		4751.22	3		I	
4890.07		1	II		4822.47		1	II		4749.948	2	30	II	
4888.99		3	II		4822.010		3	II		4749.55		1	II	
4888.18	25	1	I		4821.58		2 e	III		4749.06	1	5	II	
4887.662		2	II		4820.74		1	II		4748.71		2	II	
4885.45	90	3	I		4820.242	400	1000	II	4	4748.08		2 d	II	
4884.205		4	II		4819.59	20	1	I		4746.68	10	150	II	6
4882.15	2		I		4818.371	100	600	II	4	4745.483	1	20	II	
4880.674		8	II		4816.43	5000	600	I	1	4745.27	2		I	
4880.190		10	II		4815.612		6	II		4743.57		3	II	
4875.852		2	II		4815.28		1	II		4743.356	250	7	I	3
4873.180		2	II		4813.92	2	7	II		4741.574	8		I	
4871.670	2	40	II	7	4812.918	400	40	I	3	4739.70	1	10	II	
4871.150	10	90	II	7	4811.89	1		I		4739.330	1		I	
4870.288	30		I		4810.51	40	4	I		4738.656	5	7	II	
4868.511	8		I		4809.451	2	30	II		4736.89	1		I	
4863.87		3	II		4808.502	2	50	II		4736.69		2	II	
4863.56		1	II		4804.571	3		I		4736.525	15		I	
4863.295	40		I		4803.653		10	II		4732.935	1	25	II	
4862.802		4 e	III		4801.473		2	II		4732.505	18		I	
4862.524	2		I		4800.535	2		I		4732.14	2		I	
4860.84		2	II		4799.96		1	II		4732.025	30	200	II	6
4859.49		2	II		4798.72		3	II		4731.70		2	II	
4857.542	50	1	I		4795.829	80	1	I		4731.04	2		I	
4856.50	1		I		4794.96	1		I		4729.25		3	II	
4855.922	15		I		4794.85	1		I		4728.109		8	II	
4854.92	1		I		4794.57	1		I		4727.901		7	II	
4853.826	500	7	I	1	4792.63		3	II		4726.54		1	II	
4853.347		7	II		4792.336		2	II		4726.08	1000	3000	II	4
4851.150	300	600	II	7	4790.61	1	15	II		4725.14		2	II	
4850.848	1	10	II		4788.924		5	II		4723.85	1		I	
4849.265		2	II		4786.61	2000	8000	II	4	4723.404		4	II	
4849.034	100	1	I		4784.54	70	9	I		4722.53	2		I	
4848.455	50	300	II		4781.867	10000	2000	I	1	4722.148	10		I	
4846.873	1	15	II		4781.17		2 d	II		4720.955		2 e	III	
4846.612	4	20	II		4780.32	400	15	I	1	4720.79	2000	50	I	2

792-867 O-66-6

TABLE 1.—*Emission spectra of ytterbium*—Continued

Wavelength in air Å	Intensity Meggers lamp	Intensity Thompson lamp	Spectrum	Zeeman type
4720.390		2	II	
4718.56	3000	500	I	3
4718.34	200	2	I	
4717.375	30		I	
4715.672		3	II	
4715.16	6		I	
4714.70	700	40	I	
4712.78	40	200	II	5
4712.73	2		I	
4709.96	15	1	I	
4709.330	40	1	I	
4706.81	2		I	
4706.700	2		I	
4705.40		4	II	
4705.04		7	II	
4704.886	300	20	I	
4704.23		1	II	
4703.012		4	II	
4702.982	10		I	
4702.355	200	10	I	
4700.77		1 e	III	
4699.045		6	II	
4698.62	10	40	II	
4697.688		2	II	
4697.34		3	II	
4696.842	1	15	II	
4696.286	40	2	I	
4695.832	7		I	
4695.70	2		I	
4693.06	1		I	
4692.41		2	II	
4691.982		4	II	
4690.810	20	90	II	
4689.807	1	7	II	
4689.069	15		I	
4688.515	40	100	II	4
4688.38	5	20	II	
4687.593	1000	50	I	1
4685.876		6	II	
4685.28	4		I	
4685.071		3	II	
4684.268	1500	80	I	7
4683.810	200	1000	II	7
4681.666	10	1	I	
4681.514	3		I	
4681.088		3	II	
4680.136	6	1	I	
4679.625	15		I	
4678.171	2	6	II	
4677.432	90	1	I	
4676.67	6		I	
4675.66	2	4	II	
4675.20	1		I	
4674.644		1	II	
4674.493	1	3	II	
4673.62	1		I	
4672.125	1		I	
4671.701	30	1	I	
4671.386		3	II	
4670.586	50	200	II	4
4669.510	2		I	
4669.280		4	II	
4667.05	1	1	II	
4666.735	200	10	I	7
4666.145	2	1	II	
4664.565	30		I	
4663.873	5		I	
4663.44	1		I	
4661.878	5		I	
4660.906		4	II	
4660.68		2 e	III	
4660.057	4		I	
4659.910		5	II	
4659.780	20		I	
4659.60		1	II	
4658.87	4 d		I	
4658.746		3	II	
4658.443	2	2	I,II	
4657.43		1	II	
4656.971	3000	500	I	2
4654.46	4		I	
4654.070	1	5	II	
4653.310	5		I	
4652.667		5	II	
4652.279		2	II	
4651.67	500	20	I	3
4650.99	3		I	
4650.05	1500	100	I	7
4649.756		2	II	
4647.076		2	II	
4646.91	7		I	
4646.532		2 e	III	
4645.05		10	II	
4644.54	3000	100	I	1
4643.14		5	II	
4641.945	6	2	I	
4640.11		15	II	
4639.14		40 e	III	
4639.04		1	II	
4638.81	3		I	
4637.88		1 e	III	
4637.341	3		I	
4637.226		3	II	
4635.01		1	II	
4634.38	4		I	
4634.014	20	200	II	7
4633.406		3 e	III	
4633.196	30	4	I	
4631.09	2		I	
4630.614		3	II	
4630.522	20		I	
4629.833	200	3	I	
4629.75		2	II	
4628.861	2		I	
4628.43	2		I	
4627.556	4		I	
4627.23	5		I	
4626.054	2		I	
4625.47	2		I	
4624.93		2	II	
4624.585		4	III	
4624.41	1200	50	I	2
4623.91		1	II	
4623.060		3	II	
4621.83		2	II	
4621.80	3		I	
4620.51		2	II	
4618.487	15		I	
4617.900	5		I	
4617.46	1		I	
4615.947	300	15	I	1
4615.740		2	II	
4615.427	3		I	
4614.020	1	3	II	
4611.90		1	II	
4610.70		1	II	
4610.172	600	30	I	3
4609.600		1	II	
4608.131		15	II	
4608.061	3		I	
4607.004		3 e	III	
4606.854	1		I	
4602.354	2		I	
4600.300		2	II	
4598.85		2	II	
4598.361	300	800	II	5
4597.980	5	30	II	
4597.279	2	30	II	
4597.087		1	II	
4596.342		7	II	
4595.556		1	II	
4594.033	10		I	
4593.375	30	5	I	
4593.214		4	II	
4592.443		10	II	
4591.780	5		I	
4591.333		4	III	
4590.834	2000	200	I	3
4590.578	10		I	
4589.211	1000	150	I	2
4588.677		1	II	
4587.547		2	III	
4587.075		15	II	
4585.916	40	4	I	7
4585.767		10	II	
4585.634	15		I	
4585.528		2	III	
4582.924	60	6	I	
4582.695	50	6	I	
4582.355	6000R	600	I	3
4581.222	7		I	
4580.724	9	1	I	
4580.649	40	6	I	
4579.536		6	II	
4578.620		3	II	
4578.142		7	II	
4577.722	10		I	
4576.209	10000R	1000	I	1
4574.800		2	II	
4572.740		1	II	
4572.027		1	II	
4571.660		3	II	
4571.064		1	II	
4570.081		1	II	
4569.172		2	III	
4568.853	200	50	I	3
4567.368	700	60	I	2
4563.95	2000	200	I	1
4563.680		3	II	

TABLE 1.—*Emission spectra of ytterbium*—Continued

Wavelength in air Å	Intensity: Meggers lamp	Intensity: Thompson lamp	Spectrum	Zeeman type
4562.440		5	II	
4561.533		2	III	
4560.022		3	II	
4558.906		3	III	
4558.095	2		I	
4557.936	20	150	II	
4555.50		2	II	
4555.47	3		I	
4554.217		5 e	III	
4554.032	1	3	II	
4553.576	500	1500	II	6
4552.619		8	II	
4552.351	6		I	
4552.175		2	II	
4551.792		2 d	II	
4550.601		6	II	
4548.359	40	80	II	
4547.960		3	II	
4547.788	10		I	
4547.032	1	20	II	
4546.866	30	1	I	
4545.770	8	1	I	
4545.383		1	II	
4545.216		2	II	
4544.420	30	1	I	
4543.879	2	40	II	
4543.680	2		I	
4543.452		4	II	
4543.302		3	II	
4542.588	1 h	5	II	
4542.371		1	II	
4541.598		2	II	
4541.452	1		I	
4541.325	20	100	II	5
4540.046	8	2	I	
4539.323	5	20	II	
4538.678	4		I	
4538.027		3	II	
4537.494		2	II	
4536.805		3	II	
4536.313	2		I	
4535.718		2	II	
4534.250		1	II	
4533.506	1000	50	I	3
4533.006	150	8	I	
4532.702	50	2	I	
4531.333	1500	200	I	1
4530.657		3	II	
4530.23		4	III	
4529.87	3000	400	I	1
4528.882		5	II	
4527.526		2	II	
4525.535		1	II	
4525.108		3	II	
4524.810		2	II	
4524.549	1	4	II	
4523.161		2	II	
4521.338		4	III	
4520.918	2		I	
4520.746		8	II	
4520.510	5	2	I	
4520.161	200	2	I	
4517.584		100	III	
4517.218		2	II	
4517.051		1	II	
4516.094	1	2	II	
4515.636		2	II	
4515.161	200	800	II	4
4514.846		10	II	
4513.990	6	20	II	
4513.408	1000	80	I	3
4512.909		1	II	
4511.725		3	II	
4510.744		3	II	
4509.700		3	II	
4508.788	1	9	II	
4506.95		2 d	II	
4506.045	1	4	II	
4505.900		5	II	
4505.345		3	II	
4504.850		2	II	
4504.331	1	9	II	
4504.076		3	III	
4503.636	600	50	I	3
4503.463		5	II	
4503.21	150	5	I	
4500.542		3	II	
4500.304		1	II	
4499.621		3	II	
4499.462		1	II	
4498.098	1		I	
4495.840	1		I	
4495.520		1	II	
4493.965	50	150	II	6
4493.244		1	II	
4492.120	4		I	
4491.422		1	II	
4490.240		1	II	
4490.161	2		I	
4488.282	1000	60	I	1
4487.266	50	200	II	7
4487.03		2 h	II	
4486.794		1	II	
4486.225		1	II	
4485.986		1	II	
4485.326		6	II	
4485.040		2	II	
4484.466	20	60	II	
4484.280	1	5	II	
4483.152	8	1	I	
4482.422	1500	150	I	3
4478.271	30	1	I	
4475.666		2	II	
4474.115		3	II	
4473.884		1	II	
4473.005	20	2	I	
4472.470	1500	300	I	7
4472.146		8	II	
4470.958		1	II	
4469.566		3	II	
4468.520	4		I	
4468.18	10	1	I	
4467.642		1	II	
4467.128	1	10	II	
4466.002		7	II	
4465.663		2	II	
4463.965		2	II	
4463.855	1	8	II	
4463.493	1	9	II	
4461.72	7		I	
4460.923	1	5	II	
4450.405		1	II	
4459.181		1	II	
4457.428		2	II	
4457.311		1	II	
4456.994		4	II	
4455.651	4	1	I	
4452.663		3	II	
4452.153		1	II	
4451.930		20	II	
4451.11		2 d	II	
4450.60		1	II	
4444.860		3	II	
4444.108		2	III	
4442.075		3	II	
4441.484		2	II	
4441.031	9	2	I	
4440.415		3	III	
4440.011	4		I	
4439.19	7000R	500	I	2
4438.142		7	II	
4436.366	4		I	
4435.150		5	II	
4434.795	20	1	I	
4434.178	40	100	II	
4432.041	1		I	
4431.595		1	II	
4430.208	900	150	I	3
4429.689		2	III	
4428.980	30	1	I	
4428.782	700	100	I	
4428.153		3 h	II	
4428.02	3		I	
4427.387	600	200	I	
4423.129		1	II	
4422.150		3	II	
4422.070	1		I	
4419.616	3		I	
4419.495		1	II	
4418.132		3	II	
4417.814		1	II	
4417.080		3	II	
4415.202	1		I	
4414.548		1	II	
4412.075		2	III	
4411.095	500	30	I	3
4410.740		2 h	II	
4410.230	200	8	I	
4409.685		2 h	II	
4409.346	200	300	II	5
4408.220		1	II	
4407.650	1	4	II	
4407.081	5	1	I	
4405.496		1	II	
4404.208		1	II	
4403.037		1	II	
4402.824		5	II	
4402.605	40	2	I	7
4402.300	40	200	II	4

TABLE 1.—*Emission spectra of ytterbium*—Continued

Wavelength in air Å	Intensity: Meggers lamp	Intensity: Thompson lamp	Spectrum	Zeeman type
4401.824		1	II	
4401.445	1	6	II	
4400.583		1	II	
4400.332	50	2	I	
4399.391		1	II	
4398.96	2000	100	I	3
4396.499	10	40	II	
4396.254	100	5	I	7
4395.52	1		I	
4394.973	70	3	I	
4394.177	25	2	I	
4393.688	2000	400 h	I	7
4392.825	50	100	II	6
4390.49		1	II	
4390.43		1	II	
4389.764	50	200	II	
4389.15		1	III	
4388.528		8	II	
4387.46		1	II	
4387.32	30	2	I	
4387.144	1	10	II	
4386.50	200	5	I	
4385.97	2	20	II	
4385.82		1	III	
4385.66	3	10	II	
4385.14	100	2	I	
4384.72		2	II	
4384.39		4	III	
4384.29	3		I	
4383.93		10	II	
4383.11		1	II	
4383.02		2	II	
4382.16		1	II	
4382.08		2	II	
4381.87	2	1	I	
4381.80		20	II	
4380.30		4	III	
4380.07		10	III	
4379.91		8	III	
4379.50	20	300	II	
4379.452	200	20	I	
4379.268	60	3	I	
4377.80		1	II	
4377.527	3000	300 h l	I	
4376.851	1	40	II	
4376.649		2	II	
4376.456	2000	200	I	3
4375.814		6	II	
4374.861		3	II	
4373.116	20	1	I	
4372.854		1	II	
4372.65		2	II	
4372.560	2	30	II	
4371.083		3	II	
4371.05		1	II	
4370.810	200	2000	II	6
4368.89		1	II	
4368.678	100	5 h	I	
4368.520		1	II	
4368.23	10		I	
4366.284	1000	200 h l	I	
4365.948		2	II	
4364.056		5	II	
4363.71	3		I	
4363.54		1	II	
4363.280	6	90	II	
4362.333		4	II	
4362.156	1	6	II	
4361.868		2	II	
4361.639	100	7 h	I	
4361.468	1	10	II	7
4360.663		4	II	
4360.140	1	2	II	
4359.958		20	II	
4359.528	1000	150 h	I	3
4359.165	3	2	I,II	
4356.676	500	40	I	2
4356.468		5	III	
4356.160		3	II	
4355.58		1	II	
4354.191	3	10	II	
4354.037	2	1	I	
4353.570	500	90 h l	I	
4352.948	2000	400	I	3
4351.67	1		I	
4351.07		4	III	
4350.801		15 e	III	
4350.44		2	III	
4350.006	40	1	I	
4349.952		2	II	
4349.470	2	1	I	
4348.807		8	III	
4348.087	3	15	II	
4347.66	3		I	
4347.358		3	II	
4347.223	10	20	II	
4347.13		1	II	
4347.013		4	III	
4346.00		1	II	
4345.054		3	III	
4344.894	1	20	II	
4344.762	300	20	I	
4344.204	60	300	II	4
4343.845		5	II	
4343.632	3		I	
4343.110	2		I	
4342.753		3	II	
4342.151	6	80	II	5
4341.646		10	II	
4340.673	2	7	II	
4340.269		1	II	
4340.147	1	15	II	
4339.71	4		I	
4339.38	30		I	
4339.082	150	1000	II	4
4337.599	80	20	I	
4337.235		2	II	
4336.430	1000	150 h l	I	
4336.30		1	II	
4335.360	20	1	I	
4334.914	3	4	II	
4333.909	400	40	I	
4332.809		4	II	
4331.942		2	II	
4331.762		3	II	
4331.318		1	II	
4331.032		5	II	
4330.488	20	1	I	
4329.818		15	II	
4329.718	70	4	I	7
4329.654		1	II	
4327.853		9	II	
4327.238		2	II	
4326.637	1	15	II	
4326.556		9	II	
4326.404	2000	200	I	1
4325.240	6	90	II	
4325.033		2	II	
4324.962		1	II	
4324.500		7	II	
4324.160		1	II	
4323.630		8	II	
4323.554	1	5	II	
4322.851		1	II	
4322.56	2	30	II	
4322.53	1	20	II	
4322.230	200	2000	II	6
4320.995		2	III	
4320.723		2	II	
4319.556	1	9	II	
4318.978		1	II	
4318.820		1	II	
4318.750		2	II	
4318.459	2	10	II	
4318.010		3	II	
4317.751	1	15	II	
4316.954	2000	8000	II	4
4315.302		3	II	
4315.15		1	II	
4314.65		1	III	
4314.306		2	III	
4313.567	30	1	I	
4313.156	70	4	I	
4312.991	60	3	I	
4312.356	600	40	I	
4311.86	2		I	
4311.714		5	III	
4310.230	1	10	II	
4310.124		20	II	
4309.886		15	II	
4309.823	3000	300	I	7
4309.308		4	II	
4309.085		3	III	
4308.73		2	III	
4308.586		7	II	
4307.820	300	10	I	
4307.583		4	II	
4307.29		3	II	
4306.494	2	80	II	
4305.966	5000	2000	I	3
4305.484	150	20	I	
4305.369		9	III	
4304.879		5	III	
4304.512		2	II	
4304.458		3	III	
4304.422		2	II	
4304.01		20	III	
4303.675		2	II	
4301.74		3	III	

TABLE 1.—*Emission spectra of ytterbium*—Continued

Wavelength in air	Intensity		Spectrum	Zeeman type	Wavelength in air	Intensity		Spectrum	Zeeman type	Wavelength in air	Intensity		Spectrum	Zeeman type
	Meggers lamp	Thompson lamp				Meggers lamp	Thompson lamp				Meggers lamp	Thompson lamp		
Å					Å					Å				
4301.496	5	15	II		4267.590	50	100	II		4242.425	4	60	II	
4301.135		40	III		4267.132	500	30 h l	I		4242.299		4	II	
4300.984	1000	80	I	7	4266.983	300	30	I		4241.67	2	6	II	
4300.736		4	II		4266.952	10	100	II		4241.24		2	II	
4298.498		2	III		4266.70	20	1	I		4241.159	1	15	II	
4298.075		1	II		4266.156	3		I		4241.116		5	II	
4296.696		3	II		4266.115	2		I		4240.95	6		I	
4296.338		3	II		4265.976		2	II		4239.455		1	II	
4295.88	3		I		4265.498		1	II		4238.84		1	II	
4295.04	300		I		4265.144		1	III		4238.63	2	1	I	
4295.023	500	50 h s	I		4264.802	1	30	II		4238.345		1	II	
4294.598		3	III		4264.520		1	II		4238.157	2	30	II	
4294.473	30	2	I		4264.282		5	II		4237.284		3	II	
4293.421		8	II		4264.029		6	II		4237.00	5		I	
4293.319		3	III		4262.826	2	5	II		4235.69	7		I	
4292.99	3		I		4262.691		6	II		4235.565	1	20	II	
4292.946		5	III		4262.273		1	II		4235.49	2		I	
4292.615	10	1	I		4261.56		8	III		4235.012	1	20	II	
4292.083	70	2	I		4261.346	20	1	I		4234.545	50	800	II	6
4291.954	3	2	I		4260.761		2	III		4233.777		1	I	
4290.357		7	II		4260.678		7	II		4233.445	150	8	I	
4289.91		1	II		4260.068		3	III		4232.427		1	II	
4289.64		20	III		4259.17		1	II		4231.972	10000	1000	I	3
4289.605	1		I		4258.98		4	III		4231.648		6	II	
4288.840	80	7	I		4258.743	200	20 h l	I		4231.073		15	III	
4288.800		9	II		4258.194	2	20	II		4230.184	100	400	II	4
4286.839		7	II		4257.640	200	2000	II	4	4229.767		4	III	
4286.625		4	III		4257.550	40	10	I		4229.681		3	II	
4285.878		9	II		4257.36	60	3	I		4229.657	4		I	
4285.816		1	II		4257.198		6	II		4229.271	3	30	II	
4285.258	1	9	II		4256.756	1000	100	I		4227.952	50	700	II	6
4285.127	2	15	II		4255.765	500	2000	II	4	4226.85		2	II	
4284.942	7	80	II		4254.775	200	800	II	6	4226.595		4	II	
4284.170	2000	500 h	I	7	4254.000		9	II		4226.523		4	III	
4283.782		7	III		4253.790		1	II		4226.273	1	20	II	
4283.453		1	II		4253.488		7	III		4226.152	300	10 h	I	
4282.808		10	II		4253.363	3		I		4225.998		8	II	
4282.098	40	2	I		4253.292	1		I		4225.548	10	30	II	
4281.972	20	50	II		4252.941	20	1	I		4225.303		1	III	
4281.850	20	1	I		4252.806		3	II		4224.196	20	150	II	4
4281.584		5	II		4252.515	300	3000	II	4	4224.064		1	II	
4281.384		2	III		4252.040		15	II		4223.621	50	2	I	
4280.636		2	II		4251.521	3000	200	I	3	4223.466		2	II	
4280.594		1	II		4250.21		5	II		4222.486		10	II	
4277.738	4000	1000	I	3	4249.861		2	II		4222.32	5		I	
4277.326		8	III		4249.81		2	II		4222.057		4	II	
4277.092		2	II		4249.748		4	II		4220.831		10	III	
4276.78		1	II		4248.12		2	II		4220.69		4	III	
4276.21		2	III		4247.885	40	300	II	6	4220.507	7	1	I	
4275.694		4	III		4247.04		2	II		4220.260		1	II	
4275.66	5		I		4246.88	4		I		4219.706	500	20 h	I	
4275.63	5		I		4246.835		10	II		4219.646		10	II	
4275.48	2		I		4246.586	4	20	II		4219.247	1000	200	I	
4273.74	10	1	I		4245.740	3	15	II		4218.693	3000	600	I	7
4273.340	20	150	II	5	4245.597		2	II		4218.565	1000	5000	II	4
4272.647	400	40 h l	I		4245.245	10	1	I		4217.79		2	II	
4272.103	1000	40	I		4244.73		1	II		4217.69		2	II	
4271.963		2	II		4244.51		8	II		4217.110		4	II	
4271.798	600	70 h l	I		4244.21	6	80	II	5	4216.885	6	60	II	
4270.515	4	60	II		4244.054	6	15	II		4216.766	20		I	
4268.986		4	III		4243.92	3		I		4216.704	60	300	II	4
4268.882		1	II		4243.494		9	II		4216.569		2	II	
4268.39	1		I		4242.86	4		I		4216.417		8	II	

TABLE 1.—*Emission spectra of ytterbium*—Continued

Wavelength in air Å	Intensity: Meggers lamp	Intensity: Thompson lamp	Spectrum	Zeeman type
4216.14		1	III	
4215.519	6	20	II	
4215.485	2		I	
4215.416		2	III	
4215.178		2	III	
4214.942	2	15	II	
4214.29	3		I	
4213.962	50 d	20 h	I	
4213.856		2	II	
4213.641		300	III	
4213.407		3	II	
4213.106	10	1	I	
4212.361		6	II	
4211.957		1	II	
4211.82	2000	300	I	2
4211.502		2	II	
4211.298		4	II	
4210.664	4	40	II	7
4210.48	5		I	
4210.299	200	20	I	7
4210.225	15		I	
4209.870		5	II	
4209.342	8	1	I	
4208.625		4	II	
4208.519		1	II	
4208.138		6	III	
4207.65		1	II	
4207.32	6	1	I	
4206.042		1	III	
4205.907	2		I	
4205.785	80	6 h	I	
4205.608		4	II	
4204.195	300	5	I	
4204.058		5	II	
4203.254		2	II	
4202.907	6	2	I	
4202.666		2	II	
4202.44	15	30 h l	II	
4201.991		1	II	
4201.864	3	1	I	
4201.460	2	20	II	
4201.291	200	8 h	I	
4200.841		5	II	
4200.72	60	1	I	
4199.939		4	II	
4199.713		10	II	
4198.863		1	II	
4198.738		10	III	
4198.18	2		I	
4197.876	400	100 h	I	
4196.632	1	9	II	
4196.54	1		I	
4195.056	2		I	
4194.95		100	III	
4194.39	2		I	
4194.34		30	III	
4194.23	2		I	
4194.19	2		I	
4193.807	2	10	II	6
4193.533		4	II	
4192.725		3	II	
4191.473		2	II	
4191.36	1		I	
4190.297	200	2000	II	4
4189.15	3		I	
4188.993	70	5 h	I	
4188.723		7	II	
4188.371		2	II	
4188.130	1	20	II	
4187.73	1		I	
4186.83	15	300	II	7
4186.75	1		I	
4186.027		2	II	
4185.565	2	30	II	5
4184.635	1	20	II	7
4184.289	2	1	I	
4184.164		3	II	
4183.905		1	II	
4183.402		4	III	
4183.129	5		I	
4183.06		3	III	
4182.553		2	II	
4182.353		2	III	
4182.07	9	1	I	
4180.809	10000	20000	II	4
4179.95	20		I	
4179.084	10	80	II	
4178.585	4	6	II	
4178.225		8	II	
4177.81	4	80	II	4
4177.40	2	50	II	
4176.204		3	II	
4175.928	10	90	II	
4175.868	100	10	I	
4175.835		30	II	
4175.602	2	30	II	4
4175.545	1	20	II	
4174.56	3000	300	I	2
4174.399		6	II	
4174.259	80	4 h	I	
4173.134	9	1	I	
4172.95		60	III	
4172.422	200	20	I	
4172.15		20	II	7
4171.222	20	1	I	
4170.106	200	2000	II	5
4169.499	2	8	II	
4169.260	50	5 h	I	
4169.141	50	5	I	
4167.37		1	III	
4166.743	40	3	I	
4165.692		2	II	
4165.143		6	II	
4165.08		1	III	
4164.660	5	50	II	
4164.587		15	II	
4163.770	3		I	
4163.502	10	2	I	
4162.717		100	III	
4162.023		5	II	
4161.572		1	II	
4161.178		7	III	
4160.299		2	II	
4160.243	4		I	
4160.090	3	40	II	
4159.008	6	1	I	
4157.755	100	200	II	
4157.292		8	III	
4156.575	1	4	II	
4156.444		1	II	
4155.385	8	1	I	
4155.123	50	2 h	I	
4154.83	4		I	
4154.484		7	III	
4153.88		6	II	
4153.758		4	II	
4153.197		7	II	
4153.11		15	III	
4152.79		3	II	
4152.38		5	III	
4152.290	2		I	
4152.058	3		I	
4151.64		7	III	
4151.19	9	1	I	
4150.04		10	III	
4149.066	20000R	2000	I	7
4148.440		8	II	
4147.774	1	30	II	
4146.984		2	II	
4146.870	80	5	I	
4146.764	1	30	II	
4146.160		3	II	
4144.700	1	20	II	
4144.273	1	15	II	
4143.498	500	30 h	I	
4143.070		4	II	
4142.364	1	30	II	
4141.457	2	60	II	5
4140.307	8	1	I	
4139.397	2		I	
4139.332	10	30	II	
4139.051	500	20	I	
4138.445		4	II	
4138.166		3	II	
4138.13		1	II	
4138.11		1	II	
4137.985		2	II	
4137.378		4	II	
4136.930		7	II	
4136.872		1	II	
4136.35		2	III	
4135.88		3	III	
4135.088	500	5000	II	6
4134.730	20	1	I	
4134.476	20	80	II	6
4132.722		6	III	
4132.465		4	II	
4132.165	15	2	I	
4132.063		2	II	
4131.600	2	20	II	
4131.325		3	II	
4131.255	2		I	
4131.15		4	II	
4131.024	6	40	II	
4130.878	1	4	II	
4130.645	2		I	
4129.413		1	II	
4129.329		2	II	
4129.157	2	30	II	4

TABLE 1.—*Emission spectra of ytterbium*—Continued

Wavelength in air Å	Intensity: Meggers lamp	Intensity: Thompson lamp	Spectrum	Zeeman type
4128.934	100	4 h	I	
4128.815	30	2	I	
4128.115	4		I	
4128.046		3	II	
4127.202		4	II	
4127.170	1		I	
4126.992	20	30	II	
4126.726	1	15	II	
4126.030		2	II	
4125.955	3		I	
4125.538	150	5 h	I	
4125.185	20	1	I	
4124.736	2	30	II	
4124.564		1	II	
4123.75	6	1	I	
4123.180	1	20	II	
4122.853	50	500	II	4
4122.274	4	1	I	
4122.143	8	1	I	
4121.902	200	20	I	
4121.345		3	II	
4121.062		15	III	
4120.071	1	40	II	
4119.812		2	II	
4119.464	200	1500	II	5
4119.25	20	30	II	
4119.087	30	3	I	
4119.046	3	60	II	
4118.395		3	II	
4118.180	8	2	I	
4118.07	10	1	I	
4117.177	1	30	II	
4116.89	1		I	
4116.654		4	II	
4116.000	4		I	
4115.70	1		I	
4115.454		9	II	
4114.694	1		I	
4114.591	2	30	II	
4114.31		1	III	
4113.879	1	20	II	
4113.805	2		I	
4113.707		5	II	
4113.389	40	2 h	I	
4113.046	40	400	II	6
4112.768		3	III	
4111.966		3	III	
4111.381		6	II	
4111.07	8		I	
4110.448		2	II	
4110.168		10	II	
4109.79	40	2	I	
4109.654		400	II	4
4109.574	3000	400	I	2
4109.306	2	40	II	
4108.845	5	15	II	
4108.542	8	1	I	
4108.399		4	III	
4107.222	20	3 h	I	
4106.284		3	II	
4106.070		5	II	
4104.60	2		I	
4104.05	4		I	
4103.416	1	10	II	
4103.113		2	II	
4102.478	20	10	II	
4102.264		5	II	
4101.335	30	3	I	
4100.877		1	II	
4100.160		8	II	
4099.820		2	II	
4099.482		3	II	
4099.338	20	1	I	
4098.920	4		I	
4098.848		2	II	
4098.232		20	III	
4098.096		2	II	
4097.885	100	600	II	5
4097.080	6	2	I	
4096.968		1	II	
4096.785		3	II	
4096.644	2	20	II	
4096.156	1	15	II	
4094.351		2	II	
4093.634	2	20	II	
4092.959		10	II	
4092.052	1	4	II	
4091.53	6	100	II	
4091.466	2	40	II	
4090.666		20	III	
4090.594		3	II	
4089.908	20	4	I	
4089.68	10000R	3000	I	3
4088.633		2	II	
4088.528		1	II	
4087.67	5	1	I	
4087.480	30 d	5 d	I	
4087.343	20	3	I	
4086.61	7	100	II	7
4087.492		8	III	
4085.66	1	8	II	
4085.05		3	II	
4084.845		3	II	
4084.515		1	II	
4084.47	4		I	
4083.870		1	II	
4083.648	15	4 h	I	
4083.346	4		I	
4082.992	500	20	I	
4082.814		4	II	
4082.64		1	II	
4082.586	2		I	
4082.529		1	II	
4081.05		1	II	
4079.991	2	40	II	6
4079.88		6	II	
4079.542		3	II	
4079.164	2	20	II	
4078.36	7	70	II	4
4078.000	10 h		I	
4077.713	10	20	II	
4077.276	200	2000	II	5
4076.82		1	II	
4076.198		3 h	II	
4076.09		3 h	II	
4075.873		3	II	
4074.705	8	60	II	5
4074.528		20	III	
4074.359	3		I	
4074.074		1	II	
4073.846	8		I	
4073.288	1		I	
4072.923	2		I	
4071.442		1	II	
4071.334		3	II	
4071.115	2		I	
4070.527	8	50	II	
4069.013		4	II	
4068.50		2	II	
4068.229		2	II	
4067.461	4		I	
4067.115	30	2	I	
4067.031		2	II	
4067.00	1		I	
4066.809		15	II	
4066.520		2	II	
4065.963	20 h	1	I	
4064.757		15	II	
4063.927	1	30	II	
4063.726	1000	150	I	2
4063.455	3000	500	I	3
4062.35		1	II	
4062.100		2	II	
4061.614		7	II	
4061.382	10	1	I	
4060.180		1	II	
4060.04		1	II	
4059.893		2	II	
4059.470	40	7	I	7
4058.625	60	6	I	
4058.404	150	15	I	
4058.238		1	II	
4058.065	1	6	II	
4056.142	500	2000	II	4
4055.468		3	II	
4055.24	2		I	
4054.588		1	II	
4053.547		2	II	
4053.235		1 h	II	
4053.11		10	II	
4052.860		20	II	
4052.283	5000	1000	I	1
4052.072	1000	60	I	1
4051.935	30	3	I	
4051.339	20	60	II	4
4050.083	20	150	II	4
4049.982		5	II	
4049.335		7	II	
4048.683		5	II	
4048.554		2	II	
4048.21		1	II	
4048.090		2	II	
4047.38	20	200	II	5
4046.998		2	II	
4046.56		1	II	
4046.52		1	II	
4046.37	1		I	
4046.297		4	II	
4045.605		1	II	

TABLE 1.—*Emission spectra of ytterbium*—Continued

Wavelength in air Å	Intensity: Meggers lamp	Intensity: Thompson lamp	Spectrum	Zeeman type
4045.302	6	80	II	
4044.657		2	II	
4044.464	3	1	I	
4043.426		4	II	
4043.05	20	300	II	5
4042.532	3	40	II	
4042.328		4	II	
4040.563	1	30	II	4
4040.498		8	II	
4040.29		1	I	
4040.08	60	1000	II	5
4039.938	15	1	I	
4039.613		4	II	
4039.140		3	II	
4038.97	2	1	I	
4038.94	2		I	
4038.187		6	II	
4037.916		9	II	
4037.822	20	50	II	7
4036.772	20	15	I,II	
4036.550	1	15	II	
4035.855	5	3	I	
4035.51	5	1	I	
4035.315	9	90	II	6
4034.438		6	II	
4033.695		4	II	
4033.029		10	III	
4032.869	10	100	II	5
4032.756		2 h	II	
4032.441		2	II	
4030.712		1	II	
4029.844	2	60 d	II	
4028.138		2000	III	2
4027.580		10	II	
4027.19		1	II	
4026.922		2	II	
4025.740		2	II	
4024.375		4	II	
4023.987	6	30	II	5
4022.712	3	40	II	
4021.956		1	II	
4021.56	2	1	I	
4020.310		2	II	
4019.852	1	10	II	
4019.35	6	150	II	4
4018.966	30	3	I	
4018.264		2	II	
4018.134		2	II	
4017.94		1	II	
4017.060		3	II	
4016.976		9	II	
4015.296		4	II	
4015.004		1	II	
4013.579	1	15	II	
4013.464		3	II	
4012.704		1	II	
4012.204		1	II	
4010.84		2	II	
4010.825	3		I	
4009.237		20	II	
4008.94	4	1	II	
4008.775		3	II	
4007.962	10	5	I	
4007.518		20	II	
4007.356	2000	500	I	3
4006.962		2	II	
4006.828	15	2	I	
4006.672		1	II	
4006.53		2	II	
4005.65	2 h		I	
4005.619		1	II	
4005.218		1	II	
4003.574		1	II	
4003.224		2	II	
4002.798		2	II	
4002.68		1	II	
4002.326		10	II	
4002.04	3 h		I	
4002.002		1	II	
4000.808	5	150	II	7
4000.46	10		I	
4000.212	4	1	I	
3999.777	2	40	II	
3998.879	2	1	I	
3998.430		7	II	
3998.38		1	II	
3998.133	3		I	
3997.667		10	III	
3997.244		4	II	
3995.859		1	II	
3995.432	1	20	II	7
3994.563		2	II	
3994.300		1	II	
3993.753	100	10	I	3
3992.826		1	II	
3992.09		8	II	
3991.945		4	III	
3991.74		10	III	
3991.09		1	II	
3990.885	10000R	1000	I	3
3990.603		2	II	
3990.473		2	II	
3990.280		1	II	
3989.717		6	II	
3988.666		70	II	
3987.99	50000A	30000	I	7
3986.962		5	II	
3986.830		5	II	
3986.179		10	II	
3985.564		100	III	
3985.125		1	II	
3984.765		3	II	
3983.748		1	II	
3983.314	2	60	II	4
3983.179		1	II	
3982.009	2	20	II	4
3981.574		1	II	
3981.160		5	II	
3980.78		1	II	
3980.318		10	II	
3979.710	10	2	I	
3979.095	60	4	I	
3978.543	2	10	II	
3977.342	2	20	II	
3977.113		1	II	
3976.527		1	II	
3976.148		7	II	
3975.283	2000	100	I	2
3974.91		1	II	
3974.30		2	II	
3973.87	10	3	I	
3972.91		1	II	
3972.848		3	II	
3972.517		4	II	
3972.267		3	II	
3972.18	3		I	
3972.08		1	II	
3972.01	7		I	
3971.739		2	II	
3971.014		2 h	II	
3969.89	4	1	I	
3969.519		1	II	
3969.461		1	II	
3969.082		3	II	
3968.79		20	II	
3968.68		1	II	
3968.024	10	100	II	5
3966.062		2	II	
3965.416		1	III	
3964.584		1	II	
3964.459	1	20	II	4
3964.364		1	III	
3963.301		2	II	
3963.07	5		I	
3962.457		4	II	
3961.98	70	6	I	1
3961.832		4	II	
3961.731	5	1	I	
3961.503	5	1	I	
3961.288		1	II	
3961.104		2	II	
3960.866		2	II	
3960.34		1	II	
3960.27		1	II	
3959.730		1	II	
3959.060	1	9	II	
3958.818		2	II	
3958.376		3	II	
3957.270	6	2	I	
3957.05	5		I	
3954.266		4	II	
3953.546		1	II	
3951.08		10	II	
3949.91	10	100	II	6
3949.58	100	200	II	5
3949.307		2	III	
3948.64		4	II	
3948.18	20	100	II	5
3946.94	20	150	II	4
3945.577		2	II	
3944.55		1	II	
3944.509		1	II	
3943.692		2	II	
3943.29	4	1	I	
3942.72		6	II	
3939.780	10	1	I	
3939.517	1	20	II	
3938.53	40	400	II	
3938.25	40	500	II	6

TABLE 1.—*Emission spectra of ytterbium*—Continued

Wavelength in air	Intensity		Spectrum	Zeeman type	Wavelength in air	Intensity		Spectrum	Zeeman type	Wavelength in air	Intensity		Spectrum	Zeeman type
	Meggers lamp	Thompson lamp				Meggers lamp	Thompson lamp				Meggers lamp	Thompson lamp		
Å					Å					Å				
3937.984		1	II		3904.447		1	II		3872.338		8	II	
3936.596		2	II		3903.74		1 h	II		3871.946		1	II	
3936.385		5	II		3903.397		4	II		3870.447		2	II	
3935.086		3	II		3903.288		3	II		3870.197		2 h	II	
3934.30	4	100	II		3902.814		5	II		3868.907	4	1	I	
3934.182	3000R	200	I		3902.43		3 h	II		3868.838		4	II	
3933.87		2	II		3902.386	10 h	4	I		3868.602	1	9	II	
3933.25		2 h	II		3902.109		5	II		3868.570	1	20	II	
3931.90	10	100	II	6	3902.042	1	20	II		3867.75		1	II	
3931.634		2	II		3901.44		1	II		3867.675		3	II	
3931.44		1	II		3901.06	10	1	I		3867.48		5 h	II	
3931.273	4		I		3900.85	4000R	500	I	3	3867.378		1	II	
3931.227		500	III		3899.245		3	II		3866.862		1	II	
3930.900		1	II		3899.07	4	80	II	7	3865.95	3 h		I	
3930.004		2	II		3898.450		1	II		3865.43	1		I	
3929.885		1	II		3897.946		8	II		3865.351		1	II	
3929.30	1		I		3897.555	10	2	I		3865.255		3	II	
3929.053		6	II		3897.34		2 d	II		3865.14	1		I	
3928.068		10	II		3897.060		1	II		3864.33	20 h		I	
3927.60		1	II		3896.966		4	II		3863.784		2	II	
3926.962		1	II		3896.742	20	3	I		3863.455	200	800	II	5
3926.724	30	3	I		3896.55		150	III		3863.046	10	100	II	
3926.651		2	II		3895.884		2	II		3862.59	2		I	
3924.656		2	II		3895.758	1	30	II		3862.511	1	20	II	5
3924.527	10	2	I		3893.740		2	II		3862.46	1		I	
3923.230		4	II		3892.285		1	II		3862.18	10	1	I	
3922.443	1	15	II		3891.696		1	II		3861.792		3	II	
3921.201		2	II		3890.850	2	50	II	4	3861.730		2	II	
3920.745		4	II		3890.767	20	3	I		3861.566		1	II	
3920.602		2 h	II		3889.664		2	II		3861.467		1	II	
3919.980	1	15	II		3887.826		10	II		3860.975	2		I	
3918.804		9	II		3887.50		1	II		3860.917		1	II	
3917.685		3	II		3887.290	20	300	II	4	3860.815	10		I	
3917.473		5	II		3887.166		20	III		3860.64	3	1	I	
3916.892		2	II		3886.63		1	II		3859.887		2	II	
3916.783	2	15	II		3886.378		4	II		3859.35		2 h	II	
3916.702		1	II		3885.647		1	II		3858.555	10	100	II	4
3916.425		10	II		3885.470		1	II		3858.434		1	II	
3916.316		1	II		3885.195		4	II		3858.07		9	II	
3916.268		1	II		3884.833		1	II		3857.860		2	II	
3915.427		10	II		3883.638		1	II		3857.586	10	20	II	
3914.690		3	II		3883.105		1	II		3856.514		3	II	
3913.923		7	II		3882.583		10	III		3856.009		2	III	
3913.729		7	II		3882.068	40	4	I		3856.00	3		I	
3913.347	30	200	II	4	3881.738		3	II		3855.883	50	8	I	
3913.234		20	III		3880.684		1	II		3854.91	4	30	II	
3912.746		15	III		3880.332		2	II		3854.806	20	100	II	5
3911.272	600	60	I	3	3880.197	5	70	II	4	3854.116	2		I	
3910.911		6	II		3880.044		1	II		3854.09	2		I	
3910.653	20	4	I		3879.985		20	III		3853.731		3	II	
3910.429		2	II		3879.140		7	II		3853.238	1	2	II	
3910.364		4	II		3878.023		4	II		3852.562		10	II	
3909.98		1	II		3877.06	4	60	II		3852.160	4	40	II	
3909.186		1	II		3876.902		1	II		3851.80		2	II	
3908.020		5	II		3876.776	1	20	II	5	3851.65	1		I	
3907.355	2	40	II	4	3876.33		2 h	II		3851.36	5		I	
3906.960	4	30	II	6	3875.76	1		I		3851.242		1	II	
3906.64		3	II		3874.610		3 h	II		3851.090		2	II	
3906.196	4	30	II		3874.066		10	II		3850.98	7		I	
3905.832	20	200	II	6	3873.497		4	II		3850.366		4	II	
3905.51	5	1	I		3873.246	5	1	I		3850.32		2	II	
3904.812	100	1500	II	5	3872.852	5000R	1000	I	7	3849.54	1		I	
3904.537		2	II		3872.555		5	II		3848.792	5	1	I	

TABLE 1.—*Emission spectra of ytterbium*—Continued

Wavelength in air Å	Intensity: Meggers lamp	Intensity: Thompson lamp	Spectrum	Zeeman type
3847.473	30	200	II	4
3846.237		4	II	
3846.186	1	15	II	
3845.79	1		I	
3845.64	3		I	
3845.402		4	II	
3845.35	2		I	
3844.988	2	6	II	
3844.349	1	15	II	
3843.811		6	II	
3843.420	5	80	II	6
3843.30	2		I	
3843.032	1	20	II	
3842.653		1	II	
3841.950	1	9	II	
3841.296	1	10	II	
3840.70		1	II	
3840.341	3	70	II	7
3840.297	2	40	II	
3840.013		2	II	
3839.907	1500	80	I	1
3839.469	30	300	II	5
3839.382	1	20	II	
3838.900	10	100	II	4
3838.67		2	II	
3838.287	80	4	I	2
3838.123		3	II	
3838.02	7	1	I	
3837.57	5	1	I	
3837.411		4	II	
3836.677		2	II	
3836.541		1	II	
3836.46	5	1	I	
3835.952		2	II	
3835.872		1	II	
3835.495		3	II	
3834.35	1		I	
3833.884		9	II	
3832.701		4	II	
3832.664		1	II	
3832.180		3	II	
3832.108		3	II	
3831.610	3	20	II	7
3831.288		1	II	
3831.13		1	II	
3830.905	2		I	
3830.178		2	II	
3829.767		2	II	
3829.736		1	II	
3828.673	20	5	I	
3827.494		4	II	
3827.030		2	II	
3826.768		8	II	
3826.620	5	1	I	
3826.51		1	II	
3824.956	1		I	
3823.241	5	1	I	
3822.216		1	II	
3822.17		1	II	
3821.526		1	II	
3821.224		1	II	
3820.825		8	II	
3820.288		5	II	
3819.916	1	15	II	
3818.365		1	II	
3817.777	3	20	II	5
3817.624		7	II	
3817.09	1		I	
3816.345	15	150	II	6
3816.189	30	300	II	4
3815.640		1	II	
3815.203	200	10	I	
3814.310		10	II	
3814.215	15	200	II	4
3814.084		4	II	
3813.665		3	II	
3811.584		2	II	
3809.04	5	30	II	
3808.809	10	1	I	
3808.544		1	II	
3808.460	1	2	II	
3808.35		2	II	
3808.315		2	II	
3807.574	50	500	II	
3807.545	100	1000	II	4
3806.996		3	II	
3806.869		1	II	
3806.818		2	II	
3806.73	2		I	
3806.188	2	20	II	
3806.011		1	II	
3804.99		1	II	
3804.431	4	40	II	5
3804.35		2	II	
3803.680		1	II	
3802.47		1	II	
3802.28		1	II	
3801.752	1	20	II	
3801.386	2		I	
3801.263	10	1	I	
3801.026		3 h	II	
3800.622	20	80	II	5
3799.054		1	II	
3798.960	4	20	II	
3798.854		1	II	
3798.402	4000	400	I	2
3798.162	3000	300	I	1
3797.915		2	II	
3797.219		2	II	
3797.181		3	II	
3796.950		10	II	4
3796.495	2		I	
3796.157	7	80	II	6
3795.916		4	II	
3795.878		3	II	
3795.785	3	1	I	
3795.061		4	II	
3794.906		3	II	
3793.934		4	II	
3793.104		3	II	
3792.86		4	II	
3792.557		1	II	
3792.39		2	II	
3791.741	7000	600	I	1
3791.336		2	II	
3789.457		6	II	
3789.37		1	II	
3788.267		4	II	
3787.418	1	5	II	
3787.080	1	10	II	
3786.465		1	II	
3785.960		1	II	
3785.666	1	20	II	7
3785.330	6	80	II	4
3784.512		1	II	
3784.384	7	100	II	6
3784.144	1	10	II	
3783.914		1	II	
3782.80	1		I	
3782.736		4	II	
3782.540	70	700	II	5
3781.684		8	II	
3781.415	1		I	
3781.268		1	II	
3781.046		3	II	
3780.605		1	II	
3780.217	2	20	II	
3779.838		1	II	
3779.472		2	II	
3779.286	20	150	II	6
3779.184	1	15	II	
3778.800		2	II	
3778.452		3	II	
3777.906	1	20	II	
3777.534	2	30	II	6
3776.520	3	40	II	5
3776.362		1	II	
3775.906		2	II	
3774.956		2	II	
3774.323	700	40	I	2
3773.625		1	II	
3773.428	200	600	II	6
3772.517	20	100	II	5
3772.294	3	40	II	5
3771.768		3	III	
3771.596		2	II	
3771.350		3	II	
3771.155	1	10	II	
3770.814		1	II	
3770.28		1	II	
3770.195	2	40	II	
3770.095	2000R	500	I	7
3769.35		1	II	
3769.189		1	II	
3768.966		2	II	
3767.891		10	II	
3767.714	8	2	I	
3767.175		1	II	
3766.925	2	20	II	5
3766.736		8 h	II	
3766.527		4	II	
3766.101	20	200	II	4
3765.080	1	8	II	
3764.59	1		I	
3764.56		3 h	II	
3764.03		1	II	
3763.35		1	II	
3763.27		1	II	
3763.045	1	6	II	

TABLE 1.—*Emission spectra of ytterbium*—Continued

Wavelength in air Å	Intensity: Meggers lamp	Intensity: Thompson lamp	Spectrum	Zeeman type	Wavelength in air Å	Intensity: Meggers lamp	Intensity: Thompson lamp	Spectrum	Zeeman type	Wavelength in air Å	Intensity: Meggers lamp	Intensity: Thompson lamp	Spectrum	Zeeman type
3762.98		1	II		3735.606		9	II		3708.218		3	II	
3762.93	1		I		3735.352		10	II		3707.707		2	II	
3762.550	40	400	II	4	3734.96		1	II		3707.486	1	7	II	5
3762.12		1	II		3734.694	3000R	300	I	1	3707.234		1	II	
3761.31		1	II		3734.435	1000	100	I	1	3707.020		4	II	
3760.999	10	200	II	6	3734.150		8	II		3706.833		4	II	
3760.481	200	6	I		3734.12		2	II		3706.32		1	II	
3760.23		2 d	II		3733.989		10	II		3706.023	10	5	I	
3757.355		1	II		3733.762		5	II		3705.745	1		I	
3756.888		2	II		3733.19		1	II		3705.64	2	30	II	7
3756.445		6	II		3732.458		5	II		3704.750		20	II	
3755.762		2	II		3732.33	1	10	II		3704.300		1	II	
3755.32		1	II		3731.166		7	II		3703.92		7	II	
3754.83		2	II		3731.044		8	II		3703.423	10	200	II	7
3754.74		1	II		3730.409	20	200	II	4	3702.94		6	II	
3754.606	2	6	II		3729.81	10	100	II	4	3702.42	1	5	II	
3753.897	8	100	II	5	3728.24		2	II		3702.07		8	II	
3753.65		1	II		3727.073		1	II		3700.580	1000	40	I	2
3753.49		2	II		3726.169	1	5	II		3699.800	5	100	II	7
3753.053	4	60	II		3725.84	5	70	II		3699.514	3000	100	I	
3752.730		4	II		3724.91		3	II		3698.81	2		I	
3752.56		1	II		3724.36	200		I		3698.596	40	400	II	6
3751.847	10	40	II	6	3724.213	150	800	II	5	3698.446	2	40	II	
3751.62	1		I		3723.06		2	II		3698.070		2	II	
3751.206	1	2	II		3722.626		7	II		3698.012		6	II	
3751.13	1		I		3722.296	40	600	II	7	3697.688		2	II	
3751.030		1	II		3720.98	6	100	II	5	3694.190	100000A	80000	II	6
3750.045		8	II		3720.846		3	II		3692.072		4	II	
3749.688	40	400	II	5	3720.584		2	II		3691.67	2	6	II	
3749.388	1	6	II		3720.192		3	II		3691.472	10	200	II	6
3748.55	1		I		3719.924		3	II		3691.34		1	II	
3748.345	3	10	II		3719.148		2	II		3691.230	1	10	II	
3748.204		2	II		3718.887		1	II		3690.560	30	300	II	7
3748.102		1	II		3718.749		2	II		3689.99		8	II	
3747.817	2	20	II		3718.482	1	10	II		3688.937		4	II	
3747.229		10	II		3718.139		4	II		3688.81	10		I	
3746.67		1	II		3718.052	3	15	II		3688.490		1	II	
3746.33	3		I		3717.885		2	II		3688.438	10	1	I	
3744.943	40	5	I		3717.412		3	II		3687.598	20	150	II	6
3744.762		1	II		3717.28	3		I		3687.142	7	80	II	6
3744.166		4	II		3717.23	1		I		3685.973		15	II	
3744.09	2		I		3717.15		1	II		3684.997	500	40	I	3
3743.97		1	II		3716.596		2	II		3684.068		1	II	
3743.390		3	II		3716.139	10	40	II		3683.352	2	30	II	7
3743.26		6	II		3715.725		4	II		3683.277	1	15	II	
3743.138		15 h	II		3715.440		10	II		3682.777		2	II	
3742.627		1	II		3715.409	50	4	I		3682.20		1	II	
3742.358		1	II		3714.186	50	150	II	6	3681.29		1	II	
3742.036	4	20	II		3713.93		1	II		3681.195		15	II	
3741.642	3	15	II		3713.70		2	II		3680.770		7	II	
3741.59	8	80	II	4	3713.298		2	II		3680.667		4	II	
3741.296	50	6	I		3712.666	10		I		3679.932	200	20	I	
3740.772		10	II		3712.438	1	10	II		3679.521		2	II	
3740.59		2	II		3712.416		4	II		3678.26		1	II	
3739.59		1	II		3712.06		1	II		3678.15		1	II	
3739.56		1	II		3711.95	1		I		3677.906		6	II	
3739.411	30	3	I		3711.907	1	400	III	7	3677.853	1	15	II	
3738.009		10	II		3711.245		6	II		3677.81	2		I	
3737.80	2		I		3710.825		3	II		3677.25	2		I	
3737.537	1	40	II		3710.340	100	1000	II	6	3676.89		1	II	
3737.123		6	II		3710.090		2	II		3676.14		2	II	
3736.901	7	10	II	4	3708.97		10	II		3675.782		20	III	
3736.237	400	100	I	3	3708.663	150	600	II	4	3675.720	20		I	

TABLE 1.—*Emission spectra of ytterbium*—Continued

Wavelength in air	Intensity		Spectrum	Zeeman type	Wavelength in air	Intensity		Spectrum	Zeeman type	Wavelength in air	Intensity		Spectrum	Zeeman type
	Meggers lamp	Thompson lamp				Meggers lamp	Thompson lamp				Meggers lamp	Thompson lamp		
Å					Å					Å				
3675.085	300	2000	II	7	3647.25	1		I		3614.593		6	II	
3674.065	2	20	II		3646.277	1	10	II		3614.048	5	100	II	4
3673.900		8	II		3646.24		7	II		3613.894		200	III	
3673.423		8	II		3645.72		7	II		3613.38		3	II	
3673.286		1	II		3644.236	40	400	II	5	3613.340		3	II	
3670.69	50	600	II	5	3643.28	1	10	II		3613.295		2	II	
3669.69	2000 r	6000	II	6	3642.63		3	II		3612.950		4	II	
3668.992	3	50	II		3642.37		7 h	II		3611.994	20	1	I	
3668.16		1	II		3642.24		4	II		3611.300	60	800	II	4
3667.951		8	II		3640.79		1	II		3610.233	100	700	II	6
3666.67	1	30	II		3639.97		1	II		3609.24		1	II	
3666.62	200	4	I	7	3639.746	1	15	II		3608.936		3	II	
3666.522		5	II		3639.445	20	8	I		3608.488	10	150	II	5
3666.09		10	II		3639.030		2	II		3608.356	3		I	
3664.895	3	40	II		3637.757	2000R	3000	II	6	3607.703	700	70	I	
3664.744	40	200	II	5	3636.899		2	II		3607.186		2	II	
3664.560	8	90	II	7	3636.23		2	II		3606.478	300	2000	II	5
3663.74		30	III		3635.330		1	II		3605.347	2	20	II	6
3663.11		6	II		3634.86		2	II		3605.208		1	II	
3662.545	1	20	II		3634.74		1	II		3603.848	20	300	II	5
3662.297		2	II		3634.525	30	20	I,II		3602.237		1	II	
3662.061		7	II		3634.40		10	II		3601.917	2	20	II	6
3662.033		5	II		3634.27		2	II		3601.209	2	15	II	
3661.656		2	II		3633.858		10	II		3600.966	10	100	II	
3661.135		2	II		3633.70	1	20	II	7	3600.763	20	300	II	
3661.08		6	II		3632.595	20	150	II	5	3600.663	2	30	II	
3660.99		1	II		3632.415	20	100	II	5	3600.383	10	150	II	6
3660.73	1	8	II		3631.86		8	II		3598.87		2 h	II	
3660.64		1	II		3631.073	7	80	II	4	3598.662	9	1	I	
3660.58	1	15	II		3630.975	4		I		3598.043	2	20	II	
3660.42		1	II		3630.621		4	II		3597.60		1	II	
3660.137	1	10	II		3630.337		2	II		3597.078		10	II	
3659.835		30	III		3630.301		4	II		3596.488	1	30	II	
3659.427	4		I		3629.919	30	300	II	6	3596.416	3		I	
3658.78	1		I		3629.58	3		I		3596.300		4	II	
3658.605	5	70	II		3629.233	800	15	I	7	3595.844		5	II	
3657.665		3	II		3628.340		6	II		3595.649		2	II	
3657.233	3 h		I		3627.89	2	30	II		3595.162		9	II	
3657.131		1	II		3627.205	2	30	II	5	3594.93	1		I	
3657.007		2	II		3627.078		1	II		3594.864	1	10	II	
3656.81		1	II		3626.80	1	6	II		3593.882		1	II	
3656.672		2	II		3625.230	2	60	II		3593.728		2	II	
3656.312	10	2	I		3624.634	15	200	II	6	3593.060		1	II	
3655.729	2000R	100	I	1	3624.109	10	1	I		3592.734	1	20	II	
3655.48	1	20	II		3623.627	1	10	II		3592.217	1	10	II	
3654.417	1	5	II		3622.320	20	80	II	6	3591.844	150	15	I	
3654.28	1	20	II		3621.873		7	II		3591.24		1	II	
3653.041	2	20	II		3621.80		2	II		3591.18		2	II	
3652.953	3	40	II		3621.743	400	10	I		3591.141		4	II	
3652.538	1	15	II		3621.513	1	15	II		3590.657	5	50	II	7
3651.24	1	10	II		3621.18		1	II		3589.997		1	II	
3651.15		1	II		3620.988	30	400	II	7	3589.186		7	II	
3650.80	4	50	II	4	3620.65	2		I		3588.832	1	20	II	
3649.739	10	150	II	5	3620.362		4	II		3588.456		2	II	
3649.084		6	II		3619.803	700 r	3000	II	4	3587.736		7	II	
3648.827		2	II		3618.887		1	II		3587.569		1	II	
3648.676		1	II		3618.040	50	200	II	6	3586.824	30	90	II	6
3648.440	10	100	II	6	3617.045	1	10	II		3586.536		6	II	
3648.38	4	50	II		3616.395		10	II		3585.878		8	II	
3648.29		1	II		3616.031		3	II		3585.794	1	20	II	
3648.242		2	II		3615.957		2	II		3585.466	2000R	4000	II	5
3648.150	150	15	I		3614.994	50	7	I	7	3583.96		4 h	II	
3647.730	2	40	II	7	3614.63		1	II		3583.827	7	70	II	

TABLE 1.—*Emission spectra of ytterbium*—Continued

Wavelength in air Å	Intensity: Meggers lamp	Intensity: Thompson lamp	Spectrum	Zeeman type
3583.532		5	II	
3583.26		7	II	
3583.180		1	II	
3582.841	3	40	II	
3582.20		3	II	
3580.755		10	II	
3580.640	1	15	II	
3580.474		1	II	
3580.404	100	10	I	
3580.125	100	20	I	
3579.511	3	40	II	7
3578.95		1	II	
3578.710	10	2	I	
3578.561	600	60	I	1
3577.985		1	II	
3577.690	1	10	II	
3577.504		3	II	
3577.008	30	300	II	7
3576.288		8	II	
3576.188		1	II	
3575.905	1	20	II	
3575.704		5	II	
3575.573	3	60	II	5
3575.125	20	2	I	
3574.58		30 h	II	
3573.750	1	10	II	7
3573.67		1	II	
3573.458	3	3	I,II	
3573.41		4	II	
3573.247	20	2	I	
3572.498	200	800	II	4
3572.448	50		I	
3572.212	2	15	II	
3570.987	1	8	II	
3570.566	200	1000	II	5
3569.925	2	20	II	
3569.500	2		I	
3569.308		2	II	
3569.094	1	10	II	
3568.430	5	50	II	4
3567.130	50	500	II	6
3566.905	2	1	I	
3566.519		2	II	
3565.891		4	II	
3565.823		1	II	
3565.477		6	II	
3565.404		3	II	
3564.955		1	II	
3563.941	200	800	II	5
3563.712	2	20	II	
3562.706	7	80	II	6
3561.738	1	10	II	
3561.444	2	6	II	
3561.309		2	II	
3560.704	500 r	2000	II	6
3560.327	2000R	3000	II	7
3559.570	10		I	
3559.139		4	II	
3559.032	1000	50	I	7
3557.825		2	II	
3557.466		1	II	
3557.100	2	20	II	7
3556.940		4	II	
3556.435		3	II	
3556.263	200	15	I	
3556.124		1	II	
3556.042		1	II	
3556.013	10		I	
3555.204	5	30	II	4
3555.055		3	II	
3554.347		5	II	
3553.82		1	II	
3553.340		7	II	
3553.192		3	II	
3553.153		3	II	
3552.324	100	1000	II	5
3551.405	1		I	
3550.87		300	III	
3549.822	200	2000	II	6
3548.470		2	II	
3548.18	50	7	I	
3548.096		7	II	
3547.756	5	1	I	
3546.085		1	II	
3545.725	1	40 h	II	
3544.162	10	1	I	
3543.890		1	II	
3543.324	1	10	II	
3543.159	30	200	II	4
3542.395	7	100	II	6
3542.272	1	6	II	
3541.924	8	1	I	
3541.375	7	80	II	5
3540.926		3	II	
3540.61		1	II	
3540.21		2	II	
3540.09		1	II	
3540.02		1	II	
3539.932		3	II	
3539.362	20	200	II	4
3539.33	200		I	
3538.369		2	II	
3537.964		1	II	
3537.127		6	II	
3536.815	3 h		I	
3536.068	1	8	II	
3534.752	4	20	II	
3534.13		2	II	
3534.05	50	100	II	5
3533.80		3	II	
3533.107	20	60	II	6
3531.725	20	1	I	
3531.24	5	100	II	4
3530.58		1	II	
3530.16		3	II	
3530.05		1	II	
3529.715	2	20	II	
3529.458		2	II	
3529.085	8	100	II	6
3528.771		2	II	
3528.075	2		I	
3527.501	1	15	II	7
3527.332	2	20	II	7
3526.477		1	II	
3525.722	5	50	II	6
3525.456		3	II	
3525.171		2	II	
3525.05		1	II	
3524.82		1	II	
3524.044		1	II	
3523.734		3 h	II	
3523.148	3	2	I,II	
3522.826		3	II	
3522.747	1	10	II	
3522.021		1	II	
3521.773	5		I	
3521.727		3	II	
3521.664		2	II	
3521.585	1	7	II	
3521.224		7	II	
3521.007	5	20	II	
3520.917		10	II	
3520.293	600 r	3000	II	6
3519.82	2		I	
3519.690		2	II	
3519.417	5	50	II	7
3519.10		1	II	
3518.89		1	II	
3518.795		3	II	
3518.674		1	II	
3518.457	300	20	I	1
3518.353	1	10	II	
3518.156	20	300	II	7
3517.001	500	60	I	3
3516.60		1	II	
3516.180		2	II	
3515.865	30	300	II	4
3515.610	10	50	II	6
3515.238	20	2	I	
3515.138	1	15	II	
3513.640		4	II	
3513.573	400	30	I	3
3513.412		2	II	
3512.708	2	20	II	
3512.441		6	II	
3511.283		8	II	
3510.942		3	II	
3510.764	600	50	I	1
3510.500	1	15	II	
3509.86	1	10	II	
3509.776		3	II	
3508.95		1	II	
3507.830	200	2000	II	4
3506.125	8	200	II	5
3505.282	50	150	II	4
3504.936	3	15	II	
3504.737	3		I	
3504.542	1	15	II	
3503.988	20	7	I	
3503.690	4	40	II	4
3503.277		2	II	
3503.190		3	II	
3503.011		1	II	
3502.572		4 h	II	
3502.180	10	100	II	4
3500.863		5	II	
3500.813	10	5	I	
3500.131	10	30	II	
3499.886		3	II	

TABLE 1.—*Emission spectra of ytterbium*—Continued

Wavelength in air Å	Intensity: Meggers lamp	Intensity: Thompson lamp	Spectrum	Zeeman type
3499.85		1	II	
3499.791		2	II	
3499.636	1	9	II	
3499.419	5	10	II	
3498.392	2	40	II	
3497.86		2	II	
3496.858	5	20	II	
3495.90		50 h	II	
3495.780		3	II	
3495.623	10	1	I	
3493.154	1	15	II	
3492.807	5	30	II	
3491.624	6	100	II	
3491.133	2		I	
3491.063		3	II	
3490.880		2 h	II	
3490.58		1	II	
3490.213	1	20	II	
3489.746	60	15	I	
3489.399	8	1	I	
3488.855	200	1	I	
3488.786	200	700	II	5
3488.43		10 h	II	
3488.34	6	50	II	
3487.971	20	5	I	
3487.603	2		I	
3487.402		3	II	
3487.233	6	100	II	
3487.041		2	II	
3486.137	1	8	II	
3485.757	200	1500	II	7
3484.656		1	II	
3484.38		2	II	
3484.176	7		I	
3484.143	1	15	II	
3484.09		2	II	
3484.06		2	II	
3483.782	1	10	II	
3482.942	1	10	II	
3482.564	5	30 h	II	
3482.390		1	II	
3481.706		2	II	
3481.68	30		I	
3481.302	1	20	II	
3479.912		2	II	
3478.835	3000 r	10000	II	5
3477.022	20	30	II	
3476.303	10000A	8000	II	4
3474.82	60	400	II	4
3474.512		3	II	
3473.996		5	II	
3473.75		3	II	
3473.01		2	II	
3472.58		1	II	
3472.324	5	20	II	
3471.891		2	II	
3471.46		1	II	
3470.79	8	80	II	5
3470.106	10	3	I	
3469.975		20	III	
3469.925	5	70	II	4
3469.253	3	5	II	
3468.395	1	20	II	
3468.00		3 h	II	
3467.26	10		I	
3467.066	10	200	II	7
3466.346		10	II	
3465.898	3	40	II	6
3465.792		3	II	
3464.905		1	II	
3464.37	30000A	2000	I	7
3464.190	100	20	I	
3463.511		150	III	
3463.325	2	30	II	
3463.179	2	20	II	
3462.79		1 h	II	
3462.338	20	15	I	
3461.719	30	300	II	4
3461.327		5	II	
3461.004	100	9	I	
3460.269	3000R	60	I	7
3460.137		4	II	
3460.092		10	II	
3459.902		2	II	
3459.828		4	II	
3459.663	100	10	I	7
3459.183	10	40	II	4
3459.095	60	3	I	
3458.792		2	II	
3458.391	1000	20	I	7
3458.286	200	1500	II	5
3457.333		2	II	
3457.10		2	II	
3457.04		1	II	
3456.953		1	II	
3456.774		6	II	
3456.525	10		I	
3456.231	5	20	II	
3456.181		40	III	
3455.863		5	II	
3454.92		3	II	
3454.75	10		I	
3454.215	50	300	II	
3454.080	2000 r	10000	II	4
3453.524		5	II	
3453.207		2	II	
3452.398	300	30	I	3
3452.264		7	II	
3451.82	2		I	
3451.33	1	20	II	
3451.305		3	II	
3450.929		2	II	
3450.269		5	II	
3449.362		1	II	
3449.15		7 h	II	
3448.906		1	II	
3447.993	4	40	II	7
3447.668	1	20	II	7
3446.887	100	600	II	6
3445.950	7	100	II	5
3445.107		3	II	
3444.544		2	II	
3443.895		2 h	II	
3443.587	30	20	I,II	7
3443.391		6 h	II	
3442.586	10	5	II	
3442.368	3	40	II	6
3442.058	1	10	II	
3441.354		7	II	
3441.30		1	II	
3441.07	3		I	
3440.894		8 h	II	
3440.016		5	II	
3439.648	1	20	II	
3438.848	400 r	2000	II	6
3438.709	200	1500	II	6
3438.516		10	II	
3437.754		3	II	
3437.222		2	II	
3437.17	5	1	I	
3437.114		2	II	
3436.452	100	700	II	5
3435.74		4 h	II	
3435.516		2	II	
3435.429		3	II	
3434.610	200	600	II	5
3434.244	1	10	II	
3433.650		1	II	
3433.167	100	10	I	
3433.160		10	II	
3432.942		80	III	
3432.732	1	3	II	
3432.261	1	30	II	
3432.143	150	15	I	
3431.780		4 h	II	
3431.63		1	II	
3431.512		2	II	
3431.377	5	9	II	
3431.140	700	20	I	7
3431.107	3000R	80	I	7
3430.872		3	II	
3430.65		1	II	
3430.632		2	II	
3429.96		1	II	
3429.80		1	II	
3428.782	700	30	I	7
3428.463	200	2000	II	6
3427.808	1	20	II	
3427.508		3	II	
3426.878	150	30	I	
3426.558		2	II	
3426.43		1	II	
3426.044	3000R	100	I	7
3425.71		1	II	
3424.750		5	II	
3424.610	1		I	
3424.554	3	15	II	
3424.295	1		I	
3424.182		1	II	
3422.454		6	II	
3421.409		1	II	
3420.345	150	20	I	
3419.807	3		I	
3419.742	2	20	II	7
3419.606	20	100	II	4
3418.571		1	II	
3418.390	400	50	I	7
3417.565	3	30	II	5
3417.345	1	10	II	

TABLE 1.—*Emission spectra of ytterbium*—Continued

Wavelength in air	Intensity		Spectrum	Zeeman type	Wavelength in air	Intensity		Spectrum	Zeeman type	Wavelength in air	Intensity		Spectrum	Zeeman type
	Meggers lamp	Thompson lamp				Meggers lamp	Thompson lamp				Meggers lamp	Thompson lamp		
Å					Å					Å				
3417.044	250	20	I		3389.439		4	II		3363.645	10	20	II	
3416.894	40	200	II	4	3388.523		7	II		3362.770	1		I	
3416.314		1	II		3387.760		3	II		3362.705	4	6	II	
3415.974	10	100	II	5	3387.505	200 r	50	I	1	3362.438	10	70	II	
3415.853		2	II		3387.370	20	2	I		3362.145	1		I	
3415.610		6	II		3387.293	2	20	II		3361.927	4		I	
3415.062	10	80	II	7	3387.120		2	II		3361.573	15	100	II	4
3414.838	20	200	II	6	3387.073		3	II		3361.467	1	8	II	
3413.357	5	15	II	5	3386.560		1	II		3361.329	3	30	II	
3412.507		5	II		3385.883	20	40	II		3359.49		1	II	
3412.453	80	40	I	7	3385.559	10	100	II	6	3359.193		3 h	II	
3411.750		6	II		3385.329	2		I		3358.612		2	II	
3411.240	10	8	I		3384.682	200	15	I		3358.254		50	III	
3410.880		4	II		3384.560		1	II		3357.802	5	40	II	
3410.689	1	6	II		3384.352		4	II		3356.966	20	200	II	5
3410.566	50	60	II	7	3384.007		2000	III	7	3356.683		1	II	
3410.487	1	10	II		3383.862	3	20	II	6	3356.305	6	40	II	
3409.875	6	70	II		3382.537	20	20	I,II		3355.870	20	200	II	6
3409.568	1	10	II		3381.255		1	II		3355.618	1		I	
3409.022		3	II		3381.060	2	15	II		3354.020		3	II	
3408.95	2		I		3380.820	1	20	II	4	3353.966	2	30	II	
3408.516	10	100	II	4	3380.644		1	II		3353.733	20	150	II	4
3408.20		3	II		3380.340		1	II		3353.607	1		I	
3408.058		7	II		3379.986	40	100	II	5	3353.563	1	6	II	
3407.922	2		I		3379.788	100	700	II	4	3353.200	3	40	II	4
3406.536	1	6	II		3379.517	6	70	II	5	3352.880	60	4	I	
3406.200	200	5	I		3379.386	2	2	I,II		3352.491	10	30	II	
3405.79		1	II		3378.698	50	3	I		3351.382	6		I	
3405.249	5	30	II		3378.404	10	100	II	6	3351.265	20	20	I,II	
3405.093		2	II		3378.286	60	4	I		3351.087	6	60	II	5
3405.03		1	II		3377.792	3	40	II		3350.967	5	40	II	5
3404.103	150	800	II	5	3377.456		3	II		3350.357	1		I	
3402.640		5	II		3376.780		2	II		3350.209	3		I	
3402.273	200	300	II	6	3376.623	3	30	II		3349.942	20	150	II	7
3401.010	200	1000	II	5	3375.483	2000 r	5000	II	6	3349.713	1		I	
3400.603		4 d	II		3375.079	30	70	II		3349.074	10	60	II	4
3400.445		3	II		3374.184		1	II		3347.537	150	1000	II	7
3399.548		3	II		3374.07		1	II		3347.016	2		I	
3398.649	2	10	II		3373.873	2	20	II		3346.504	30	30	I,II	
3397.661		100	III		3373.736		1	II		3346.192		7	II	
3397.446	2	20	II		3373.033	1	10	II		3345.958	2		I	
3397.125	2	20	II		3372.576	500	40	I		3345.921		7	II	
3397.037	50	2	I		3372.00		1	II		3345.575	5		I	
3396.328	40	400	II	5	3371.325	100	10	I		3345.187		9	II	
3395.14		5 h	II		3371.090	2		I		3345.012	20		I	
3394.519	3		I		3369.886	10	80	II	6	3344.715		3	II	
3394.437	60	300	II	5	3369.544	70	200	II	5	3344.507	1		I	
3394.152		1	II		3369.344	20	60	II	5	3344.212	30	3	I	
3393.972	30	3	I		3367.738		6	II		3343.78		1	II	
3393.815		1	II		3367.324	1		I		3343.705		2	II	
3393.636		2	II		3367.077		4	II		3343.566		2	II	
3393.252		1	II		3366.964		3	II		3343.071	80	400	II	6
3392.555		150	III		3366.937	3		I		3342.93	20 h	100 h	II	
3392.390	7	100	II	5	3366.923	10		I		3342.310		1	II	
3392.356	2	20	II		3365.969	80	800	II	6	3341.097	3	40	II	5
3392.276		4	II		3365.658		2	II		3340.791		1	II	
3391.104	100	900	II	4	3365.444		1	II		3339.644	2		I	
3390.817	3	40	II		3365.181	5		I		3339.476		3	II	
3390.63		1	II		3365.059		4	II		3339.305		3	II	
3390.421	1 h	30 h	II		3364.471		4	II		3339.274		1	II	
3390.246	1 h	40 h	II		3364.302		20	III		3339.075	10 h		I	
3389.985		2	II		3364.125		2	II		3339.022		1	II	
3389.904	8 h		I		3363.886		1	II		3338.749	1	8	II	

TABLE 1.—*Emission spectra of ytterbium*—Continued

Wavelength in air Å	Intensity: Meggers lamp	Intensity: Thompson lamp	Spectrum	Zeeman type
3337.581		1	II	
3337.420	5	20	II	5
3337.171	30 r	100	II	7
3337.005		5 h	II	
3336.88		1	II	
3336.718		4	II	
3336.68	20	1	I	
3335.826	1	10	II	
3335.435		2	II	
3335.327		3	II	
3334.321	1	3	II	
3333.800		4	II	
3333.057	200	1000	II	4
3332.774		7	II	
3332.150	9		I	
3331.95	1		I	
3331.220	5	50	II	4
3330.238		1	II	
3329.93	4		I	
3329.50	3	5	II	
3329.382	50	100	II	6
3329.087		4	II	
3329.017	3	10	II	
3328.584		8	II	
3328.51	2		I	
3328.39		1	II	
3327.756	8	80	II	6
3327.485	1	15	II	
3327.195	3	3	I,II	
3326.949	2	20	II	5
3326.745		4	II	
3326.266	40	200	II	5
3325.512	1	2000	III	3
3325.104	9	50	II	4
3324.80		2	II	
3324.470	10	70	II	4
3324.172	40	300	II	5
3324.043	2	12	II	
3323.46		3 h	II	
3322.963	20	250	II	5
3322.87	1	2	II	
3322.58		1	II	
3320.802		1	II	
3320.642		2	II	
3320.314	10	200	II	5
3320.032	5	30	II	
3319.737		2	II	
3319.674	5		I	
3319.412	700 r	50	I	7
3319.180	80	500	II	5
3318.973	50	100	II	5
3318.590		1	II	
3318.283	3	40	II	5
3317.939	2	30	II	
3317.094		3	II	
3316.834	10	200	II	4
3316.496	300	30	I	1
3315.390	20	200	II	5
3315.101	1 h	15 h	II	
3314.720	10	20	II	
3314.533	20	5	I	
3314.52		10	II	
3314.27	1		I	
3313.763	5	40	II	7
3313.039		3	II	
3312.450	1	20	II	
3311.742	2	10	II	
3311.630	3	8	II	
3311.180		2	II	
3311.050	4	30	II	
3310.937	10	80	II	7
3310.815		1	II	
3310.20		1	II	
3309.512	10	70	II	
3309.470	2	20	II	
3309.372	70	300	II	5
3309.185	5	50	II	
3308.461		2	II	
3308.210		1	II	
3306.783	100	400	II	7
3305.733	500 r	2000	II	6
3305.252	20	20	I,II	
3304.770	70	400	II	6
3304.558	80	400	II	5
3304.346		6	II	
3303.926		1	II	
3303.864		2	II	
3303.449		1	II	
3303.203		2	II	
3302.978	3		I	
3302.368	7		I	
3302.202		1	II	
3301.780	1	10	II	
3301.711	10	20	II	6
3301.481	1		I	
3301.328		1	II	
3299.828	200	10	I	7
3299.647	2		I	
3299.447		1	II	
3299.400	1	6	II	
3298.896		8	II	
3298.826	1	10	II	
3298.102		2	II	
3297.851	10	100	II	6
3297.486	8		I	
3296.501		4	II	
3295.825		4	II	
3294.58		2	II	
3294.341	7	100	II	6
3293.836		2	II	
3293.685	7		I	
3293.66		3	II	
3293.25		1	II	
3293.19	10		I	
3292.92		1	II	
3292.26	20		I	
3292.089	5	20	II	
3291.967		10	II	
3291.946	20		I	
3291.028		4	II	
3290.554		8	II	
3290.14		4	II	
3289.370	60000A	50000	II	4
3287.81		1	II	
3286.960	10	70	II	5
3285.78		1	II	
3285.35		1	II	
3285.168		2	II	
3283.494	4	40	II	4
3282.33	3		I	
3282.03		5	II	
3281.715	1	7	II	
3280.850		4	II	
3280.335	1	10	II	
3279.89		4	II	
3279.32		4	II	
3278.99		1	II	
3278.614	50	1	I	
3278.56	5		I	
3278.400	2	20	II	4
3278.057	7	70	II	6
3277.73		4	II	
3277.607	4	15	II	
3277.575		1	II	
3277.07		1	II	
3276.218	15		I	
3275.801	50	200	II	6
3275.19		7	II	
3275.14		1	II	
3275.01	1	8	II	
3274.96		2	II	
3274.770	6		I	
3273.940	7	70	II	
3273.65		1	II	
3272.98		2	II	
3272.644	30		I	
3271.528	20	150	II	
3271.247	2	20	II	
3271.190	10	40	II	
3271.125	3	30	II	
3270.57		2	II	
3269.265	50	200	II	
3268.94		2	II	
3268.84		1	II	
3268.811	2		I	
3267.890	150	2	I	
3267.313	10		I	
3266.915		6	II	
3266.39		4 d	II	
3266.163		4	II	
3265.930	3	30	II	
3265.247	2		I	
3265.068	7	60	II	
3264.889	8	80	II	
3264.114		4	II	
3263.938	1	10	II	
3263.79		1	II	
3262.296	6	60	II	
3261.759	5	50	II	
3261.686	20	200	II	6
3261.508	500	1500	II	5
3261.02		1	II	
3260.82		5	II	
3259.99	1	8	II	
3259.100	100	500	II	6
3258.663	1	10	II	
3258.453		8	II	
3256.86		1	II	
3256.030	5	50	II	

TABLE 1.—*Emission spectra of ytterbium*—Continued

Wavelength in air Å	Intensity: Meggers lamp	Intensity: Thompson lamp	Spectrum	Zeeman type
3255.24		1	II	
3254.62		2	II	
3254.197	100	300	II	
3253.911	10	100	II	
3253.545	20	1	I	
3253.340	20	120	II	
3253.023	3		I	
3252.106	1	10	II	
3250.505	1	5	II	
3249.80		1	II	
3249.57		1	II	
3249.17		4	II	
3248.446	2	10	II	
3247.932	1	5	II	
3246.85		1	II	
3246.657	1	7	II	
3246.28		1	II	
3246.060		10	II	
3245.70		5	II	
3245.05		6	II	
3244.46	2		I	
3243.46		5	II	
3243.00	4	30	II	
3242.12	1	10	II	
3242.048	4	50	II	
3241.86	30	1	I	
3240.946	20	1	I	
3240.57		3	III	
3239.580	200	5	I	
3239.39	1	3	II	
3239.195	50	200	II	6
3237.888	10		I	
3237.215		5	II	
3236.488	20	60	II	
3236.24	10		I	
3236.160	40	300	II	4
3235.975	3	30	II	
3235.858		6	II	
3235.635	2		I	
3235.61		8	II	
3235.520	4		I	
3234.740	2	10	II	
3233.487	3	40	II	
3233.38		1	II	
3232.29		4	II	
3231.986	50	300	II	6
3231.90	1	10	II	
3231.81		10	II	
3231.376	10	50	II	
3231.228		2	II	
3229.93	2		I	
3229.814	50	150	II	6
3229.475	2	20	II	
3228.575		2000	III	
3228.503	5	40	II	
3227.478	100	2	I	
3226.725	20	80	II	4
3225.885	100	400	II	6
3225.78	20	200	II	7
3224.890		4	II	
3224.752		3	II	
3224.43		4	II	
3224.25		1	II	
3223.854	4	20	II	
3223.105	4	40	II	
3222.696	150	3	I	
3222.55		1	II	
3222.11		5	II	
3221.486	10	70	II	5
3221.246	15	150	II	4
3220.96		2	II	
3220.814		8	II	
3219.633		8	II	
3219.408	2	9	II	
3219.325	1	10	II	
3218.913	2	15	II	
3218.323	100	600	II	7
3217.96		1	II	
3217.66		3	II	
3217.45		1	II	
3217.40	5		I	
3217.29	1	7	II	
3217.176	200	1000	II	5
3216.66	2		I	
3216.273		50	III	
3215.927	10	100	II	
3215.68		2	II	
3215.456	10	60	II	
3215.38		2	II	
3214.330	2	20	II	
3214.14		1	II	
3213.172		6	II	
3212.485		5	II	
3210.84		7	II	
3210.112	20	200	II	5
3208.01		3	II	
3207.870	2		I	
3207.702	4	30	II	5
3207.538	2	10	II	
3207.40		1	II	
3207.380	6		I	
3206.148	20	200	II	7
3205.863	20	50	II	
3205.58		1	II	
3204.681	20	200	II	4
3203.989	1	10	II	
3202.76		2	II	
3201.35	5	30	II	
3201.160	800 r	2000	II	5
3200.69		1	II	
3199.785	5	50	II	
3199.24		1	II	
3198.647	400	1000	II	5
3196.354	10	50	II	7
3196.052	2	20	II	
3195.585	20	200	II	5
3195.349	15		I	
3194.765	10	100	II	7
3194.242	8	70	II	6
3192.885	1000 r	3000	II	7
3192.62	4	30	II	
3192.45	1	8	II	
3192.15		5	II	
3191.352		800	III	1
3190.780	8	30	II	
3190.58		5	II	
3188.26		1	II	
3187.51		2	II	
3187.01		3	II	
3186.580	10	100	II	4
3185.64		1	II	
3185.03		1	II	
3184.71		1	II	
3183.90	3		I	
3183.498	1	5	II	
3183.46	1	5	II	
3183.07	2		I	
3182.86		4	II	
3182.52	1	8	II	
3182.165	2	10	II	
3182.09	1		I	
3181.64		1	II	
3181.27	1	4	II	
3181.03	1	9	II	
3180.919	200	800	II	5
3180.48		1	II	
3179.94	1	10	II	
3179.344	30	70	II	
3178.85		1	II	
3177.815		1	II	
3177.78		2	II	
3176.26		3	II	
3176.06		1	II	
3175.759	25	150	II	6
3174.22		2	II	
3173.797	20	150	II	7
3171.176	100	300	II	6
3169.558	10		I	
3169.056	200	1200	II	5
3168.985	3	10	II	
3168.405	8	60	II	5
3167.72		1	II	
3167.044	1	8	II	
3166.727	2	20	II	
3166.644	10		I	
3166.407	10		I	
3165.981	1	5	II	
3165.875		7	II	
3165.206	60	500	II	4
3164.973	6	15	II	
3163.985	4		I	
3163.796	100	600	II	7
3162.737	4		I	
3162.293	50	5	I	
3161.80		2	II	
3161.55	2		I	
3160.894	1	8	II	
3160.12		1	II	
3160.01		3	II	
3159.79		2	II	
3159.59		1	II	
3159.49		2	II	
3159.34		1	II	
3159.04		2	II	
3158.869	5	10	II	
3158.43	1	7	II	
3158.300	40	300	II	5
3158.145	1		I	
3157.043		7	II	

792-867 O-66-7

TABLE 1.—*Emission spectra of ytterbium*—Continued

Wavelength in air Å	Intensity: Meggers lamp	Intensity: Thompson lamp	Spectrum	Zeeman type	Wavelength in air Å	Intensity: Meggers lamp	Intensity: Thompson lamp	Spectrum	Zeeman type	Wavelength in air Å	Intensity: Meggers lamp	Intensity: Thompson lamp	Spectrum	Zeeman type
3156.365		4	II		3126.012	5	4000	III	7	3092.496	5	3000	III	3
3155.798	30	40	II		3125.885	1	10	II		3092.10	1	8	II	
3155.52		2	II		3125.700	5	20	II		3091.10	1	6	II	
3155.284	5	50	II		3125.443	50	100	II		3090.924	6	15	II	
3155.183	40	200	II	6	3124.25		2	II		3090.747	1	10	II	
3154.194	5	40	II		3123.870		6	II		3089.61	3	20	II	
3153.880	100	700	II	7	3123.510	8	60	II		3089.102	150 r	500	II	4
3153.616	20	100	II		3122.74		1	II		3089.04	10		I	
3153.180	40	300	II	5	3122.48		3	II		3088.823	3	30	II	
3152.880	2		I		3122.185	2	20	II		3088.78	1	9	II	
3152.44	4	40	II		3121.38		2	II		3088.66		3	II	
3151.90		1	II		3119.73		1	II		3087.998	1	15	II	
3151.436	15	100	II		3119.37		2	II		3087.720		6	II	
3151.255	3	8	II		3119.10		1	II		3087.46		2	II	
3150.46	3	30	II		3117.806	1000 r	3000	II	6	3086.971	10	100	II	4
3150.19		6	II		3117.318	2		I		3086.508	8	40	II	
3150.12		2	II		3116.702	60	300	II	5	3085.817	10	70	II	6
3148.998	30	200	II		3116.487	10	70	II		3085.434	9	60	II	
3148.43		2	II		3116.342	10	40	II		3085.21	8		I	
3148.08		1	II		3116.070	15	70	II	6	3084.347	7	70	II	6
3147.450	1		I		3115.340	100	400	II	7	3083.809		3	II	
3146.134	8	60	II		3115.25	1	8	II		3083.44		1	II	
3145.540	150	500	II		3114.905	3	20	II		3082.34		1	II	
3145.063	80	600	II	6	3114.69		1	II		3082.264		6	II	
3142.813	1	7	II		3114.505		4	II		3082.05		1	II	
3142.74		2	II		3112.980	1	10	II		3081.625		8	II	
3141.733	60	400	II	4	3112.91		4	II		3081.18		1	II	
3141.17		3	II		3112.742	5		I		3081.142	2		I	
3140.936	1000 r	2000	II	6	3111.047	1	6	II		3080.552	3	30	II	6
3140.28		2	II		3109.786	5	40	II		3080.49		3	II	
3139.75	1	6	II		3109.52		2	II		3080.17	3	20	II	
3139.27		2	II		3109.10	1	5	II		3079.593		7	II	
3138.577	1	1000	III		3107.902	1000 r	3000	II	4	3079.264	7	1	I	
3138.276		5	II		3107.760	100	500	II	5	3078.450	1	10	II	
3138.07		2	II		3106.97		2	II		3078.31	1	10	II	
3137.622		10	II		3106.94	1	6	II		3077.82		2	II	
3137.51		1	II		3106.740	2	10	II		3077.34		7	II	
3136.760	80	400	II	6	3106.133		3	II		3077.18		8	II	
3136.67	1	10	II		3106.007		4	II		3077.14		6	II	
3136.18		2	II		3105.37		1	II		3076.50		1	II	
3135.989		4	II		3103.81		4	II		3076.013	30	150	II	6
3135.93		1	II		3103.36		1	II		3075.10		2	II	
3135.43		1	II		3102.71		2	II		3074.92		2	II	
3135.316	1	10	II		3102.18		20	III		3074.84		3	II	
3135.12	4	30	II		3102.074	30	150	II	5	3074.63	3		I	
3133.96		1	II		3101.688		5	II		3074.60	2		I	
3133.845		3	II		3101.361	50	250	II	4	3074.50	1	10	II	
3133.778		3	II		3101.004	15	100	II		3073.89		3	II	
3132.628	15	150	II	6	3100.745	5		I		3073.680	20	100	II	
3132.478	2	15	II		3100.25		4	II		3073.19		3	II	
3132.294	1	8	II		3100.03		2	II		3072.486	6	60	II	
3131.397		1	II		3099.114	1	10	II		3072.41		4	II	
3131.38		3	II		3098.850	4	10	II		3071.583	5	50	II	
3130.862	2		I		3098.384		3	II		3071.26		1	II	
3129.145	8	80	II	5	3097.331	1	8	II		3070.98	1		I	
3128.60		1	II		3096.278		4	II		3070.28	2	7	II	
3127.866	20	120	II	6	3096.10		1	II		3069.34		2	II	
3127.64		2	II		3095.415	30	60	II		3068.69	1	10	II	
3127.49		2	II		3095.221	10	60	II	6	3068.284	7	60	II	
3127.31		2 h	II		3094.894	100	200	II		3067.986	2	10	II	
3127.138	4	40	II		3093.870	200 r	1000	II	5	3067.365	10	70	II	6
3126.25	1	5	II		3093.423	3	30	II	6	3066.54		2	II	
3126.192	4	20	II		3093.40	1	10	II		3066.487	2	6	II	

TABLE 1.—*Emission spectra of ytterbium*—Continued

Wavelength in air	Intensity		Spectrum	Zeeman type
	Meggers lamp	Thompson lamp		
Å				
3065.74		7	II	
3065.52		2	II	
3065.48		1	II	
3065.040	300 r	1000	II	4
3064.868	30	150	II	
3064.75		2	II	
3063.80		4	II	
3063.671	20	100	II	
3063.350	2	10	II	
3063.125	40	200	II	5
3062.524		4	II	
3062.06		1	II	
3061.646		6	II	
3060.440	5		I	
3060.394		7	II	
3059.568		7	II	
3059.362		4	II	
3058.71		2	II	
3058.66		5	II	
3058.288		4	II	
3058.20		1	II	
3057.29		1	II	
3056.01		2	II	
3055.60		1	II	
3055.46		2	II	
3055.350	5	15	II	
3055.157	10	60	II	4
3054.649	1	10	II	
3053.928	2	20	II	
3053.452		8	II	
3053.084	1	10	II	
3052.20		2	II	
3052.021	1	7	II	
3051.98		2	II	
3051.11		2	II	
3050.64		1	II	
3050.50		6	II	
3049.84		2	II	
3049.14		7	II	
3048.82		2	II	
3048.41		6	II	
3048.15		2	II	
3047.052	20	100	II	6
3046.482	30	200	II	4
3046.27		3	II	
3045.91		2	II	
3045.84		1	II	
3045.46		4	II	
3045.044	1	7	II	
3044.83	10	60	II	6
3044.004	20	100	II	4
3043.93		4	II	
3043.07		1	II	
3042.78		3	II	
3042.650	50	300	II	4
3042.34		2	II	
3041.180	7		I	
3040.83		2	II	
3040.652		30	III	
3040.504	5	30	II	
3040.444	2	15	II	
3040.235	5	15	II	
3039.665	40	300	II	4
3039.276		6	II	
3038.81		2	II	
3038.75	2	10	II	
3038.531	5	30	II	
3037.992	15	90	II	6
3036.820	10	60	II	
3036.13		1	II	
3035.945	1	7	II	
3034.99	1	5	II	
3034.642	40	200	II	4
3034.52		2	II	
3034.32		1	II	
3033.860	30	100	II	
3033.664	2	10	II	
3033.40		2	II	
3033.28		1	II	
3033.14		1	II	
3031.625		100	III	
3031.110	5000A	3000	II	4
3029.486	2	2000	III	3
3028.38	2	20	II	
3027.476	7		I	
3026.669	100	700	II	4
3025.76		2	II	
3025.38		6	II	
3024.935	2	15	II	
3023.614	5	30	II	6
3022.58		1	II	
3022.454	10	60	II	7
3021.27		1	II	
3020.99		4	II	
3020.703	20	100	II	5
3020.345	2	10	II	
3020.211		5	II	
3019.440	2	15	II	
3019.17		2	II	
3019.058	8	40	II	
3017.560	100	800	II	5
3016.95		6	II	
3016.40		1	II	
3014.97		2	II	
3014.526	10	60	II	7
3014.427	40	200	II	5
3014.02		8	II	
3013.08		2	II	
3012.80		3	II	
3012.28		1	II	
3011.842		4	II	
3011.218	7		I	
3011.00		1	II	
3010.735	2		I	
3010.625	50	300	II	4
3009.392	100	500	II	4
3009.21	2		I	
3007.923	5	30	II	
3007.56		3	II	
3006.863	10	70	II	5
3006.30		3	II	
3006.14	5	40	II	
3005.766	800 r	3000	II	4
3005.118	5		I	
3004.642	1	15	II	
3004.46	3	10 h	II	
3004.097	1	5	II	
3003.60		2	II	
3002.608	30	200	II	
3002.47		2	II	
3002.035	5	30	II	5
3001.864	2	10	II	
3001.283	4	40	II	4
3000.987	2	15	II	
3000.865	2		I	
3000.465	100	300	II	4
3000.13		2	II	
2999.642	5	10	II	
2999.43		8	III	
2998.377	4	30	II	
2998.000	1	800	III	
2996.75		2	II	
2996.373		5	II	
2995.862	20	100	II	5
2995.03	6	30	II	
2994.94	2	20	II	
2994.805	150 r	600	II	6
2994.53	2	20	II	
2994.48	1	10	II	
2993.939	10	70	II	6
2992.28		5	II	
2991.872	40	200	II	5
2991.70	5	9	II	
2991.33		1	II	
2991.240	1	6	II	
2990.366	30	200	II	5
2989.768	2	15	II	
2989.376	6	10	II	
2989.20	2	20	II	6
2988.95		5	II	
2988.56		1	II	
2988.30		2	II	
2987.862	1	10	II	
2987.25	1	6	II	
2986.64		2	II	
2986.47		1	II	
2985.876	10	70	II	4
2985.078	50	300	II	5
2984.84	7	60	II	
2984.44		1	II	
2983.990	200 r	1000	II	6
2983.702	15	100	II	
2983.369	4	8	II	
2982.659	10	70	II	4
2982.494	20	150	II	4
2982.055	2	8	II	
2982.01		5	II	
2981.519	3	20	II	
2980.482		5	II	
2979.859	10	60	II	4
2979.658	3	20	II	4
2979.44		1	II	
2978.906	6	40	II	4
2977.835		50	III	
2977.76		1	II	
2977.695		4	II	
2977.525	10	60	II	6
2977.270	1	9	II	
2976.53		1	II	

792-867 O-66-8

TABLE 1.—*Emission spectra of ytterbium*—Continued

Wavelength in air Å	Intensity: Meggers lamp	Intensity: Thompson lamp	Spectrum	Zeeman type
2975.567	3	20	II	
2975.238		6	II	
2973.36		1	II	
2972.94		6	II	
2972.47	3	30	II	7
2970.84	20	200	II	6
2970.564	4000A	3000	II	6
2969.70	1	7	II	
2967.72		4	II	
2966.763	20	100	II	7
2965.168	8	60	II	
2964.82		4	II	
2964.755	100 r	500	II	5
2964.39	15	100	II	6
2963.96		4	II	
2963.46	40	300	II	6
2963.255	10	70	II	
2963.17	8	50	II	
2962.522	40	250	II	6
2961.801	4	30	II	
2961.150	1	6	II	
2960.850	10	60	II	4
2958.425		3	II	
2957.632	40	150	II	
2957.05		3	II	
2955.61		2	II	
2955.318	40	200	II	5
2955.09	1	4	II	
2954.45		1	II	
2953.016	5	40	II	4
2952.55	4		I	
2952.475		4	II	
2952.253	1	10	II	
2951.716	1	8	II	
2951.406	5	40	II	
2951.022	8	50	II	
2950.80	2	8	II	
2950.64		1	II	
2950.52	2	20	II	
2950.326	20	150	II	4
2949.840		5	II	
2948.65		2	II	
2947.76		3	II	
2947.131	4	30	II	
2946.95		5	II	
2946.852	2	20	II	
2946.765	10	70	II	5
2946.305	30	200	II	6
2945.907	100 r	600	II	5
2945.22		3	II	
2944.465	5	30	II	
2944.336	5		I	
2944.19		2	II	
2943.20		2	II	
2943.15		1	II	
2942.823	10	50	II	4
2942.60		2	II	
2942.038	15	80	II	6
2941.77	1	4	II	
2941.11		1	II	
2940.517	25	150	II	5
2940.25		2	II	
2939.534	20	100	II	5
2938.84	1	4	II	
2938.51	3	20	II	
2938.188	7	50	II	6
2937.186	15	100	II	5
2935.52		4	II	
2935.245	1	7	II	
2935.108	30	200	II	5
2934.360	60	3	I	
2933.82		6	III	
2932.90		1	II	
2932.21		1	II	
2932.08		2	II	
2931.27		1	II	
2929.70		5	II	
2929.48		3	II	
2929.44		1	II	
2928.973		300	III	
2928.62	3		I	
2927.850	10	70	II	5
2927.48	3		I	
2927.42		1	II	
2927.116	1	10	II	
2926.65	2	15	II	
2926.28		1	II	
2924.65	2	9	II	
2924.560		4	II	
2924.235	20	100	II	4
2922.35	2	7	II	
2922.235	4		I	
2921.85		1	II	
2921.64		2	II	
2921.119	40	200	II	6
2920.16	1	10	II	
2919.346	400 r	1000	II	6
2919.08		4	III	
2918.89		2	II	
2918.53		1	II	
2916.83	2	10	II	
2916.61	7	30	II	
2916.431	10	70	II	4
2915.99		4	II	
2915.275	150 r	300	II	4
2915.14		4	II	
2914.84	1	8	II	
2914.48	7	40	II	6
2914.210	100 r	600	II	4
2913.75		3	II	
2913.12	1	10	II	
2912.865	10	50	II	4
2912.51		5	II	
2912.25		2	II	
2911.61		3	II	
2911.523	40	200	II	6
2910.43		2	II	
2909.88		4	II	
2909.48	30	150	II	5
2909.19	20	100	II	7
2908.55	1	9	II	
2908.33	10	50	II	4
2908.15		4	II	
2908.09	5	40	II	
2906.88	7	60	II	6
2906.313	1	1000	III	3
2905.61		3	II	
2904.97		3	II	
2904.79	1	7	II	
2904.20		1	II	
2902.924	8	80	II	5
2902.41	6	40	II	6
2901.86		1	II	
2901.60		1	II	
2900.39		2	II	
2899.705	40	200	II	4
2899.236	5	40	II	5
2898.30		600	III	7
2897.98		2	II	
2897.31		4	II	
2896.902	10	100	II	4
2895.06	2	15	II	
2894.95	3	30	II	5
2893.620	10	100	II	4
2891.384	3000A	2000	II	4
2891.16	4	40	II	
2890.28	1	8	II	
2888.24	15		I	
2888.04	100 r	300	II	6
2887.74	2	7	II	
2886.263	30	200	II	5
2885.97	10	70	II	4
2885.594		7	II	
2885.02	1	8	II	
2884.51		2	II	
2883.87	1	10	II	6
2883.686	10	1	I	
2883.01		6	II	
2882.155	7	50	II	7
2882.01		1	II	
2881.93	7	60	II	5
2881.10		6	II	
2879.83		1	II	
2879.159	10	70	II	5
2876.45		1	II	
2875.86		400	III	7
2874.83		1	II	
2874.11		6	II	
2873.490	15	1	I	
2873.14		3	II	
2872.82		1	II	
2872.11	2	10	II	
2871.712	2	10	II	
2870.57		3	II	
2870.51		3	II	
2870.061	20	100	II	5
2869.61		1	II	
2869.546	1	15	II	
2868.536		5	II	
2867.90		7	II	
2867.58	5	15	II	
2867.20	1	7	II	
2867.065	100 r	500	II	4
2866.179	4	30	II	6
2865.96	1	6	II	
2865.74		1	II	
2865.60	1	7	II	
2865.328	5	30	II	6
2864.725	4	40	II	4

TABLE 1.—*Emission spectra of ytterbium*—Continued

Wavelength in air Å	Intensity: Meggers lamp	Intensity: Thompson lamp	Spectrum	Zeeman type
2864.62	1	10	II	
2864.19		1	II	
2863.13	5	30	II	
2862.97	2	5	II	
2862.85	1	8	II	
2861.34	20	200	II	6
2861.212	40	300	II	5
2861.11	5	30	II	
2860.70	3	15	II	
2860.393	20	100	II	7
2859.94	4	20	II	
2859.805	1000R	1000	II	4
2859.392	30	200	II	6
2858.460	8	40	II	4
2858.332	15	60	II	6
2857.75		2	II	
2857.29	4	20	II	5
2857.13		3	II	
2855.85	1	7	II	
2854.490	10	50	II	4
2854.144	10	60	II	4
2854.04	4	40	II	
2853.68	3	30	II	4
2853.409	5	60	II	6
2852.63		1	II	
2851.92		4	II	
2851.86	10	70	II	5
2851.126	500R	1000	II	4
2850.64		3	II	
2850.13		1	II	
2849.90		3	II	
2849.84		1	II	
2849.71		1	III	
2849.336	6	40	II	6
2848.88	1	7	II	
2848.445	20	100	II	4
2847.97		3	II	
2847.75		2	II	
2847.64		2	II	
2847.28		4	II	
2847.175	400 r	1000	II	5
2847.03		1	II	
2846.324		5	II	
2846.183	1	5	II	
2845.355		4	II	
2844.685	4	20	II	
2844.067	4	10	II	
2843.83	3	15	II	
2843.702	1	7	II	
2842.955		300	III	7
2842.586	6	30	II	6
2842.51	2	8	II	
2842.291	1	7	II	
2842.140	3	15	II	7
2841.308	2	20	II	6
2841.26		1	II	
2841.02		2	II	
2839.91		2	II	
2839.85		1	II	
2839.17		1	II	
2838.64	3	15	II	
2837.92		2	II	
2837.09		1	II	
2835.95		1	II	
2835.48		2	II	
2835.13		1	II	
2834.972	10	70	II	6
2834.63		4	II	
2833.68		1	II	
2832.201	4	20	II	4
2830.989	30 r	200	II	5
2830.88	4	30	II	7
2830.639	1	8	II	
2828.48	1	10	II	
2827.921	3	20	II	7
2827.81	1	5	II	
2826.735		3	II	
2826.522		2	II	
2826.013		15	III	
2824.974	20	100	II	5
2824.86	1	4	II	
2824.54	2	9	II	
2824.20	2	10	II	
2823.95		1	III	
2823.585	7	50	II	7
2823.320		4	II	
2821.52		3	II	
2821.152	30 r	200	II	4
2820.12		3	II	
2819.75		2	II	
2819.49	2	10	II	6
2819.24	2		I	
2818.722	6	1000	III	1
2817.66		2	II	
2816.915		600	III	7
2816.368	2	8	II	
2816.317	4	20	II	
2815.20		1	II	
2814.87	2	10	II	
2814.528	20	100	II	6
2814.241	2	10	II	
2814.14	2		I	
2813.00		1	II	
2812.612	2	6	II	
2811.133	3	8	II	
2810.723	5	20	II	4
2810.109	4	15	II	
2809.326	2	9	II	
2808.75		2	II	
2808.514	2	50	III	
2808.305	4	20	II	5
2807.83	2	10	II	
2807.744	2	6	II	
2807.32	1	4	II	
2807.22		10	III	
2807.180	2	8	II	
2806.43		1	II	
2806.057	1	4	II	
2804.807	1	3	II	
2804.260	5	30	II	4
2803.427	2	1000	III	7
2803.319		400	III	7
2801.598	1	5	II	
2801.272		1	II	
2800.109	2	10	II	
2800.060	6	30	II	
2800.006	8	50	II	
2799.376	30	40	II	5
2798.211	20	100	II	6
2797.796	10	80	II	5
2797.28		2	II	
2796.764		2	II	
2795.60	5	600	III	1
2795.292	6	20	II	6
2795.074	8	40	II	4
2794.774	7	40	II	7
2794.441	10	70	II	5
2794.08	2	10	II	
2793.280	10	60	II	4
2792.54		3	II	
2790.47		3	III	
2789.665	3		I	
2789.431	3	15	II	
2788.245		300	III	
2787.965	7	30	II	5
2787.010	1	7	II	
2786.025	1	5	II	
2785.903	2		I	
2785.750	8	30	II	5
2785.066		2	II	
2784.966	4		I	
2784.656	30	150	II	6
2783.16		2	II	
2782.58		3	II	
2782.54	1	5	II	
2782.203	1	5	II	
2782.102	1	2	II	
2781.493		2	II	
2780.820	1	3	II	
2780.125		3	II	
2780.032	2	15	II	
2779.412		3	III	
2776.688	1	5	II	
2776.280	60 r	200	II	6
2775.440	2	10	II	6
2774.304	5	20	II	7
2773.91		2	II	
2771.86		2	II	
2771.324	20	100	II	4
2770.405		2	II	
2769.412		2	II	
2768.281	2	20	II	
2766.624	2	7	II	
2766.167	1	3	II	
2765.495		100	III	
2765.046	2	8	II	
2764.414	10	50	II	6
2762.716	1	3	II	
2761.70		4	II	
2761.373	10	70	II	7
2760.780	10	70	II	5
2759.532	3	20	II	
2759.257		3	II	
2759.003	7	40	II	4
2758.263		1	II	
2758.065		1	II	
2757.542		3	II	
2756.76		200	III	
2755.94		200	III	

TABLE 1.—*Emission spectra of ytterbium*—Continued

Wavelength in air Å	Intensity: Meggers lamp	Intensity: Thompson lamp	Spectrum	Zeeman type	Wavelength in air Å	Intensity: Meggers lamp	Intensity: Thompson lamp	Spectrum	Zeeman type	Wavelength in air Å	Intensity: Meggers lamp	Intensity: Thompson lamp	Spectrum	Zeeman type
2754.943	3	20	II	6	2719.005	3	15	II	7	2681.180		2	II	
2754.105		2	II		2718.349	40 r	200	II	7	2680.993		2	III	
2753.584	5	20	II		2717.76		2	II		2680.404	6	40	II	6
2751.452	20	80	II	4	2717.661	3	10	II		2678.847	1	3	II	
2750.477	600R	500	II	4	2717.617	1	4	II		2677.394	1	500	III	3
2749.907	3	500	III	7	2717.106	4	20	II	7	2676.131	3	6	II	
2749.624	3	20	II		2716.463		2	III		2674.866	3	10	II	4
2748.664	50 r	150	II	5	2716.354	3	5	II		2673.331		30	III	
2748.56	3	10	II		2716.177		3	II		2672.656	200R	200	II	4
2748.036	5	30	II	4	2715.94	3	15	II	7	2672.028		2	II	
2747.641	3	10	II		2715.640	1	4	II		2671.958	1000A	10	I	7
2747.580	20	80	II	5	2715.383	4	7	II		2671.554		2	II	
2746.83		1	II		2715.17		1	II		2670.605		1	II	
2745.712	5	30	II	5	2714.408	4	30	II	6	2669.305		1	II	
2745.115	2	8	II		2714.18		2	II		2669.131	1	3	II	
2744.782	1	3	II		2714.052		1	III		2668.94		2	II	
2744.372		1	II		2713.718		2	II		2668.752	8	40	II	
2742.741		2	II		2712.658	15	80	II	4	2668.707	4	20	II	7
2742.651	1	5	II		2712.321	2	400	III	3	2668.587	1	3	II	
2741.779	4	15	II		2711.785	20	30	II	5	2668.092		2	III	
2741.714	8	40	II	5	2711.09		1	II		2667.965		2	II	
2741.150	2	8	II		2710.674	6	30	II	6	2666.994	20	2000	III	7
2740.79	3	9	II		2710.544	20	80	II	5	2666.132	20	2000	III	7
2740.551	3	6	II		2710.046	2	5	II		2665.038	60	100	II	6
2740.397	1	4	II		2709.715	4	20	II	4	2664.894		70	III	
2740.215	2	6	II		2708.842	5	30	II	6	2664.39		2	II	
2739.475	1	2	II		2708.46		2	II		2663.900	2	5	II	
2738.818	2	8	II	7	2708.035		30	III		2661.888		3	II	
2738.31		1	II		2705.108		3	II		2660.861	1	4	II	
2737.61	3	15	II	5	2704.75		2	II		2660.73		2	II	
2736.553	4	20	II		2704.53	3	15	II		2659.983		100	III	
2736.050		2	II		2702.133	1	4	II		2659.635		2	II	
2735.673	2	6	II		2701.733	1	4	II		2659.267	4	20	II	4
2734.928		2	II		2701.130	3	5	II		2657.46		1	II	
2734.413		1	II		2700.797	6	40	II	5	2657.20		2	II	
2734.087	5	30	II	7	2698.617	2	8	II		2656.838	2	15	II	5
2733.724		4	II		2698.447		1	II		2656.125	10	40	II	4
2733.65		2	II		2696.625	4	20	II	7	2653.75	1000R	1000	II	7
2733.112	5	10	II	5	2696.150		2	II		2652.28	2		I	
2732.942	1	4	II		2695.556		2	II		2652.25	2	700	III	2
2732.742	30 r	150	II	4	2695.427	8	60	II	6	2651.74	3	1000	III	2
2732.50		1	II		2694.99		1	III		2651.68	2		I	
2732.033		1	II		2694.622	1	4	II		2650.795	2	10	II	
2731.83		1	II		2692.703	2	10	II		2650.728	9	30	II	4
2731.573		3	II		2692.408	3	15	II	6	2649.787	10	40	II	6
2731.517		3	II		2691.996	5	30	II	6	2649.165		3	II	
2730.62		1	II		2691.49		3	II		2648.803	6	30	II	4
2729.50	2	8	II	5	2691.44		2	II		2647.455	8	40	II	5
2729.093	1	5	II		2691.012	2	500	III	3	2647.233	2	10	II	
2728.47		1	II		2690.669	2	2	II		2646.442	6	30	II	5
2728.420	6	20	II	4	2690.298	1	3	II		2645.691		2	II	
2727.66		1	II		2689.85		1	III		2644.306	20	80	II	6
2727.22		1	II		2689.338		2	III		2643.62		100	III	
2724.65	1	3	II		2688.22		1	II		2643.237		3	II	
2724.41		2	II		2687.980	4	30	II	6	2642.815		5	II	
2723.338		3	II		2687.900	1	5	II		2642.558	10	1000	II	6
2722.759		2	II		2687.08		1	II		2641.97	2	10	II	
2722.475	1	5	II		2685.990	2	10	II		2641.886	50	50	II	5
2722.205	8	40	II	7	2685.30		2	III		2641.485		2	II	
2721.895		3	II		2685.022		2	III		2640.482		300	III	
2721.183		3	II		2684.747	10	70	II	6	2639.448	10	40	II	4
2720.522	1	5	II		2683.895		2	II		2638.596	4	5	II	
2719.996		2	II		2683.416	4	30	II	6	2638.055	1	500	III	3

TABLE 1.—*Emission spectra of ytterbium*—Continued

Wavelength in air Å	Intensity: Meggers lamp	Intensity: Thompson lamp	Spectrum	Zeeman type
2637.637		2	II	
2637.378	2	2	II	
2636.519	1	6	II	6
2636.399		3	II	
2636.275	2	8	II	
2635.37		30	III	
2635.197	1	4	II	
2634.50		2	III	
2634.306	30	40	II	6
2634.183		3	II	
2632.69	2	8	II	
2631.73	3	15	II	4
2630.36		1	III	
2628.80	2	7	II	
2628.605	1	4	II	
2628.424		2	II	
2628.07	3	20	II	6
2627.07		300	III	
2624.949	3	5	II	
2624.52		2	II	
2623.22	2	9	II	4
2621.67	4	20	II	
2621.11	1	600	III	3
2619.93	3	15	II	
2619.074	4	20	II	5
2618.948		2	II	
2618.800	40	1	I	
2617.01	100 r	100	II	6
2615.35	1	5	II	
2615.262	6	30	II	4
2614.55	1	3	II	
2614.45	2	3	II	
2612.63	2	10	II	
2612.041	4	20	II	
2611.645	2	2	II	
2610.860	5	30	II	7
2610.531	1	4	II	
2609.14		30	III	
2608.498	1	4	II	
2607.864	5	30	II	4
2607.22		2	III	
2605.43	2	3	II	
2604.69		2	II	
2604.58		4	III	
2604.053	5	30	II	5
2602.40		2	II	
2601.87	20	1	I	
2600.850	2	9	II	
2600.508	1	2	II	
2600.21	3	15	II	
2599.75	1	2	II	
2599.144	1	800	III	1
2598.43	2	6	II	
2598.11		2	II	
2597.69	1	3	II	
2597.619	2	2	II	
2597.495	1	5	II	
2597.23	1	500	III	2
2596.735	3	30	II	
2596.320	6	80	II	6
2596.16	6	80	II	6
2594.493	3	20	II	
2594.20	3	15	II	6
2592.694		20	III	
2591.026	3	10	II	6
2590.711	2	5	II	
2590.328		2	III	
2588.617		100	III	
2586.30	3	10	II	7
2585.67		2	III	
2584.76		2	III	
2583.748	1	4	II	
2582.489		2	II	
2582.38		7	III	
2582.068		3	II	
2581.41	1	4	II	
2581.092		3	II	
2580.36	3		I	
2579.57	4	1000	III	1
2577.74	3	10	II	
2577.605	5	20	II	
2576.09		2	II	
2574.78	2	10	II	
2573.147	6	30	II	7
2572.15	1	4	II	
2571.69	1	2	II	
2571.36	7	50	II	4
2569.61	1	2	II	
2568.60		2	II	
2568.17	3	10	II	
2567.607	7	2000	III	7
2566.78		100	III	
2565.573	10	40	II	
2564.439		5	III	
2564.32		3	III	
2563.92	2	2	II	
2561.66		10	III	
2560.56		100	III	
2559.972	2	5	II	
2559.094		3	III	
2558.40	3	2	II	
2557.804	4	5	II	
2557.703	1	5	II	
2557.259	4	20	II	7
2556.30		3	II	
2555.29	1	300	III	3
2554.641		2	II	
2552.88	2	2	II	
2552.70	10	60	II	7
2552.147	15	80	II	7
2550.786		1	II	
2550.68	3	10	II	
2550.39		40	III	
2550.060	10	20	II	
2550.023		3	II	
2548.756	3	15	II	7
2548.00		3	II	
2547.498	2	8	II	
2547.23	2	5	II	
2547.20		2	II	
2546.886	1	2	II	
2546.28	2	5	II	
2545.871	2	4	II	
2545.545		3	II	
2544.72		2	II	
2542.76	3	10	II	
2542.318	4	10	II	
2541.82		1	II	
2541.16	2	6	II	
2540.60		1	II	
2539.64		4	II	
2538.79	2	20	II	
2538.67	300A	200	II	6
2538.203	4	30	II	
2537.65	10	70	II	7
2537.240	1	5	II	
2537.08		1	II	
2536.962	2	10	II	6
2536.027	4	20	II	5
2534.05		2	II	
2532.55	2	6	II	
2532.19	2	3	II	
2531.00		1	II	
2529.98	1	3	II	
2529.50	3	9	II	
2529.14		20	III	
2528.836	1	1	II	
2528.339	3	25	II	7
2527.954		3	II	
2527.864	4	30	II	5
2527.49		2	II	
2527.165		2	III	
2526.31	2	5	II	
2526.189		3	II	
2524.990	2	10	II	
2524.573	4	8	II	
2524.30		3	III	
2522.438	15	50	II	6
2522.07		15	III	
2521.04	3	15	II	
2520.329		8	III	
2519.39		2	II	
2518.59		2	II	
2518.47		1	II	
2518.01	3	10	II	6
2516.82	50	300	II	7
2516.35	6	30	II	6
2516.118	1		I	
2516.031	3	15	II	
2515.600	2	7	II	7
2515.460	2	3	II	
2515.165		2	II	
2514.69		1	II	
2514.248	7	20	II	7
2513.64		1	II	
2512.87		2	II	
2512.524	5	20	II	5
2512.061	50 r	100	II	4
2511.868	4	20	II	
2510.50	2	7	II	
2510.29	1	2	II	
2510.18		1	III	
2510.03	1	1	II	
2509.86	2	5	II	
2508.073	10	20	II	
2506.69		1	III	
2506.52		4	III	
2506.25		40	III	
2505.477	6	30	II	6

TABLE 1.—*Emission spectra of ytterbium*—Continued

Wavelength in air Å	Intensity: Meggers lamp	Intensity: Thompson lamp	Spectrum	Zeeman type
2503.46		1	II	
2502.02	30	70	II	4
2501.21	1	3	II	
2500.568	2	6	II	
2498.73		2	II	
2498.36	2	5	II	
2496.85		2	II	
2495.63	5	20	II	
2495.05	4	3	II	
2493.64	3	10	II	
2493.50		2	III	
2491.69		20	III	
2491.15	3	5	II	
2490.42		200	III	7
2488.92		3	II	
2487.08	1	3	II	
2484.89	5	20	II	6
2484.29		5	III	
2481.42	1	3	II	
2481.35		2	II	
2481.03	1	2	II	
2479.29		2	II	
2479.15	1	5	II	
2477.76		1	II	
2476.62		2	II	
2475.92		2	II	
2474.52	2	1	II	
2474.27	1	3	II	
2473.95		1	II	
2473.16		2	II	
2471.06	2	3	II	
2470.85		2	II	
2469.89	1	2	II	
2469.52		1	II	
2467.24		2	II	
2466.63	5	20	II	6
2465.13		2	II	
2464.59	1	10	II	
2464.50	1000A	10	I	7
2463.79		1	II	
2463.35	2	4	II	
2463.04		1	II	
2462.71		1	II	
2461.98		2	II	
2461.83		1	II	
2461.40	3	10	II	
2460.25	10	40	II	7
2460.00	1	1	II	
2459.93	1	4	II	
2458.637		10	III	
2458.22		2	II	
2457.73		2	II	
2456.74		1	II	
2456.35		1	II	
2456.08		6	II	
2455.97		3	II	
2454.75	1	10	II	
2454.52	3	20	II	
2453.51		2	II	
2451.94	2	3	II	
2451.15		1	II	
2450.26	3	5	II	
2449.71	1	3	II	
2449.45		2	II	
2447.26	3	10	II	
2446.41		1	II	
2445.92	1	2	II	
2444.64		2	II	
2443.74		2	II	
2442.64	1	3	II	
2440.43		20	III	
2440.01		1	II	
2439.72		2	II	
2439.59	3	5	II	
2439.31		20	III	
2438.27		100	III	
2437.24	4	7	II	
2436.87	1	2	II	
2436.06		5	II	
2434.71	1	9	III	
2434.02		2	II	
2433.74		1	II	
2433.62	1	3	II	
2433.43		20	III	
2433.16	1	2	II	
2433.05		1	II	
2432.62	2	3	II	
2432.01		2	II	
2431.69		1	II	
2429.18		10	III	
2429.01	1	10	II	
2428.74		1	II	
2428.30		1	II	
2428.12		6	II	
2427.66		1	II	
2427.20		1	II	
2426.19		1	II	
2425.68		1	II	
2424.61	4	6	II	
2423.96		1	II	
2422.84	10	20	II	
2421.35	10	50	II	4
2420.03	1	4	II	
2419.41		1	II	
2419.20		2	II	
2418.38		2	II	
2417.01		3	II	
2415.39		2	II	
2414.33	2	6	II	
2413.77		2	II	
2413.66	1	5	II	
2412.33		60	III	
2411.53		9	III	
2410.77		8	III	
2410.04		20	III	
2409.44		1	II	
2409.06		5	II	
2407.98		1	II	
2407.76		1	II	
2406.79		1	II	
2406.09	1	10	II	
2404.62		2	III	
2403.95		50	III	
2403.41		4	II	
2402.71		2	II	
2399.93		1	II	
2398.02	40	20	II	
2397.87		3	II	
2397.73		3	II	
2397.34		1	II	
2390.74	20R	70	II	4
2390.57	2	8	II	
2389.18		3	II	
2388.40	2	7	II	
2386.75		2	II	
2385.94		1	II	
2385.01	1	5	II	
2383.44		1	II	
2382.98		2	II	
2382.57	1	10	II	
2380.39	2	15	II	
2377.22		20	III	
2375.18		3	II	
2374.74		1	II	
2374.52	1	5	II	
2374.32		3	II	
2373.89	2	20	II	7
2373.06		7	II	
2371.64		1	II	
2369.99		30	III	
2369.59		2	II	
2369.42		50	II	
2367.46		50	III	
2366.97		2	II	
2365.68		2	III	
2365.43		200	III	
2364.10		2	II	
2363.49	1	9	II	
2362.89	10	60	II	
2362.30		1	II	
2361.08		40	III	
2358.67		2	II	
2358.53		6	III	
2357.84	1	7	II	
2355.03		1	II	
2350.06		2	II	
2349.39		7	II	
2347.41		1	II	
2345.63		3	III	
2344.66	4	20	II	
2344.09	4	7	II	
2340.78		1	II	
2340.40	1	6	II	
2339.61		1	II	
2337.97		200	III	
2336.83		1	II	
2335.44	2	10	II	
2335.11		1	II	
2333.28		7	III	
2332.28		1	II	
2331.56		1	II	
2330.39		1	II	
2328.06		1	II	
2327.74		3	II	
2327.38		1	II	
2326.92	1	10	II	
2324.44	30	9	I	
2323.18		4	II	
2323.02		1	II	

TABLE 1.—*Emission spectra of ytterbium*—Continued

Wavelength in air Å	Intensity Meggers lamp	Intensity Thompson lamp	Spectrum	Zeeman type	Wavelength in air Å	Intensity Meggers lamp	Intensity Thompson lamp	Spectrum	Zeeman type	Wavelength in air Å	Intensity Meggers lamp	Intensity Thompson lamp	Spectrum	Zeeman type
2322.63		1	II		2263.12		3	II		2148.60		5	III	
2321.38		1	II		2262.26		100	III		2144.77		15 e	IV	
2320.81	200A	150	II	4	2257.03		200	III		2142.21		2	II	
2318.65		2	II		2255.48		3	II		2139.98		10 e	IV	
2315.20	3	10	II		2253.97		1	II		2138.35		4 e	IV	
2314.81		8	III		2253.27		2	II		2137.71		4	II	
2314.49	1	200	III	7	2251.93		1	II		2135.27		3	II	
2312.59	1	3	II		2244.28		100	III		2131.40	6	5	II	
2311.18		1	II		2243.18		1	II		2126.74	100	80	II	
2309.54	2	5	II		2240.11		300	III		2125.57		4	II	
2309.27		100	III		2237.51		2	II		2120.36		3	II	
2307.39	1	6	II		2231.56		5	III		2119.18		20	III	
2306.30		2	II		2227.71		5	III		2117.62		6	II	
2305.32	2	300	III	1	2224.89		1	II		2116.67	100	80	II	
2303.28		2	II		2224.46	100	80	II	4	2114.56		3	III	
2303.16		1	II		2222.25		1	II		2113.39		1	III	
2298.67		2	II		2216.20		1	II		2110.20		4	III	
2297.91		4	II		2214.68		3	II		2109.54		50	III	
2296.63		2	II		2213.06		1	II		2106.71		10	III	
2292.83		4	II		2212.60	3		I		2102.73	5	20	II	
2292.19		3	II		2211.91		1	II		2102.10		4	III	
2291.61		1	II		2203.11		2	II		2098.36		30	III	
2289.76	4		I		2202.27		80	III		2096.79		15	III	
2288.96	2	10	II		2201.20		3	II		2095.31		80	III	
2288.14		1	II		2198.14		20	III		2094.77		10	III	
2288.04	1		I		2189.45		6	II		2093.13		6	III	
2285.79		4	II		2185.71	100	80	II	5	2092.26		20	III	
2284.99		30	II		2178.70		4	II		2091.23		20	III	
2283.40	3	9	II		2174.28	1	3	II		2087.98		50	III	
2282.99	1	150	III		2169.79		2	II		2087.37		10	III	
2279.44		1	II		2165.21		3	II		2086.53		4	III	
2276.11		1	II		2163.89		4 e	IV		2078.05		30	III	
2275.07		3	II		2161.60	10	40	II		2073.64		10	III	
2271.31		1	II		2160.20		6	II		2067.52		4	III	
2271.11	40	2	I		2159.89		1	II		2066.49		10	III	
2269.57		1	II		2155.88	3		I		2054.80		20	III	
2268.57		4	II		2155.50		30	II		2029.54		6	III	
2268.31		3	II		2155.20		3	II		2022.03		2	II	
2267.16		3	II		2154.19		20 e	IV		2021.36		2	II	
2265.67		200	III		2152.32		3	II		2018.08		2	II	
2263.89		1	II		2148.94		2	II		1998.17		40	III	

The senior author gratefully acknowledges the cooperation of George R. Harrison in obtaining the first Zeeman spectrograms of ytterbium in 1939. He is happy to thank Jack Sugar for the first Yb spectrograms showing reversals that he made in 1961, and Nissan Spector for infrared spectrograms of the sliding spark in 1963. He also thanks Mrs. John B. Peterson most sincerely for her expert assistance with wavelength calculations and compilations of many thousands of ytterbium lines.

4. References

[1] W. F. Meggers and B. F. Scribner, Arc and spark spectra of ytterbium, J. Res. NBS **19,** 651–664 (1937), RP1053.
[2] W. F. Meggers, The second spectrum of ytterbium, J. Opt. Soc. Am. **37,** 988 A (1947).
[3] A. Gatterer and J. Junkes. Spektren der Seltenen Erden. pp. 307–314 (Vatican City Press, 1945).
[4] C. J. Humphreys and E. Paul, Jr., Infrared Atomic Spectra, Quarterly Report Foundational Research Projects NOVORD Report 5970, NOLC Report 473, 57–67 (1959).
[5] B. W. Bryant, The spectra of doubly and triply ionized ytterbium, Johns Hopkins Spectroscopic Report Number 21, 82 pp. (1961).
[6] L. Allen, The Zeeman effect of the arc and spark spectra of ytterbium and thulium, United Kingdom Atomic Energy Authority Research Group Report, AERE–R4029, 34 pp (1962).
[7] W. F. Meggers, Present experimental status of rare-earth spectra, J. Opt. Soc. Am. **50,** 405–406 (1960).
[8] C. H. Corliss, W. R. Bozman, and F. O. Westfall, Electrodeless metal-halide lamps, J. Opt. Soc. Am. **43,** 398–400 (1953).
[9] C. H. Corliss and W. F. Meggers, Improved description of hafnium spectra, J. Res. NBS **61,** 269–324 (1958), RP2904.
[10] W. F. Meggers and F. O. Westfall, Lamps and wavelengths of mercury 198, J. Res. NBS **44,** 447–455 (1950), RP2091.
[11] M. Zelikoff, P. H. Wyckoff, L. M. Aschenbrand, and R. S. Loomis, Electrodeless discharge lamps containing metal vapors, J. Opt. Soc. Am. **42,** 818–819 (1952).
[12] J. J. Thompson, On the discharge of electricity through exhausted tubes without electrodes, Phil. Mag. **32,** 321–336, 445–464 (1891).
[13] V. L. Bloch and E. Bloch, Spectres d'Etincelle d'Ordre Superieur du Mercure, J. Phys. Rad. **4,** 333–348 (1923).
[14] J. Sugar, Light source for producing self-reversed spectral lines, J. Res. NBS **66A** (Phys. and Chem.), No. 4, 321–324 (1962).
[15] J. Sugar, Analysis of the third spectrum of praseodymium, J. Opt. Soc. Am. **53,** 831–839 (1963).
[16] G. R. Harrison and F. Bitter, Zeeman effects in complex spectra at fields up to 100,000 gauss, Phys. Rev. **57,** 15–20 (1940).
[17] W. F. Meggers and C. H. Corliss, First spectrum of ytterbium, Yb I, J. Opt. Soc. Am. **50,** 1136A (1960).
[18] E. Back and A. Landé, Zeemaneffekt und Multiplett-struktur der Spektrallinien, p. 168 (Julius Springer, Berlin, 1925).

(Paper 70A1–386)

Washington, August 10, 1965.

JOURNAL OF RESEARCH of the National Bureau of Standards—A. Physics and Chemistry
Vol. 70A, No. 1, January–February 1966

Publications of the National Bureau of Standards*

Selected Abstracts

Error analysis of phase-integral methods. I. General theory for simple turning points, F. W. J. Olver, *J. Res. NBS* **69B** (*Math. and Math. Phys.*), *No. 4, 271–290 (Oct.–Dec. 1965).*
An approximate general solution of the differential equation

$$d^2w/dz^2 = f(z)w$$

is

$$w \approx Af^{-1/4} \exp\left(\int f^{1/2}dz\right) + Bf^{-1/4} \exp\left(-\int f^{1/2}dz\right).$$

To represent a particular solution throughout a given complex domain, differing pairs of values of the arbitrary constants A and B are generally needed in various subdomains. Strict error bounds are established in this paper for the coefficients in the linear equations connecting the pairs of values of A and B, in the case in which the z-domain under consideration is unbounded and contains a simple zero and no singularities of $f(z)$.
The results are used to place the "WKBJ" method on a firm mathematical foundation.

Error analysis of phase-integral methods. II. Application to wave-penetration problems, F. W. J. Olver, *J. Res. NBS* **69B** (*Math. and Math. Phys.*), *No. 4, 291–300 (Oct.–Dec. 1965).*
A study is made of the differential equation

$$d^2w/dz^2 = \{f(z) + h(z)\}w,$$

in which $f(z)$ and $h(z)$ are real and regular on the real axis, and $f(z)$ has exactly two zeros there. Strict error bounds are derived for the coefficients in the formulas which connect the asymptotic solutions at $z = +-$ with the asymptotic solutions at $z = -$. Applications are made to two physical problems.

A random walk model of chain polymer adsorption at a surface. II. Correlation between neighboring steps, R. J. Rubin, *J. Res.* **69B** (*Math. and Math. Phys.*), *301–312 (Oct.–Dec. 1965).*
A random walk lattice model of adsorption of an isolated polymer chain at a solution surface is investigated. The model is a modification of a simple cubic lattice in which there is a correlation between successive steps. The direction of each step is at right angles to the direction of the preceding step (all bond angles are 90°). One-dimensional characteristics of the monomer unit distribution are determined analytically in the limit of long polymer chains neglecting the self-excluded volume. The mean number of monomer units adsorbed in the surface layer $\nu(\theta, N)$ is determined assuming that one end of the polymer chain lies in the surface layer, where N is the mean number of monomer units in the chain and θ is the adsorption energy of each monomer unit in the surface layer measured in units of kT. In addition, the mean distance of the free end of the chain from the surface layer $z(\theta, N)$ is determined. The properties of this correlated step model are qualitatively similar to the properties which have been found in uncorrelated step models. In particular, there is a critical value of the adsorption energy θ_c such that for $\theta > \theta_c$, $\nu(\theta, N)$ is proportional to N. Numerical values of $N\,\nu(\theta, N)$ and $z(\theta, N)$ are presented for $\theta > \theta_c = \ln(\sqrt{5}-1)$.

Single crystal x-ray diffraction at high pressures, C. Weir, S. Block, and G. Piermarini, *J. Res.* **69C** (*Engr. and Instr.*), *No. 4, 275–281 (Oct.–Dec. 1965).*
Construction and operation of a high-pressure single-crystal x-ray diffraction precession camera is described. The instrument appears applicable to single crystal studies to pressures as high as at least 30 kbars and temperatures of at least 250 °C. Application of the instrument is illustrated by single crystal studies of ice VI and ice VII. Unit cell parameters are given for these two forms of ice. Further modifications and applications are discussed.

The Sondheimer-Wilson-Kohler formula in platinum resistance thermometry, R. J. Corruccini, *J. Res. NBS* **69C** (*Engr. and Instr.*), *No. 4, 283–286 (Oct.–Dec. 1965).*
An attempt was made to determine the ideal resistivity versus temperature function for platinum by a parameter-variation method using the Sondheimer-Wilson-Kohler formula for the deviation from Matthiessen's rule. At the same time a test of the applicability of the SWK formula for practical thermometry was made by examining the accuracy with which it could fit the resistance-temperature functions of selected thermometers, the characteristics of which were restricted in a manner believed to favor their accurate representation. No ideal resistivity function could be found such that most of the thermometers could be accurately represented.

Thermodynamic and related properties of parahydrogen from the triple point to 100 °K at pressures to 340 atmospheres, H. M. Roder, L. A. Weber, and R. D. Goodwin, *NBS Mono. 94 (Aug. 10, 1965), 75 cents.*
Experimental programs on parahydrogen at this laboratory have provided pressure-density-temperature relations and heat capacities at temperatures from 15 to 100 °K and at pressures from 2 to 350 atm. The two types of data have been correlated to yield a consistent set of functions. The properties tabulated for selected isobars and isochores are temperature, volume or pressure, the isotherm derivative $(\partial P/\partial \rho)_T$, the isochore derivative $(\partial P/\partial T)_\rho$, internal energy, enthalpy, entropy, the specific heats at constant volume and at constant pressure, and the velocity of sound. Also presented are the derived Joule-Thomson inversion curve and some comparisons with normal hydrogen near 100 °K.

Standard Reference Materials: Methods for the chemical analysis of white cast iron standards, J. I. Shultz, *NBS Misc. Publ. 260–6 (July 16, 1965), 45 cents.*
The procedures described in this publication are those used at the National Bureau of Standards in the analysis of white cast iron standard reference materials for the ten (10) major elements; namely, carbon, manganese, phosphorus, sulfur, silicon, copper, nickel, chromium, vanadium, and molybdenum.
Carbon and sulfur are determined by combustion; manganese, chromium, and vanadium by titrimetry; phosphorus, copper, and molybdenum by photometry; and silicon and nickel by gravimetry. These procedures, which are slight modifications of well-established and previously published methods, were selected for their accuracy and dependability.

Interrelations between cement and concrete properties, Part 1. Materials, techniques, water requirements and trace elements, R. L. Blaine, H. T. Arni, B. E. Foster, et al., *NBS Bldg. Sci. Series* **2**, *Pt. 1 (Aug. 20, 1965), 35 cents.*
The studies of the interrelations between cement and concrete properties are presented in a series of related articles. This first section presents the type classification of the cements and the areas from which they were procured together with the tests performed on the cements and concretes. Also presented are the methods employed in the statistical treatment of the data and a discussion of the significance of the various statistical techniques employed in the following sections dealing with specific aspects of the interrelations between cement and concrete properties.

Accuracy in measurements and calibrations, 1965, W. A. Wildhack, R. C. Powell, and H. L. Mason, *NBS Tech. Note 262 (June 15, 1965), $1.00.*

This publication contains a comprehensive picture of the degree of accuracy in measurement now existing in the United States for many of the physical quantities of importance to science and industry. The information is conveyed through charts which plot the limits of uncertainty of a given quantity ranging from pico units to giga units. Brief discussions prepared by various NBS scientists cover the six basic quantities of the International System and derived quantities in the fields of electricity, metrology, mechanics, thermal, radiation, and radio. Some charts show present estimates of precisions or accuracies for NBS standards available as calibration services to science and industry; others indicate values sought as near-term goals. In some cases an area designated "Non-NBS State of the Art" is given on the chart to indicate how commercial and other Government laboratories are progressing in the field of measurement.

Electrochemical analysis: Studies of acids, bases, and salts by EMF conductance, optical and kinetic methods, July 1964 to June 1965, ed. R. G. Bates, *NBS Tech. Note 271 (Sept. 6, 1965), 60 cents.*
This survey of the activities of the Electrochemical Analysis Section, Analytical Chemistry Division, covers the period July 1964 to June 1965. An attempt is made to summarize a year's progress on the technical projects of the Section in such a way as to stress the program and capabilities of the organizational unit as a whole. Consequently, a description of facilities and equipment is presented first and is followed by brief summaries of the several lines of work currently under way. Emphasis is given to the reasons why each study was undertaken. The main areas of investigation include the study of acidity and solvent effects in water, deuterium oxide, and water-methanol solvents by emf methods; the development of reference indicator bases for nonaqueous media and reference materials for dielectric measurements; measurement of the thermodynamic properties of mixed salt solutions; and investigation of special problems in trace analysis by conductometric and kinetic methods. The survey concludes with lists of the members of the Section staff, publications and manuscripts produced during the year, and talks given by the staff.

Solubility of solids in dense gases, J. M. Prausnitz, *NBS Tech. Note 316 (July 1965), 35 cents.*
The thermodynamics of solid-dense gas equilibria is discussed, and two techniques are described for calculating the solubility of a solid component in a gas at high pressure. The first one is based on the recent empirical equation of state of Redlich which, in turn, is derived from Pitzer's generalized tables of fluid-phase volumetric properties. The second one is based on the Hildebrand-Scatchard theory of solutions. Both methods give good semiquanitative results but cannot accurately predict solubilities from pure-component data alone.

Emission spectrum of CF, T. L. Porter, D. E. Mann, and N. Acquista, *J. Mol. Spectry.* **16,** *228 (June 1965).*
Eighteen bands of the $A^2\Sigma^+ - X^2\pi$ system of CF in the region 2190–2965 Å have been analyzed and several molecular constants calculated, including rotational constants for levels up to $v'=1$ and $v''=9$. The rotational analyses were carried out with the help of a digital computer program which searched wavenumber lists for rotational branches, these being series of lines with constant second differences. Consideration of potential curves and dissociation energies indicates that, in the first approximation, the potential curve of the stable A state is crossed by a repulsive curve of the same symmetry. Application of the noncrossing rule leads to the conclusion that the potential curve of this state has a maximum resulting in predissociation, and that the originally repulsive state is in fact stable and may be identified with a previously known B state.

High pressure x-ray diffraction studies, G. J. Piermarini, *Proc. 13th Chemical Engineering Conf., Montreal, Canada, Oct. 19–23, 1963, pp. 182–185 (Chemical Institute of Canada, 1963).*
A device containing an opposed diamond-anvil pressure cell and capable of obtaining x-ray diffraction powder patterns photographically of materials subjected to pressures of up to 70 kilobars or more is described. Experimental results obtained with this apparatus are presented which serve to illustrate its range of application, and its usefulness as a crystallographic tool in high-pressure research.

Radiolytic stress relaxation of an ethylene-propylene copolymer, H. Yu and L. A. Wall, *J. Phys. Chem.* **69,** *2072–2078 (June 1965).*
The kinetics of network chain scission, induced by γ-rays, has been studied by stress relaxation at a constant elongation in vacuum and in air. The rate of chain scission of 1:1 ethylene-propylene copolymer was found to be independent of initial network chain density, and the initial rates were roughly the same in air and in vacuum. Parameters for crosslinking, induced by γ-rays, were obtained by sol extraction and by measurement of elastic properties of the resulting networks. G-values for scission and crosslinking and gel dose, obtained by stress relaxation and elastic properties and by sol extraction, were found to be in an agreement with each other.

The determination of beta-emitting radionuclides in aqueous formamide solutions, A. Schwebel, *Proc. Bioassay and Analytical Chemistry Meeting, Argonne Natl. Lab., Argonne, Ill., Oct. 1962, ANL Publ. 6637, p. 29 (1962).*
A method is described for the radioassay of β or $\beta-\gamma$ emitting nuclides in an aqueous formamide solution placed in a windowless flow counter.

The half-life of carbon-14; comments on the mass-spectrometric method, E. E. Hughes and W. B. Mann (*Proc. Radio-Carbon Dating Conf., Cambridge, 1962*), *Intern. J. Appl. Radiation Isotopes* **15,** *97–100 (1964).*
An assessment has been made of the mass-spectrometer results in the recent NBS determination of the half-life of carbon-14. Evidence is presented to show that the uncertainties due to effusive separation and the dependence of the sensitivity constant on the isotopic abundance of carbon-14 are well within the 0.8% uncertainty already assigned to these sources.

The heats of solution and oxidation of sulfur dioxide, W. H. Johnson and S. Sunner, *Acta. Chem. Scand.* **17,** *1919–1924 (1963).*
The heat of solution of sulfur dioxide from 0.013 M to 0.23 M and the heat of oxidation of aqueous sulfur dioxide to sulfuric acid by liquid bromine have been determined by calorimetric methods.

The kinetics of positive ion desorption from polycrystalline tungsten and rhenium, M. D. Scheer and J. Fine (*Proc. Intern. Symp. Condensation and Evaporation of Solids, Dayton, Ohio, Sept. 12–14, 1962*), *Book, Condensation and Evaporation of Solids, Paper 20, p. 327 (Gordon & Breach, New York, N.Y., 1963).*
The mean adsorption lifetimes (τ_3) of Cs^+ on tungsten and Cs^+ and Ba^+ on rhenium have been measured in the millisecond region. Under atomically clean conditions and low surface coverage:

$$\tau_3 = (1.0 \pm 0.5) \times 10^{-12} \exp\left[\frac{23{,}600 \pm 500}{T}\right] \text{sec}; \quad 1070 < T < 1194\ ^\circ\text{K}$$

was obtained for Cs^+ on W; for Cs^+ on Re

$$\tau_3 = (1.9 \pm 0.9) \times 10^{-13} \exp\left[\frac{23{,}300 \pm 500}{T}\right] \text{sec}; \quad 950 < T < 1080\ ^\circ\text{K}$$

was found; and

$$\tau_3 = (0.6 \pm 0.4) \times 10^{-13} \exp\left[\frac{54{,}700 \pm 2400}{T}\right] \text{sec}; \quad 2100 < T < 2300\ ^\circ\text{K}$$

was measured for Ba^+ on Re.
Both the $Cs^+ - W$ and $Cs^+ - Re$ bonding can be attributed to the electrostatic image energy of the Cs^+ ion on an electrically conducting surface. The $Ba^+ - Re$ interaction on the other hand, must include a large exchange force in addition to the electrostatic image force because of the unpaired valence electron remaining in the univalent Ba^+ ion. The presence of an adsorbed layer of residual vacuum gases decreased the $Cs^+ - W$ and the $Cs^+ - Re$ binding energies by about 0.5 eV and increased the pre-exponential factor by about two orders of magnitude.

Theoretical electromotive forces for cells containing a single solid or molten fluoride, bromide, or iodide, W. J. Hamer, M. S. Malmberg, and B. Rubin, *J. Electro. Chem. Soc.* **112,** *No. 7, 750–755 (July 1965).*
Theoretical electromotive forces have been calculated for reversible cells of the type: metal|metallic halide|halogen for fluorides, bromides, and iodides from 25 to 1500 °C using available thermodynamic data. The data for each halide type are arranged in electromotive force series and compared with the respective series in aqueous solutions.

Thermogravimetric study of some new transition metal-Schiff base coordination polymers, E. Horowitz, M. Tryon, and R. G. Christensen, *J. Appl. Polymer Sci.* **9,** *2321–2336 (1965).*
A condensation reaction between 5-amino-8-hydroxyquinoline and terephthalaldehyde yielded a bis-bifunctional Schiff base ligand, 5,5′-[*p*-phenylenebis(methylidynenitrilo)] di-8-quinolinol, which was used to produce coordination polymers containing Mn(II), Co(II), Ni(II), Cu(II) or Zn(II) in the form of insoluble powders. The thermal stabilities of these polymers were evaluated in vacuum over the temperature range of 25°–700 °C using a newly constructed thermobalance having improved sensitivity. The results relate the decomposition of the polymers to the metal in the backbone as well as to the organic ligand to which the metal is coordinated. Some discussion is devoted to the possible modes of decomposition of these polymers.

Fracture topography of brittle polymers, S. B. Newman, *Polymer Engr. Sci.* **5,** *No. 3, 159–165 (July 1965).*
Fracture surfaces record the kinetics of failure at two levels in the structure of polymeric solids. The first is evidenced by the formation of geometric markings resulting from the interaction of the primary fracture front with secondary fractures developing radially just ahead of the primary fracture. These markings are often visible to the unaided eye and have minimal dimensions in the micron range. The second fracture phenomenon appears to involve the orientation of molecular chains or bundles. Such orientation manifests itself in the interference-color producing film found on the fracture surfaces of poly(methylemethacrylate) and polystyrene. It is also apparent in the free or adherent film found on the surfaces of large fractured crazes. Some evidence is presented for the existence in these films of chain bundles 30 A or less in diameter. Similar mechanisms are apparently operating in the production of "craze matter" and of fracture surface films.

Gold in dentistry, W. T. Sweeney and C. L. Burns, *American Society for Metals Monograph on Gold. Properties and Applications, ch. 13, pp. 227–235 (D. Van Nostrand Co., Inc., Princeton, N.J., 1964).*
This is a resume of the use of gold in dentistry to be included in monograph on Gold. It was prepared at the request of the editor, Dr. E. M. Wise. The data are chiefly from similar articles in the Metals Handbook. This chapter contains no data not already published.

Measurement of very-high pressures, E. C. Lloyd and A. A. Giardini, *Acta Imeko* **2,** *305 (1964).*
The state-of-the-art in measurement of pressures above a few kilobars is summarized in a graph of accuracy of measurement versus pressures over the pressure range of interest for each of a number of present and possible future techniques. Problems involved in the measurement of high pressures in solid pressure media are discussed. Construction, performance and characteristics of several devices for measurement of high pressures to 100 kilobars are described. These devices utilize (1) a deadweight loaded piston-and-cylinder configuration for pressures to 30 kilobars; (2) a multiple-event calibration cell utilizing polymorphic transitions of bismuth, thallium, and barium; (3) a modification of Bridgman's manganin wire gage for use in solid systems; (4) an ionic pressure sensor; and (5) an inductive pressure sensor. The last two devices constitute novel continuous-reading cells of high sensitivity.

Atomic scattering factors for the lithium and beryllium isoelectronic sequences from accurate analytic Hartree-Fock wave functions, C. M. Womack, Jr., and J. N. Silverman, *Z. Kryst.* **118,** *No. 5–6, 422–433 (Sept. 1963).*
The most widely used atomic scattering factors are based on numerical self-consistent field (SCF) wave functions, some of which are of low accuracy. Atomic scattering factors obtained from recent analytic Hartree-Fock wave functions of higher accuracy than the older numerical SCF functions are reported here for the lithium- and beryllium-isoelectronic sequences. In both sequences, the calculations are made for the nuclear charges $3 \leq Z \leq 10$. These results represent previously unreported SCF factors for the two sequences except for Li, Be, and C^{+2}. The present factors for Li, Be, and C^{+2} are found to be in excellent agreement with the corresponding factors determined from recent, accurate numerical Hartree-Fock solutions. The use of such analytic functions permits high precision evaluation of the form factors for arbitrary values of $\lambda^{-1} \sin \theta$, an operation which is less readily performed using the conventional numerical solutions. In addition, the influence of increasing nuclear charge on various approximate wave functions is examined by comparing the SCF factors for these isoelectronic sequences with the factors derived from other types of wave functions. In this connection, the relative reliability of the SCF factors is discussed. Finally, an explanation is given for the observation that for a given atomic or ionic species of the sequences, the various scattering curves obtained from different approximate wave functions tend to cross in such a manner so that the areas beneath them are approximately equal.

Calculation of electronic energies in HCO_2^+, HCO_2 and HCO_2^-, W. H. Kirchhoff, J. Farren, and J. W. Linnett, *J. Chem. Phys.* **42,** *No. 4, 1410–1422 (Feb. 15, 1965).*
The π-electron energies of the formyloxy cation, radical and anion (formate ion) have been calculated using several methods. The use of wave functions in which the individual electrons were placed in non-paired spatial orbitals gave a substantial improvement, as judged by comparison with a more accurate configuration-interaction function, over wave functions of the molecular-orbital and valence-bond types. All calculations were then duplicated using electron-electron repulsion integrals which were similar in magnitude to the empirical values of Pariser and Parr but which were derived from the split-*p* method of Dewar. In this case the use of non-paired spatial orbitals also gave improvements over the other methods but the advantage was not so great. The implications of these results as well as the technical problems involved in the use of non-paired spatial orbitals are discussed. Finally, a comparison is made between the results obtained here and those obtained for the isoelectronic allyl system.

Impurity controlled properties of ionic solids, A. D. Franklin (*Proc. Symp. Physics and Chemistry of Ceramics, Pennsylvania State Univ., University Park, Pa., May 28–30, 1963*), *Book, Physics and Chemistry of Ceramics, pp. 77–109 (Gordon and Breach, New York, N.Y., 1963).*
The influence of trace amounts of impurities on the physical properties of ionic solids is reviewed. The properties are classified according to the way in which the impurities influence them, as directly or indirectly influenced. The directly influenced properties are in turn subdivided into additive localized, additive non-localized, domain, and scattering effects. Data drawn from the literature is used to illustrate these impurity effects. An extended discussion is given for paramagnetic resonance, dielectric and anelastic relaxation, the photographic effect, dislocation pinning, thermal conductivity, and impurity-induced dislocation climb.

Laboratory measurement of the rate of the reaction $O^+O_2 \rightarrow O_2^+O$ at thermal energy, F. C. Fehsenfeld, P. D. Goldan, A. L. Schmeltekopf, and E. E. Ferguson, *Planet. Space Sci.* **13,** *579–582 (Mar. 1965).*
The rate for the reaction

$$O^+ + O_2 \rightarrow O_2^+ + O$$

has been measured to be $2 \pm 1 \times 10^{-11}$ cm^3 sec^{-1} at 300 °K. It is believed that this measurement resolves an order of magnitude discrepancy between previously reported laboratory measurements. A brief discussion of rates which have been used for this reaction in ionospheric models is presented.

Nuclear magnetic resonance in bulk nickel samples, L. H. Bennett, *Phil. Mag.* **12,** *No. 115, 213–215 (July 1965).*

Nuclear magnetic resonance (NMR) experiments in bulk metals suffer from a small effective filling factor due to the small penetration depth of the rf field. We have found that the NMR signal in bulk Ni metal, however, is extraordinarily intense.

Relation of the stacking fault energy to segregation at stacking faults and to the occurrence of phase boundaries in F. C. C. binary alloys, R. DeWit and R. E. Howard, *ACTA Met.* **13,** *655–661 (June 1965).*
Since the stacking fault energy in many FCC (face-centered cubic) metals is lowered by alloying, thermodynamic equilibrium requires that some segregation of solute atoms to the stacking faults takes place to lower the total free energy. Instead of assuming that the width of the extended dislocations remains fixed during the segregation, we suppose that the width always has the equilibrium value corresponding to the local concentration at the stacking fault and thus changes continually. Two general conditions of thermodynamic equilibrium are found. The first is the same as that derived previously without the above assumption by Dorn and Suzuki; it gives the relation between the solute concentration in the faulted region and the matrix if the stacking fault energy dependence on the local concentration is known. The second is a new expression for the stacking fault width in terms of the stacking fault energy and an entropic term, and can be interpreted in terms of the balance of forces on each partial dislocation. It is found that the locking stress, which is the resolved shear stress required to free a dislocation from its segregated atmosphere, is not changed by the above extension of the theory. On the assumption that the stacking fault energy is exactly the difference in the free energy of the FCC and HCP (hexagonal close-packed) structures of the same composition and temperature, it is shown that the FCC and HCP phase boundary concentrations of the alloy may be related to the concentration dependence of the stacking fault energy. A numerical example for a hypothetical alloy illustrates the various aspects of the theory.

The determination of work function from the ratio of positive to negative surface ionization of an alkali halide, J. Fine, T. E. Madey and M. D. Scheer, *Surface Sci.* **3,** *227 (1965).*
The work function and its temperature dependence has been measured for a (110) oriented tungsten surface in the temperature range 1800 to 2200 °K. The method consisted of determining the ratio of positive to negative surface ionization of a NaCl beam impinging on the (110) tungsten surface. The recent spectroscopic determination of the halogen electron affinities makes possible a reliable calculation of the work function from these data. The results are in reasonable agreement with those obtained independently by the more conventional retarding potential method. Mean values for the parameters in the equation $\phi = \phi_0 + \alpha T$ for the (110) tungsten surface are $\phi_0 = 5.05 \pm 0.10$ eV and $\alpha = -(1.4 \pm 0.2) \times 10^{-4}$ eV/°K.
The indicated uncertainties are standard errors of the coefficients derived from fitting a straight line to the data by least squares.

Theoretical aspects of polymer crystallization with chain folds: bulk polymers, J. D. Hoffman, *SPE Trans.* **4,** *No. 4, 315–362 (Oct. 1964).*
The theory of crystallization of bulk linear polymers with chain folding is discussed in terms of recent developments. Specific topics covered are: (a) rate of crystal growth and size of folded nuclei, (b) theoretical and experimental estimates of the fold surface free energy, and estimates of the surface free energy of "fringed micelle" and "switchboard" type crystals, (c) basic causes of essentially regular folding in bulk, (d) rejection of short chain species during crystallization, (e) melting behavior of thin chain-folded lamellae, (f) gradual thickening of lamellae on isothermal storage, (g) homogeneous, pseudohomogeneous, and heterogeneous nucleation, (h) voids and included point defects as a part of the concept of the degree of crystallinity, and (i) phenomena occurring in stage 1 and stage 2 of bulk crystallization isotherms (annealing). A comparison of theory and experiment is carried out using data, some previously unpublished, on polyethylene and polychlorotrifluoroethylene. The theory with essentially regular folding is found to be satisfactory.

Volume relaxations in amorphous polymers, R. S. Marvin and J. E. McKinney, *Book, Physical Acoustics, Ed. W. P. Mason, IIB, ch. 9, 165–229 (Academic Press Inc., New York, N.Y., 1965).*
Volume relaxations in amorphous polymers are treated along with the effect of static hydrostatic stress on time dependent molecular motion. The relationship between a linear viscoelastic constitutive equation and a general phenomenological equation is discussed, and the linear equation related to molecular mechanisms through a free volume concept. Experimental techniques and results involving dilatation are reviewed, and information from such measurements on amorphous polymers summarized and evaluated. These data indicate that the simple free volume concept is applicable in some cases. In general, polymers for which the primary molecular motions seem to involve large segments of the polymer molecule agree closely with the predictions of the combined phenomenological and molecular theories available. Other types of motion, which are not specifically considered in most current theories, appear to give rise to more complicated behavior.

Dissociation constant of acetic acid in deuterium oxide from 5 to 50°. Reference points for a *p*D scale, R. Gary, R. G. Bates, and R. A. Robinson, *J. Phys. Chem.* **69,** *No. 8, 2750–2753 (1965).*
Electromotive force measurements of a cell without liquid junction have been used to determine the dissociation constant of acetic acid in deuterium oxide from 5 to 50°. The enthalpy, entropy, and heat capacity changes on dissociation of acetic acid have been calculated. Values of $-\log (a_D + \gamma_{Cl^-})$ and the conventional pa_D values for the equimolal (0.05 *m*) acetic acid-sodium acetate buffer solutions have been determined. These provide a second fixed point for standardizing the *p*D scale, supplementing the equimolal mixture of KD_2PO_4 and Na_2DPO_4 established in an earlier investigation.

Frequency-dependent transport coefficients in fluid mechanics, R. Zwanzig, *J. Chem. Phys.* **43,** *No. 2, 714–720 (July 15, 1965).*
Exact time-correlation formulas for frequency dependent shear viscosity, bulk viscosity, and thermal conductivity are presented. These formulas are evaluated for a fluid composed of molecules with internal degrees of freedom, in the limit of very weak coupling of internal and translational motions. In this limit, the shear viscosity is unaffected by internal modes. The bulk viscosity consists of two parts, one due to translational motions, and the other due to relaxation of the energy contained in internal modes. The thermal conductivity consists of two parts, one due to translational motions, and the other due to diffusion of energy in internal modes (the Eucken correction). The resulting excess sound absorption is in complete agreement with the predictions of the thermodynamic theory of relaxation in fluids.

Drift mobility and diffusion for impurities in ionic crystals, J. R. Manning, *Phys. Rev.* **139,** *No. 6A, A2027–A2034 (Sept. 13, 1965).*
An electric field exerts a force on the charged ions in an ionic crystal and causes a net flow of ions and vacancies. In calculations of the drift mobility μ and diffusion coefficient D, it has been customary to assume that the vacancy flow does not alter the average vacancy concentrations at sites that are second-nearest neighbors or farther from the impurity. In the present treatment, this approximation is avoided. Instead vacancies are presumed to be at equilibrium only at vacancy sources-and-sinks and on the symmetry plane containing the impurity. The resulting equations for μ/D include terms $\Sigma_i k_i \triangle w_i$. Here, $\triangle w_i$ is the difference between the vacancy-jump frequencies in the positive and negative x-directions from site i in the absence of a field, and the k_i are coefficients. The summation, which is over all sites in the crystal, simplifies in a number of special cases. Whenever the vacancy jump frequency for association of a vacancy-impurity complex differs from the vacancy jump frequency far from an impurity, extra terms which have not appeared in previous expressions for μ/D are obtained.

Energy levels of polarons in a magnetic field, D. M. Larsen, *Phys. Rev.* **135,** *No. 2A, A419–A426 (July 20, 1964).*
A variational method closely related to the intermediate coupling method Lee, Low, and Pines is used to calculate the ground state energy and low lying excited states of the Frohlich Hamiltonian with a uniform time independent magnetic field. The energy is calculated in a power series in $\frac{\omega_c}{\omega}$ to order $\left(\frac{\omega_c}{\omega}\right)$ where ω_c is the cyclotron

resonance frequency of the electron in the absence of electron-phonon interaction and ω is the frequency of the longitudinal optical phonons. It is shown that in the presence of electron-phonon interaction the energy of the nth magnetic level is no longer proportional to n and that the effective mass for motion along the direction of the magnetic field is a function of n. The calculated variational energies approach the corresponding energies obtained by Lee, Low, and Pines when $\frac{\omega_c}{\omega} \to 0$, and in the weak coupling limit the ground state energy becomes exact to order $\left(\frac{\omega_c}{\omega}\right)^2$.

Excitation of optically forbidden states in the ionization continuum by electron impact, J. A. Simpson, G. E. Chamberlain, and S. R. Mielczarek, *Phys. Rev.* **139,** *No. 4A, A1039–A1041 (Aug. 1965).*
The inelastic electron scattering resonances in the ionization continuum of He, Ne and Ar were recorded as a function of primary energy. The energy resolution was ~ 0.1 eV, the angular resolution $\Delta\phi$ was ~ 10^{-2} radian about the forward direction and the primary energy was between 60 and 400 eV. The strength of resonances due to optically forbidden transitions from the ground state compared to those due to optically allowed transitions increases as the energy is reduced as was expected. A marked difference between ^1D and ^1S behavior exists and certain resonances, notably that due to the $(2s2p^63p)^1P$ state in Ar, change shape as the energy is reduced. At the highest energies used the resonances due to optically forbidden transitions were still apparent.

Investigation of the anomaly in the response of silicon semiconductor radiation detectors at low temperatures, W. R. Dodge, S. R. Domen, A. T. Hirshfeld, and D. D. Hoppes, *IEEE Trans. Nuclear Sci.* **NS–12,** *295 (Feb. 1965).*
Investigation of the response anomaly in silicon semiconductor radiation detectors cooled to temperatures below 40 °K has been continued. Experiments with surface barrier detectors show that the mean temperature at which normally ionized impurity atoms accept electrons (as deduced from dE/dx measurement of the depletion depth) is a slowly varying function of the impurity concentration. This behavior is expected from the dependence of the Fermi level on the temperature, impurity concentration and ionization energy. Below the narrow temperature interval in which the majority of the impurity atoms accept electrons and hence become electrically neutral, particles which produce low ionization densities (beta particles) produce pulse heights with room temperature magnitudes, while particles with high ionization densities (alpha particles) produce pulse heights which are lower than those characteristic of room temperature operation and which depend on the detector bias voltage. The results of experiments conducted to investigate polarization effects in lithium-drifted semiconductor radiation detectors are described.

Matter transport in solids, R. E. Howard and A. B. Lidiard, *Rept. Progr. Phys.* **XXVII,** *161–240 (1964).*
This article reviews the transport of atoms through crystalline solids under the influence of external electric fields, chemical and isotopic concentration gradients and thermal gradients. The main emphasis is on the statistical and thermodynamic description of these phenomena via the theory of mobile lattice imperfections – vacancies and interstitial atoms. In discussing the various phenomena in detail (§ 5) extensive use is made of non-equilibrium thermodynamics as providing a convenient general formalism. Particular attention is given wherever possible to the physical interpretation of the descriptions provided by this formalism.
An introductory survey of the properties of vacancies and interstitials in relation to diffusion phenomena is given in § 2. This includes a summary of the various defect models applicable to different solids – metals, ionic solids, semiconductors and insulators. Section 3 deals in greater detail with certain necessary aspects of the statistical thermodynamics of solids containing defects. Section 4 briefly summarizes the basic theory of non-equilibrium thermodynamics, oriented towards matter transport in crystalline solids; attention is drawn to several pitfalls in this approach. Finally, § 5 is the main object of the review; it applies the material developed in §§ 3 and 4. This section deals with (i) isothermal diffusion in metal alloys, including chemical diffusion, and isotopic tracer diffusion, particular attention being given to dilute systems, (ii) electrolytic conductivity, ionic mobility and both solute and solvent diffusion in ionic solids, special attention being given to the relation between these quantities and to a generalized form of the Nernst-Einstein relation, (iii) the Soret effect and thermal diffusion, especially in metals and dilute alloys, and (iv) thermoelectric phenomena in ionic solids. The article does not deal with grain boundary or surface diffusion and does not specifically discuss diffusion-controlled chemical reactions, sintering or creep. Discussions of these aspects of the subject are given in the works listed in the bibliography.

Optical properties of beryllium in the ultraviolet from electron energy absorption, R. E. LaVilla and H. Mendlowitz, *Appl. Opt.* **4,** *No. 8, 955–960 (Aug. 1965).*
A method for obtaining the optical constants of beryllium in the far ultraviolet based upon electron energy loss experiments is described. This method correlates the electron interaction with the target material with the optical properties of the material. The n and k values and the reflectivity are presented for photon energies in the range $12 \leq E \leq 28$ eV. The n and k values are given and are checked for internal self-consistency by means of the Kronig-Kramers dispersion relations. The optical data have been fitted by a two parameter Drude model with a plasma energy of $\hbar\,\omega_p = 18.4$ eV and a relaxation time of 1.4×10^{-16} sec.

The annealing of vacancies in dilute alloys, R. E. Howard and A. B. Lidiard, *Phil. Mag.* **11,** *No. 114, 1179–1187 (June 1965).*
The annealing of vacancies in dilute alloy is analysed using a more general phenomenological model than that employed in previous discussions. Specific results are presented also for an f.c.c. alloy in which the impurities and vacancies interact only at short range. It is shown that the effective vacancy diffusion coefficient contains another term additional to those obtained by Damask and Dienes using their rate equation model. This additional term is associated with jumps of vacancies from positions where they are free to positions where they are in interaction with impurity atoms. In the special case of an f.c.c. alloy with only nearest neighbor impurity-vacancy interactions the additional term does not alter the qualitative predictions of the Damask and Dienes model about the dependence of vacancy flux, J_v, upon these interactions; but one expects this term to become increasingly important as the range of interaction increases. The associated impurity flux, J_b, however, may not be correctly given in their model. Only for strongly bound impurity-vacancy pairs with high vacancy jump rates, is J_b in the same sense as J_v. For weakly bound pairs it is in the opposite sense. The rate equation model always predicts that both J_b and J_v are towards vacancy sinks.

Other NBS Publications

J. Res. NBS 69B (Math. and Math. Phys.), No. 4 (Oct.–Dec. 1965), 75 cents.
Table of Dedekind sums. R. D. Shipp.
Lattice points in a sphere. M. Bleicher and M. I. Knopp.
Error analysis of phase-integral methods. I. General theory for simple turning points. F. W. J. Olver. (See above abstracts.)
Error analysis of phase-integral methods. II. Application to wave-penetration problems. F. W. J. Olver. (See above abstracts.)
A random walk model of chain polymer adsorption at a surface. II. Correlation between neighboring steps. R. J. Rubin. (See above abstracts.)
Groups of unimodular circulants. R. H. Austing.
A generalization of a result of Newman on multipliers of difference sets. R. L. McFarland.
The bridge tournament problem and calibration designs for comparing pairs of objects. R. C. Bose and J. M. Cameron.
The condition of certain matrices. L. F. Shampine.
Some number-theoretic calculations. K. E. Kloss.

Thermodynamic and related properties of parahydrogen from the triple point to 100 °K at pressures to 340 atmospheres, H. M. Roder, L. A. Weber, and R. D. Goodwin, NBS Mono. 94 (Aug. 10, 1965), 75 cents.

Standard Reference Materials: Methods for the chemical analysis of white cast iron standards, J. I. Shultz, NBS Misc. Publ. 260–6 (July 16, 1965), 45 cents.

Hydraulic research in the United States 1965, ed. H. K. Middleton, NBS Misc. Publ. 270 (July 22, 1965), $1.25.

Guide to instrumentation literature, J. F. Smith and W. G. Brombacher, NBS Misc. Publ. 271 (July 7, 1965), $1.25. Supersedes Cir. 567.

Interrelations between cement and concrete properties, Part 1. Materials, techniques, water requirements and trace elements, R. L. Blaine, H. T. Arni, B. E. Foster, et al., NBS Bldg. Sci. Series 2, pt. 1 (Aug. 20, 1965), 35 cents.

Quarterly radio noise data March, April, May 1964, W. Q. Crichlow, R. T. Disney, and M. A. Jenkins, NBS Tech. Note 18–22 (Aug. 2, 1965), 50 cents.

Accuracy in measurements and calibrations, 1965, W. A. Wildhack, R. C. Powell, and H. L. Mason, NBS Tech. Note 262 (June 15, 1965), $1.00.

Electrochemical analysis: Studies of acids, bases, and salts by EMF conductance, optical and kinetic methods July 1964 to June 1965, ed. R. G. Bates, NBS Tech. Note 271 (Sept. 6, 1965), 60 cents.

Analysis and purification section: Summary of activities July 1964 to June 1965, ed. J. K. Taylor NBS Tech. Note 273 (Oct. 1, 1965), 50 cents.

Solubility of solids in dense gases, J. M. Prausnitz, NBS Tech. Note 316 (July 1965), 35 cents.

A numerical representation of CCIR report 322 high frequency (3–30 MC/S) atmospheric radio noise data, K. L. Lucas and J. D. Harper, Jr., NBS Tech. Note 318 (Aug. 5, 1965), 55 cents.

Characteristics of insoluble protein of tooth and bone—I, Fluorescence of some acidic hydrolytic fragments, S. A. Mancewicz and K. C. Hoerman, Arch. Oral. Biol. **9,** 535–544 (Oct. 1964).

Electrical properties, A. J. Curtis, Book, Crystalline Olefin Polymers, ed. R. A. V. Raff, **2,** 105–130 (Interscience Publ. Inc., New York, N.Y. 1964).

Energy loss straggling of protons and mesons: tabulation of the Vavilov distribution, S. M. Seltzer and M. J. Berger, Natl. Acad. Sci.-Natl. Res. Council Publ. 1133. Studies in the Penetration of Charged Particles in Matter, ch. 9, pp. 187–203 (1964).

High temperature measurements and standards: 1000–3000 °C, R. F. Walker (Proc. Intern. Symp. High Temperature Technology, International Union of Pure and Applied Chem., Asilomar, Pacific Grove, Calif., Sept. 1963), Book, High Temperature Technology. Suppl. to Pure and Applied Chem., p. 7 (Butterworths Inc., Washington, D.C., 1964).

H_2-transfer reactions in the gas-phase radiolysis of hydrocarbons, P. Ausloos and S. G. Lias, J. Chem. Phys. **43,** No. 1 (July 1, 1965).

Osmotic and activity coefficients of tris(hydroxymethyl) aminomethane and its hydrochloride in aqueous solution at 25 °C, R. A. Robinson and V. E. Bower, J. Chem. Engr. Data **10,** No. 3, 246–247 (1965).

Oxidation of asphalt in the presence of ozone, J. R. Wright and P. G. Campbell, Am. Chem. Soc. Div. Petroleum Chem. Preprint **9,** No. 2, B99 (Apr. 1964).

Oxygen atoms reaction with condensed olefins, R. Klein and M. D. Scheer, Science **144,** 1214 (1964).

Present status of project HAYSTAQ, E. C. Marden and H. R. Koller (Proc. 3rd Annual Meeting Comm. Intern. Cooperation and Information Retrieval Among Examining Patent Offices, Vienna, Austria, Sept. 17–26, 1963), Book, Information Retrieval Among Examining Patent Offices, ed. H. Pfeffer, p. 163 (Spartan Books Inc., Baltimore, Md., 1964).

Radiochemical determination of uranium of low activity, L. A. Currie, G. M. France, III, and P. A. Mullen, Health Phys. **10,** 751–755 (1964).

Reaction of deuterated polystyrenes with hydrogen and deuterium atoms, L. A. Wall and R. B. Ingalls, J. Chem. Phys. **41,** No. 4, 1112–1120 (Aug. 1964).

Sampling of leather for physical and chemical examination, J. Mandel and J. R. Kanagy, Book, The Chemistry and Technology of Leather **4,** ch. 59, 223–242 (Reinhold Publ. Corp., New York, N.Y., 1965).

Some electrochemical aspects of germanium dissolution. Simultaneous chemical and electrochemical oxidation, W. E. Reid, Jr., J. Phys. Chem. **69,** No. 7, 2269–2277 (July 1965).

Stress relaxation of γ-irradiated fluorocarbon elastomers, T. Yoshida, R. E. Florin, and L. A. Wall, J. Polymer Sci. **A3,** No. 5, 1685–1712 (May 1965).

The molecular symmetry of iodopentaborane, L. H. Hall, J. Am. Chem. Soc. Commun. to Editor **86,** No. 21, 4729 (Nov. 5, 1964).

The role of carbon dioxide in the bone char process, F. G. Carpenter, V. R. Deitz, and D. Larry, Proc. 1963 Sugar Industry Technologist **22,** No. 2, 27–45 (Chemistry Inst., New York, N.Y., May 1963).

The structure of carbon suboxide, W. J. Lafferty and A. G. Maki, Chemistry **37,** No. 7, 19 (July 1964).

Thermodynamics of solid carbon dioxide solubility in liquid solvents at low temperatures, A. L. Myers and J. M. Prausnitz, Ind. Engr. Chem. **4,** No. 2, 209–212 (May 1965).

Weathering: theoretical and practical aspects of asphalt, J. R. Wright, Book, Bituminous Materials: Asphalts, Tars, and Pitches, ed. A. J. Hoiberg, Vol. **2.** Asphalts, pt. 1, ch 8, 249–306 (John Wiley and Sons, New York, N.Y., 1965).

X-ray study of isothermal thickening of lamellae in bulk polyethylene at the crystallization temperature, J. D. Hoffman and J. J. Weeks, J. Chem. Phys. Note **42,** No. 2, 4301–4302 (June 15, 1965).

A liquid-medium step-function pressure calibrator, R. O. Smith, J. Basic Eng. Series D, **86,** No. 4, 723–727 (Dec. 1964).

Are our neighbors from abroad aware of standards and what standards can do for them? A. T. McPherson, Proc. 13th Annual Meeting Standard Engineering Society, New York, N.Y., Sept. 3, 1964, pp. 11A1–11A2 (1965).

Automatic optical design, O. N. Stavroudis, Book, Advances in Computers, ed. F. L. Alt and M. Rubinoff, IV, 227–255 (Academic Press Inc., New York, N.Y., 1964).

Clinical evaluation of complete dentures made of 11 different types of denture base materials, J. B. Woelfel, G. C. Paffenbarger, and W. T. Sweeney, J. Am. Dental Assoc. **70,** No. 7, 1170–1188 (May 1965).

Comments on the paper "A liquid-medium step-function pressure calibrator", by R. O. Smith, J. L. Cross, Trans. Am. Soc. Mech. Eng. Series D, **86,** 729 (1964).

Comments on three papers on fire tests, J. V. Ryan, ASTM Fire Test Symp., Oct. 1, 1962, Am. Soc. Testing Material Spec. Tech. Publ. No. 344, 52 (Oct. 1963).

Digitizing pictorial information with a precision optical scanner, R. T. Moore, M. C. Stark, and L. Cahn, Photogrammetric Eng. **XXX,** No. 6, 923 (Nov. 1964).

Dimensional changes of dental amalgam associated with strain release in the silver alloy particles, G. Dickson and R. M. Waterstrat, J. Dental Res. **44,** No. 3, 620 (May–June 1965).

Discussion of paper 63–39 I, "The measurement of short duration impulse voltages," by F. C. Creed, M. M. C. Collins, and H. N. Cones, IEEE Trans. Commun. Electron. **EC-69,** 629 (Nov. 1963).

Effect of surface texture on diffuse spectral reflectance, Part B, surface texture measurement of metal surfaces, D. B. Spangenberg, A. G. Strang, and J. L. Chamberlin (Symp. Measurement of Thermal Radiation of Solids, San Francisco, Calif., Mar. 4–6, 1964), NASA Spec. Publ. SP–55, Session II, Paper 17, pp. 169–177 (1965).

Guide to dental materials, 1964–1965, G. C. Paffenbarger, J. W. Stanford, and W. T. Sweeney, Am. Dental Assoc. 2d ed., 159 pages (Chicago, Ill., 1964).

Intense resonance line sources for photochemical work in the vacuum ultraviolet region, H. Okabe, J. Opt. Soc. Am. **54,** 478 (Apr. 1964).

Interferometer test of the 26-inch refractor at Leander McCormick Observatory, J. B. Saunders, Astron, J. **69,** No. 6, 449 (Aug. 1964).

Letter to the Editor of Industrial Research in answer to letters regarding "Synthesis of Food," A. T. McPherson, Ind. Res. Feedback Col. **4,** No. 5, 15–16 (May 1962).

Liquid hydrogen bubble chambers, H. P. Hernandez and B. W. Birmingham, Book, Technology and Uses of Liquid Hydrogen, ch. 8, pp. 228–284 (Pergamon Press, Inc., New York, N.Y., 1964).

Programmed maneuver-spectrum fatigue test of aircraft beam specimens, L. Mordfin and N. Halsey, Am. Soc. Testing Mater. Spec. Tech. Publ. 338, 251–272 (1963).

Some physical characteristics of agar impression materials, M. Ohashi, G. C. Paffenbarger, and J. W. Stanford, J. Nihon Univ. Sch. Dent. **7,** No. 1, 1–11 (Mar. 1965).

Spectral distribution of typical daylight as a function of correlated color temperature (condensed version), D. B. Judd, Illum. Eng. **60,** No. 4, 272–278 (Apr. 1965).

Summary of symposium on methods of metallographic specimen

preparation, L. L. Wyman, Am. Soc. Testing Mater. Spec. Tech. Publ. 285, 130 (May 1961).

The cement and concrete reference laboratory inspection service for concrete testing laboratories, J. R. Dise, Concrete Construc. **9,** No. 8, 234 (Aug. 1964).

The Institute for Applied Technology, D. A. Schon, Engineer **V,** No. 2, 3 (Summer 1964).

The liquefaction of hydrogen. 3A. Basic principles, P. C. Vander Arend and D. B. Chelton, Book, Technology and Uses of Liquid Hydrogen, ch. 3, pp. 38–55 (Pergamon Press, Inc., New York, N.Y., 1964).

The liquefaction of hydrogen. 3B–2. Large scale hydrogen liquefaction facilities, P. C. Vander Arend and D. B. Chelton, Book, Technology and Uses of Liquid Hydrogen, ch. 3, pp. 79–105 (Pergamon Press Inc., New York, N.Y., 1964).

The work of NOMAD–1, W. Hakkarinen, Proc. Buoy Technology Symp., Washington, D.C., Mar. 24–25, 1964, p. 443 (Marine Technology Society, 1964).

What is needed next in the simulation of the arterial street? M. C. Stark, Proc. Highway Conf. Progress Related to the Future of Surveillance, Simulation and Control, Washington, D.C., Sept. 14–15, 1964, p. 144 (Bureau of Public Roads, Washington, D.C., 1964).

What's new in control standards, H. L. Mason, Control Eng. **11,** No. 6, 85–87 (June 1964).

Address encoding—A study of the double-binary keyboard as a link in the machine—sorting of mail, J. R. Cornog, J. F. Hockman, and J. C. Craig (Proc. Winter Annual Meeting, American Society of Mechanical Engineers, Philadelphia, Pa., Nov. 17–22, 1963), ASME Publ. 63–WA–338 (1964).

Approximations to the distribution of quadratic forms, M. M. Siddiqui, Ann. Math. Stat. **36,** No. 2, 677–682 (Apr. 1965).

Estimation for a one-parameter exponential model, J. A. Speckman and R. G. Cornell, J. Amer. Stat. Assoc. **60,** 560–572 (1965).

How people influence experimental results, J. R. Cornog, Proc. Social Statistics Section Convention, American Statistical Association, Cleveland, Ohio, pp. 119–122 (1964).

Inequalities for permanents and permanental minors, R. A. Brualdi and M. Newman, Proc. Cambridge Phil. Soc. **61,** pt. 3, 741–746 (Jan. 26, 1965).

Mortality patterns in eight strains of flour beetles, D. B. Mertz, T. Park, and W. J. Youden, Biometrics **21,** No. 1, 99–144 (Mar. 1965).

On the binary collision expansion of the classical N-body Green's function, J. Weinstock, Phys. Rev. **126,** No. 1, 341–344 (Apr. 1, 1962).

On matching problems, J. Edmonds, A. J. Goldman, C. Witzgall, C. T. Zahn, Jr., Proc. ARO Working Group on Computers, ARO-D Report 65–1, pp. 46–50 (Office Chief Res. and Develop., Feb. 1964).

Paths, trees, and flowers, J. Edmonds, Can. J. Math. **17,** 449–467 (1965).

Plasma oscillations with collective correlations, C. M. Tchen, Proc. 6th Intern. Conf. Ionization Phenomena in Gases, Paris, France, July 8–13, 1963, I, 195–199 (P. Hubert Assoc., EURATOM-CEA Centra-d-Etudes Nuclearies de Fontenay-aux-Roses, Paris, France, 1963).

Realization of semi-multipliers as multipliers, H. Fell and A. J. Goldman, Am. Math. Mo. **72,** No. 6, 639–641 (June–July 1965).

Some remarks on certain generalized Dedekind sums, H. Rademacher, Acta Arithmetica **9,** Sec. 1, 97–105 (1964).

Stochastic theory of diffusion in a plasma across a magnetic field, C. M. Tchen, Proc. Intern. Symp. Diffusion, Feldafing, Germany, June 29–July 3, 1964, pp. 118–123 (1964).

The current status of graphic storage techniques: their potential application to library mechanization, S. N. Alexander (Proc. Conf. Library Automation, Airlie Foundation, Warrington, Va., May 26–30, 1963), Book, Libraries and Automation, ed. B. E. Markuson, pp. 111–140 (Library of Congress, Washington, D.C. 1964).

Accurate length measurement of meter bar with helium-neon laser, K. D. Mielenz, H. D. Cook, K. E. Gillilland, and R. B. Stephens, Science Letter **146,** No. 3652, 1672–1673 (Dec. 1964).

Comments on "Application of experimental design to the study of a test method," R. T. Thaxter and P. D. Hubbe. J. Mandel, Tappi **46,** No. 12, 193A–194A (Dec. 1963).

Direct quantitative analysis of microstructures by a digital computer, G. A. Moore, Am. Soc. Metals Tech. Report No. 16.3 (1964); (condensed version). Book. Computer Applications in Metallurgical Engineering, p. 111 (Am. Soc. Metals, Metals Park, Ohio, 1964).

Educating metrologists, T. R. Young, Ordnance **XLIX,** No. 268, 432–435 (Jan.–Feb. 1965).

Measurement—R & D looks to future, W. A. Wildhack, Control Eng. **12,** No. 1, 75–76 (Jan. 1965).

Metrology as related to microminiaturization processes, T. R. Young, Proc. Microminiaturization Congress, New York, N.Y., Mar. 10–13, 1962 (American Watchmakers Inst., New York, N.Y., Mar. 1963).

The definition of alginate impression materials by a specification, M. Ohashi, G. C. Paffenbarger, and J. W. Stanford, J. Nihon Univ. School Dent. **7,** No. 1, 12–28 (Mar. 1965).

The statistical construction of a single standard from several available standards, E. L. Crow, IEEE Trans. Instr. Meas. **IM–13,** No. 4, 180–185 (Dec. 1964).

Calculations of the hyperfine splitting for the lithium atom, J. B. Martin and A. W. Weiss, J. Chem. Phys. Letter **39,** No. 6, 1618–1620 (Sept. 15, 1963).

Calculation of the radiative tail in the inelastic scattering of electrons, L. C. Maximon and D. B. Isabelle, Proc. Intern. Conf. Nuclear Physics, Paris, France, July 2–8, 1964, 2, 1031–1033 (1964).

Coupling of particle-hole states and two particle-two hole states: splitting, W. Greiner and M. Danos, Compt. Rend. Congres Intern. Physique Nucleaire, ed. P. Gugenberger, II, 617 (Editions du Centre National de la Recherche Scientific, Paris, France, 1964).

Connection between shielding and stability in a collisionless plasma, F. Engelmann, M. Feix, and E. Minardi, Il Nuovo Cimento, Serie X **30,** 830–836 (Nov. 1963).

Dynamic theory of the nuclear collective model, M. Danos and W. Greiner, Phys. Rev. **134,** B285 (1964).

Electromagnetic properties of a quantized relativistic electron-positron gas, L. A. Steinert, Il Nuovo Cimento, Serie X, 36, 935–953 (Apr. 1965).

Experimental verification of the WLF superposition technique, A. J. Bur, Proc. Electrical Insulation Conf., Cleveland, Ohio, Oct. 1964, Natl, Acad. Sci.-Natl. Res. Council Publ. 1238, pp. 70–71 (1965).

Experimental fires in enclosures, D. Gross and A. F. Robertson, Proc. 10th Symp. (Intern.) Combustion, Cambridge, England, Aug. 1964, pp. 931–942 (1965).

General report on fundamental spectroscopic data, C. E. Moore, (Proc. Intern. Astronomical Union Commission 14 Meeting, Hamburg, Germany, Aug. 1964), Trans. Intern. Astron. Union **XIIA,** 156 (July 1965).

Gas mixtures and pressures for optimum output power of RF excited helium-neon gas lasers at 632.8 nm, K. D. Mielenz and K. F. Nefflen, Appl. Opt. Letter **4,** 565 (May 1965).

Hypervelocity cratering data and a crater depth model for the regime of partical fluidity, O. G. Engel, Proc. 6th Hypervelocity Impact Symp., Cleveland, Ohio, Apr. 30–May 1, 1963, II, pt. II, 337–366 (U.S. Army Ballistics Res. Lab., Aberdeen Proving Ground, Md., Aug. 1963).

Introduction, Book, Technology and Uses of Liquid Hydrogen, R. B. Scott, pp. 1–8 (Pergamon Press Ltd., London, England, 1964).

Minutes of the Meeting at Tokyo, Japan, of the Triple Commission for Spectroscopy, September 9, 1962, C. E. Moore, J. Opt. Soc. Am. **53,** No. 7, 883–893 (July 1963).

On the possibility of the measurement of the nuclear 2^4-pole deformation, M. Danos, W. Greiner, and C. G. Kohr, Physics Letters **12,** No. 4, 344 (1964).

Optical constants in the vacuum ultraviolet and electron energy losses, L. L. Marton, J. Quant. Spectr. Radiative Transfer **2,** 671–678 (May 1964).

Preliminary studies on the characterization of solution-grown ADP crystals, R. D. Deslattes, J. L. Torgensen, B. Paretzkin, and A. T. Horton, Advan. X-Ray Anal. **8,** 315–324 (1965).

The gamma-ray distribution from oriented cerium-141 and its application to thermal contact at low temperature, J. F. Schooley and D. D. Hoppes (Proc. 8th Intern. Conf. Low Temperature Physics, Queen Mary College, London, England, Sept. 1963), Book, Low Temperature Physics, ed. R. O. Davies, pp. 435–436 (Butterworth Inc., Washington, D.C., 1963).

The sprin lattice relaxation time of some paramagnetic dispersions, P. H. Fang (Proc. XI Colloque Ampere, Eindhoven, The Netherlands, June 1962), Book, Magnetic and Electric Resonance and Relaxation, pp. 123–128 (1963).

Utility of the Tait equation relating volume and pressure in the study of transitions in polymers, L. A. Wood, J. Polymer Sci. **B2,** No. 7, 703–707 (July 1964).

Unorthodoxy in science, L. A. Wood, J. Wash. Acad. Sci. **51,** 30 (Mar. 1961).

Vapor-phase growth kinetics of potassium and mercury crystals, R. L. Parker and S. C. Hardy (Proc. Intern. Symp. Condensation and Evaporation of Solids, Dayton, Ohio, Sept. 12–14, 1962), Book, Condensation and The Evaporation of Solids. Section II. Condensation of Solids, p. 649 (Gordon and Breach, New York, N.Y., 1964).

Volume relaxation of As_2O_3 in the glass transformation, A. B. Bestul, Proc. Intern. Conf. on Physics of Non-Crystalline Solids, Delft, The Netherlands, July 1964, pp. 426–435 (North-Holland Publ., Amsterdam, The Netherlands, 1965).

Wave functions for anharmonic oscillators by perturbation methods, A. M. Shorb, R. Schroeder, and E. R. Lippincott, J. Chem. Phys. **37,** 1043 (Sept. 1, 1962).

Dependence of the critical frequency of the ionospheric *E*-layer on solar zenith angle and the annual variation in *E*-layer ionization, T. Shimazaki, Nature **205,** No. 4974, 889–891 (Feb. 27, 1965).

Justification for neglecting the compressibility of the ionosphere in VLF radio propagation, J. R. Wait, IEEE Trans. Ant. Prop. **AP–13,** 480–481 (May 1965).

National Bureau of Standards Central Radio Propagation Laboratory, Boulder, C. G. Little, Astron. J. **69,** No. 9, 698–700 (Nov. 1964).

Natural electromagnetic phenomena below 30 kc/s, R. M. Gallet, NATO Advanced Study Institute, Bad Hamberg, pp. 167–204 (Plenum Press Inc., New York, N.Y., 1964).

Propagation and technical factors in radiospectrum utilization, J. W. Herbstreit, Radio Spectrum Utilization, ed. J. W. Herbstreit, A report of the Joint Tech. Adv. Comm. of Inst. Elec. Electron. Eng. Inc., and the Electron Ind. Assoc., ch. III, pp. 30–208 (1964).

Representation of diurnal and geographic variations of ionospheric data by numberical methods. II. Control of stability, W. B. Jones and R. M. Gallet, Telecommun. J. pp. 1–12 (Place des Nations, Geneva, Switzerland, Jan. 1965).

The ionosphere; new guide, how to listen to the world, A. H. Shapely, World Publ. **11,** 15–18 (Hellerup, Denmark, Mar. 1965).

Adhesive bonding of various materials to hard tooth tissues. I. Method of determining bond strength, R. L. Bowen, J. Dental Res. **44,** No. 4, 690–695 (July–Aug. 1965).

Crystal growth as chemical research, H. S. Peiser and J. L. Torgesen, Chemistry **38,** 15–20 (1965).

Determining moisture in solid materials by reaction with calcium carbide, S. Dahl, Mater. Res. Std. **5,** No. 9, 446–453 (Sept. 1965).

Infrared spectrum of the free radical NCN, D. E. Milligan, M. E. Jacox, J. J. Comeford, and D. E. Mann, J. Chem. Phys. **43,** No. 2, 756–757 (July 15, 1965).

Mass spectrometric study of the reaction of nitrogen atoms with ethylene, J. T. Herron, J. Phys. Chem. **69,** No. 8, 2736–2740 (Aug. 1965).

Thermal decomposition of 2,3-dimethylbutane in a single-pulse shock tube, W. Tsang, J. Chem. Phys. **43,** No. 2, 352–359 (July 15, 1965).

Xenon photosensitized formation of metastable nitrogen, M. D. Scheer and W. M. Jackson, Science **148,** 3678 (1965).

Focused-beam electron bombardment evaporator, D. H. Blackburn and W. Haller, Rev. Sci. Instr. **36,** No. 7, 901–903 (July 1965).

The effect of environment on the fatigue strengths of four selected alloys, T. R. Shives and J. A. Bennett, NASA Contractor Report CR–267, 2–22 (Aug. 1965).

The temporal dimensional stability of surface-hardened steels, M. R. Meyerson, Metal Treating **15,** No. 6, 5 (Dec. 1964–Jan. 1965).

Analysis of the spectrum of triply ionized praseodymium (Pr IV), J. Sugar, J. Opt. Soc. Am. **55,** No. 9, 1058–1061 (Sept. 1965).

A method for measuring polarization in the vacuum ultraviolet, K. Rabinovitch, L. R. Canfield, and R. P. Madden, Appl. Opt. 4, No. 8, 1005–1010 (Aug. 1965).

A one-dimensional model of polymer adsorption, E. A. DiMarzio and F. L. McCrackin, J. Chem. Phys. **43,** No. 2, 539–547 (July 1965).

Experiments in electron scattering, L. L. Marton, Lab. Invest. **14,** No. 6, pt. II, 754 (1965).

Historical background of image formation, L. Marton, Lab. Invest. **14,** No. 6, pt. I, 739 (1965).

Letter to the Editor "Physical significance of the Fulcher equation," A. B. Bestul, Phys. Chem. Glasses **6,** No. 3, 108–110 (June 1965).

Localized-introduction concept on a curved vortex and motion of an elliptic vortex ring, R. J. Arms and F. R. Hama, Phys. Fluids **8,** No. 4, 553–559 (Apr. 1965).

Thermal diffusion of substitutional impurities in metals, R. E. Howard and A. B. Lidiard, Acta Met. **13,** No. 4, 433–444 (1965).

**Publications for which a price is indicated are available by purchase from the Superintendent of Documents, U.S. Government Printing Office, Washington, D.C., 20402 (foreign postage, one-fourth additional). Reprints from outside journals and the NBS Journal of Research may often be obtained directly from the authors.*

U.S. GOVERNMENT PRINTING OFFICE : 1966 OL—792–867

OCT 46129
UNIVERSITY MICROFILMS INC
SERIALS SECTION
313 NORTH FIRST ST
ANN ARBOR MICH

UNITED STATES
GOVERNMENT PRINTING OFFICE
DIVISION OF PUBLIC DOCUMENTS
WASHINGTON, D.C. 20402

OFFICIAL BUSINESS

POSTAGE AND FEES PAID
U.S. GOVERNMENT PRINTING OFFICE

JOURNAL OF RESEARCH of the National Bureau of Standards
A. Physics and Chemistry

Vol. 70A, No. 1 January–February 1966

Contents

Page

Optical and magnetic spectra of bis-*N*-propylsalicylaldiminato copper (II). Curt W. Reimann, Gerald F. Kokoszka, and Harry C. Allen, Jr. 1

Phase equilibria in the system niobium pentoxide-germanium dioxide. Ernest M. Levin. 5

Phase equilibria in the system pentoxide-boric oxide. Ernest M. Levin. 11

The solution to a nonlinear Lamm equation in the Faxén approximation. Irwin H. Billick and George H. Weiss. 17

A line formula notation system for coordination compounds: III Deviations from idealized configurations. E. Silverton and R. F. Pasternack. 23

The spherulitic crystallization of isotactic polypropylene from solution: on the evolution of monoclinic spherulites from dendritic chain-folded crystal precursors. F. Khoury. 29

Wavelengths, intensities, and Zeeman patterns in ytterbium spectra (Yb I, II, III, IV). William F. Meggers and Charles H. Corliss. 63

Publications of the National Bureau of Standards. 107

Library of Congress Catalog Card Number: 62–37059

For sale by the Superintendent of Documents, U.S. Government Printing Office, Washington, D.C., 20402. Price $1.00 (single copy)
Subscription price: $5 a year; $1.00 additional for foreign mailing.
UNITED STATES GOVERNMENT PRINTING OFFICE, WASHINGTON : 1966